Coiled-coil based 3D scaffolds as highly specialized biological microenvironments

Inaugural-DISSERTATION

to obtain the academic degree

Doctor rerum naturalium (Dr. rer. nat.)

submitted to the Department of Biology, Chemistry, Pharmacy

of Freie Universität Berlin

by

Katharina Saskia Hellmund, geb. Hagen, Dipl. Chem.

from Berlin, Germany

December 2019

At the department of Chemistry and Biology at the *Freie Universität Berlin*, this doctoral thesis was carried out in the working group of Prof. Dr. Beate Koksch starting in May 2015 and finishing in December 2019.

1st Referee: Prof. Dr. Beate Koksch

2nd Referee: Prof. Dr. Rainer Haag

Disputation at the 24th February 2020

Declaration

I confirm that I have prepared this dissertation entitled *"Coiled-coil based 3D scaffolds as highly specialized biological microenvironments"* autonomously and without impermissible help. All external sources and resources have been specified and properly cited or acknowledged. This thesis has not been submitted, accepted, rated as insufficient or rejected in any other doctorate procedure.

Berlin, December 2019 ***Katharina Saskia Hellmund***

To my family

Science doesn't always go forwards. It's a bit like doing Rubik's cube. You sometimes have to make more a mess with a Rubik's cube before you can get it to go right.

Jocelyn Bell Burnell

Publications

K. S. Hellmund, B. Koksch, Self-Assembling Peptides as Extracellular Matrix Mimics to Influence Stem Cell's Fate, *Front. Chem.* **2019**, *7:172,* DOI: 10.3389/fchem.2019.00172.

Oral Presentations at Conferences and Workshops

"Functionalized coiled-coil peptide hydrogels as tunable extracellular matrix mimics", - Short Poster Talk; 5. International Symposium of the SFB 765 "Multivalency in Chemistry and Biology", Berlin/Germany, October 2019

"Functionalized coiled-coil peptide hydrogels as extracellular matrix mimics" - Short poster talk; 14th German Peptide Symposium, Cologne/Germany, March 2019

"Functionalized Coiled-coil peptides: A versatile tool with multiple applications" - Short poster talk; 8th Peptide Engineering Meeting, Berlin/Germany, November 2018

"Coiled-coil-based peptide hydrogels as synthetic extracellular matrix for stem cell differentiation"; Non-PI-Meeting of the 9th International Meeting 2017 of the Stem Cell Network North Rhine Westphalia, Münster/Germany, May 2017

Poster presentations at conferences

"Functionalized coiled-coil peptide hydrogels as tunable extracellular matrix mimics", 5. International Symposium of the SFB 765 "Multivalency in Chemistry and Biology", Berlin/Germany, October 2019

"Functionalized coiled-coil peptide hydrogels as extracellular matrix mimics"; 14th German Peptide Symposium, Cologne/Germany, March 2019

"Functionalized Coiled-coil peptides: A versatile tool with multiple applications"; 8th Peptide Engineering Meeting, Berlin/Germany, November 2018

"Functionalized coiled-coil peptide hydrogels as potential ECM mimics"; 35th European Peptide Symposium, Dublin/Ireland, August 2018

"Coiled-coil-based peptide hydrogels as synthetic ECM mimics for stem cell differentiation"; 9th Münster Symposium on Cooperative Effects in Chemistry, Münster/Germany, March 2018

Publications, Oral - and Poster Presentation

"Coiled-coil-based peptide hydrogels as synthetic extracellular matrix for stem cell differentiation"; 9th International Meeting 2017 of the Stem Cell Network North Rhine Westphalia, Münster/Germany, May 2017

"Coiled-coil-based synthetic extracellular matrix for stem cell differentiation"; 6. Berliner Chemie Symposium, Berlin/Germany, April 2018

"Coiled-coil-based synthetic extracellular matrix for stem cell differentiation"; 13th German Peptide Symposium, Erlangen/Germany, March 2017

Invention disclosure

Invention disclosure "Funktionalisierbare, coiled-coil basierte Peptid-Hydrogele als Trägersysteme für Erkennungsmotive als künstliche extrazelluläre Matrix für biologische und medizinische Anwendungen"; reported to patent and licensing service of Freie Universität Berlin on 29th August 2019; FU-reference: koks005; Freie Universität Berlin claimed the invention on 14th November 2019; European patent application in process.

Acknowledgement

First of all, I would like to thank Prof. Dr. Beate Koksch for the opportunity to do my PhD thesis in her group and the interesting and challenging projects as well as her encouraging and scientific support and the freedom she granted me and my research. I also thank Prof. Dr. Rainer Haag for his support and many helpful scientific advices in the context of the SFB 765 and being second supervisor of my thesis.

The best ideas will only remain as these if they could not be realized in that excellent and inspiring research atmosphere of the whole Koksch lab. Every current and former group member contributed to the unforgettable character of all the discussions, coffee breaks, cake times and group activities. Especially, many thanks to Allison for several scientific and non-scientific discussions, various helpful advices in English writing and proof-reading of scientific texts. Further thanks to Johann and Susanne for the fruitful discussions and nice time. My students Michelle, Paul and Annika, who supported my experimental work and contributed to my research within their master and bachelor thesis or internship and the secretaries for the support during my thesis.

Prof. Dr. Nan Ma is thanked for scientific advices regarding stem cell research, Dr. Falko Neumann for introducing me into cell culture and Dr. Marie Weinhardt for providing NIH/3T3 cells. Further thanks to Dr. Katharina Achazi and the whole “Biolab team” for the opportunity to do my cell culture experiments in their labs and especially Johanna Scholz for supporting me in working in the “Biolab”. For providing stem cells and many motivating and helpful advices in handling cells, a special thanks to M.Sc. Yong Hou.

I wish to especially thank M.Sc. Benjamin von Lospichl for the excellent cooperation and introducing me into the field of rheology and neutron diffraction and patiently answering the plenty of questions I had at the beginning. In this context, I would also like to thank Prof. Dr. Michael Gradzielski for his advices and giving me new thoughts in understanding the structure of hydrogels. Further, I would like to thank M.Sc. Malte Hilsch for our cooperation and many fruitful discussions, which also opened a lot of new ideas about multivalent structures.

All the staff members of the Core Facility BioSupraMol is thanked for providing an excellent infrastructure and the friendly support and advices I got during my thesis. Especially I would like to thank PD Dr. Christoph Böttcher and Dr. Kai Ludwig for the cooperation. Many thanks Frau Leo and the all the staff members of the Material Management for their friendly service and support. I am grateful to the SFB 765 for financial support and its whole team for their awesome management of the numerous events.

Acknowledgement

I am very thankful to my family and friends who were always there for me. Especially, to my friend Morten Droas, who is always willing to listen to me and enquires for my progress.

Especially I am grateful to my family, my mother Renate and my husband Markus, for their constant appreciation in me. Thank you for your moral and emotional support and your unconditional trust and love to strength me all the time. I am thankful for your unremittingly support, Markus.

Table of Contents

Table of Contents

Abbreviations

ACN	acetonitrile
AOSP	all on solid phase
ASC	adult stem cell
AUC	analytical ultracentrifugation
bFGF	basic fibroblast growth factor
BMHP	bone Marrow Homing Peptide
BMP	bone morphogenic protein
Boc	*tert*-butyloxycarbonyl
CCK-8	Cell Counting Kit-8
CD	circular dichroism
CMP	collagen mimetic peptide
COMU	(1-Cyano-2-ethoxy-2-oxoethylidenaminooxy)dimethylamino-morpholino-carbenium hexafluorophosphate
CuAAC	Copper-Catalyzed Azide-Alkyne Cycloaddition
D-PBS	Dulbecco‘s Phosphate-Buffered Saline
DBU	1,8-Diazabicyclo[5.4.0]undec-7-ene
DIC	N,N‘-diisopropylcarbodiimide
DIPEA	*N*,*N*-diisopropylethylamine
DMEM	Dulbecco's Modified Eagle Medium
ECM	extracellular matrix
EDT	1,2-ethandithiol

Abbreviations

EDTA	ethylenediaminetetraacetic acid
ESC	embryonic stem cell
ESI-ToF	electron spray ionization - time of flight
FCS	fetal calf serum
FF	fiber forming
Fmoc	9-*N*-fluorenylmethyloxycarbonyl
G'	storage modulus
G''	loss modulus
GA	glutaric anhydride
GAG	glycosaminoglycans
Gal	galactose
HA	hemagglutinin
HAI	hemagglutination inhibition
HATU	1-[bis(dimethylamino)methylene]-1*H*-1,2,3-triazolo[4,5-b]pyridinium 3-oxide hexafluorophosphate
HBTU	3-[Bis(dimethylamino)methyliumyl]-3*H*-benzotriazol-1-oxide hexafluorophosphate
HFIP	1,1,1,3,3,3-hexafluoro-2-propanol
hG	high glucose
hMSC	human mesenchymal stem cell
HOAt	1-hydroxy-7-azabenzotriazole
HOBt	1-hydroxy-benzotriazole
HPLC	high performance liquid chromatography

hPSC	human pluripotent stem cell
IAV	Influenza A Virus
iPSC	induced pluripotent stem cell
Man	mannose
MS	mass spectrometry
Mtt	4-methyltrityl
MWCO	molecular weight cut-off
NA	neuraminidase
NAD	nicotinamide adenine dinucleotide
NADP	nicotinamide adenine dinucleotide phosphate
NAIP	neuronal apoptosis inhibitory protein
NMP	*N*-Methyl-2-pyrrolidone
NMR	nuclear magnetic resonance
ODF	Oligomer stater discrimination factor
PDB	protein data bank
PEG	polyethylene glycol
PHP	PolyHIPE polymer
pip	Piperidine
PNA	Peptide nucleic acid
PTA	phosphotungstic acid
RNA	ribonucleic acid
RP	reversed Phase

Abbreviations

RP-HPLC	reversed phase high performance liquid chromatography
RS	recognition sequence
SAF	self-assembling fibres
SAM	self-assembled monolayer
SANS	small angle neutron scattering
SC	stem cell
SPPS	solid phase peptide synthesis
TBTU	*O*-(Benzotriazol-1-yl)-*N*,*N*,*N*',*N*'-tetramethyluronium tetrafluoroborat
TEM	transmission electron microscopy
TFA/$CFCl_3$	trifluoroacetic acid
TIS	triisopropylsilane
VT	vitronectin
w/o	without
WHO	world health organisation
WST-8	(2-(2-methoxy-4-nitrophenyl)-3-(4-nitrophenyl)-5-(2,4-disulfophenyl)-2H-tetrazolium, monosodium salt)
WT	wild type
wt%	weight percent
cryo-TEM	cryo transmission electron microscopy

Amino acid codes used for synthesis of peptides and building blocks

Abbreviations of the 20 canonical amino acids are consistent with the one- and three-letter code recommended by the IUPAC-IUB Joint Commission on Biochemical Nomenclature (JCBN) [*Eur. J. Biochem.* **1984**, *138*, 9-37].[1]

Ala	A	Alanine
Arg	R	Arginine
Asn	N	Asparagine
Gln	Q	Glutamine
Glu	E	Glutamic Acid
Gly	G	Glycine
His	H	Histidine
Ile	I	Isoleucine
Leu	L	Leucine
Lys	K	Lysine
Met	M	Methionine
Phe	F	Phenylalanine
Pro	P	Proline
Ser	S	Serine
Thr	T	Threonine
Val	V	Valine

If not stated otherwise, the abbreviations correspond to L-amino acids.

Abz **o-*aminobenzoic acid***

List of protected canonical and non-canonical amino acid building blocks for solid-phase peptide synthesis used within the scope of this thesis.

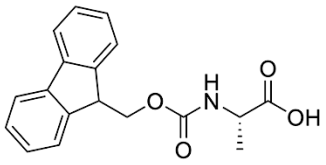

Fmoc-L-Ala-OH

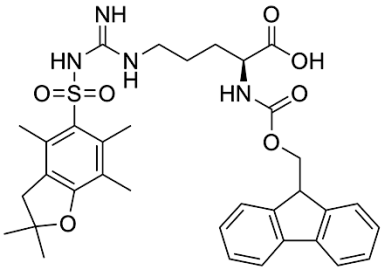

Fmoc-L-Arg(Pbf)-OH

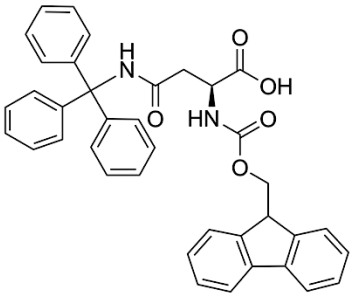

Fmoc-L-Asn(Trt)-OH

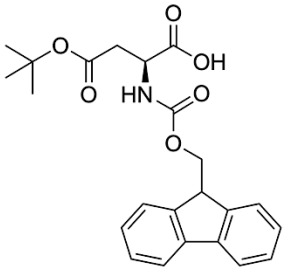

Fmoc-L-Asp(OtBu)-OH

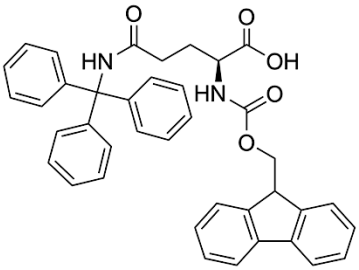

Fmoc-L-Gln(Trt)-OH

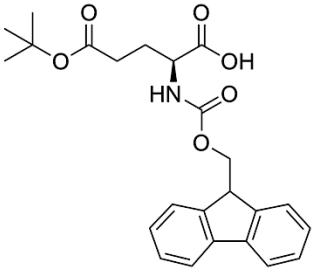

Fmoc-L-Glu(OtBu)-OH

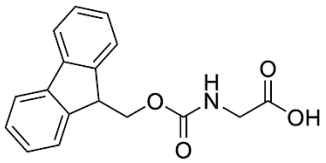

Fmoc-Gly-OH

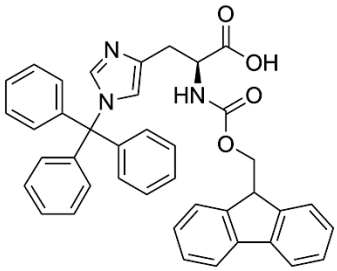

Fmoc-L-His(Trt)-OH

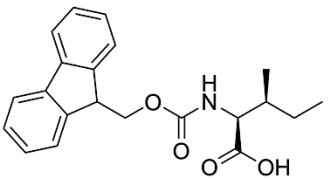

Fmoc-L-Ile-OH

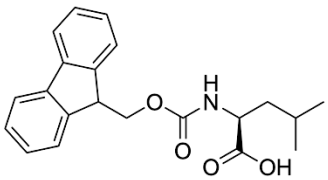

Fmoc-L-Leu-OH

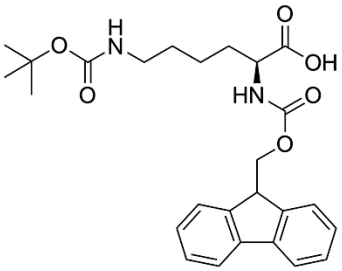

Fmoc-L-Lys(Boc)-OH

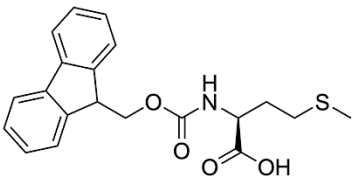

Fmoc-L-Met-OH

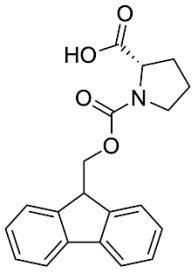

Fmoc-L-Pro-OH

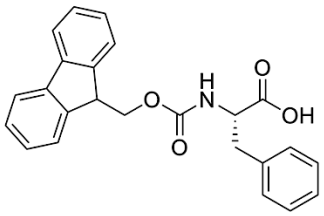

Fmoc-L-Phe-OH

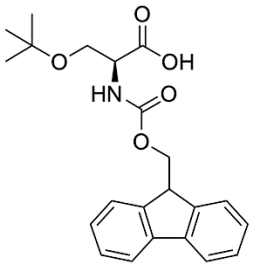

Fmoc-L-Ser(tBu)-OH

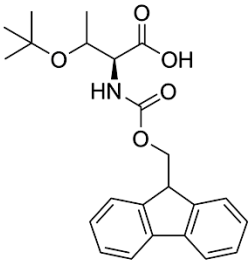

Fmoc-L-Thr(tBu)-OH

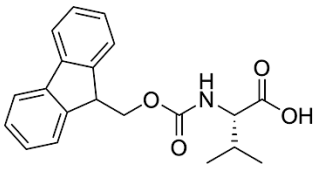

Fmoc-L-Val-OH

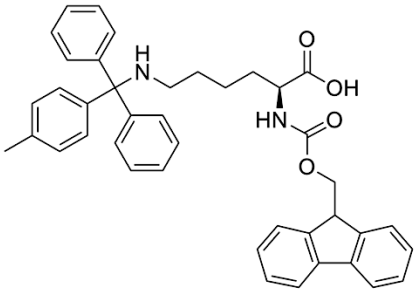

Fmoc-L-Lys(Mtt)-OH

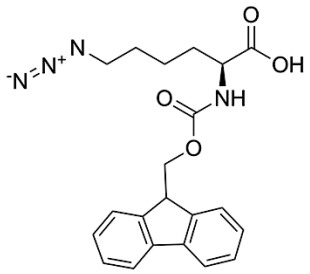

Fmoc-L-Lys(N_3)-OH

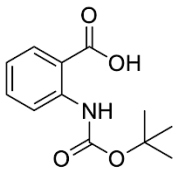

Boc-2-Abz-OH

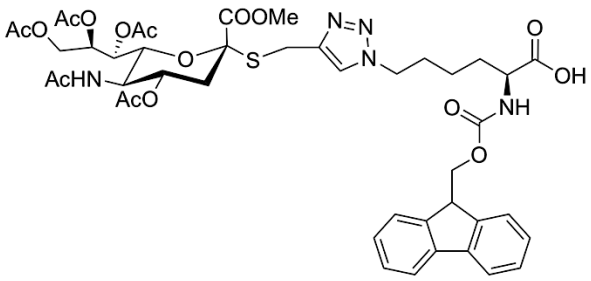

Fmoc-L-Lys-Sial-OH

1 Abstract

Peptides, as natural and highly specific and biocompatible substrates, fibers or active compounds, are developed since their first descriptions by Crick, Corey and Pauling in the 1950's. Inside this diverse field, coiled-coil peptides have been increasingly investigated as suitable substrates due to their self-assembly properties, which enable multivalent ligand presentation.

This thesis has the aim to develop various highly specific and stable coiled-coil peptides as possible 2D or 3D scaffolds for stem cell differentiation. Related to the up to date research in the field of cell culture materials for biological and *"created by extracted own cells"* implants for the human body, the goal is to direct the stem cell fate to the specific cell type needed e.g. as heart muscle tissue. Therefore, a library of different undecorated peptides was synthesized and their properties were compared to known standards. Furthermore, their impact on self-assembly and formation of stable hydrogels had to be evaluated as possible 2D or 3D scaffolds. With regard to the information, a hydrogelating fiber forming coiled-coil peptide (hFF03-*b*A*c*A) was chosen and functionalized by conjugation with biologically relevant ligands. Due to varying the density and ligands presented, the structural and mechanical properties could be adjusted. Combining all these parameters, two main applications for testing the designed peptide as suitable biomaterial were developed.

On the one hand, hFF03-*b*A*c*A presenting biological relevant ligands was tested as a tailored artificial 3D material to mimic the so-called extracellular matrix (ECM). Therefore, the system was either functionalized with carbohydrates or peptide-epitopes as signal molecules and mixed with each other in different ratios. The aim was to create a suitable 3D scaffold, which presents the desired signal molecules in a multivalent fashion. Structural and rheological characterizations revealed that the coiled-coil systems build fibrous networks with viscoelastic properties. Moreover, embryonic mouse fibroblast populations showed excellent viability profiles, when cultured on these peptide hydrogels.

On the other hand, peptide-carbohydrate conjugates were evaluated as potential inhibitors for Influenza A Virus. Therefore, sialic-acid was conjugated to fiber forming coiled-coil peptides and tested regarding density of ligands and suitability as substrates for virus inhibition. Hemagglutination-inhibition tests showed that sialic-acid conjugated coiled-coil peptides enable inhibition of Influenza A Virus in the micromolar range and are therefore promising substrates as diagnostic tool or anti-influenza drugs.

In conclusion, the developed and established approaches represent a simple and efficient methodology to design 3D scaffolds based on coiled-coil peptide structures presenting in a defined and exactly adjustable density of biologically active ligands for specialized applications in the fields of tissue engineering, regenerative medicine and infectious diseases, like growing implants out of extracted steam cells.

2 Kurzzusammenfassung

Coiled-coil Peptide wurden seit ihrer Entdeckung in den 1950iger Jahren durch Crick, Corey und Pauling immer interessanter für medizinische Anwendungen für ihren Einsatz als natürliche und selektive Substrate, Fasern oder aktive Komponenten. Die Anforderung an diese Biomaterialien sind neben einer hohen Biokompatibilität auch eine hohe Stabilität und die multivalente Präsentation von Liganden.

Im Kontext dieser Doktorarbeit werden verschiedene hochspezialisierte und stabile coiled-coil Peptide als potentielle 2D oder 3D Trägersysteme für die Differenzierung von Stammzellen entwickelt. Im Vergleich zur aktuellen Forschung für Zellkulturmaterialien und Substrate für biologische und personalisierte Implantate, die aus körpereignen Zellen gezüchtet werden, sollen Stammzellen in gewebsspezifische Zellen differenziert werden, wie z.B. Herzmuskelgewebe. Hierfür wurde eine Bibliothek verschiedener coiled-coil Peptide synthetisiert und auf ihre Eignung als künstliches Zellkultursubstrat getestet.

Weiterhin wurden ihre Eigenschaften hinsichtlich der Ausbildung von selbstassemblierten Aggregaten und die Ausbildung von Hydrogelen für ihren Einsatz als 2D oder 3D Trägersysteme untersucht. Als vielversprechendster Kandidat wurde ein hydrogelierendes faserbildendes coiled-coil Peptid (hFF03-*b*A*c*A) ausgewählt und mit biologisch relevanten Liganden ausgestattet. Die strukturellen und mechanischen Eigenschaften des Hydrogels wurden durch Variierung der Ligandendichte erreicht. Deren Eignung als Trägersystem wurde in zwei verschiedenen Anwendungen evaluiert.

Durch die Präsentation verschiedener Liganden und -dichten am Peptid hFF03-*b*A*c*A sollen maßgeschneiderte 3D Substrate für die Zellkultur, die sogenannte Extrazelluläre Matrix entwickelt werden. Hierzu wurde das System mit verschiedenen Liganden, wie Kohlenhydraten und kleinen Peptidsequenzen (sogenannte Epitope) ausgestattet. Durch Vermischung der verschiedenen Peptide in verschiedenen Konzentrationen wurde die Ligandendichte variiert und so ein anpassbares 3D Substrat entwickelt, welches die gewünschten Liganden zudem multivalent präsentiert. Die systematische Charakterisierung hinsichtlich Rheologie, Struktur und Toxizität gegenüber embryonalen Mausfibroblasten zeigte, dass die Vermischung unterschiedlicher Liganden-präsentierender Peptidsequenzen ein vielversprechender Ansatz für die Biomaterialforschung darstellt. Die getesteten Hydrogele zeigten durchgehend ein viskoelastisches Verhalten und eine hohe Biokompatibilität.

Weiterhin wurde untersucht, inwiefern coiled-coil Peptide als Trägersysteme für die Präsentation von Sialinsäure zur Inhibition des Influenza A Virus geeignet ist.

Hämagglutinations-Inhibitionstests zeigten, dass diese Peptide-Kohlenhydrat-Konjugate eine inhibierende Wirkung im mikromolaren Bereich hervorrufen können und daher geeignet Substanzen für die Entwicklung von Diagnostika und anti-Influenza Wirkstoffen sind.

Zusammenfassend stellen die in dieser Doktorarbeit entwickelten und ausgiebig untersuchten Modellsysteme eine effiziente und leicht zugängliche Methode dar, um eine Plattform zu kreieren, die für die Präsentation einer exakt einstellbaren und definierten Dichte unterschiedlicher Wirkstoffmoleküle spezialisiert ist. Dieses bietet somit vielversprechende Möglichkeiten für die Entwicklung von Biomaterialien in der regenerativen Medizin, dem *„Tissue Engineering“* und der Behandlung von Infektionskrankheiten.

3 Introduction

Since the earlies 1950s peptides are investigated and developed as pharmaceutical active compounds due to their high variation in structural motifs and behaviors.[2,3] They can also be used as defined architectures existing of α-helices and/or β-sheets, which are relevant for molecular recognition in biological processes. Their defined structural properties encoded by their amino acid sequences (primary structure), makes them suitable as scaffolds in applications inside the fields of tissue engineering, regenerative medicine and infectious diseases

The phenomenon of building α – or β – structures and the question, if these polymers are a coiled-coil system, was already described by Crick[2] or Pauling and Corey[3] in the beginning of 1950s. In this time, the possibility of forming coiled-coil structures was described for different peptidic structures, like α – or β – keratin as well as many synthetic polymers, like polyglycine, poly-y-methyl-L-glutamate or further different polypeptides.

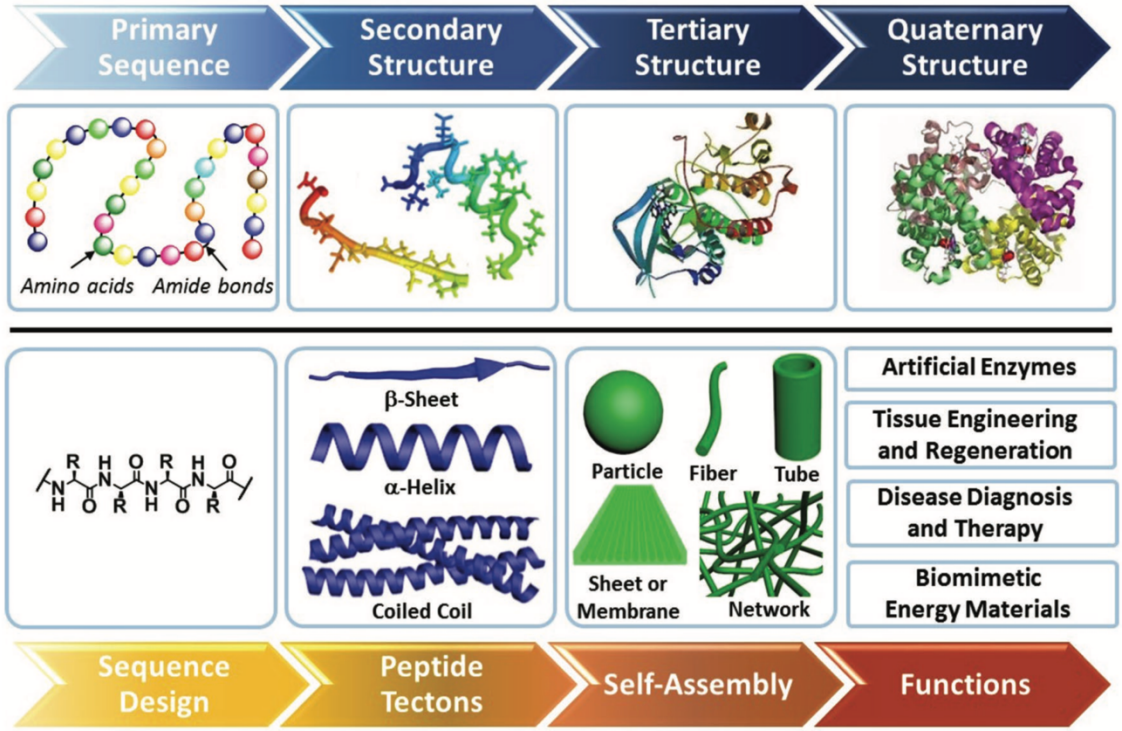

Figure 3.1. Development of defined peptide-nanostructures starting with its sequence design inspired by natural pathway of synthesis of complex protein structures. This picture was reproduced with the allowance of Wiley VCH, according to the Creative Commons Attribution License.[4]

As exemplarily described in Figure 3.1 peptides can adopt different structures from linear amino acid sequences to complex quaternary structures which highlights their diversity. Especially coiled-coil peptides, are excellent candidates for the development of 2D and 3D scaffolds, because of their biodegradability and biocompatibility.[5] In the following part the coiled-coil folding motif and developed applications are described with regard to biomaterials design for cellular and diagnostic applications.

The coiled-coil folding motif

Coiled-coil peptides are used in a variety of applications since a report by F. H. C. *CRICK*[2] determining α-keratin as possible coiled-coil peptide. Since then various structural investigations to clarify assembly and oligomerization behavior of coiled-coils[6] were performed and their versatility for implementation as tunable material was evaluated.[7] Today, we know that the most occurring structural motif in nature is the α-helical secondary structure, which appears in a lot of natural proteins, e.g. collagen or α-keratin. Single α-helices are slightly stable in solution and are mostly stabilized by salt bridges based on their arginine, glutamic acid and lysine rich sequences.[8] They are also stabilized by hydrophobic side chains which are found between three to four residues to wreath the α-helix with 3.6 residues per turn.[9,10] This leads to a more stabilized packing geometry and arrangement of α-helices, when they are wound around each other to form the so-called coiled-coil structure. Coiled-coils consists of two up to seven α-helical strands forming a left-handed superhelical twist with a pitch angle of 20° (see Figure 3.2 a and b).[9,11,12] The heptad repeat, its primary amino acid sequence, is characterized by a seven residue periodicity, denoted by *a*-*b*-*c*-*d*-*e*-*f*-*g* and are depicted in a so-called helical wheel diagram, to visualize helical formation of the sequence (Figure 3.2).

The heptad repeat sequences are formed according to the following “rules”[9]

- Positions *a* and *d* are commonly occupied by nonpolar amino acids forming the hydrophobic core[11] that directs the folding and packing of the amphipathic structure.[9]
- Positions *e* and *g* are mostly charged amino acid residues and provide intermolecular ionic interactions within the bundle.[11,13]
- Positions *b*, *c* and *f* are directed toward the outside of the bundle and are solvent exposed.

Following these rules, α-helices with 3.5 residues per turn will be achieved in comparison to approximately 3.6 residues per turn found in single α-helices.[9] The hydrophobic effect

is the driving force of coiled-coil formation. Thus, the hydrophobic core of coiled-coils denoted by amino acid residues *a* and *d* such as leucine, isoleucine and valine is stabilized by hydrophobic and van-der-Waals interactions.[7] The selection of the type of hydrophobic amino acids represented in positions *a* and *d* defines the oligomeric state of the helix bundle, due steric effects.[7,9,14] The wounded helices are packed in regular, tight side-chain interface which is commonly named as knobs-into hole packing (see Figure 3.2 c).[12]

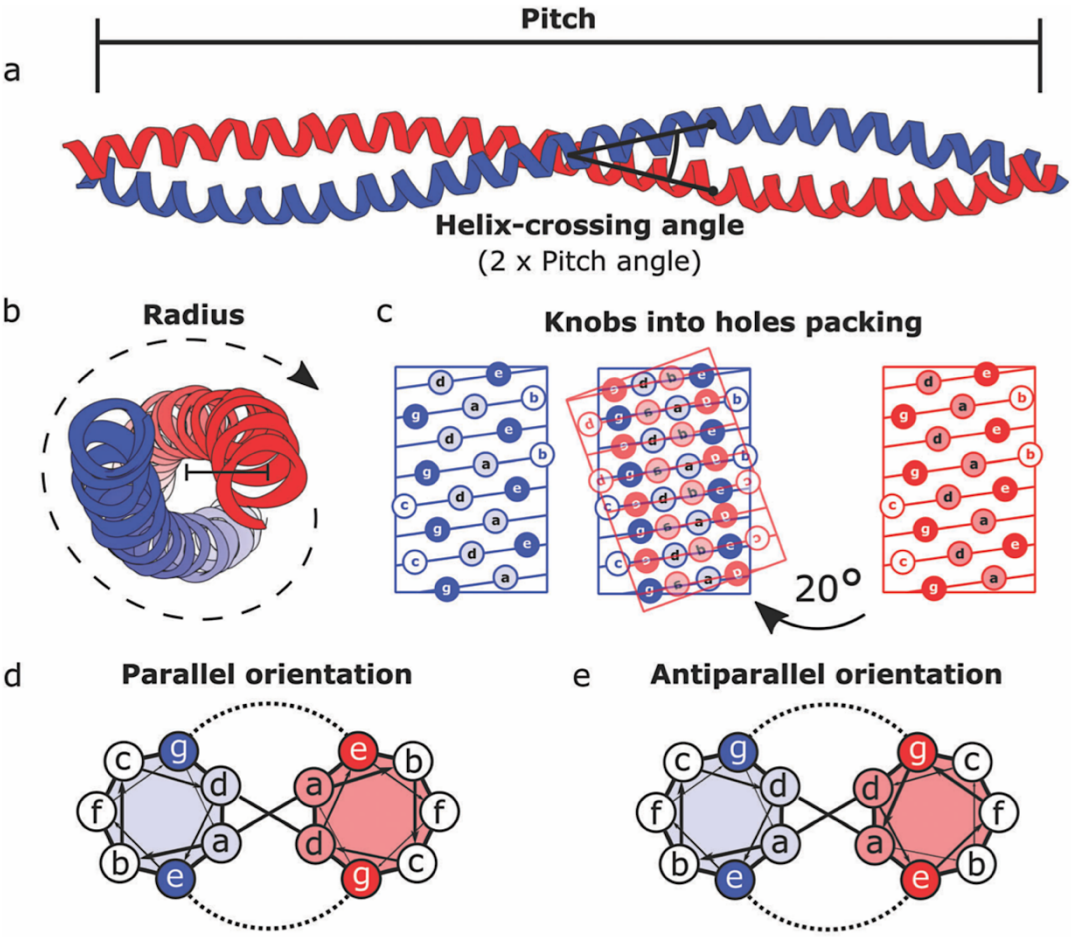

Figure 3.2. Schematic representation of the structure of a coiled-coil dimer (PDB code: 1C1G). (a) Horizontal side view along the superhelical axis depicting the pitch angle of 20° and (b) top view along the axis of the superhelix showing the left-handed orientation of the single-strands wrapped around each other. (c) Scheme of knobs into holes packing of coiled-coil dimer. Helical projection of a (d) parallel and a (e) antiparallel coiled-coil dimer. This picture was reproduced with the allowance of the Chemical Society according to Creative Commons Attribution 3.0 Unported License.[12]

Positions *e* and *g* are occupied by charged amino acids. Electrostatic interactions between complementary charged amino acid residues like glutamic acid and lysine stabilize the

coiled-coil bundle.[7,9] Both effects are influencing the structural properties of the coiled-coil bundle, namely its oligomeric state and parallel or antiparallel orientation of the strands (see Figure 3.2 d and e). The strands can be there of the same sequence (homotypic) or distinct sequences (heterotypic). Solvent exposed positions *b*, *c* and *f* are suitable to occupy by helix-favoring residues like alanine, glutamate, glutamine and lysine[9], are responsible for solubility of the peptide and are appropriate for modifications e.g. carbohydrate or peptide ligands.[15,16]

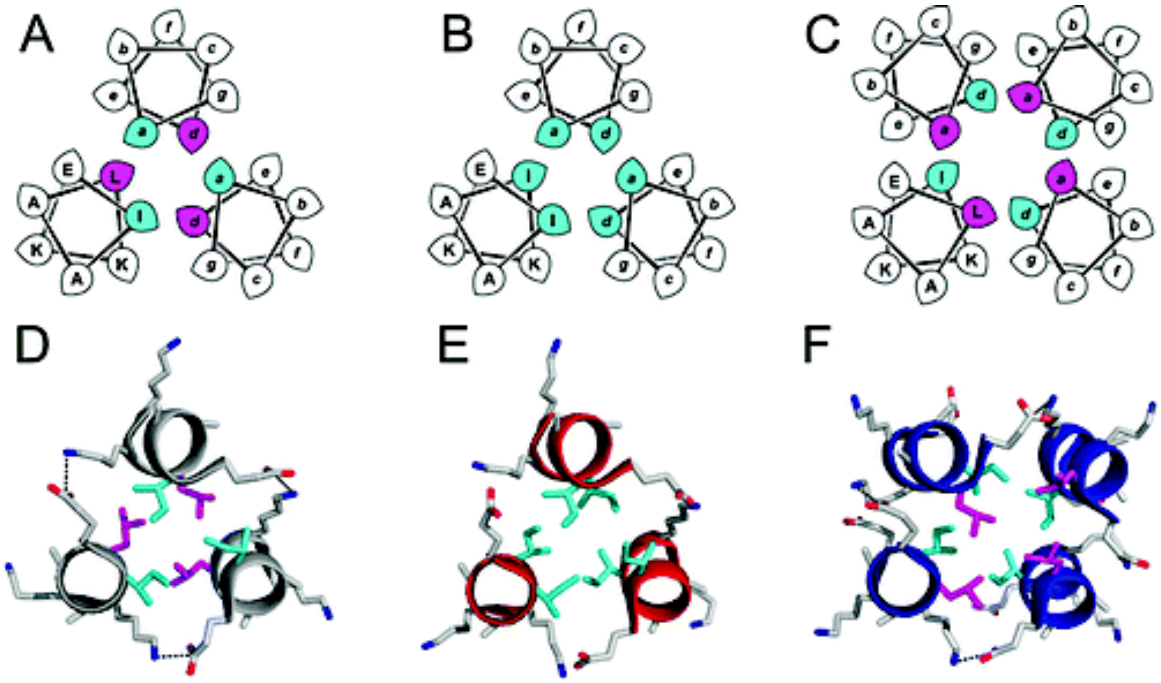

Figure 3.3. Helical wheel projections and structures of the coiled-coils as view along the axis of the superhelices from N-terminal end to C-terminal end of the coiled-coils CC-pIL (A and D, PDB code: 4DZN), CC-pII (B and E, PDB code 4DZL) and CC-pLI (C and F, PDB code 3R4A) showing knobs-into-hole packing by hydrophobic core amino acids isoleucine (turquoise) and leucine (pink). Dashed line represents electrostatic interactions between positions g (glutamic acid) and e (lysine). Reprinted with permission from (J. M. Fletcher, A. L. Boyle, M. Bruning, Sg. J. Bartlett, T. L. Vincent, N. R. Zaccai, C. T. Armstrong, E. H. C. Bromley, P. J. Booth, R. L. Brady, et al., ACS Synth. Biol. 2012, 1, 240–250.). Copyright (2012) American Chemical Society. [17]

In fact, primary sequence analysis has shown that nearly 2 - 3 % of natural proteins contain coiled-coils. Prominent examples are collagen and α–keratin.[6,18] The regularity of this structural motif makes them attractive and versatile tools for peptide and protein designers for a variety of different applications. The simplest type are coiled-coil dimers. One example is the parallel homodimeric coiled-coil GCN4, which is a transcription factor in yeast and is represents a starting point for several studies regarding the relation between

the roles of hydrophobic core occupancy, sequence and oligomerization properties.[12] The group of Harbury explored the effect of hydrophobic core substitutions on the oligomerization behavior of the coiled-coil leucine-zipper GCN4-p1.[14] They replaced amino acids in positions *a* and *d* with leucine, isoleucine or valine, respectively and demonstrated the influence on the oligomerization state.[12,14] Substitutions in positions *a* and *d* in different combinations resulted in dimers for isoleucines in positions *a* and leucines in positions *d*, whereas isoleucines in all positions *a* and *d* results in trimeric oligomerization state and positions *a* substituted by leucines and *d* by isoleucines gives tetramers.[19]

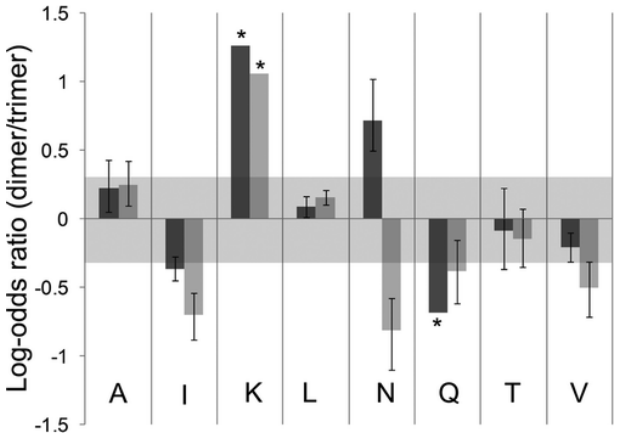

Figure 3.4. Oligomer-state discrimination factors (ODFs) for amino acids A, I, K, L, N, Q, T and V as log10 of the ratio of normalized percentages of respective amino acid in positions a (black bars) and d (grey bars) in dimeric and trimeric parallel coiled-coil homomers. Shaded region emphasizes the range of +/- 0.3.[17] Reprinted with permission from (J. M. Fletcher, A. L. Boyle, M. Bruning, Sg. J. Bartlett, T. L. Vincent, N. R. Zaccai, C. T. Armstrong, E. H. C. Bromley, P. J. Booth, R. L. Brady, et al., ACS Synth. Biol. 2012, 1, 240–250.). Copyright (2012) American Chemical Society.[17]

The control over oligomerization by modifications of the hydrophobic core of coiled-coils was also successfully demonstrated by the group of Woolfson, who designed several dimeric, trimeric and tetrameric coiled-coils outgoing from the hydrophobic core combinations of Harbury (see Figure 3.3).[17] Their studies confirm the revealed rules of Harbury on GCN4-p1 and additionally showed that they can be applied not only for natural coiled-coil sequences but also for *de novo* designed coiled-coil backbones.[17] However, it was also demonstrated that the targeted dimer namely CC-pIL (*a*= Ile, *d*= Leu) either forms a trimer in solution and its crystal state (see Figure 3.3) indicating that this rule is not sufficient in itself for the specification of dimers.[17] By a single-substitution of isoleucine to asparagine (position *a, 17*) in the center of the coiled-coil sequence the problem was solved by proving the dimeric state of the more specified designed peptide CC-Di. The

reason why this peptide switches from the trimeric state into the dimeric state by a punctual mutation of position *a* to asparagine could be explained by the so-called oligomer-state discrimination factor (ODF), which describes a normalized ratio (in %) of a considered amino acid in the hydrophobic core positions in a dimeric coiled-coil and a trimeric coiled-coil depicted as $\log_{10}$ (see Figure 3.4).[17] Comparing positive valued ODFs only amino acids asparagine and lysine have values above 0.3. However, asparagines seem to strongly favor dimers, whereas lysines seem to favor both dimer and trimer.

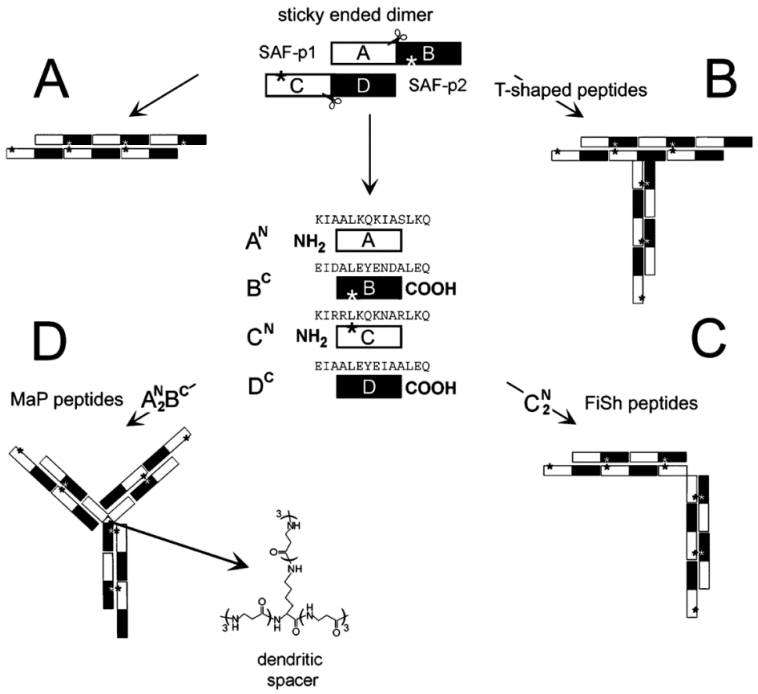

Figure 3.5. Schematic representation of SAF system, which enables T-shaped, Fiber Shaping (FiSh) peptides and Matrix-Programming peptide designs. (A) Elongated fiber assembly of SAF peptides, which form dimers with sticky ends. (B) Branched architecture by mixing SAF peptides with T-shaped peptides obtaining branched fibrils.[20] (C and D) AN and BC, as well as CN and DC designed chemically distinct halves of SAF peptides. Superscript indicates the terminal end that is free in the parent peptide.[21] (C) Kinked architecture by FiSh peptide C2N.[22] (D) Hyperbranched and networked architecture by a tridirectional peptide built around a dendritic spacer like A2NBC.[21] Reprinted with permission from (M. G. Ryadnov, D. N. Woolfson, *J. Am. Chem. Soc.* **2005**, *127*, 12407–12415). Copyright (2005) American Chemical Society.[21]

The detailed understanding of coiled-coil design and the accompanying control over self-assembly and oligomerization behavior makes coiled-coil peptides attractive for the development of several functional and functionalized designer materials with defined structural features in the range of biological and medical applications.[7] An appropriate example of *de novo* designed fibrous coiled-coil biomaterials is the self-assembling fiber

(SAF) system developed by Woolfson and co-workers.[23] The system enables fiber formation after mixing complementary strains SAF-p1 and SAF-p2. The design of the SAF sequences includes a hydrophobic core with isoleucines in *a* positions and leucines in *d* positions to promote dimerization, whereas glutamic acids and lysines occupy positions *e* and *g* to trigger sticky-end assembly and asparagine in different, complementary heptads of the two peptides for parallel orientation of the heterodimeric coiled-coil.[9,23] Application of these rules into the design of the coiled-coil system led to a versatile and tunable tool with the ability to create different engineered peptide fiber morphologies.[7,21,22]

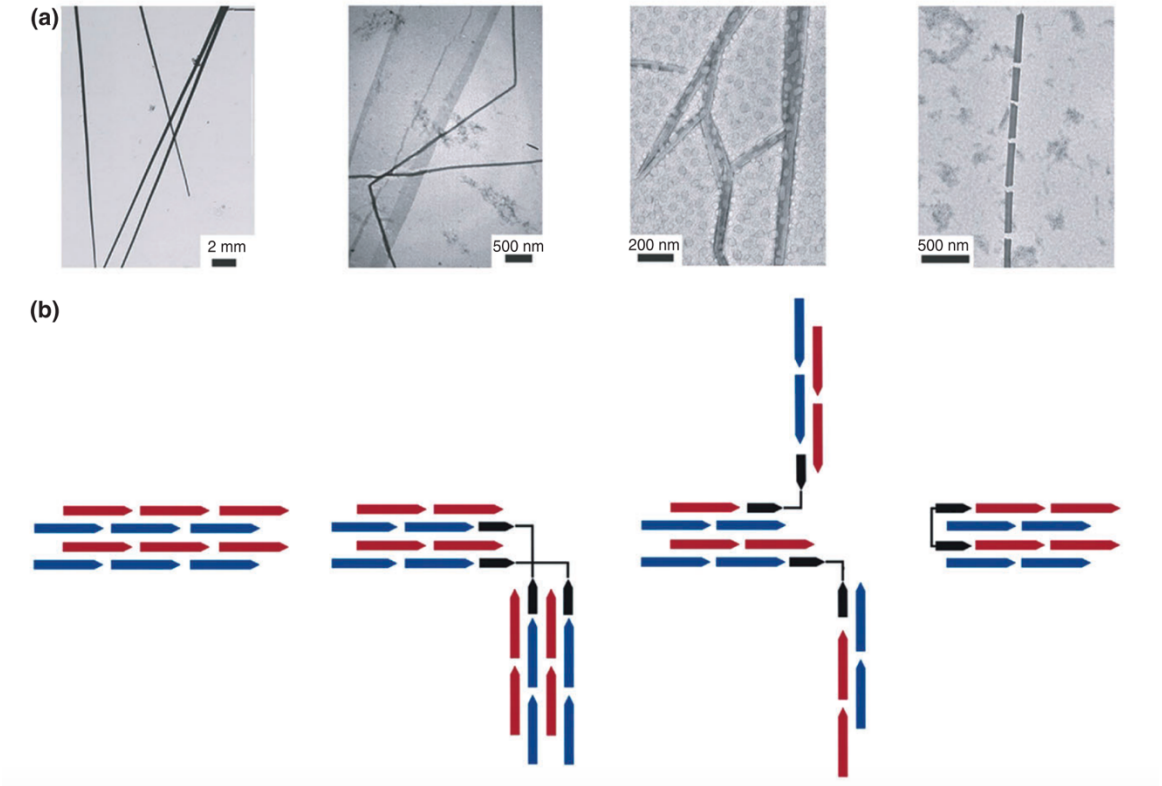

Figure 3.6. Examples of different morphologies produced by different combinations of SAF peptide units. (a) TEM micrographs of straight (standard SAF), kinked homotrimer C3N, interconnected network of SAF peptides and MaP peptide and segmented SAF fiber assemblies with B2C (left to right).[21] (b) Scheme of assembly modes of different presented architectures. Blue and red arrows represent dimeric SAF coiled-coil and black lines show the introduced structural elements.[7] Adapted with permission from (M. G. Ryadnov, D. N. Woolfson, J. Am. Chem. Soc. 2005, 127, 12407–12415). Copyright (2005) American Chemical Society, Copyright 2006 and with permission from Elsevier.

As an example the introduction of flexible β-alanine containing linkers can lead to kinked morphologies of the SAF-system.[21,22] Furthermore, the SAF peptides can be divided into distinct regions and each of them can be combined in different ratios to produce e.g.,

straight, network or segmented morphologies (see Figure 3.6).[21] Application of all known design principles into the sequence development was investigated *via* computational analysis in comparison with experimental examination of solution behavior of a designed antiparallel, homo-tetrameric coiled-coil peptide bundle.[24] Two sequences, namely BNDL1 and BNDL2, both of 29 amino acids were the focus of the study. The sequence of BNDL1 was designed with expected solubility.[25] Both peptides contain alanine – and isoleucine residues (*a* and *d* positions) in their hydrophobic core except of the first amino acid (*a* position) occupied by aspartic acid for BNDL1 and arginine for BNDL2.

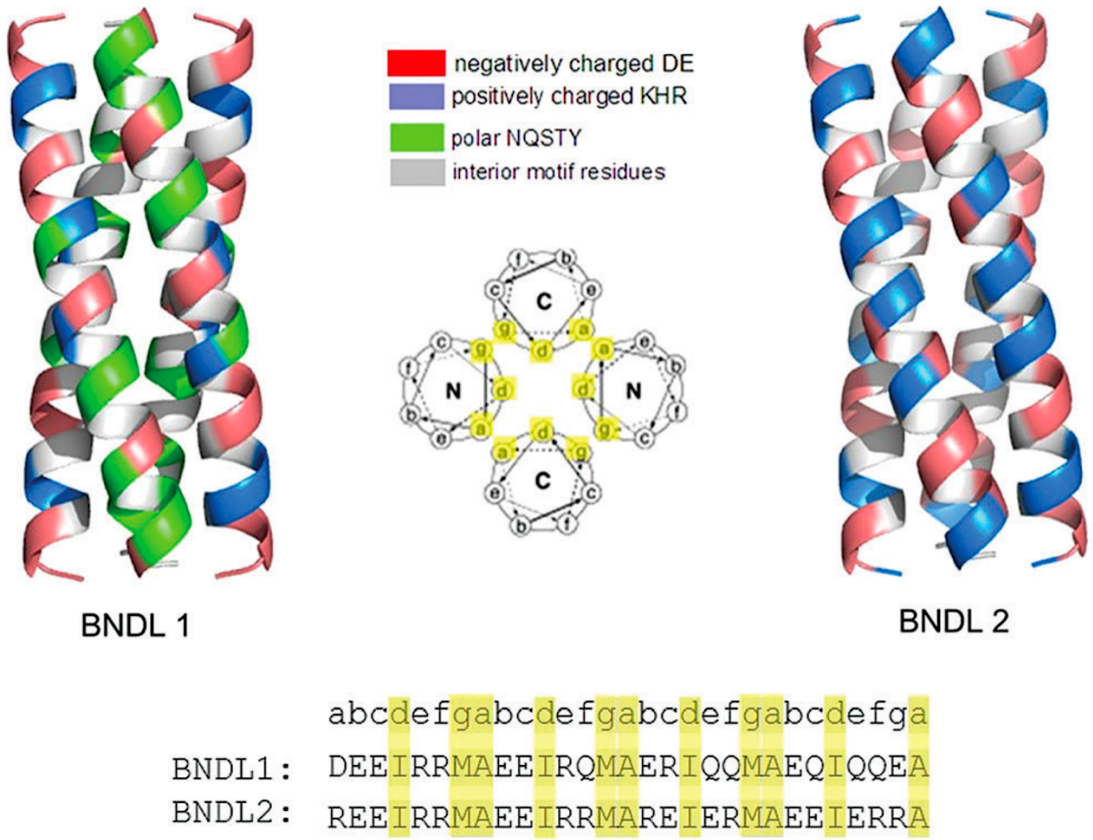

Figure 3.7. Coiled-coil bundles BNDL1 and BNDL2 computationally designed. According to their chemical properties the residues are color coded demonstrating their properties on the surface of the helix bundle. Helical wheel diagram and sequences according to the oligomerization degree and orientation of the coiled-coil strains of BNDL1 and BNDL2. Amino acids which participate in the hydrophobic core of the bundle are marked yellow. Reproduced from M. J. Haider, H. V. Zhang, N. Sinha, J. A. Fagan, K. L. Kiick, J. G. Saven, D. J. Pochan, Soft Matter 2018, 14, 5488–5496 with permission from The Royal Society of Chemistry.[24]

The computational design includes occupancy of charged positions to result in antiparallel arrangement of the monomeric strains. Experiments show that assembled coiled-coil

bundles are robust and have a high stability and solubility in solution, even in the milli-molar range. Circular Dichroism (CD) and analytical ultracentrifugation (AUC) confirmed tetrameric coiled-coil formation.[24] The aggregation behavior of the peptides in solution at high concentration was supported by small angle neutron scattering (SANS) which revealed that the peptides form soluble bundles also at 15 mM peptide concentration.[24] The experimental data harmonize with the computational simulations and show the applicability of coiled-coil design principles.

To sum up, current and former examples on coiled-coil design and application as versatile materials makes them an excellent platform for the development of 2D and 3D materials. Their properties are also able to simulate by computational analysis comparable with experimental data which opens several opportunities in biomaterials design. With these tools in hand peptide designers are able to develop materials with predictable structural properties following the previously described rules to promote α-helical fibrillar scaffolds.[26] As one of the most recently studied structural elements of biological organism is the extracellular matrix (ECM). Successful mimicking and engineering of the latter opens the possibilities for tissue engineering and applications in regenerative medicine e.g. in combination with different types of stem cells. The principles of native ECMs and the basis of the development of peptide-based stem cell supporting materials as synthetic microenvironments are summarized within the next paragraph.

3.1 Extracellular matrix mimicking by self-assembling peptides[1]

3.1.1 The ECM as an important component of the stem cell niche

The ECM as an important part of the stem cell niche theory and was firstly described by Ray Schofield in 1978,[27] and can influence the stem cell fate evaluated in numerous studies.[28] This specialized environment regulates the stem cell behavior due to signals of all components inside[29,30] and describes how stem cells were supported or influenced by the defined microenvironment, for instance, physical interactions between the stem cells and other cells, by secretion of signal molecules or the presentation of molecules on the surface of other cells like integrins.[29–32] Stem cells have specific characteristics, they are able to differentiate into individual cell-types[33,34] and are contributing to the regeneration of these tissues.[30,34] Additionally an unlimited self-renewal by an asymmetric cell division into a specialized and an unspecialized daughter cell summarizes the main characteristics of stem cells.[35,36] Within the asymmetric cell division two daughter cells with different fates originate from one parent cell. Their fate is a feature which will be identified by different sizes, morphology and gene expressions of the two daughter cells.[35] Figure 3.8 represents schematically the stem cell division into two daughter cells with different fates triggered by intrinsic and extrinsic factors.

Two different types are known: embryonic stem cells (ESCs) and adult stem cells (ASCs).[30,34] ESCs are derived from the inner cell mass of the blastocyst[30,33] and have a pluripotent differentiation potential.[30,37] They have the ability to differentiate into cells of all three germ layers (ectoderm, mesoderm and endoderm).[30,33,34] ASCs are unspecialized, multipotent cells derived from adult tissues and can differentiate into restricted types of specialized cells.[33,34] These multipotent cells are important for tissue homeostasis.[30,32] The most common type of ASCs are the mesenchymal stem cells (MSCs)[34] and have wide a differentiation potential.[38] ASCs need a defined microenvironment in an adult organism to maintain their stem cell properties.

[1] *The whole Chapter 3.1 is adapted and extended based on the mini-review; K. S. Hellmund, B. Koksch, Front. Chem. 2019, 7, 172. Copyright © Hellmund and Koksch.*[43] The text was partially modified with the allowance of the authors and copyright owners.

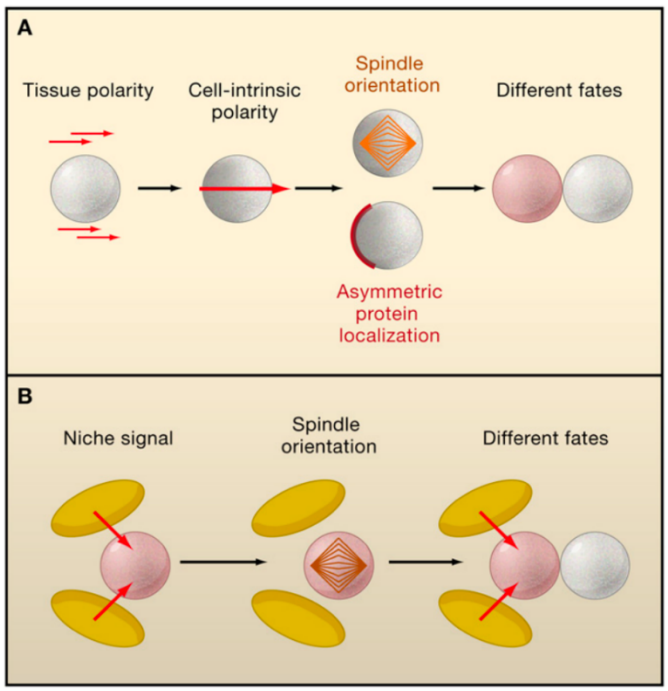

Figure 3.8. Stem cell self-renewal by extrinsic and intrinsic regulation. This figure was used with Copyright © 2008 Elsevier Inc. [35]

The composition of the natural ECM can depend and differ on its tissue of origin consisting of different adhesion proteins like collagen, fibronectin and laminin.[30,39,40] More detailed, these proteins have cell-binding epitopes, which are small peptide sequences, namely, RGD from collagen, RGDS from fibronectin and IKVAV and YIGSR from laminin.[41] These cell-binding epitopes can induce a physical interaction between the stem cells and other cells, the secretion of signal molecules, or the presence of molecules on the surface of other cells, like integrins. The (stem) cell senses the environment in which it is embedded and is able to modify its form and function accordingly; this is its main mechanism of proliferation and differentiation (Figure 3.8). Understanding this mechanism in detail is of paramount importance to the development of new biomaterials for stem cell biology and regenerative medicine.[42]

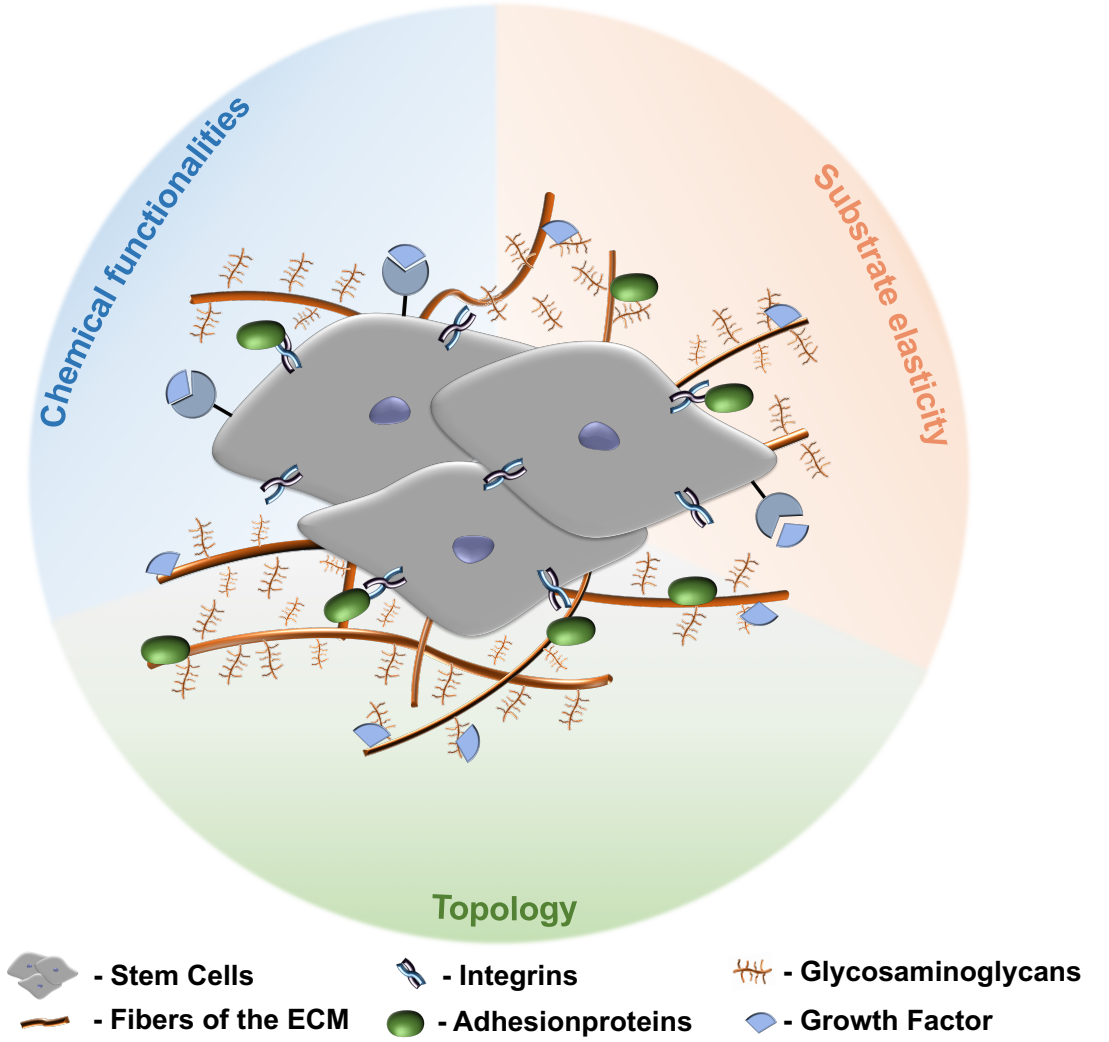

Figure 3.9. Schematic representation of the extracellular matrix of stem cells. Stem cells are surrounded by fibers and adhesion proteins which recruit integrins. Their fate is directed by aspects of the ECM like stiffness, cell-cell interactions, and composition with respect to solubility factors, adhesion proteins, and glycosaminoglycans. Topological signals can be epitopes presented by the latter to direct cell behavior. According to the biomaterial design principles discussed, peptide materials can be designed to comply with the requirements of the natural ECM. This picture was reproduced and adapted with the allowance of the authors Hellmund and Koksch, in accordance to the Creative Commons Attribution License (CC BY), *K. S. Hellmund, B. Koksch, Front. Chem. 2019, 7, 172.*[43]

3.1.2 Peptide based materials to mimic the ECM of stem cells

The development of cell culture materials is a challenging task for the chemistry community, but its successful realization would allow cellular behavior to be directly influenced in order to optimize their applications in regenerative medicine. By tuning the properties of such materials, i.e., stiffness or the presence of chemical inducers like recognition motifs, it is possible to tailor the stem cell's microenvironment to give

information regarding proliferation and differentiation. I.e. a stiff ECM induces differentiation towards stiff tissues, i.e., osteogenesis. Depending on the specific mechanical properties, for example, MSCs can differentiate into tissue cells according to stiffness of tissues the cells are specializing in. The strongest tissue with elastic moduli from 25 kPa to 40 kPa is osteoblast entrapping bone tissue; elastic moduli between 8 to 17 kPa was determined for muscle tissue and entraps myoblasts; elastic modulus of 3 kPa is typical for cartilage tissue and entraps chondrocytes; pancreatic tissue has an elastic modulus of about 1.2 kPa and the elastic modulus of brain tissue ranges from 0.1 kPa to 1 kPa and can entrap neurocytes.[44,45] The properties of each peptide-based material can be adjusted by the primary structure, and they are generally easy to procure by means of standard peptide synthesis protocols. Peptide structures, folding processes and stability are also for the most part well established in the literature.[5,46]

With these characteristics in mind, peptides and peptide derivatives are excellent candidates for the development of 2D and 3D cell-culture materials, thanks to their biodegradability and biocompatibility, and make it possible to tailor biomaterials for different applications in tissue engineering and regenerative medicine.[5,41] Specific types of peptide-based materials possess specific advantages: whereas 2D scaffolds present highly sensitive ligands bound to an inert substrate, elasticity and stiffness are key in obtaining differentiation signals for stem cells embedded in 3D scaffolds. The Kiessling group developed an array of self-assembled monolayer and displayed heparin-binding peptides in different densities that interact with glycosaminoglycans (GAGs) on the cell surface.[47] They showed that only low surface densities of the GAG-binding peptide GKKQRFRHRNRKG derived from vitronectin (VT) need to presented for adherence and proliferation of pluripotent stem cells.[47,48] This example of 2D cell culture demonstrates the possibility to tune tailored surfaces by displaying peptides as bioactive ligands.[48] A promising peptide candidate to include in screening studies is the neuropeptide substance P, which is associated to have regulatory effects on bone morphogenic protein 2 (BMP2) induced osteogenic differentiation.[49] Furthermore peptide was found to have a function as injury messenger to mobilize and recruit MSCs for tissue repair.[50,51]

One prominent example of a 3D nanofibrous scaffold supporting cell differentiation belongs to the RAD16 peptide family.[5,52] The RAD16 peptide family has exists of two ionic β-sheet forming peptides, named RAD16-I and RAD16-II, which form stable structures in water and spontaneously self-assemble into nanofiber scaffolds to mimic the ECM of tissue cells. [5,53] By functionalization with three different biologically active peptide motifs at its C-terminus three different self-assembling peptide hydrogels were developed to mimic a 3D cell environment for human adipose stem cells.[54] C-terminus of the peptides

was elongated by peptide epitopes found in Bone Marrow Homing Peptide 1 (BMHP1, SKPPGTSS, RAD/SKP), heparin binding motif (FHRRIKA, RAD/FHR) and a PRGD-peptide motif (PRGDSGYRGDS, RAD/PRGD).[54] In cell-culture the functionalized RAD16-I peptide-based hydrogels showed an increased viability of human adipose stem cells compared to RAD16-I. The largest number of human adipose stem cells showing highest biological activities including migration, proliferation and growth factor-secretion were detected in case of RAD/PRGD. These kinds of biomaterials follow simple design principles and are easy to connect with biologically relevant peptide epitopes to tune bioavailability.

Comparing the mechanical properties of each tissue in mammalian organism bone tissue has the greatest stiffness of all types. However, stem cells exist in the bone marrow niche, which is variable stiff and it is not yet been cleared how their fate will be directed after leaving their niche.[55] Besides stiffness, artificial substrates that should promote osteogenic differentiation have also to provide topological cues to induce osteogenic signals. The influence of shape and topology of a synthetic ECM on cell fate was demonstrated by covalently grafted silica-nanoribbons with a KRGDSPC peptide onto activated glass substrates and showed that the studied helical nanoribbons induced differentiation into osteoblast lineage.[56] Different biologically relevant epitopes are shown to promote osteogenic differentiation of osteoblast precursor cells by C-terminal extension of RAD16 peptides.[57] The design of peptide-amphiphiles including the recognition motif RGD and N-terminal palmitic acid resulted in a 3D-network which influences the stem cells' attachment, proliferation, and differentiation to osteogenic lineage by mixing an aqueous solution of peptide-amphiphile with MSCs.[58,59] RAD16-I conjugated to PolyHIPE polymer (PHP) spontaneously self-assembled into highly hydrated nanofibers with volume contents of 99.5% water represent a an appropriate 3D nano environment to embed cells. [60,61] The cell-number in RAD16-I coated H-PHP constructs compared to H-PHP alone significantly increased and induced osteoblast differentiation.[61] Osteoinductive materials are focusing on signals sent by molecules covalently grafted onto inert surfaces or presented in a 3D nanofiber network.

One approach to creating chondrogenesis inducing materials is to mimick the structure of adhesion proteins like collagen.[62] Due to its triple-helix structure[63–65] collagen can be mimicked by synthetic peptide-amphiphiles[62,66] and coiled-coil peptides[67] or collagen mimetic peptides (CMPs), which are able to adopt the tertiary structure of natural collagen.[68–70] CMP substrates retain their structure to help encapsulate collagen by conjugation with PEG, which maintains chondrocytes[68,70] and thus, serves as suitable substrate to enable MSCs chondrogenesis.[69,70]

Systematic investigations to study the effect of glucose, carboxylate, and sulfonate attached to a peptide nanofiber on the differentiation behavior of rat MSCs showed that the presence of the monosaccharide on the peptide nanofiber leads to osteo/chondrogenic differentiation of the tested cells.[71] Designing materials to inducing chondrogenesis have either to combine structural and morphological features of cartilage tissue. In the native ECM glycosaminoglycans play an important role in achieving stiffness. A promising proof-of-concept is the conjugation of simple functional groups to these substrates to take into consideration that native ECMs are of high complexity.

Nanofibrous structures, like the RAD16 peptides, were shown to promote neural stem cell differentiation by conjugation with BMHP1 and Bone Marrow Homing Peptide 2 (BMHP2) supported by detected gene expressions. [72] With the aim of creating a self-assembling IKVAV-linked peptide hydrogel as a 3D scaffold for enhanced differentiation of neural stem cells the peptide was found to be suitable for a potential application for the regeneration of injured brain tissue. [73] The pentapeptide IKVAV is known to promote neuronal differentiation and neurite proliferation. [74] RAD16-II, like RAD16-I, also showed to be a suitable substrate for neurite outgrowth.[5,75] Conjugation of different peptide motifs found in native ECMs to these peptide sequences lead to an increase of neuronal differentiation behavior of different stem cell lines.

3.1.2.1 Decorated coiled-coil peptides

Coming back to the coiled-coil folding motif an example is described by engineering its primary structure to engineer 3D materials to direct cellular behavior. By modelling the solvent exposed positions *b*, *c* and *f* of the SAF system, which were exchanged against alanines and glutamines to generate networks of non-covalently cross-linked fibrils, namely hydrogelating SAF (hSAF) show hydrogelation in comparison to its highly ordered original.[76] Alanine was introduced because it promotes weak hydrophobic interaction, whereas glutamine was chosen because of its affinity for hydrogen bonding. The effect of these substitutions was systematically studied and resulted for both substitutions in self-supporting gels revealed by inverting sample vials the gels were filled in. For a better understanding, the invertion of sample vials is a simple test, to verify the ability of a material to form self-supporting gel materials. The test is positive if the materials remains for at least 30 min at the inverted bottom of a flat glass vial, if it flows down the test is negative. However, both gels were shown to have different mechanical properties. Glutamine residues in the solvent exposed domain led to gel which melts at high temperatures. Alanines affected the self-assembly, and thus the gelation of the hSAF fibers into a weak gel at low temperatures whereas heating led a stiffer gel demonstrate by rheological

experiments. Gel formation of both hSAF peptides was confirmed their dominating storage modulus G' over loss modulus G''. This effect was stronger for the alanine gel-variant and increased by increasing temperature. To stabilize fibril-fibril interactions and the gel itself for cell culture applications by treatment with phosphate buffered saline (PBS) or cell-culture medium one f-position was exchanged from alanine to more hydrophobic tryptophan W.[76] With this the self-assembling α-helical coiled-coil hydrogel was shown to support the growth and differentiation of rat adrenal pheochromocytoma cells (PC12) in comparison to commonly used Matrigel®. Having in mind that Matrigel® is an *ex vivo* product and a complex mixture of different ECM proteins and growth factors, it is a hallmark to design and engineer materials out of simple building blocks like coiled-coils which perform similar ~75% to commercially available variants.[76] The resulting hSAFs are suitable and defined microenvironments for cell growth and differentiation. To increase the performance of the designed hydrogels the attachment of functionalities originally found in native ECMs is an approach to increase the complexity of these materials. Therefore Mehrban *et al.* engineered functionalized hSAF gels *via* copper-catalyzed azide-alkyne cycloaddition (CuAAC) to attach the cell-adhesion motif RGDS to azide-bearing hSAF gels.[77] By half-moon studies, were unfunctionalized gels and functionalized gels were directly compared in one cell-culture well, it was demonstrated that the cell number of seeded PC12 cells is higher on the side of the latter and indicate a higher proliferative and differentiation activity.[77] Combining these gels with neural stem cells (NSCs) it was shown that cells migrate into regions of RGDS-rich regions of the gels and formed large neurospheres.[78] To take into consideration that the ECM is of high complexity and a continuously changing environment more functionalities should be provided to the cells to enhance their proliferative and differentiation behavior.[78] α-helical peptide-based hydrogels provide an appropriate extracellular environment for different types of cells. They are an excellent starting point for biomaterial development in tissue engineering.

The approach to tailor coiled-coil scaffolds by attachment of ligands in the solvent exposed domain was also used by the Koksch group. Their approach includes the covalent attachment of monomeric carbohydrate moieties in varying positions and numbers of the ligands on the coiled-coil scaffold and the varied the distance between peptide backbone and carbohydrate to find optimal density and geometry for interaction with asialoglycoprotein receptor on hepatocytes.[16] Another strategy comprised the presentation of antigens to their target by a fiber-forming coiled-coil peptide (FF03). Prior to its assembly the peptide was loaded with a specific carbohydrate-epitope-ligand and tested for its suitability as a multivalent scaffold in bioassays and diagnostics.[15]

3.2 Influenza A Virus Inhibition

Over the last decade, the importance to develop efficient Influenza A Virus (IAV) inhibitors increased significantly. Influenza, commonly known as “flu”, is caused by infection with IAV. The World Health Organization (WHO) reported that annually 1 billion cases of flu and 3-5 million cases of severe illness occur worldwide due to infection with IAVs.[79] Every year ~ 500.000 casualties are caused.[80,81] Influenza is a global spread infection known for centuries. IAVs are able to avoid human antibodies for immune defense causing serious sickness due to its antigenic variability.[82] Over the last one hundred years four pandemics resulted from the occurrence of new influenza strains:

- the H1N1 strain in Spanish flu in 1918 caused approximately 40-50 million deaths
- the H2N2 strain in Asian flu in 1957 caused around 1-2 million deaths
- 1968 the Hong Kong flu causes 500.000 to 2 million death by H3N2 strain
- Swine flu (Mexican flu) in 2009 triggered by H1N1 strain caused up to 575.000 casualties.[83–85]

Structure of Influenza A Virus

Influenza virions are of spherical or filamentous shape with a diameter of 100 nm for spherical forms and 300 nm length for filamentous forms.[86] They are enveloped by a membrane, which is protecting its genome and viral spike proteins and supports the entry of the virus into the host organism. The membrane consists of the glycoproteins hemagglutinin (HA), neuraminidase (NA) and the matrix protein 2 (M2),[87] which overlay the virion core enclosing matrix protein 1 (M1).[86] Trimeric HA and tetrameric NA are presented as spikes on the surface of the virus and have their main role in viral entry and release.[87,88] The virus particle contains a viral ribonucleoprotein complex (vRNP) consisting of HA, NA, M1, M2, nucleoprotein (NP), polymerase basic protein 1 (PB1), polymerase basic protein 2, nonstructural protein 1 (NS1) and nuclear export protein (NS2).[89] IAVs are classified into antigenic subtypes according to the density in which they are presenting HA and NA on their surface: classification with HA occurs from H1 to H18 and classification with NA from N1 to N15, but only a few subtypes were isolated from infected humans.[90] By binding of the viral HA to receptors on the surface of the host cell the virus is able to enter the cell. Infection will be initiated by fusion of virus und membrane of the host cell (Figure 3.10).[91]

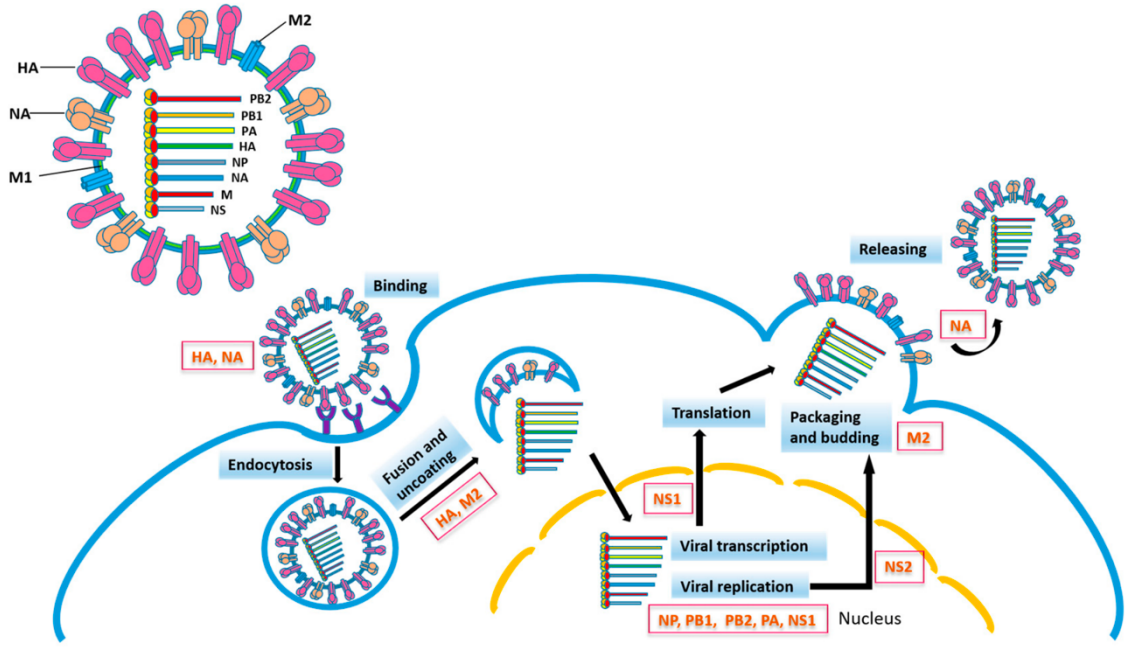

Figure 3.10. Anatomy of Influenza A Virus and its life cycle. During infection of the host cell viral proteins participate in different steps of virus infection. HA – Hemagglutinin; M1 – matrix protein 1; M2 – Matrix protein 2; NA – Neuraminidase; NP – Nucleoprotein; NS1 – nonstructural protein 1, NS2 – nuclear export protein; PB1 – polymerase basic protein; PB2 – polymerase basic protein 2. This figure was reproduced from W. Zhu, C. Wang, B. Z. Wang, Int. J. Mol. Sci. 2017, 18, 1–14 with the Creative Commons Attribution License.[89]

The enzyme NA supports the virus to leave the cell after replication by cleavage of receptor binding site followed by release of new virions (Figure 3.11).[92,93] The M2 proton channel is involved in genome release in early and late stages of replication of the virus.[91,94] Due to continuous changes in the antigenic structure of viral proteins the virus will not be neutralized by antibodies produced by the host after virus infection.[86,95] This high mutational rates of IAVs reduce therapeutic effects of current drug-candidates and require an annual updating of influenza vaccines.[88,96] Regular vaccination strategies address viral proteins that undergo these continuous changes, which limits the protection for especially elderly or immunocompromised persons and highlights the need for new strategies.[88,95]

IAV inhibition strategies

Available influenza drugs target two viral proteins, which are involved in critical stages of the virus life cycle: the M2 channel and NA.[91] Amantadine and rimantadine are common M2 ion channel inhibitors, whereas oseltamivir, zanamivir, peramivir and laninamivir are used as NA inhibitors.[79,93] The mutation potential of these proteins resulted in IAV strains

resistant against specific drugs. Examples are the common and worldwide circulating IAV H1N1 subtypes, which are resistant to adamantanes and nearly 100% of these subtypes are resistant to oseltamivir.[79] Also the global circulating subtype H3N2 mutated to adamantane resistance. Since the majority of IAVs gained resistance to M2 ion channel inhibitors, NA inhibitors are the only class of drugs currently in use.[79,93] These drugs prevent new infections of host cells by blocking NA mediated cleavage of the receptor binding of the virus to the host cell and interfere with the release of new virions (Figure 3.11).

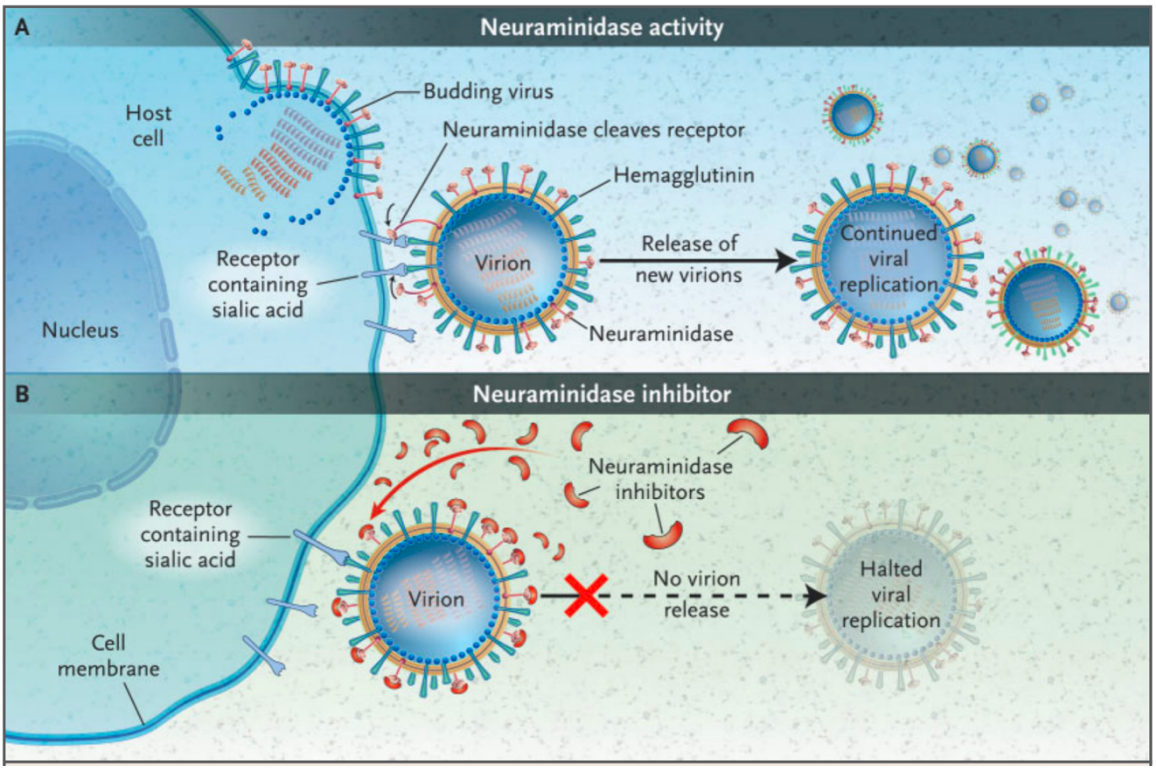

Figure 3.11. Mode of action of virus neuraminidase (A) and neuraminidase inhibitors (B). Reproduced with permission from (A. Moscona, N. Engl. J. Med. 2005, 13, 1363–1373), Copyright Massachusetts Medical Society.[93]

Further IAV inhibition strategies focus on targeting the viral HA. Finding suitable scaffolds which enable multivalent presentation of sialic acid groups is therefore of high interest. Sialic acid is a monosaccharide, which was found to bind to HA on the surface of the virus.[97] The glycoprotein interacts with sialic acid moieties resulting in infectivity-neutralizing binding sites.[98] An alternative strategy is the imitation of the host cell's surface leading to the binding of the virus by the multivalent presentation of sialic acid moieties.[81,99,100] The requirements for each scaffold are, besides their cytotoxicity and biocompatibility their structural properties to present the sialic acid moieties in an

appropriate fashion to the virus. Sialic acid conjugated polyacrylamide scaffolds were successfully used to prevent the binding of IAVs to their target cell.[81,101–103] It was shown that the presentation of multiple sialic acid moieties leads to an increasing inhibition of IAV compared to their monomeric equivalents.[102] Unfortunately, polyacrylamides are normally cytotoxic,[81,104] especially those of high molecular weight, though they are more effective in inhibiting IAV compared to their low-molecular weight forms.[101,105] *In vivo* studies of 3'-sialyllactose-polyamidoamin (PAMAM) dendrimer-conjugates showed its successful implementation as anti-infective agents in experimentally infected mice. The results of this study led to the expectation that inhibiting IAV mediated hemagglutination is appropriate to prevent IAV infection.[106] Kwon and coworkers developed the right spacings and densities by using 6′-sialyllactose-PAMAM derivates.[107] They found out that, within their tested spherical scaffolds, the distance of ligands is a crucial parameter for binding to IAV HA and not the density of ligands.[107] Typically, HA recognizes sialyl-LacNAc ligands on the surfaces of host cells, which was considered for the development of self-assembled peptide nucleic acid (PNA)-DNA complexes displaying the latter.[108] The study covered explorations regarding valency of the glycoligands, their distance and position on scaffolds presented by either flexible polyethylene glycol spacers of different length or rigid, self-assembled PNA-DNA complexes.[108,109] It was found, that the optimal distance between sialyl-LacNAc ligands is in average 50 Å.[108]

The effect of different scaffold geometries was studied by Bhatia and coworkers, who conjugated sialic acid to linear and dendritic low-molecular weight polyglycerol scaffolds. Both scaffolds varied in molecular weight and density of presented sialic acid ligands. By *in vitro* and *in vivo* studies they demonstrated that the linear polyglycerol-sialic acid conjugates have a higher potency to inhibit IAV than the dendritic derivates which may be due to steric shielding of the virus.[81] The presented agents are promising approaches and consider crucial parameters needed for successful inhibition of IAV binding to host cells. Nevertheless, finding the right geometry of the scaffold and density of sialic acid moieties to prevent binding of the virus are still major aim in this field.

4 Scientific Goals

The aim of this thesis is the development of coiled-coil peptides, which can act as carriers for recognition motifs and as 2D/3D substrates for cell culture at the same time. The main goal is the establishment of a tailored scaffold influencing the fate of stem cells. Therefore, the conjugation with defined recognition motifs is necessary, which are crucial for the stem cell environment or development.

The overall goal includes

i. Design and synthesis of a series of undecorated and decorated coiled-coil peptides with defined conformational behavior and ligand presentation.
ii. Structural characterization of the coiled-coil peptides and development of appropriate environments for stem cells.
iii. Evaluation of (binding) specificity of the developed coiled-coil peptides as 2D/3D scaffolds in cell culture or as carrier system for virus inhibition.

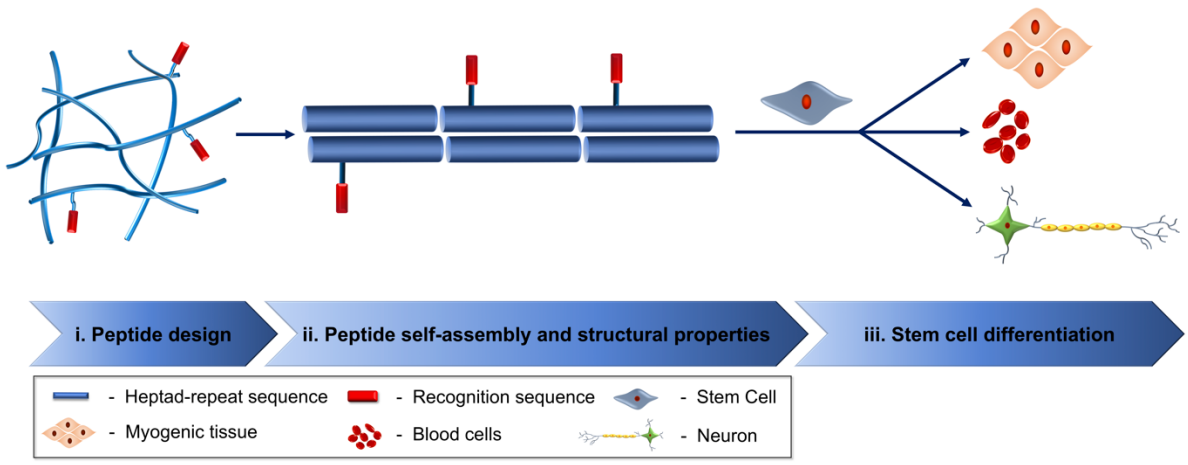

Figure 4.1. Schematic illustration of a coiled-coil peptide presenting recognition sequences in varying densities to achieve stem cell differentiation.

The design of undecorated and decorated coiled-coil peptides includes the evaluation of biologically relevant ligands to initiate cellular response. Therefore, solvent exposed position *f* of the coiled-coil folding motif was chosen to present different ligands based on peptide sequences or carbohydrates. The structural behavior and their influence as cellular substrate had to be evaluated. Consequently, their cytotoxicity and their differentiation behavior should be tested. To vary the ligand density, mixtures of the decorated and undecorated peptides should be used to find the ideal concentration. The

final goal is to evaluate coiled-coil peptide scaffold as an artificial ECM mimic. This approach enables the study of scaffolds regarding their structural properties with multivalently presented ligands by functionalized coiled-coil hetero-assemblies and will give hints regarding ideal ligand density and ligand type presented through the scaffold. Studies of cell-toxicity and cytocompatibility will help to understand design principles of the developed approach of mixing different decorated coiled-coil peptides to tailor a microenvironment for influencing cellular behavior.

Besides that, the potential of sialic-acid conjugated coiled-coil peptide as Influenza A Virus inhibitor are evaluated. Here, different densities of sialic-acid presenting peptides have to be studied. Density and scaffold of the attached ligand will be compared in order to find optimal geometry of the scaffold and optimal ligand density for increasing binding potential to hemagglutinin receptors of Influenza A Virus.

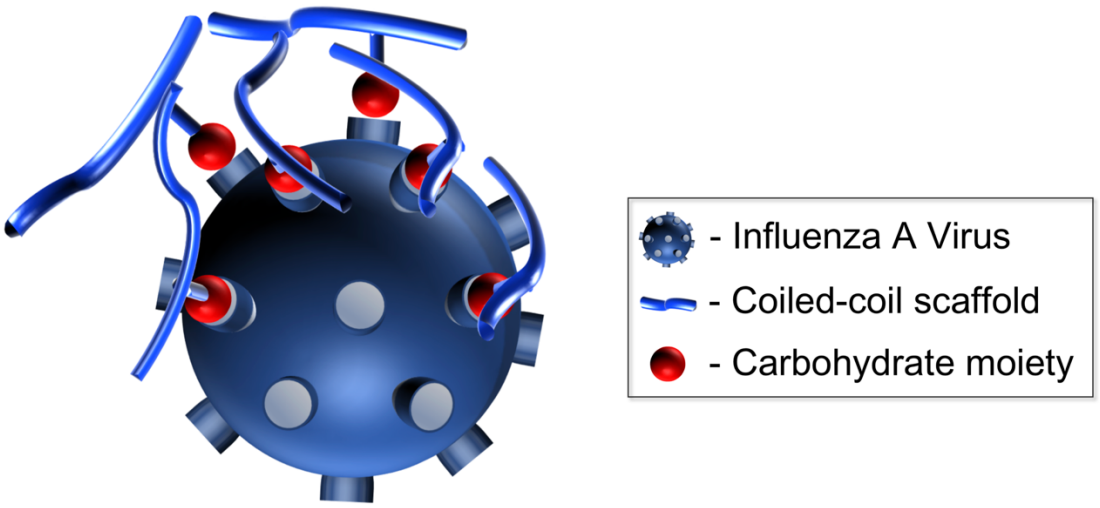

Figure 4.2. Schematic representation of a sialic acid moiety conjugated to a coiled-coil peptide occupying hemagglutinin-receptors on the surface of Influenza A Virus.

5 Result and Discussion

To successfully mimic an ECM with the aim to direct the fate of stem cells, the designed coiled-coil peptide materials need to fulfill the following features consulting the hypothesis of R. Schofield.[27]

- Ability to modulate the scaffolds to consider complexity of native ECMs.
- Defined (and multivalent) presentation of biologically relevant ligands on the surface of the peptide fibers.
- Suitable mechanical properties.

Within this thesis, various coiled-coil peptides were synthesized to accomplish the mentioned requirements. Therefore, the first aim was to design and develop a library of undecorated peptide structures for a final defined decoration with relevant ligands.

5.1 Design and development of suitable undecorated coiled-coil peptides as scaffold mimic

FF03 is a fiber-forming (FF) coiled-coil peptide, which was previously studied as a stable scaffold for the multivalent presentation of antigens.[15] In order to design a coiled-coil peptide, which is suitable as a scaffold for biomedical applications, a series of undecorated peptides was synthesized based on the sequence of FF03. Therefore, positions b, c and f of the parent peptide were systematically substituted by the hydrophobic amino acid alanine to shield the solvent-exposed domain of the peptide fiber and to promote hydrophobic interactions between the coiled-coil fibrils, a concept that was previously reported for the generation of hydrogel-forming peptides.[76] The newly designed hydrogel fiber forming (hFF) hFF03 peptide series is summarized in Table 5.1. hFF03-peptides are following the rules of the coiled-coil folding motif consisting of repeating heptad units.[110] hFF03 consists of three heptad-repeats and an additional hydrophobic core at the C-terminus.[15] At the N-terminus half a heptad creates “sticky ends” to trigger fiber-assembly.[15,110,111] The hydrophobic core of the scaffold consists of the amino acid leucine. The interaction of complementary charged amino acids lysine in position e and glutamic acid in position g are stabilizing the coiled-coil structure. Furthermore, the members of the hFF03 series are differing by the number of alanine residues presented in the solvent exposed domain, which differs from the FF03 sequence.[15] In case of hFF03-*b*A*c*A*f*A, b, c and f positions are occupied with alanine residues, whereas for the peptides hFF03-*b*A*c*A only positions b and c carry alanines and hFF03-*f*A presents alanines only in the f position. Solvent-exposed positions f of the coiled-coil scaffold hFF03-*b*A*c*A are substituted with

lysines, b and c positions of the scaffold hFF03-*f*A are occupied with lysines and glutamic acids. A schematic representation of the helical-wheel projections of the newly designed coiled-coil peptides is shown in Figure 5.1. To compare the behavior of the newly designed peptide series, the peptide FF03 was resynthesized according to the literature.[15]

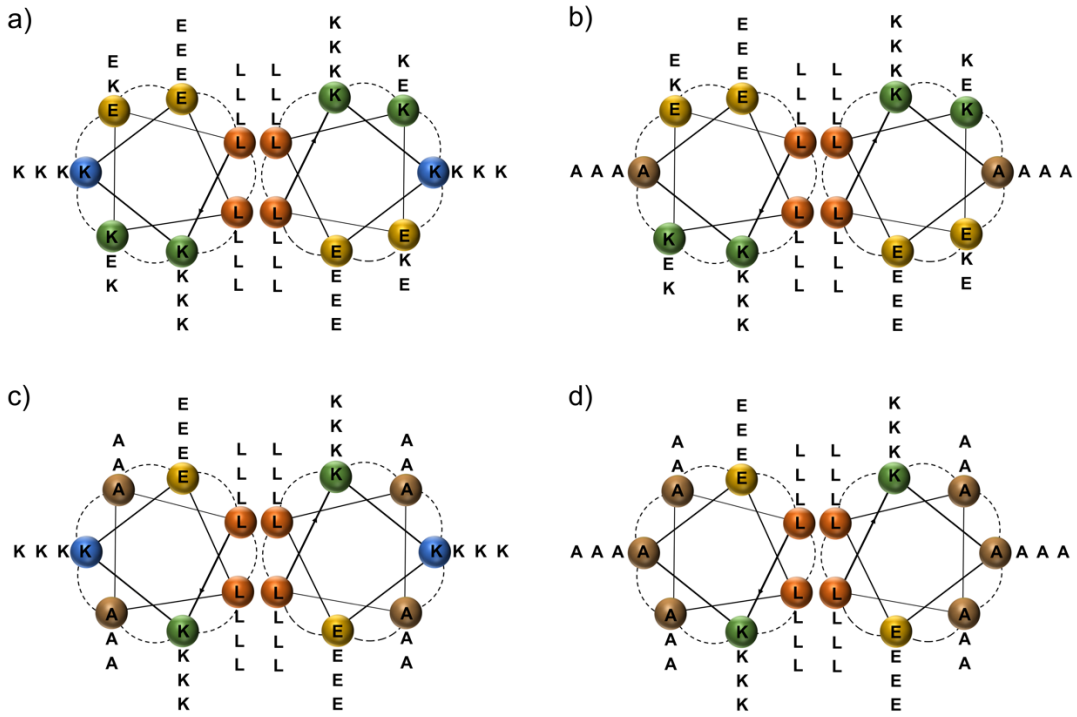

Figure 5.1. Helical-wheel projections of FF03[15] (a), hFF03-*f*A (b), hFF03-*b*A*c*A (c) and hFF03-*b*A*c*A*f*A (d), shown as dimers.

Table 5.1: Sequences of hFF03-peptides in comparison to original FF03-sequence.

	1	2	3	4	5	6	7	8	9	10	11	12	13	14	15	16	17	18	19	20	21	22	23	24	25	26
	d	e	f	g	a	b	c	d	e	f	g	a	b	c	d	e	f	g	a	b	c	d	e	f	g	a
FF03[15]	Abz	L	K	**K**	E	L	**K**	L	K	**K**	E	L	**E**	**K**	L	K	**K**	E	L	**K**	**E**	L	K	**K**	E	L
hFF03-*f*A	Abz	L	K	**K**	E	L	**A**	**A**	L	**K**	E	L	**A**	**A**	L	K	**K**	E	L	**A**	**A**	L	K	**K**	E	L
hFF03-*b*AcA	Abz	L	K	**A**	E	L	**K**	**E**	L	**A**	E	L	**E**	**K**	L	K	**A**	E	L	**K**	**E**	L	K	**A**	E	L
hFF03-*b*AcA*f*A	Abz	L	K	**A**	E	L	**A**	**A**	L	**A**	E	L	**A**	**A**	L	K	**A**	E	L	**A**	**A**	L	K	**A**	E	L
E-hFF03-*b*AcA	Abz	L	**E**	K	**E**	L	A	A	L	**E**	K	**E**	L	A	A	L	**E**	K	**E**	L	A	A	L	**E**	**E**	L
K-hFF03-*b*AcA	Abz	L	**K**	K	**K**	L	A	A	L	**K**	K	**K**	L	A	A	L	**K**	K	**K**	L	A	A	L	**K**	**K**	L

With this library in hand, structural behavior of the synthesized peptides was studied by CD spectroscopy in Dulbecco's phosphate buffered saline (D-PBS) at pH 7.4 at 20°C to verify the influence of the substitutions on the secondary structure of the peptides. The substitution of alanines in the solvent exposed domain of each hFF03-variant has no influence on the α-helical conformation of the peptides shown in Figure 5.2. Exemplary, the peptide sequences of hFF03-*b*A*c*A, hFF03-*f*A and hFF03-*b*A*c*A*f*A are highlighted.

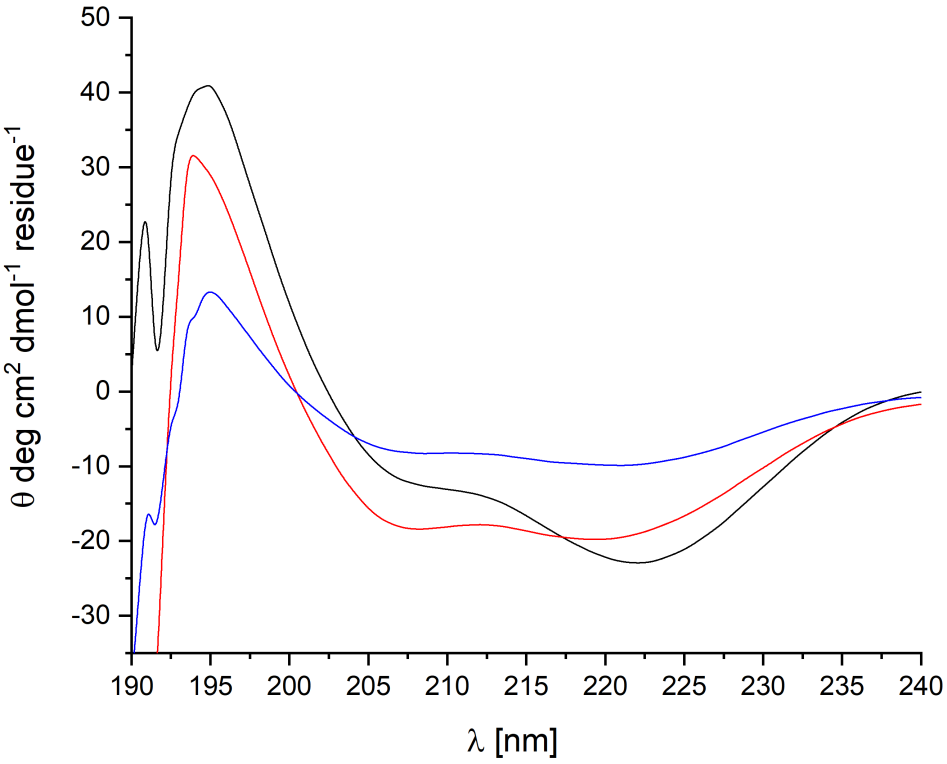

Figure 5.2. CD-spectra of hFF03-*f*A (black line), hFF03-*b*A*c*A (red line) and hFF03-*b*A*c*A*f*A (blue line) at pH 7.4 (D-PBS) at 20°C, peptide concentration 50 µM.

As next step, their ability of building self-supporting hydrogels was tested by a simple approach to get an impression about this property. All peptides were dissolved in D-PBS with a final concentration of 1000 µM, which corresponds to an average peptide content of approximately 0.3 wt% and transferred into a glass vial with a flat bottom (Figure 5.3). To test the gelation process, the glass vial was inverted after 30 min. If no liquid funnels down the vial after additional 30 min, it can be concluded that the peptide has the ability to form a hydrogel. The results showed that only peptide hFF03-*b*A*c*A has the ability to

form a hydrogel. With this rough impression in hand, further experiments were performed to characterize the mechanical and structural properties of all peptides.

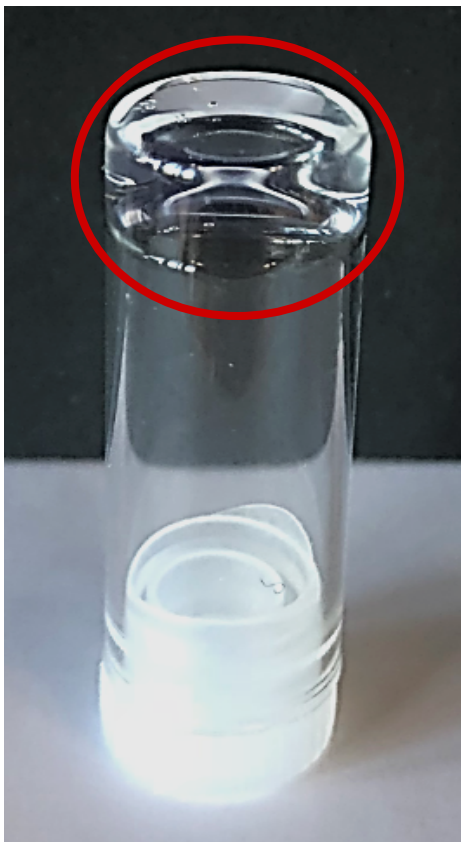

Figure 5.3. Inverted sample vial with the self-supporting coiled-coil hFF03-*b*A*c*A hydrogel at a concentration of 1000 µM in D-PBS (pH 7.4).

If the sequence is divided into an E-containing part all e and g positions of the coiled-coil sequence and a K-containing part at all charged positions e and g of the coiled-coil sequence (see Table 5.1 and Figure 5.4), the coiled-coil should only be built by mixing both monomeric sequences equally.[76,112]

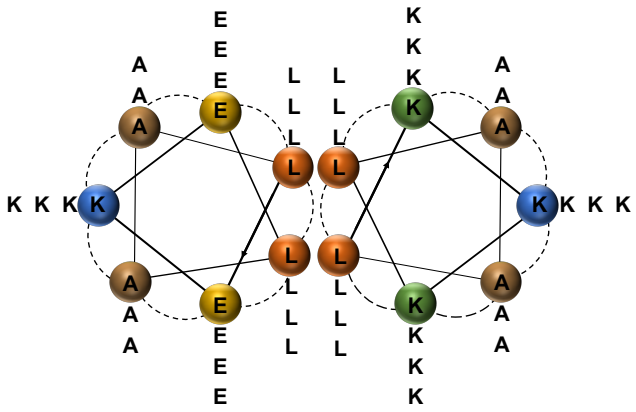

Figure 5.4. Helical-wheel projection of mixed E-hFF03-*b*A*c*A (left) and K-hFF03-*b*A*c*A (right).

Having a heteromeric coiled-coil system, which starts to gel only by mixing both monomer-sequences could enhance the handling properties of this system. The structural behavior of the monomers as well as the E-/K-mixtures were tested by CD-spectroscopy at 1000 µM each, as the parent peptide sequence was found to gel at this concentration.

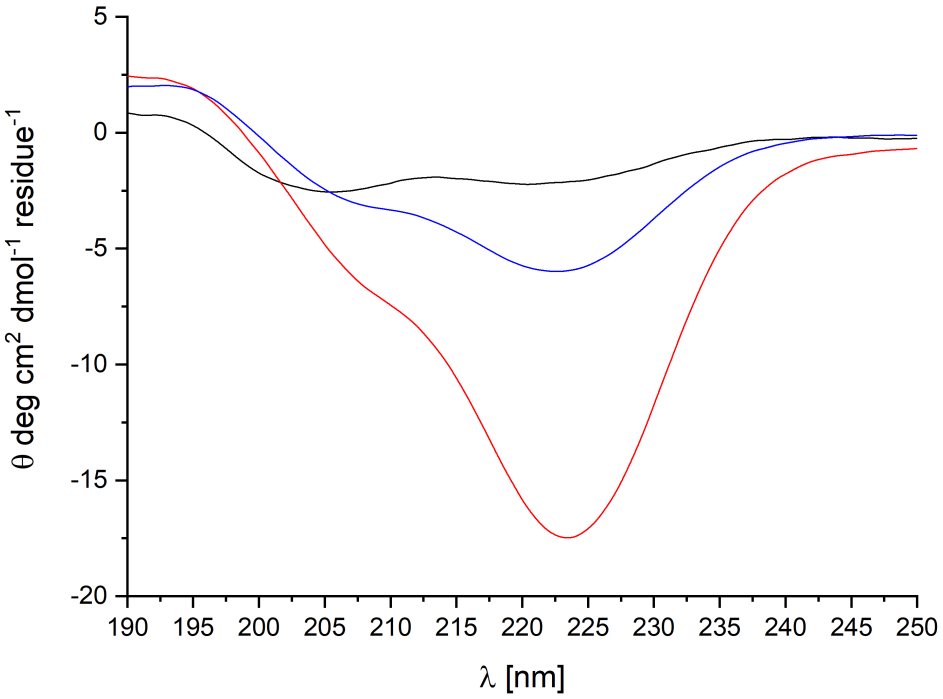

Figure 5.5. CD-profiles of E-hFF03-*b*A*c*A (black-line, 1000 µM) and K-hFF03-*b*A*c*A (red line, 1000 µM) in D-PBS at pH 7.4. Mixing both peptide sequences into an E-/K-hFF03-*b*A*c*A (blue line) coiled-coil gave also typical α-helical CD-profile. Measurements were performed directly after sample preparation.

However, CD spectroscopy confirmed that each monomeric sequence build α-helical structures (see Figure 5.5). Mixing the peptide sequences led to α-helical CD-profiles but no gel formation was confirmed for the sample, even after 24. This observation confirms the gel-properties of hFF03-*b*A*c*A is an exclusive property for this peptide sequence. The results underline that tuning the amino-acid sequences will not automatically lead to gelating properties through hydrophobic shielding of solvent exposed positions. In future, more coiled-coil systems should be tested to confirm this hypothesis. To put it in a nutshell, of all designed peptide sequences only hFF03-*b*A*c*A showed the desired properties. Based on these findings, hFF03-*b*A*c*A[2] was further decorated with peptide fragments and carbohydrate units. They can act as ligands for specific bindings to stem cells or virus particles. The different attempts are described in the following chapters.

[2] In the following chapters hFF03-*b*A*c*A will be named as hFF03.

5.2 Coiled-coil peptide hydrogels as 3D ECM mimics

The development of tailorable and biocompatible 3D hydrogels to influence cell behavior *in vitro* is of high interest for a variety of cell-based applications in the field of tissue engineering or regenerative medicine.[43,78] As the environment of native cells is continuously changing and of high complexity, a tunable peptide based 3D material is needed. This peptide hydrogel present different multifunctional properties simultaneously imitating an ECM ideally for different stages of cellular development. The cellular behavior can be influenced by structural and functional features, as well as stiffness of their embedded environment, e.g. recognition and release signals. In this thesis hFF03 is designed and synthesized in accordance with the needed parameters for a synthetic ECM. As described, hFF03 combines the possibility to act as hydrogelator and to present ligands at the same time. It was therefore chosen as a tunable cell-environment to consider the requirements of cells in different stages of their development.[78]

Cellular behavior will be controlled by the provided environment. Parameters like the stiffness of the scaffold and presented chemical cues for e.g. recognition sequences or carbohydrate moieties of GAGs are important. Native ECMs are of high complexity and need therefore ligands for cell stimulation.[78] Only a few examples are so far described in literature. One example is the α-helical coiled coil hSAF system, which is post-synthetically functionalized with a RGDS-sequence by click-chemistry after gel formation.[77,78] The approach leads to controlled functionalization of hydrogels at defined positions. A drawback is that the click-reaction is not quantitative, as some of the azide-bearing peptide fibers are shielded through the self-assembly during fiber and gel formation.[78] If the monomeric peptide sequences are decorated during synthesis, the presentation of the ligands and the resulting scaffold is more defined and quantifiable, which would compensate this disadvantage. Therefore, the influence of the ligands has to be studied regarding their ability to affect the self-assembly and hydrogel formation of the functionalized peptides. Such a functionalized coiled-coil peptide hydrogel enables to build up a fully synthetic, reproduceable, quantifiable and tunable substrate for cell stimulation. A schematic illustration, how hydrogels were prepared and how the gel formation proceeds by including different ligand presenting coiled-coil peptides is shown in Figure 5.6.

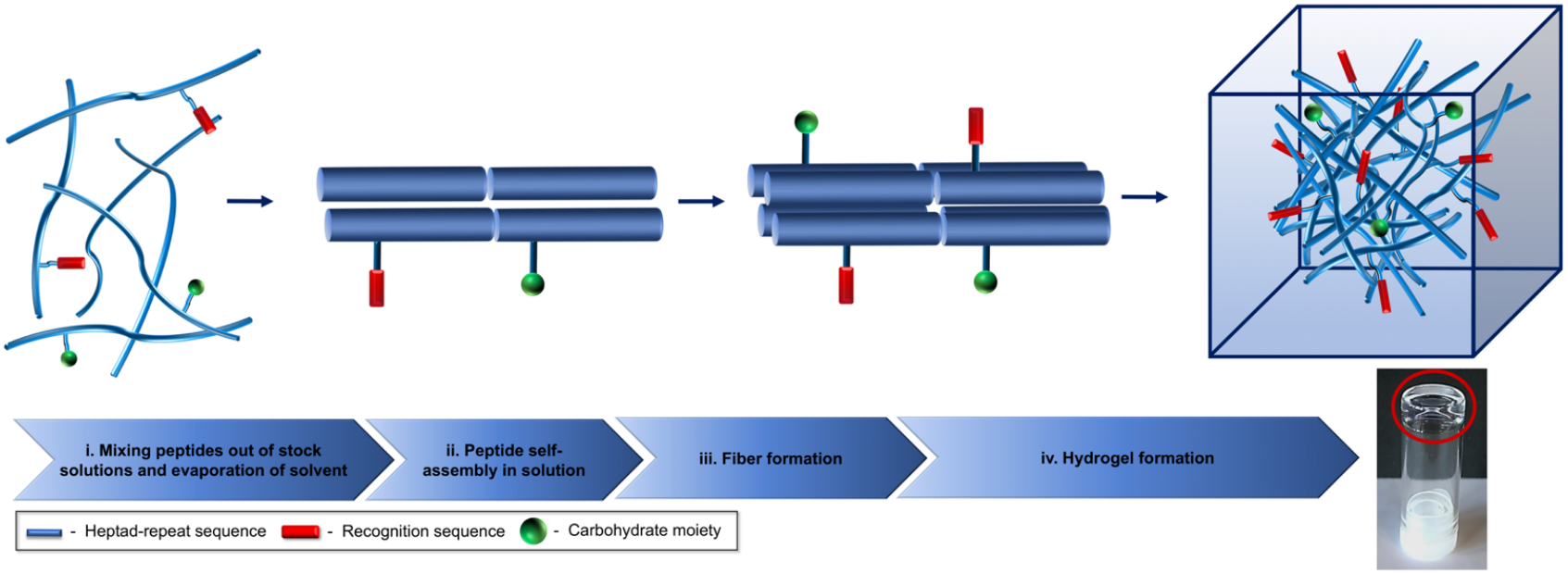

Figure 5.6. Schematic representation of hydrogel preparation and formation by mixing different ligand bearing coiled-coil peptides to build functionalized hydrogel. Coiled-coil peptides were combined out of stock solutions in Hexafluoroisopropanol and solvent was evaporated by a gentle stream of N_2. Self-assembly of the peptide fibers starts by dissolving the peptide mixture in cell culture medium or buffer solution. Fiber formation takes place as a consequence of self-assembly resulting in hydrogel formation. Hydrogel formation is tested by inverting the sample vial after sample preparation (peptide hydrogel prepared in D-PBS).

5.2.1 Design and synthesis of a decorated hFF03-library

The synthesis of hFF03 and its derivates was performed by SPPS starting from C-terminal end to the N-terminal end. After full-length synthesis of the sequence, the N-terminus was blocked with Boc-*o*-aminobenzoic acid (Abz). Position 17, the amino acid lysine, was previously evaluated as suitable for the coupling of different peptide ligands[15] and therefore protected with a methyltrityl group (Mtt), which can be removed easily under mild acidic conditions.[113] This selective deprotection allows a peptide synthesis starting from the free amino-group of the lysine side-chain by SPPS and the build-up of different peptide fragments or the connection of carbohydrate units.[15] This approach is called all-on-solid-phase (AOSP) synthesis. The following scheme is showing the synthetical strategy of hFF03 and its peptide functionalized derivates Figure 5.7.

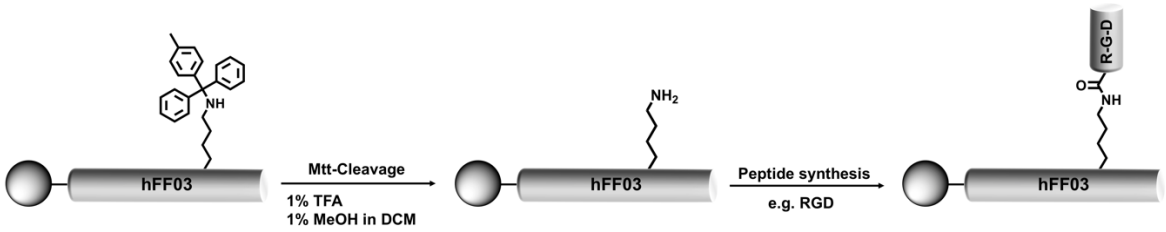

Figure 5.7. Synthesis scheme of peptide functionalized hFF03 derivatives by AOSP-approach. Synthesis starts by cleavage of Mtt-group protecting from the lysine side-chain (K17 of hFF03) followed by orthogonal.

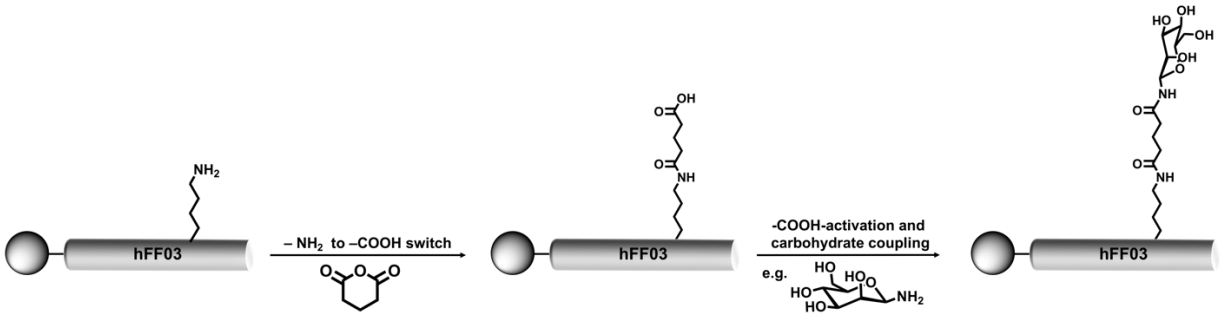

Figure 5.8. Scheme of carbohydrate coupling starting from the free-amino group presented by lysine in position 17 of hFF03 by AOSP-approach.

In case of the sugar-ligand the free amino-group of the lysine was switched to a carboxylic acid functionality by means of glutaric anhydride.[15] This free carboxy-function was activated on resin to couple the amino-functionalized sugar, respectively. In the following

scheme the coupling of monosaccharide is described Figure 5.8. The synthetic strategy enables to create a library of different functionalized coiled-coil peptides with the aim to build different 3D scaffolds for the use as artificial ECMs. Therefore, hFF03 was conjugated with the tripeptide RGD and the neuropeptide substance P (SP). SP is an epitope of the neuronal apoptosis inhibitory protein family (NAIP) and the heparin-binding domain of Vitronectin (VT). Furthermore, an another RGD-functionalized hFF03-variant was designed, namely hFF03-RGD, were the amino acids Arg, Gly and Asp were substituted into positions 9, 10 and 11 of the coiled-coil hFF03 sequence. Due to this approach the tripeptide RGD is presented on one twist of the solvent exposed domain of the coiled-coil peptide. As adhesion proteins in native ECMs present the tripeptide within their sequence, this design approach was pursued to include the sequence according to the rules of coiled-coil design. Positions 9, 10 and 11 were chosen to not interrupt the folding behavior by occupying the hydrophobic core, which is necessary for coiled-coil formation. The peptide hFF03-RGD is used as a control to check the possibility of tuning the sequence by including the recognition motif without presenting it on the surface of the peptide fiber. Finally, hFF03 was conjugated to two more monosaccharides, galactose and mannose. All synthesized hFF03 variants as well as the sequences of the attached ligands are summarized in Table 5.2.

Table 5.2. Sequence of coiled-coil peptide hFF03-RGD and peptidic and carbohydrate ligands attached to lysine in position 17 of the peptide hFF03 as scaffold.

	1	2	3	4	5	6	7	8	9	10	11	12	13	14	15	16	17	18	19	20	21	22	23	24	25	26
	d	e	f	g	a	b	c	d	e	f	g	a	b	c	d	e	f	g	a	b	c	d	e	f	g	a
hFF03-RGD	**Abz**	L	K	K	E	L	K	E	L	**R**	**G**	**D**	L	E	K	L	K	K	E	L	K	E	L	K	K	E	L
	Peptidic ligands presenting coiled-coil peptides																									
hFF03-RGD	RGD-Sequence attached to lysine side-chain in position 17																									
hFF03-K17-NAIP	SKPPGTSS – sequence attached to lysine side-chain in position 17																									
hFF03-K17-SP	RPLPNNFFGLM - sequence attached to lysine side-chain in position 17																									
hFF03-K17-VT	GKKQRFRHRNRKG - sequence attached to lysine side-chain in position 17																									
	Carbohydrate ligands presenting coiled-coil peptides																									
hFF03-K17-Gal	Galactose moiety attached to lysine in position 17																									
hFF03-K17-Man	Mannose moiety attached to lysine side-chain in position 17																									

5.2.2 Drafting extracellular matrix mimics by bottom-up approach

A strategy to combine the hydrogelating properties of the scaffold with the complexity of native ECMs was developed. In order to design a variety of different ECMs, different ligand presenting fibers were mixed with undecorated peptide hydrogel in different rates to achieve hetero functionalized coiled-coil assemblies. To incorporate a fibrous network and different chemical inducers represented by conjugated ligands presented in position 17, the recognition sequence RGD (hFF03-K17-RGD) and a Mannose moiety (hFF03-K17-Man) was conjugated to hFF03. A hetero-assembled network was achieved by mixing the undecorated coiled-coil scaffold with different amounts of the ligand presenting coiled-coil peptides. As the presenting peptide fibers are following the same heptad repeat sequence as the hydrogelator the artificial ECM consists only of the similar peptide fibers and their presented ligands in the arranged ratio. The ligands are then statistically distributed within the 3D structure of the hydrogel. Peptide hydrogels were tested with 0.15 wt%, 0.30 wt% and 0.50 wt% peptide content. Native ECMs have more than 99% water content. To take into account that native ECMs present various chemical features and as a proof-of-concept, the ligand bearing coiled-coil peptides hFF03-K17-RGD and hFF03-K17-Man were tested and characterized in the same concentration as mentioned above. Both peptides past an initial inversion test at concentrations of 1000 µM, which demonstrated that covalently attached RGD-sequences, as well as the attached monosugar are not disturbing the hydrogelating behavior of the coiled-coil peptide.

Therefore, all these peptides were chosen to systematically study the influence of the rate of conjugated ligands. Mixtures of the parent peptide hFF03 with 5% RGD-bearing hFF03 and a mixture with 1% mannose-bearing hFF03 as well as the combination with both ligand bearing species were tested, respectively. Table 5.3 summarizes all eighteen tested homo - and hetero - assembled coiled-coil mixtures. These eighteen peptide mixtures were studied as a model system to characterize their structural and mechanical features as well as their morphology and *in vitro* toxicity of biological systems.

Consequently, and for the first time, fully-functionalized peptide hydrogels are presented, and especially the first carbohydrate-functionalized coiled-coil based hydrogel. This approach provides a platform, which enables to address the complexity of native ECMs by the presentation of chemical cues quantitively within the 3D structure of the scaffold.

Table 5.3. Overview about designed coiled-coil peptide hydrogel-based model ECM mimics as a proof-of-concept approach to study materials properties and cell viabilities with regard to peptide content, presented ligand type and ligand density. Composition of hydrogel mixtures are in % with regard to concentration of hFF03. WT - wild type; CH - carbohydrate; RS - recognition sequence.

Short name	*Composition*	*Peptide content [w%/v]*
WT	hFF03	0.15
		0.30
		0.50
WT-CH	hFF03-K17-Man	0.15
		0.30
		0.50
WT-RS	hFF03-K17-RGD	0.15
		0.30
		0.50
WT + 1% WT-CH	hFF03 + 1% hFF03-K17-Man	0.15
		0.30
		0.50
WT + 5% WT-RS	hFF03 + 5% hFF03-K17-RGD	0.15
		0.30
		0.50
WT + 1% WT-CH + 5% WT-RS	hFF03 + 1% hFF03-K17-Man + 5% hFF03-K17-RGD	0.15
		0.30
		0.50

5.2.2.1 Structural characterization of the newly generated hydrogels

5.2.2.1.1 Secondary structure of functionalized coiled-coil peptides and their compositions

All synthesized peptides were characterized regarding their secondary structure by CD-spectroscopy. CD-spectroscopy of all peptides and mixtures was performed in D-PBS (pH 7.4) at 20 °C and 37 °C over a period of six days. Figure 5.9 exemplarily shows CD profiles of all tested pure peptides and mixtures at appropriate concentrations for 0.5 wt% peptides at 20 °C for proof-of-concept as ECM mimics (CD profiles for 0.3 wt% and 0.15 wt% coiled-coil peptides and mixtures are shown in the appendix).For all tested conditions pure peptides and peptide mixtures show typical α-helical CD-spectra with minima around 208 nm and 222 nm. The minimum at 222 nm has higher intensity compared to the minimum at 208 nm, which could be explained by fiber formation and elongation over the tested period.

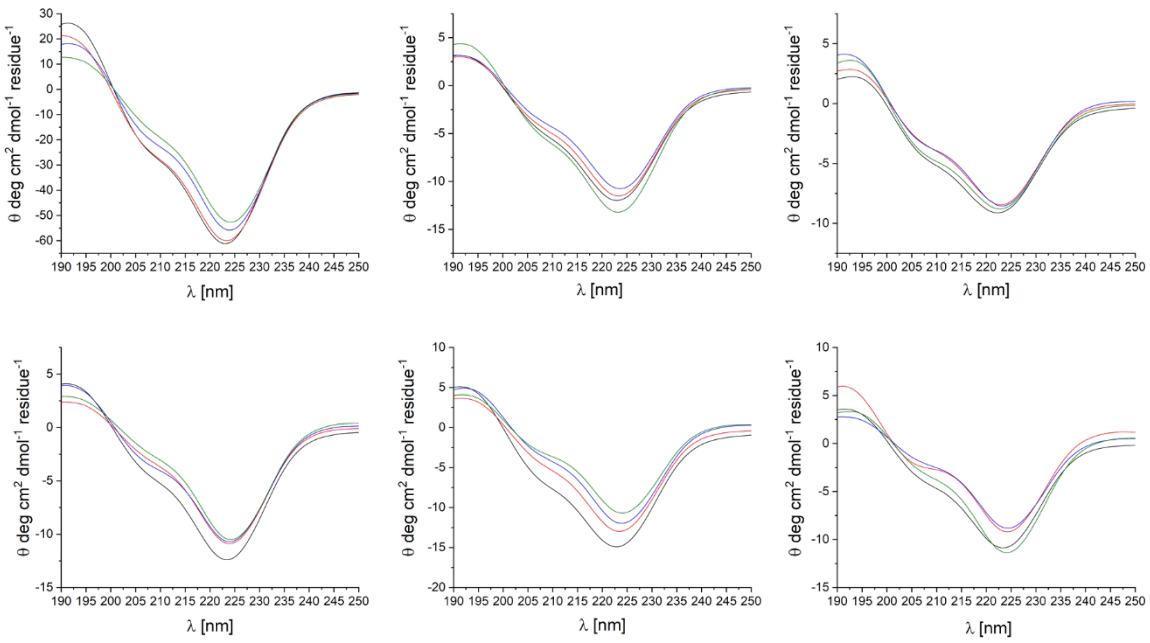

Figure 5.9. CD-spectra at 20°C over a period of six days directly after sample preparation (black line), 24h (red line), 72h (blue line) and 6 days (green line) after sample preparation to follow folding behavior of 0.50 wt% hFF03 (a), hFF03-K17-Man (b) and hFF03-K17-RGD (c). Folding behavior of peptide mixtures was followed by CD-spectroscopy as well for 0.50 wt% hFF03 samples containing 1% hFF03-K17-Man (e), 5% hFF03-K17-RGD (f) and both peptides in the same amount as for panel e) and f) (d).

As mentioned, these model ECMs (Table 5.3) were studied regarding the impact of the concentration described above for their hydrogelating properties. It was found that the attached moieties are not interfering with the self-assembly of the peptides confirmed by CD-Spectroscopy (Figure 5.9) and are not disturbing the hydrogel formation, which was confirmed by the inversion test (Figure 5.3)

5.2.2.1.2 Morphology studies of coiled-coil peptide hydrogels

As a next step, TEM and cryo-TEM measurements were performed to characterize the self-assembly and morphology of the peptides and their aggregates. As TEM measurements are not able to determine morphology of the peptides because of extraction of water during sample preparation, coiled-coil hydrogels were also characterized by cryo-TEM measurements. The TEM and Cryo-TEM measurements were performed in collaboration with *PD Dr. Christoph Böttcher*.

TEM micrograph (Figure 5.10) of hFF03, at a concentration of 1000 µM in D-PBS 24 h after sample preparation shows defined fiber bundles with a diameter of 3.5 nm. Like the parent peptide FF03, hFF03 has tendency for bundle formation, which seems to be a characteristic feature related to this coiled-coil peptide.[15,114] The study of the hFF03 series is therefore promising for the development of α-helical fibrous peptide materials with well-predictable structural properties.

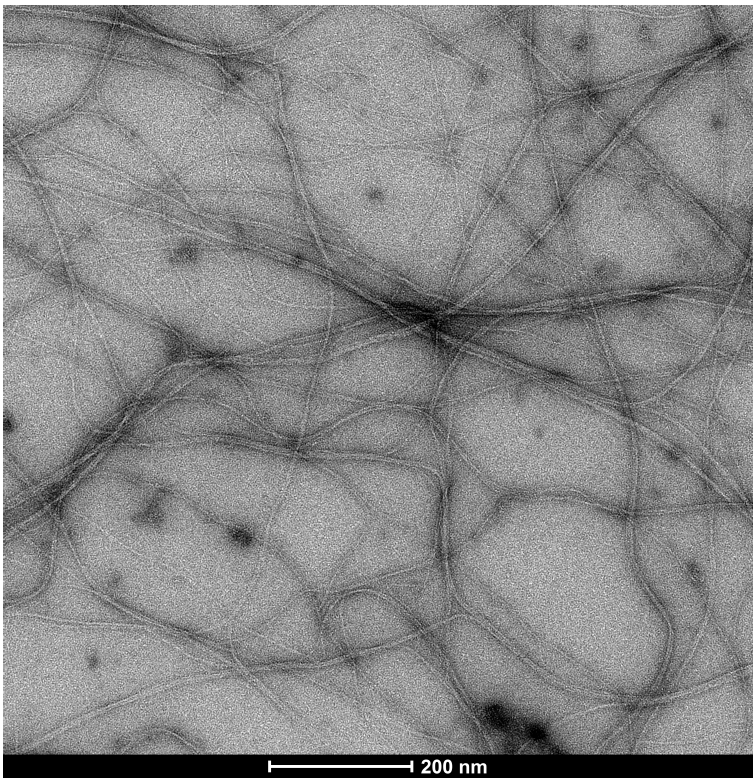

Figure 5.10. TEM micrograph of hFF03 at a concentration of 1000 µM, 24h after sample preparation. Peptide was dissolved in D-PBS at pH 7.4 and stained with a solution of 1% phosphotungstic acid (PTA).

Cryo-TEM has the advantage to measure without any supplements for contrasts and enables visualization of almost native states of the sample. Therefore, the morphology of the hydrogels was confirmed using cryo-TEM (see Figure 5.11).

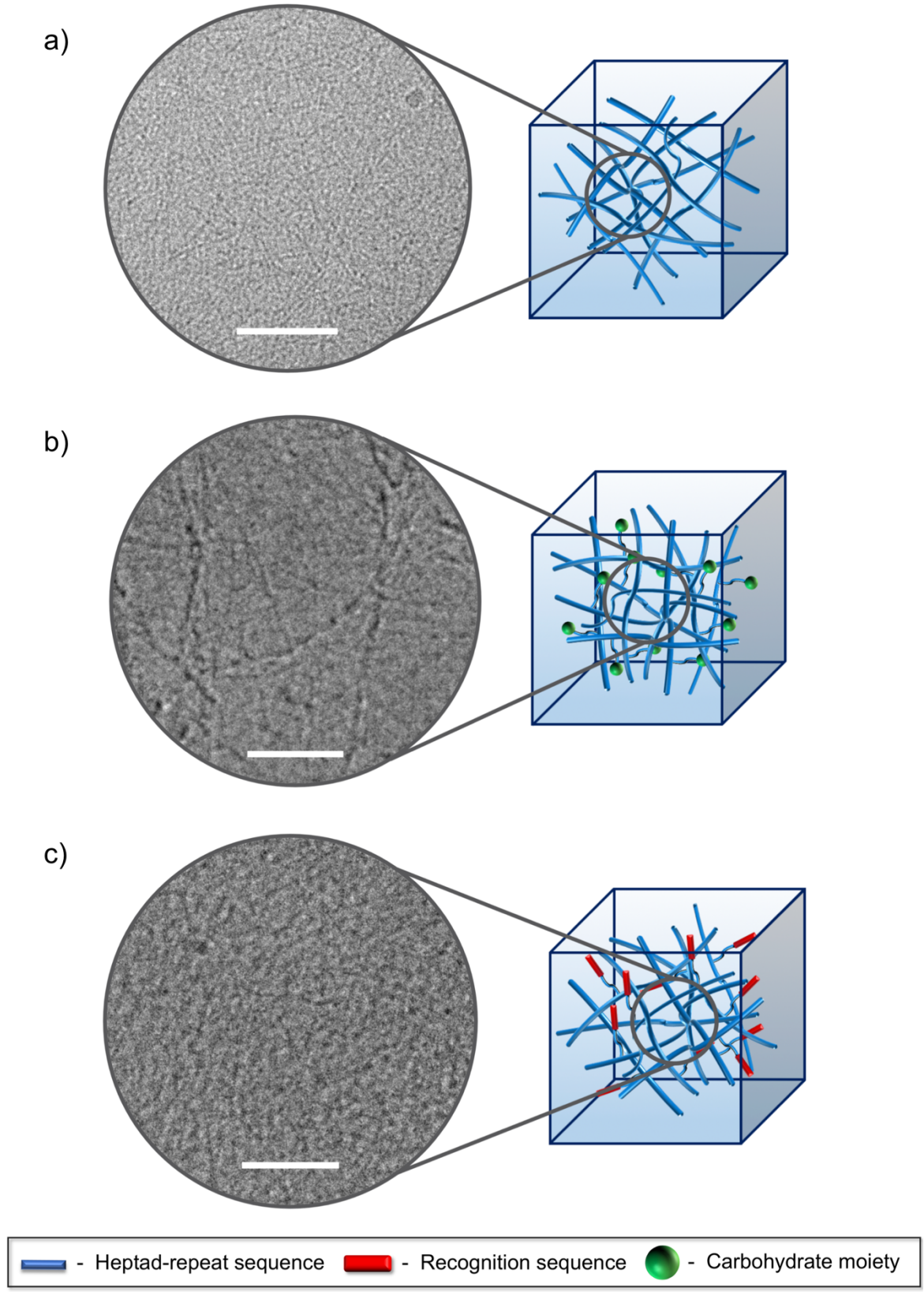

Figure 5.11. Cryo-TEM images and schematic representations of (a) 0.15 wt% undecorated hFF03 hydrogel, (b) 0.15 wt% decorated hFF03-K17-Man hydrogel and (c) 0.15 wt% hFF03-K17-RGD hydrogel. The white scale bar denotes 100 nm each.

The measurements indicate that pure 0.15 wt% hFF03 hydrogels and its mannose-decorated and its RGD-decorated analogues form a homogenous and tenuous network of peptide fiber-bundles, respectively. The fiber-bundles building the network of hFF03-hydrogel have a diameter of approximately 3 nm, whereas fibers-bundles of hFF03-K17-Man have an average diameter of 5 nm and hFF03-K17-RGD have an average diameter of 6.5 nm. Increasing fiber thickness might result of the attached ligands, as they contribute to the volume of the solvent exposed domain of the coiled-coil bundle.

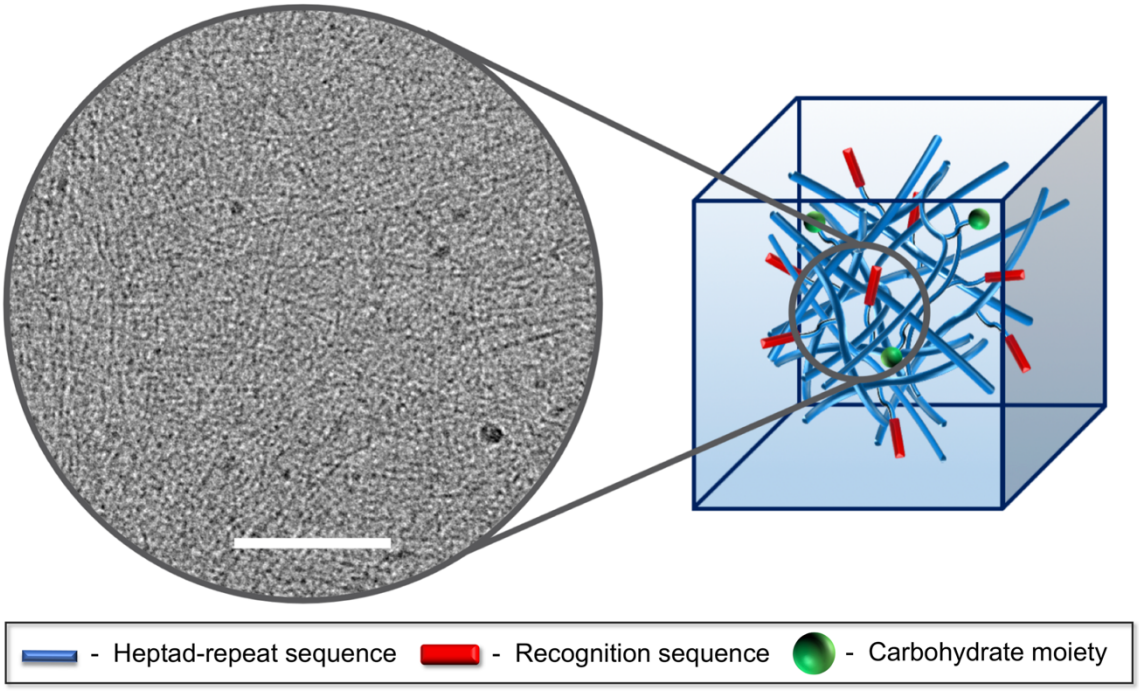

Figure 5.12. Cryo-TEM image and schematic representation of 0.15 wt% hFF03 hydrogel containing 1% hFF03-K17-Man and 5% hFF03-K17-RGD. The white scale bar denotes 100 nm.

Interestingly, 0.15 wt% hydrogel composed of hFF03 with 5% hFF03-K17-RGD and 1% hFF03-K17-Man showed an uninterrupted network of thin peptide fibers with filled vesicle-like inclusions distributed over the whole network (Figure 5.12). As cryo-TEM revealed that all three pure species have no inclusions within their network, the vesicles might result of a few hetero assembled peptide fibers occurring of the addition of 1% hFF03-K17-Man and 5% hFF03-K17-RGD.

5.2.2.1.1 Structural assessment of peptide hydrogels by SANS measurements

To get further information on the self-assembly behavior and the structure of the peptides, small angle neutron scattering (SANS) measurements were performed for all designed ECM mimics summarized in Table 5.3. SANS is a powerful technique to elucidate the structure of molecules in the range of 1 nm to more than 100 nm and can be used to study assembly, dispersion and mixing of components.[115] It is a widely used method to study hydrogen-rich biological systems due to the possibility to mark them by isotopic labeling; e.g. neutrons are sensitive to hydrogen-deuterium exchange.[115,116] By this exchange the contrast can be changed to get more detailed information about the internal microstructure of the probe.[117] The intensity measured in SANS experiments reveals information on the volume and shape of the aggregates formed in aqueous solution. It is furthermore very sensitive to changes in contrast and concentration.[115] During the SANS experiment the dissolved coiled-coil peptides are deferred to a neutron beam of a given wavelength which is scattered through the nuclei of the particles inside the sample. The intensity I(q) is recorded by a detector placed at a certain distance from the sample.[116] Figure 5.13 shows a scheme of the experimental setup.

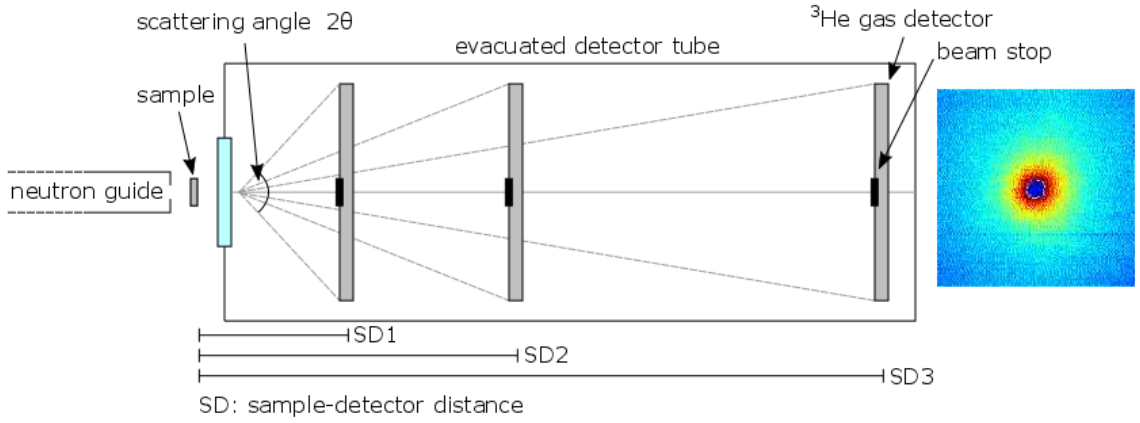

Figure 5.13. Schematic setup of a small angle scattering experiment. The sample is placed at different distances from the detector to determine the maximum value of scattering angle. The figure was kindly provided by M.Sc. Benjamin von Lospichl, Group of Prof. Michael Gradzielski, Technische Universität Berlin.

Normally, the scattering intensity I(q) is expressed as a function of the magnitude of the scattering vector q. The wavelength λ and the scattering angle θ of incident radiation contribute to q resulting as inverse length in nm^{-1} as unit.[115] Two types of scattering

contribute to I(q): coherent and incoherent elastic scattering. Coherent scattering is q-dependent and gives useful structural information on the scattered particles, whereas incoherent scattering is generated by background noise.[115,118] The contribution of the particle shape and size to the scattered intensity is expressed through a form factor P(q).[115,119] Generally, small particle features cause a low scattering at large q-values, whereas larger structures yield a higher intensity at low q-values.[115,120]

SANS measurements were performed and analyzed in accordance with the results shown by TEM and cryo-TEM measurements. Samples for SANS measurements were prepared in a deuterated buffer system according to concentration and composition of coiled-coil peptides summarized in Table 5.3. Thus, D-PBS containing salts were dissolved in deuterium oxide and used as the deuterated buffer. All SANS measurements were performed in cooperation with the Group of Prof. Dr. Michael Gradzielski, Technische Universität Berlin by *M.Sc. Benjamin von Lospichl*. The following scattering patterns of pure peptide hydrogels as a function of the concentration are shown in Figure 5.14.

All tested peptide hydrogels show a distinct trend, that is with increasing concentration the intensities are also increasing for the major part of the investigated q-range, which can be taken as an indication for larger structures to be formed. There is no difference between WT and decorated WT-hydrogels (Figure 5.14). Figure 5.15 shows results of SANS measurements of hydrogel compositions. Before the data are analyzed in more detailed with an appropriate model, a model-independent analysis is performed. Therefore, the (modified) Guinier law (Equation 1) is used to describe the data in the intermediate q range, while the Porod law (Equation 2) is taken for the description of the data in the high q regime. The obtained results are summarized in Table 5.4.

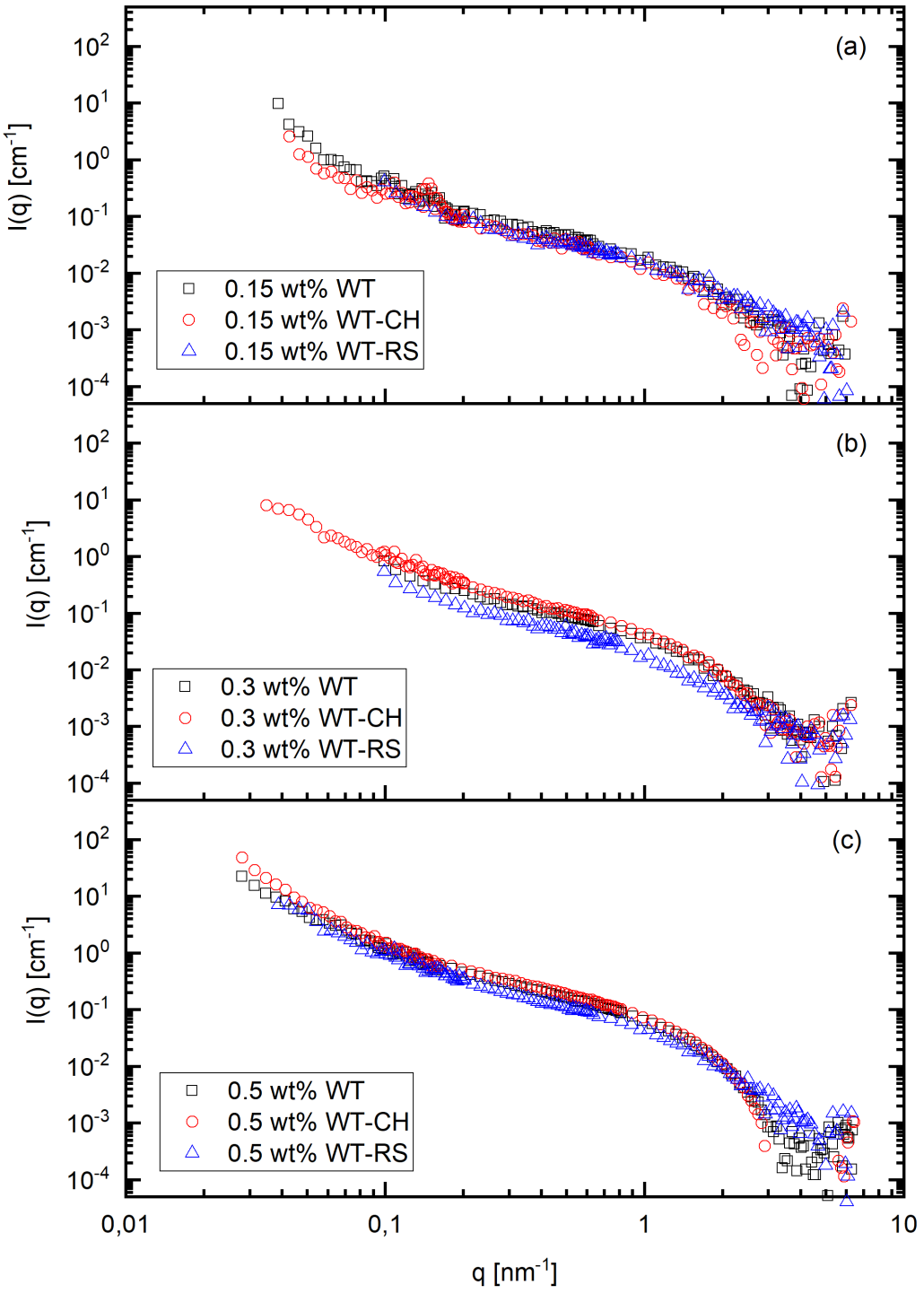

Figure 5.14. Scattering patterns of pure peptide hydrogels at concentrations of (a) 0.15 wt% (b) 0.30 wt% and (c) 0.50 wt%. Patterns are denoted by black squares for pure WT hydrogel, red circles for pure WT-CH hydrogel and blue triangles for pure WT-RS hydrogel.

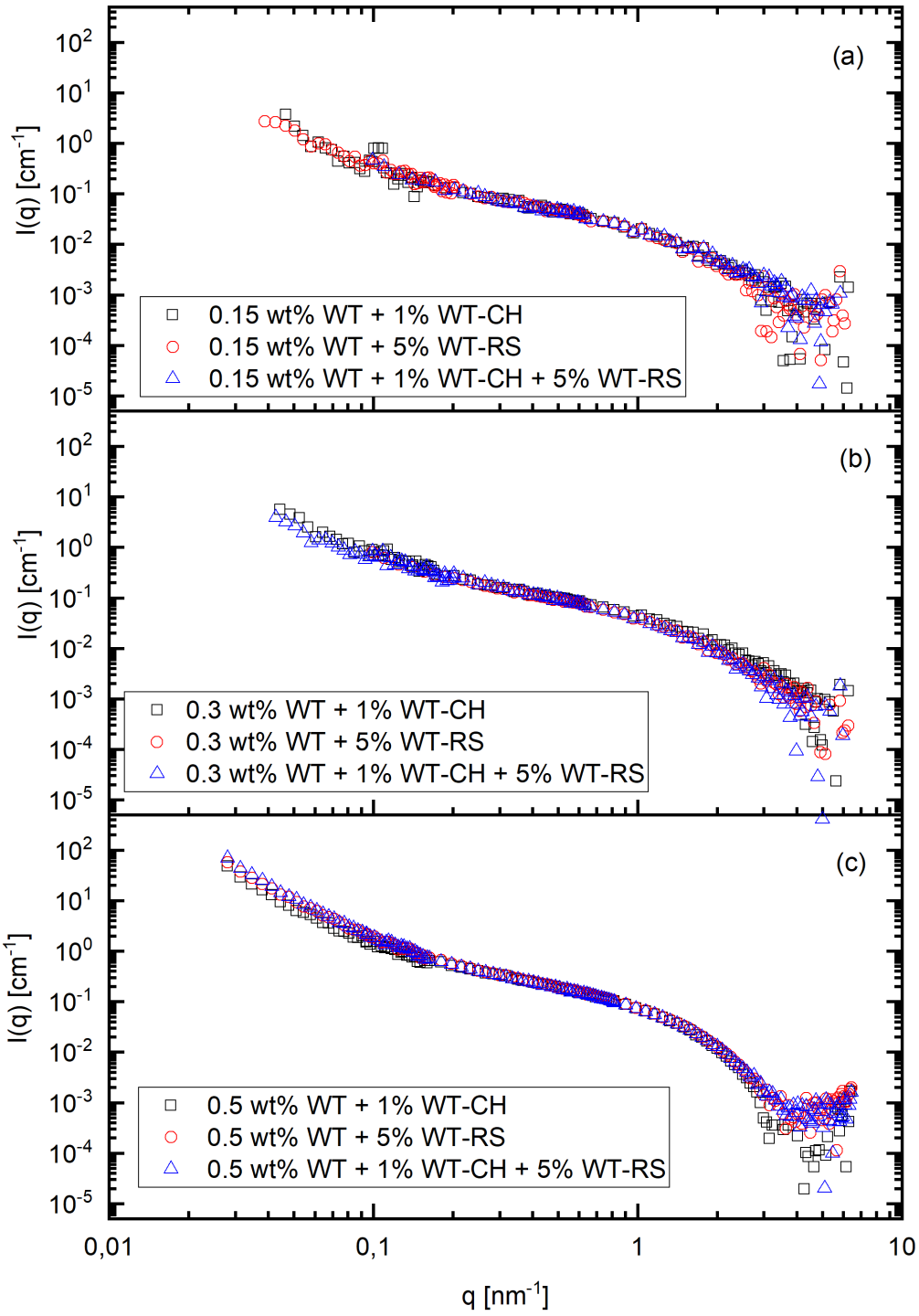

Figure 5.15. Scattering patterns of hydrogel mixtures (a) 0.15 wt% peptide hydrogels (b) 0.30 wt% peptide hydrogels and (c) 0.50 wt% peptide hydrogels. Patterns are denoted by black squares for hydrogel composition WT + 1% WT-CH, red circles for hydrogel composition WT + WT-RS and blue triangle for hydrogel composition WT + 1% WT-CH + 5% WT-RS.

To understand the way the data have been analyzed, the following paragraph shows a short theoretic introduction to the two important equations.

The scattering patterns reveal a q^{-1} behavior in the intermediate q-range which is typical for systems consisting of elongated rod-like structures. The slope changes for low q values to q^{-2}. By taking into account that the hydrogels exist of elongated structures, a modified Guinier analysis (Equation 1) can be used to fit the collected data in the intermediate q range.

Equation 1. Modified Guinier law for intermediate q range

$$I(q) = \frac{A}{q} \cdot \exp\left(-\frac{q^2 R_{g,m}^2}{2}\right) \text{ with } R_{g,m}^2 = \frac{R_{cs}^2}{2}.$$

Equation 2. Porod law describing scattering data in the high q regime

$$I(q) = \frac{C_1}{q^n} + C_0 \ .$$

The factor A (Equation 1) describes the forward scattering intensity per unit length and R_{cs} is the cross-sectional radius. In the high q regime scattering data are approximated by the Porod law (Equation 2), where the (incoherent) background is denoted by C_0, the Porod constant by C_1, and the Porod exponent by *n,* which is defined as *6 – D*. The exponent n contains thereby information on the dimensionality of the scattering objects:

- For a value of *n = 4* a smooth particle surface can be assumed
- For a value of n = 3 - 4 a rough surface of the particle is assumed.

The studied coiled-coil based peptide hydrogel system can be approximated as a polymeric system. In this case a value of *n = 2* dedicates a Gaussian chain in a dilute system, whereas a value of *n = 3* give evidence to collapsed polymer coils. Networks or branched systems can be assumed for slopes between 2 and 3, where the studied system can be supposed to be mass fractal.[121]

As mentioned before, by applying Equation 1 - Equation 2 to the data sets shown in Figure 5.14 and Figure 5.15 the relevant parameters can be extracted and are listed in Table 5.4. The results for the Porod slopes of almost all samples let us assume a mass fractal hydrogel system. Except 0.30 wt% and 0.50 wt% WT-CH hydrogel have Porod

slopes greater than 3 clearly indicating that scattered particles have a fractal surface. The cross-sectional radii obtained from the fitting of the intermediate range of q with Equation 2 display values around 1 nm which agrees with the results of TEM and cryo-TEM measurements.

Table 5.4. Results of the Porod slope n, the cross-sectional radius R_{cs}, persistence length l_p and model-depended radius R by applying to the scattering data present in Figure 5.14 and Figure 5.15.

name	**c (wt%)**	**n**	**R_{cs} [nm]**	**l_p [nm]**	**R [nm]**
hFF03	0.15	2.60(9)	1.00(8)	9.20(3)	0.95(9)
	0.30	2.53(3)	1.03(9)	13.54(3)	0.98(7)
	0.50	2.78(7)	1.29(9)	9.81(1)	1.13(6)
hFF03-K17-Man	0.15	2.56(9)	1.05(0)	8.42(0)	1.00(6)
	0.30	3.47(9)	1.18(2)	8.94(1)	1.08(9)
	0.50	3.16(1)	1.24(2)	7.49(2)	1.18(1)
hFF03-K17-RGD	0.15	1.41(1)	0.74(0)	10.40(9)	0.72(0)
	0.30	1.99(1)	1.29(8)	9.96(0)	1.08(5)
	0.50	2.46(9)	1.11(2)	8.95(0)	1.01(6)
hFF03 + 1% hFF03-K17-Man	0.15	1.71(1)	0.93(8)	10.44(4)	0.86(1)
	0.30	1.96(6)	0.77(5)	12.68(2)	0.79(2)
	0.50	3.35(0)	1.15(9)	9.09(8)	1.14(2)
hFF03 + 5% hFF03-K17-RGD	0.15	2.51(2)	1.02(6)	9.80(1)	0.97(6)
	0.30	2.38(1)	0.99(3)	14.14(7)	0.95(6)
	0.50	3.45(8)	1.16(0)	6.96(4)	1.14(1)
hFF03 + 1% hFF03-K17-Man + 5% hFF03-K17-RGD	0.15	2.51(2)	0.90(9)	10.69(8)	0.84(2)
	0.30	2.28(3)	1.03(4)	12.27(2)	0.96(7)
	0.50	3.26(4)	1.16(3)	6.58(7)	1.13(7)

For a more accurate description of the scattering intensity, the data are approximated by a form factor based on the flexible cylinder model as implemented in SasView.[122] This model originates from simulations done by Pedersen and Schurtenberger on semiflexible polymers, which take into account excluded volume effects.[123] From this model the persistence length l_p, that is a measure for the stiffness of a polymer, as well as the cross-sectional radius R_{cs} can be extracted. Comparing the obtained values for the latter one, it is found that the values are in good agreement with the model independent analysis proofing the validity of the selected model in the high q regime. The persistence length is found to be in a range of 7 to 14 nm, which is in good correspondence to the length of an extended single peptide chain of the given composition, which is 16.81 nm.[124,125]

5.2.2.2 Determination of mechanical properties of peptide hydrogels by rheological Characterization

Beside the structural features of a peptide-based material, its stiffness is a critical parameter to direct cellular behavior. To characterize the designed peptide hydrogels with regard to this feature, their elastic and viscous properties were studied by oscillatory rheology. With this technique it is possible to determine, in combination with structural investigations, the main properties of the biomaterials to evaluate possible applications. The mechanical properties of a material can be detected in a quantitative fashion by small deformations within the linear viscoelastic region of the sample.[126] The requirements of a materials to use the perception "*gel"* and the rheological criteria was previously defined by Almdal et al., who determined a gel as a soft, solid or solid-like material consisting of two or more components in liquid of significant amount.[127] Upon to their definition the criteria a material has to accomplish to be classified as a gel are their elastic and viscous qualities, namely storage modulus G' and loss modulus G'', with respect to a considerably smaller G''.[127,128] The storage modulus G' of a material defines the energy of deformation which is stored during the shear process and can be explained by the stiffness of a material, whereas the dissipated energy during the shear process, i.e. the behavior of the material like a liquid, is the loss modulus G''.[126] If G' > G'', the material behaves like an elastic solid and can be classified as gel, in case of G''>G' the material behaves like a viscous liquid.[129,130] For all rheological experiments pure peptide and peptide compositions listed in Table 5.3 were prepared in Dulbeccos Modified Eagle Medium (DMEM) to imitate the conditions for cell culture experiments.

The rheological characterization of all coiled-coil peptide hydrogels was performed in cooperation with the Group of Prof. Dr. Michael Gradzielski by *M.Sc. Benjamin von Lospichl*. Prior to every experiment an amplitude sweep in deformation mode was

performed to assure that the amplitude chosen for the subsequent frequency sweep is within the linear viscoelastic regime (LVE), i.e. the response of the samples is not depending on the amplitude at the given frequency. Ultimately, the amplitude was fixed at a deformation of 2% for all measurements to ensure conditions being equal. Elastic and viscous properties, respectively storage and loss modulus G' and G'' are commonly determined from frequency sweeps in the range of 0.05 to 20 Hz. For all tested peptide samples, it was found that the storage modulus G' dominates over the loss modulus G'' for the investigated frequency range. These findings indicate that the system has pronounced elastic properties. Data for storage and loss moduli of wildtype (WT) hydrogel and WT mixtures are shown in Figure 5.16.

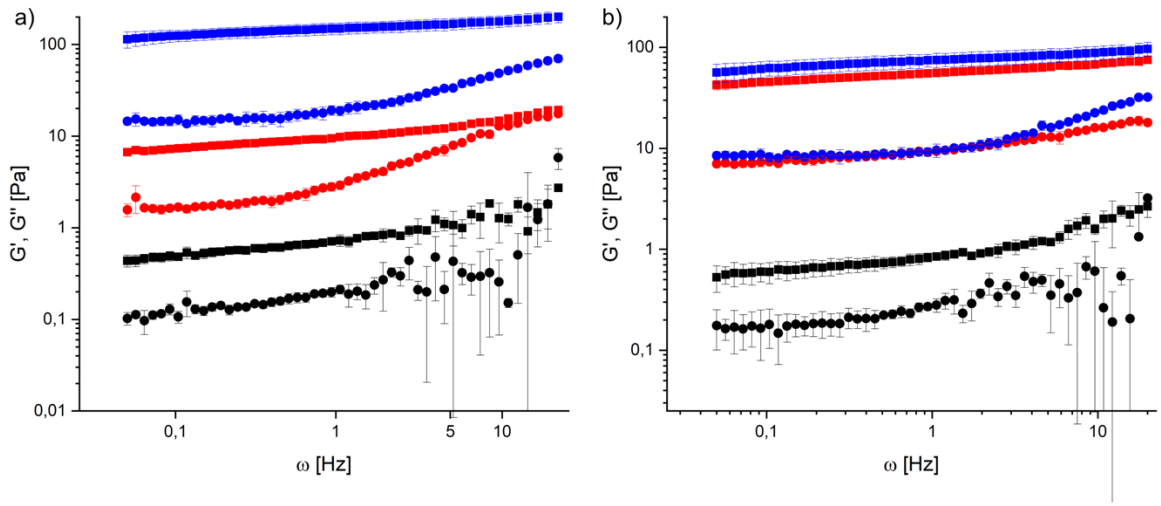

Figure 5.16. Storage modulus G' (squares) and loss modulus G'' (circles) as function of the applied frequencies for WT hydrogel (pattern a) and WT + 1% WT-CH and 5% WT-RS (pattern b) at concentrations of 0.15 wt% (black symbols), 0.30 wt% (red symbols) and 0.50 wt% (blue symbols) at 37°C.

To compare the temperature dependent properties of the hydrogels, data of all 0.50 wt% hydrogels at 25°C and 37°C are shown in Figure 5.17.

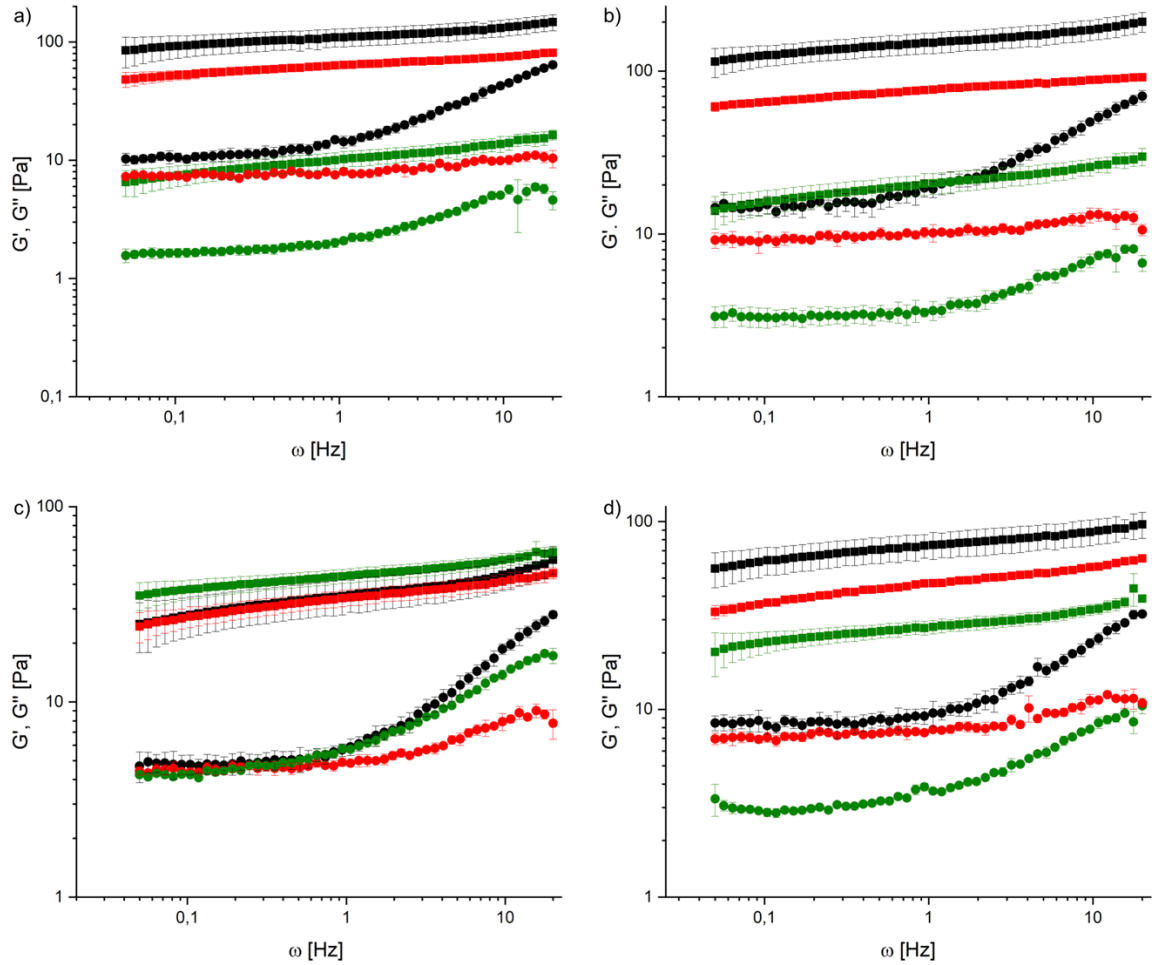

Figure 5.17. Storage modulus G' (squares) and loss modulus G" (circles) of pure (panels a and b) and mixed (panels c and d) 0.50 wt% hydrogels at temperatures of 25°C (a and c) and 37°C (b and d). Panels a and b: WT – black symbols, WT-CH – green symbols, WT-RS – red symbols. Panels c and d: WT + 1% WT-CH + 5% WT-RS – black symbols, WT + 1% WT-CH – green symbols, WT + 5%WT-RS – red symbols.

For a classification of the gels, the loss factor, respectively the phase angle of the system was taken, which is a reference for characterization of the frequency-dependent properties of the hydrogel. The phase angle is defined by equation 5.

Equation 3. Phase angle of the hydrogel (frequency dependent properties)

$$\tan(\delta) = \frac{G''}{G'}$$

Exemplary the phase angles of WT hydrogel and WT + 1% WT-CH + 5% WT-RS hydrogel composition measured at 37°C are presented in Figure 5.18.

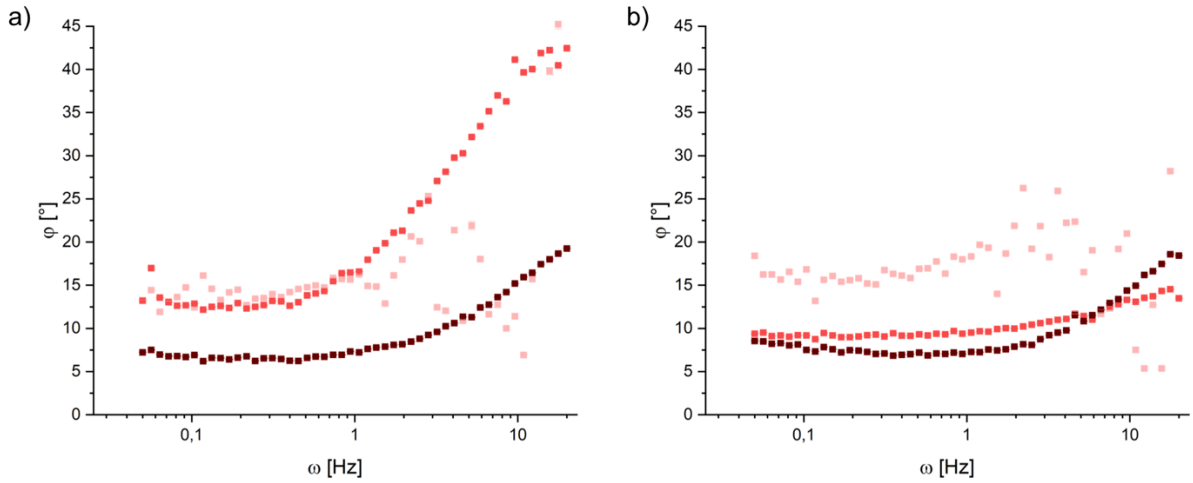

Figure 5.18. Phase angle at T2 = 37°C of (a) hFF03 and (b) hFF03 + 1%hFF03-K17-Man + hFF03-K17-RGD at concentrations referring to 0.15 wt% (bright red), 0.30 wt% (red) and 0.50 wt% (dark red).

The phase angle increases with increasing frequency for both hydrogels, which is a typical behavior of a viscoelastic solid. As the phase angle decreases with increasing concentration of the hydrogels, it can be assumed that the process of gelation is stronger at higher concentration. A commonly used model to describe the frequency-depended moduli G' and G'' within a viscoelastic solid material is the Kelvin-Voigt model. This model comprises the elastic modulus G', which is taken to be constant over the whole frequency range and therefore is directly related to the plateau modulus, and the loss modulus, which depends linearly on the frequency. The corresponding proportionality constant in the latter case is the viscosity of the material. As it is seen from the data shown before, these assumptions are not valid for the peptide system we investigated. Therefore, the so-called fractional Kelvin-Voigt model is used to approximate the data. In this model the moduli are defined as followed

Equation 4. Fractional Kelvin-Voigt model

$$G'(\omega) = E_1\omega^{\alpha}\cos\left(\frac{\pi\,\alpha}{2}\right) + E_2 \text{ and } G'' = E_1\omega^{\alpha}\sin\left(\frac{\pi\,\alpha}{2}\right)$$

A detailed derivation of these equations can be found e.g. in Refs.[131,132] The fractional viscosity E_1 (Equation 4) in units [Pa s^{α}] depends on the fractional exponent α ($0 < \alpha < 1$). The static load is denoted by E_2 and is equivalent to the plateau modulus (in the high frequency limit). Within this approximation the adequate description of G' is possible within the whole frequency range, whereas only high frequency ranges of G'' are possible to approximate. This might be an effect of an inertia behavior at low frequencies. The

crosslinking or overlapping density ${}^1N$ as well as an average mesh size ξ can be calculated by the static load E_2 through

Equation 5. Crosslinking or overlapping density 1N

$$ {}^1N = \frac{E_2}{k\,T} = \frac{1}{\xi^3} $$

Here, k denotes the Boltzmann constant and T the absolute temperature. Calculated results for ξ for both investigated temperatures are summarized in Table 5.5. For almost all tested samples the mesh size is decreasing with increasing concentration of the gel. This result is reasonable due to the fact that a low number of peptide fibers, respectively a low fiber density results in a higher mesh size. Furthermore, the mesh sizes follow for both tested temperatures, 25°C and 37°C, the same trend and are in the same order of magnitude.

Table 5.5. Average mesh size ξ and static load E2 as determined from fitting the data by the expressions for moduli given in Equation 4, which are derived from the fractional Kelvin-Voigt model. The indices refer to the corresponding temperature T1 = 25°C and T2 = 37°C, respectively.

name	*c (wt%)*	*E2(1) (Pa)*	*ξ1 (nm)*	*E2(2) (Pa)*	*ξ2 (nm)*
hFF03	0.15 0.30 0.50	0.29 3.65 95.20	242.04 104.04 35.09	0.45 6.00 57.24	211.72 89.34 42.12
hFF03-K17-Man	0.15 0.30 0.50	2.66 0.94 6.03	115.62 163.76 88.04	6.08 4.32 15.28	88.94 99.69 65.42
hFF03-K17-RGD	0.15 0.30 0.50	1.63 8.78 37.55	136.26 77.66 47.84	1.33 15.15 39.09	147.71 65.60 47.83
hFF03 + 1% hFF03-K17-Man	0.15 0.30 0.50	0.27 8.23 22.44	246.86 79.34 56.80	0.33 20.17 19.42	235.55 59.64 60.39
hFF03 + 5% hFF03-K17-RGD	0.15 0.30 0.50	1.67 17.48 24.21	135.16 61.73 55.38	2.39 23.26 32.11	121.41 56.87 51.07
hFF03 + 1%hFF03-K17-Man + hFF03-K17-RGD	0.15 0.30 0.50	0.17 16.97 32.27	290.75 62.34 50.32	0.60 16.61 39.68	192.25 63.63 47.60

It is found that the results of SANS experiment and the rheology are comparable in their orders of magnitude, namely the average lengths determined from the neutron scattering and calculated mesh sizes from rheology-data. These results clearly demonstrate that the presented results for the characterization of the coiled-coil peptides are consistent.

5.2.2.3 Biocompatibility testing of differently composed coiled-coil peptide hydrogels

For initial cytotoxicity studies NIH/3T3 mouse fibroblast were chosen as a robust cell line to get more insight into the interaction of cells and their artificial extracellular matrix. NIH/3T3 cells were cultured in 175 cm^2 cell culture flasks in DMEM culture medium containing high glucose (4.5 g/L, hG), 10% fetal calf serum (FCS) and 1% penicillin/streptomycin (P/S) in a humidified incubator at 37 °C under 5.0% CO_2 atmosphere. Medium change occurred every second. The culture was *splittet* respectively subcultured upon confluency of 70 – 80% according to the detected cell number. Toxicity of the peptide hydrogels and their compositions was tested with concentrations described above (see Table 5.3) using cell counting kit-8 (CCK-8); a colorimetric assay that allows to determine proliferation behavior of cultured cell populations. The setup of the assay includes all designed peptide hydrogels prepared in DMEM culture medium.

A transparent, tissue-culture treated 96-well plate with *Chimney-Wall* to avoid *edge effect* was filled with peptide hydrogels prior to cell culture. The *Chimney-Wall* of the well-plate was filled with D-PBS. NIH/3T3 mouse fibroblasts were seeded in the respective well-plates and cultured for 24 hours and 72 hours at 37 °C under 5 % CO_2-atmosphere in a humidified incubator, respectively. Untreated cells, which were grown only in pure cell culture medium represent the control, cells cultured on Matrigel® represent negative control and positive control is represented by cells which were treated with a 1% (w/v) solution of sodium dodecyl sulfate (SDS) to establish controlled cell-death.

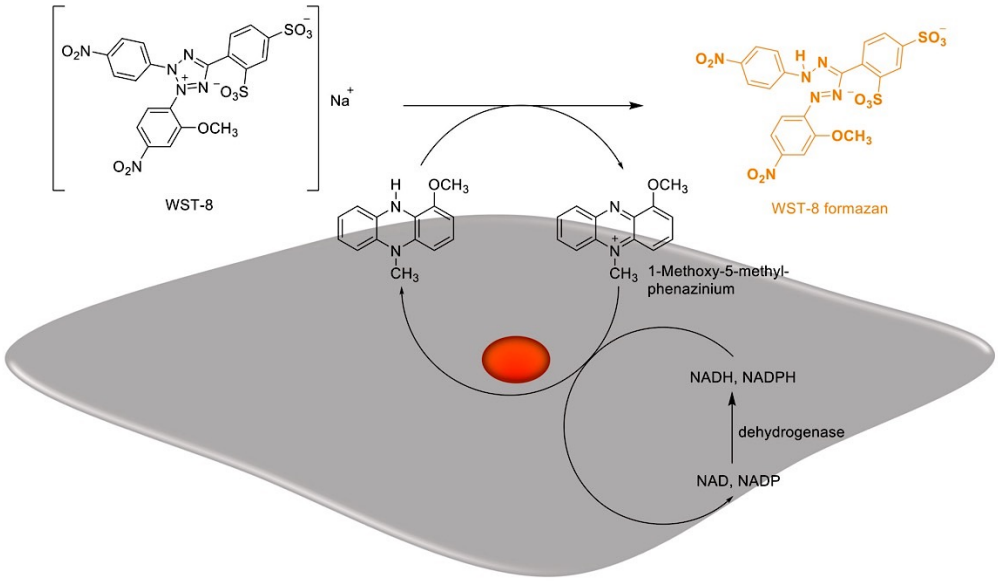

Figure 5.19. Mechanism of reduction of WST-8 to orange WST-8 formazan in viable cells.

After 24 hours and 72 hours, respectively, CCK-8 solution was added to each well. CCK-8 solution is a ready-to-use solution containing WST-8 tetrazolium salt, which will be reduced to orange formazan salt by dehydrogenases in viable cells (see Figure 5.19). The formazan can be detected by absorbance measurements at 450 nm after 90 minutes of incubation. Viability profiles of coiled-coil peptide hydrogels are illustrated in Figure 5.20. All hydrogels and hydrogel compositions show very good viability profiles for NIH/3T3 cells 24 h post-seeding. Compared to the control 0.30 wt% hFF03 hydrogel indicated viabilities higher than 160%. Lowest viability values were detected for cells cultured hFF03-K17-Man hydrogels, especially for 0.30 wt% hydrogel. Viabilities of cells on hydrogel compositions, show nearly the same levels with differences of up to 10% and best performance for 0.15 wt% candidates, respectively. Viabilities of cells evolved to lowest moderate values for hFF03-K17-Man hydrogel, particularly for 0.50 wt% with 61%. Cells cultured on 0.30 wt% hFF03-K17-Man and 0.50 wt% hFF03-K17-RGD show values below 80%. Thus, these hydrogel candidates could be classified as very low to moderate cytotoxic to NIH/3T3 cells under the tested conditions. As for cell populations on all remaining compositions viability values between 81% and 115% were determined and therefore all are classified as non-toxic. Except of hFF03-K17-Man, all hydrogels and hydrogel compositions with a peptide content of 0.15 wt% initiated viabilities above 100% compared to both controls.

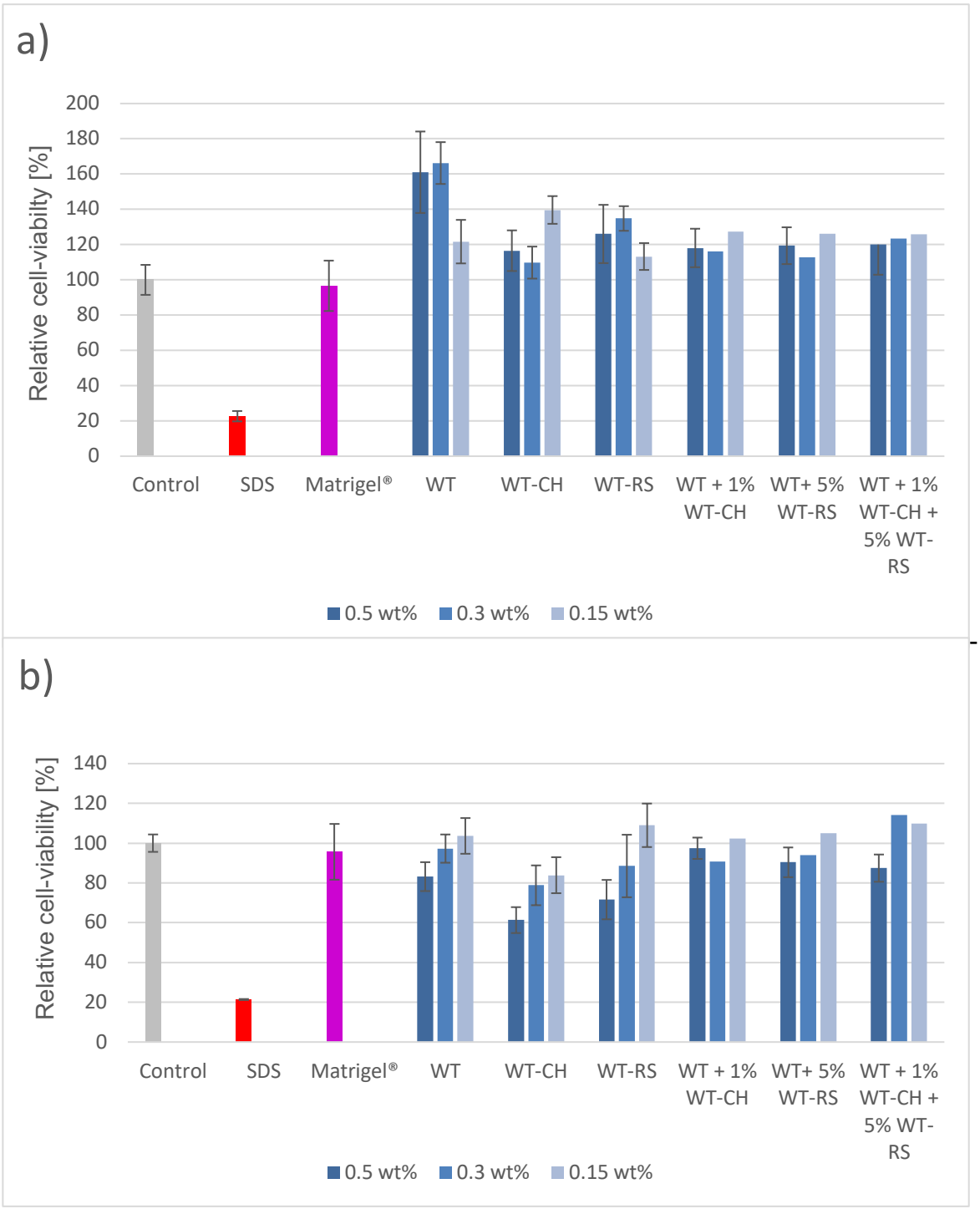

Figure 5.20. Viability profiles of seeded NIH3T3-cells on peptide hydrogels after a) 24h and b) 72h. The values were normalized against the control defined as 100% viability representing cells cultured only in medium.

In summary coiled coil peptide hydrogels initiated a significantly higher viability after 24h compared to Matrigel®. After 72h only cells cultured on WT-CH and WT-RS show less viability.

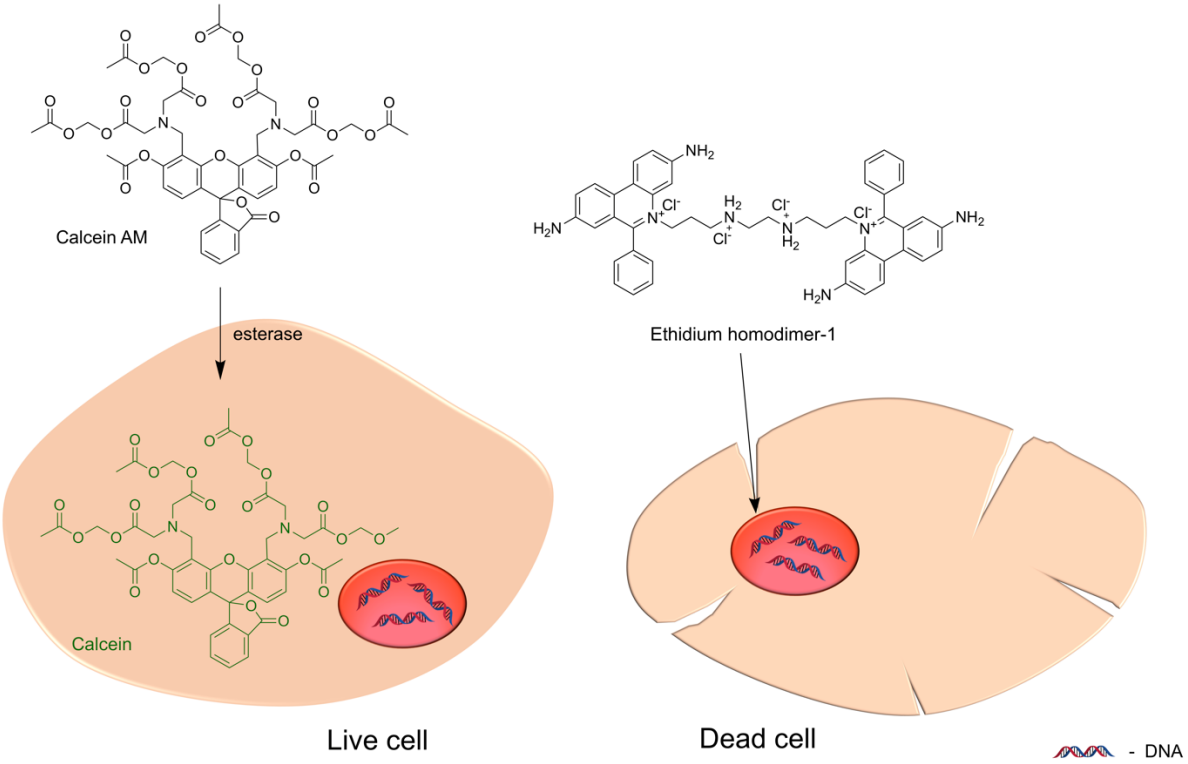

Figure 5.21. Mechanism of LIVE/DEAD-staining containing calcein AM to stain live cells and ethidium homodimer-1 to stain dead cells.

Viability of cells cultured on the hydrogels was visualized by LIVE/DEAD-staining, which enables distinguishing between live and dead cells. Live cells were stained with calcein AM and dead cells were stained with ethidium homodimer-1. Calcein AM is non-fluorescent and can diffuse through the cellular membrane. By entering the cell membrane esterases of the live cell convert calcein AM into calcein which is a green fluorescent dye. Because dead cells have no active esterases, they will not fluorescent in green. Ethidium homodimer-1 is able to pass the damaged membrane of dead cells and binds to DNA of the nucleus of the cell. The binding to DNA results in emitting red fluorescence and stains the nucleus of the cell.[133] The principle of LIVE/DEAD-staining is shown in Figure 5.21. Microscopy images confirmed high biocompatibility of tested hydrogels indorsing the results of cytotoxicity assay (Figure 5.20). In the following figure the microscopy images of LIVE/DEAD-assay after 72h are shown (Figure 5.22, images after 24h are shown in the appendix).

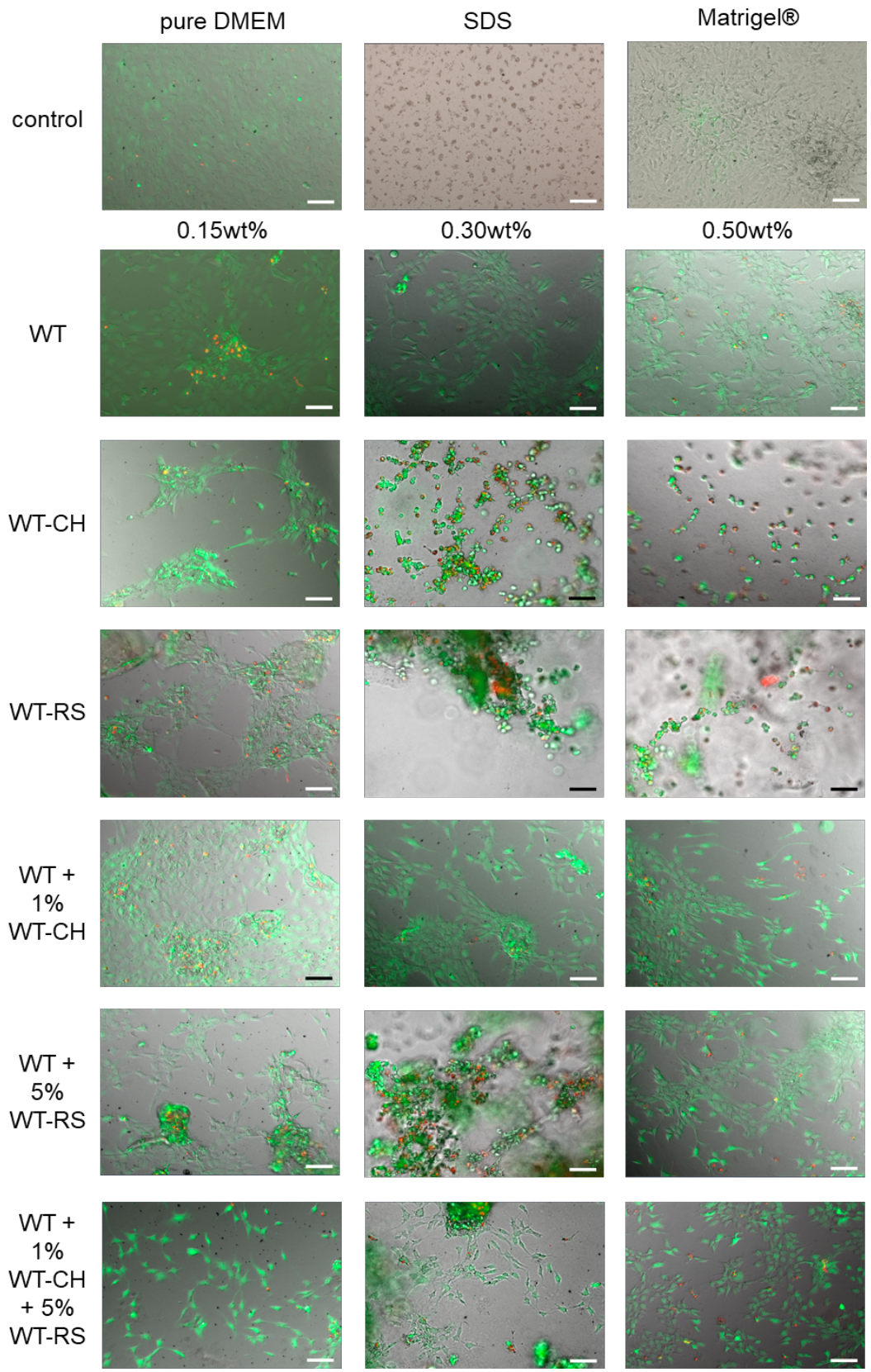

Figure 5.22. NIH/3T3 cells 72h after culturing on coiled-coil peptide hydrogels. Cells were stained by a LIVE/DEAD staining were living cells are stained green (calcein AM) and dead cells were stained red (ethidium homodimer-1). The scale bar denotes 100 μm.

5.2.3 Drafting the extracellular matrix with signal epitopes as ligands presented on coiled-coil surfaces

As the mannose-conjugated hFF03 initiated excellent viabilities when combined in 1% amount with and without 5% RGD-conjugated variant in hydrogel environment, further ligands have to be tested to verify the approach of mixing different ligands presenting coiled coil peptides to imitate the natural ECM of cells. To this end, a second monosaccharide conjugated hFF03 variant was included into the study to test the impact of the nature of the carbohydrate ligand on the cell viability. As described before, hFF03 was conjugated to several signal peptides which appear in adhesion proteins of native ECMs. A sequence of the neuronal apoptosis inhibitory protein family (SKPPGTSS, NAIP) was coupled to the surface of the coiled-coil bundle as it has, among inhibition of neural apoptosis,[134] several other functions in native ECMs and is suggested to have an important role in supporting cell viability.[135] Another peptide sequence was Substance P, as it potentially increases the expansion of MSCs *in vivo* and could induce the migration from the bone marrow into the periphery.[136] The heparin-binding peptide GKKQRFRHRNRKG derived from vitronectin is known to promote self-renewal of human pluripotent stem (hPS) cells for long-time period in defined medium.[47] The described peptide sequences are seen as promising ligands to bear in artificial substrates for culturing different cell lines and enable the study of proliferation, self-renewal and differentiation mechanism.

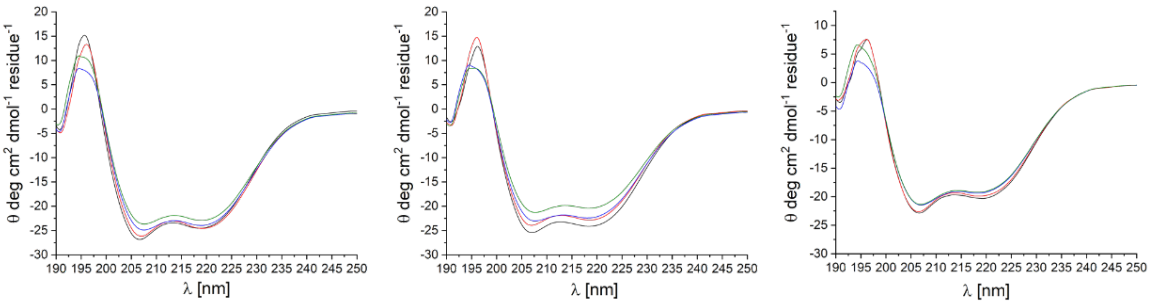

Figure 5.23. CD spectra of epitope conjugated hFF03 peptides over a period of 6 days at 20°C in D-PBS (pH 7.4). (a) hFF03-K17-NAIP, (b) hFF03-K17-SP and (c) hFF03-K17-VT. Peptide concentration is 50 µM.

As shown in the CD-spectra (Figure 5.23) the conjugated ligands are not disturbing the self-assembly of the peptides. One feature of this assay was to mix undecorated hFF03 with an amount of 1% regarding the concentration of the wild type hydrogel. As the required

epitope density is very low, these mixtures were tested regarding toxicity against NIH/3T3 cells in a five days cell culture.

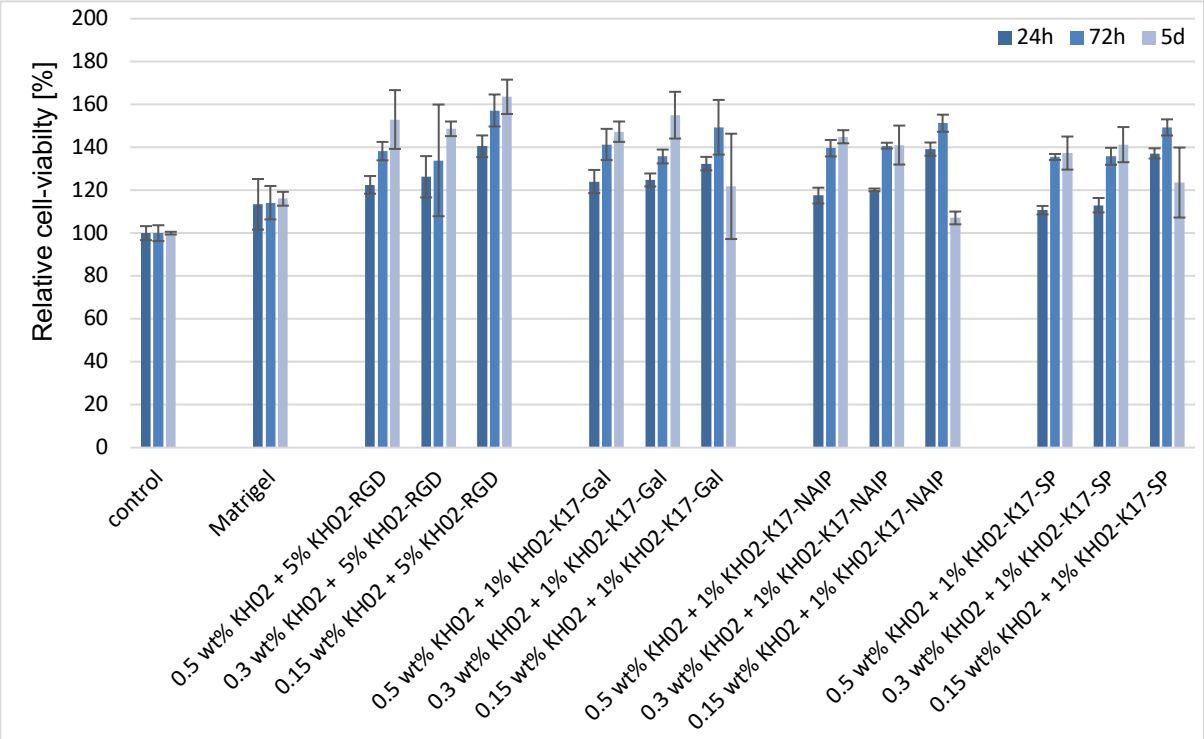

Figure 5.24. Relative viabilities of seeded NIH3T3-cells compared to control cells (NIH/3T3 cultured only in cell culture medium without any additive) on peptide hydrogels after 24h (blue column), 72h (red column) and 5d (green column).

Here, the galactose-functionalized hFF03 was used to give more insights about the tolerance of carbohydrate-functionalization within a three-dimensional microenvironment, since mannose-functionalization showed no toxicity (Figure 5.20). Also, the second RGD-functionalized hFF03-variant (hFF03-RGD) was included as a control peptide to check the difference of tolerance of NIH/3T3-cells against the presentation mode of the recognition motif – presented at the coiled coil template *versus* embedded in the coiled coil sequence. This peptide was included was an amount of 5% like its derivative hFF03-K17-RGD. This approach makes it possible to study the tolerance of NIH/3T3 cells against the epitopes inside the peptide fiber versus outside the fiber. NIH/3T3 cells were seeded on peptide hydrogels according to the same conditions as described above. One experimental run was performed in triplicates per hydrogel candidate. Overall NIH/3T3 remained viable after five days cell culture and showed excellent viability profiles.

The viability of cells seeded on hydrogel-compositions of 0.50 wt%, 0.30 wt% and 0.15 wt% showed for all tested time points viability profiles above 100 %, respectively.

Highest viability was detected for hydrogel composed of 0.15 wt% hFF03 hydrogel and 5% hFF03-RGD at all time points. For all tested peptide concentrations, a trend of viability is visible that is viability is increasing at decreasing peptide concentrations. Most of the tested hydrogel compositions showed this trend that viability of NIH/3T3 cells seeded on peptide hydrogels increases over the tested period of time indicating a high tolerance of this cell line towards all new hydrogels. Two exceptions were determined for this trend. Cells seeded on 0.15 wt% hFF03 gels containing either 1% NAIP-functionalization or SP-functionalization have lower viabilities but are comparable to viabilities of cells seeded on Matrigel. This may be due to cell death or delayed cell growth on these gels. The presentation mode of the recognition sequence RGD seems to have strong influence on the viability of cells (Figure 5.20). Furthermore, the tested cell line tolerates both tested carbohydrate functionalization and the more complex peptide epitopes, as well as fully functionalized carbohydrate and RGD-functionalized gels dependent on the peptide content, respectively.

Mesenchymal stem cells (MSCs) have a wide differentiation potential and it is therefore a promising approach to offer different chemical functionalities in a tunable three-dimensional scaffold combined with adjustable mechanical properties. As NIH/3T3 cells are tolerating all new peptide hydrogels, it motivated to study them in the context of stem cell culture. The higher sensitive bone marrow derived human MSCs (hMSCs) have to be tested regarding their viability on the presented system. At first, their survival potential over a longer time period has to be measured. Therefore, hMSCs were cultured as mentioned in the experimental part. Comparing the results of both viability tests of NIH/3T3 cells, it is obvious that best viability values were collected for 0.30 wt% and 0.15 wt% peptide hydrogels (see Figure 5.20 and Figure 5.24). Best candidates from both studies were chosen to be presented to the hMSCs to get a first impression about the toxicity. Data was collected 24 hours and 72 hours after seeding and culturing at 37°C under 5% CO_2-atmosphere in a humidified incubator, respectively. The results are presented in comparison to non-peptide control, were cells were cultured only with medium, the negative control by cells seeded on Matrigel® and a positive control represented by cells which were treated with a 1% (w/v) solution of SDS.

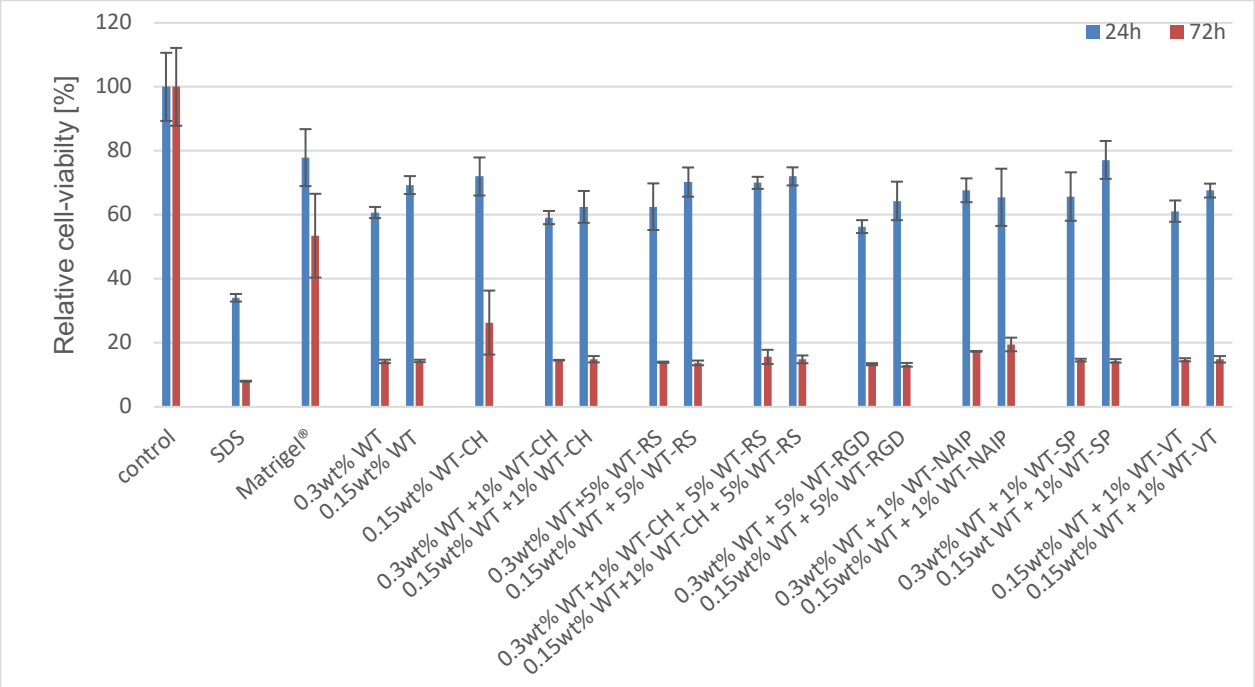

Figure 5.25. Viability profiles of seeded hMSCS (P6) on a selection of coiled-coil peptide hydrogels after 24h (blue columns) and 72h (red columns).

Viability profiles of seeded hMSCs show values between 56% and 77% compared to the non-peptide control for all tested hydrogel candidates. Most of the 0.30 wt% hydrogels are therefore classified as moderately toxic to the cultured hMSCs after 24h. Exceptions are 0.30 wt% hydrogels of the pure hFF03 peptide or hydrogel compositions containing 1% of mannose-conjugated hFF03 or 5% of hFF03-RGD which have to be classified as fully toxic to cells as their viability values are beneath 61%. Surprisingly, viability of 0.30 wt% hydrogel containing 1% mannose-conjugated and RGD-conjugated hFF03, as well as 0.15 wt% WT-CH hydrogel have an up to 12% higher viability compared to the fully toxic candidates. Overall, 0.15wt% hydrogels are more tolerated by the hMSCs than their 0.30 wt% variants after a 24h culture. Highest viability values of 77% were collected for 0.15 wt% hydrogel containing 1% Substance P conjugated hFF03 followed by the mannose and RGD-containing hydrogel with 72%. The 0.15 wt% hydrogels containing 5% RGD-conjugated hFF03 and the fully conjugated WT-CH are in the same range. These hydrogels are classified as low toxic after this time. These results show the different effects of the peptide mixtures to the seeded cells and confirm the approach of designing specialized hydrogels by mixing differently functionalized peptide into a hydrogel network. Unfortunately, the viability values of the hMSCs cultured on the peptide hydrogels decrease beneath 20 % compared to the non-peptide control after 72h of culture.

To finalize and perfect the main project of the thesis, comparing all investigated data, we can assume that the designed coiled-coil peptide materials based on the newly developed hFF03 can fulfill the following features as mentioned in the hypothesis of R. Schofield;[27]

- Ability to modulate the peptide scaffolds to address complexity of native ECMs.
- Defined and multivalent presentation of biologically relevant ligands on the surface of the peptide fibers.
- Suitable mechanical properties of newly generated hydrogels.

Within this study, a series of various carbohydrate and peptide-epitope presenting coiled-coil peptides were developed for their use as modifiable hydrogels in cell-culture applications. By studying their secondary structure, it was shown that the attached ligands are not interrupting their α-helical conformation even after several days. Herein, we could investigate a synthetic approach giving highly specialized networks with a defined density of ligands at exact positioning in the peptide. With this in hand, we could erase the disadvantage of post modification of peptides normally made and therefore test the influence of these ligands systematically with a small selection of the series including the undecorated hydrogel forming peptide hFF03, as well as mannose- and RGD-functionalized hFF03 variant, respectively. In a bottom-up approach the peptides were mixed in different rates and concentrations, to verify the influence of different ligand types, their density and the water content, i.e. peptide concentration on the structural formation of the hydrogels and microstructures inside as well as their performance in cell-culture. Morphology studies revealed a thin fibrous network of each gel candidate, whose characteristics were confirmed by SANS experiments. Mechanical properties of all hydrogels approved their gel characteristics and assessed a self-organizing behavior in the tested frequency range. Due to these characteristics, NIH/3T3 cells were cultured with these hydrogels to study their tolerance towards new hydrogels. Viabilities of the cells after 72h showed that the gels are mostly non-toxic to cells and partially induce higher viabilities than the commercially available 3D substrate, Matrigel®. These findings confirm the approach of mixing different functionalized coiled-coil peptides within the hydrogel environment. More complicated ligands from adhesion proteins were tested under the same conditions and showed an excellent viability profile for the latter cell-line in a 5 days cell culture. For a possible application in regenerative medicine the tolerance of hMSCs was tested towards the system in a three days cell culture with a selection of the best hydrogel candidates tested before. hMSCs showed low viability values after 72h. To improve these results further studies regarding hydrogel compositions and presented ligands need to be done. However, the studied hydrogel system provides a suitable

platform for developing a variety of simple to complex composed three-dimensional hydrogel materials.

The here presented approach is step forward, as it enables to mimic the complexity of native ECM and to address the necessity of cells of a continuously changing environment within different stages of cell development. As an outlook the hydrogels should be tested for their long-term stability under different conditions, to ensure a constant and continuous performance. Also, ligands of other structure should be tested to broaden the possibilities this approach offers for the design of three-dimensional hydrogel materials. Based on this methodology, it is possible to develop materials that can be used in tissue engineering, regenerative medicine and as screening-system for studying the influence of target-molecules and their density within a three-dimensional matrix on the viability of cells.

5.3 Coiled-coil peptides as multivalent scaffold for Influenza A Virus inhibition

Over the last decade, the importance to develop efficient Influenza A Virus (IAV) inhibitors increased significantly. Recent developments mimic the cell surface by the multivalent presentation of sialic acid groups of the host cell and provide an alternative approach for targeting IAV - HA binding sites.[81] Finding the optimal geometry and density of sialic acid groups presented to the virus is the main goal for the development IAV inhibitors.[99] For a conceivably application as drug the scaffold carrying the sugar moieties should have a high biocompatibility and are non-cytotoxic. Coiled-coil peptides can be suitable scaffolds to present sialic acid moieties with optimal geometry and density of the latter to act as competitive binders of IAV and, thus, prevent IAV binding to cells. Recent studies have demonstrated that high densities of sialic acid ligands presented by the scaffolds are not necessary for an effective inhibition.[81] FF03 and hFF03 were identified as stable scaffolds for the multivalent presentation of peptidic and carbohydrate ligands and successfully demonstrated their performance in biological studies (see chapter 5.2).[15] Therefore, these scaffolds were chosen as carriers for sialic acid ligands to determine and compare their inhibition potential against IAV. With this strategy, it is possible to compare a fiber forming scaffold (FF03) with a scaffold that has the ability to build three-dimensional networks (hFF03). Both geometrical features can directly be compared and, by diluting of ligand bearing scaffolds with the undecorated peptides in varying ratios, different ligand densities can be achieved. Thus, this approach allows to determine the optimal ligand density on the two different coiled-coil scaffolds for Influenza A Virus inhibition. The concept is shown in Figure 5.26.

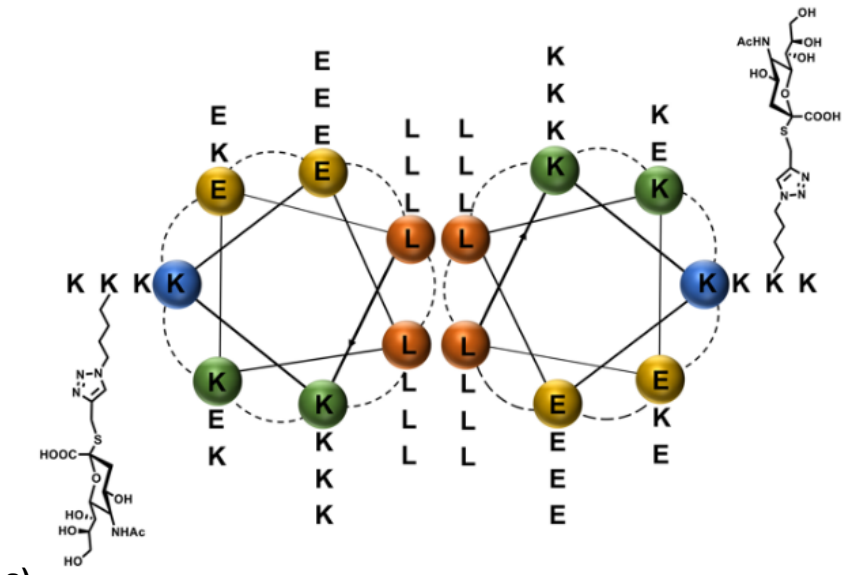

a)

	1	2	3	4	5	6	7	8	9	10	11	12	13	14	15	16	17	18	19	20	21	22	23	24	25	26
	d	e	f	g	a	b	c	d	e	f	g	a	b	c	d	e	f	g	a	b	c	d	e	f	g	a
a) FF03 Abz	L	K	K	E	L	K	E	L	K	K	E	L	E	K	L	K	**K**	E	L	K	E	L	K	K	E	L
b) hFF03 Abz	L	K	K	E	L	A	A	L	K	K	E	L	A	A	L	K	**K**	E	L	A	A	L	K	K	E	L

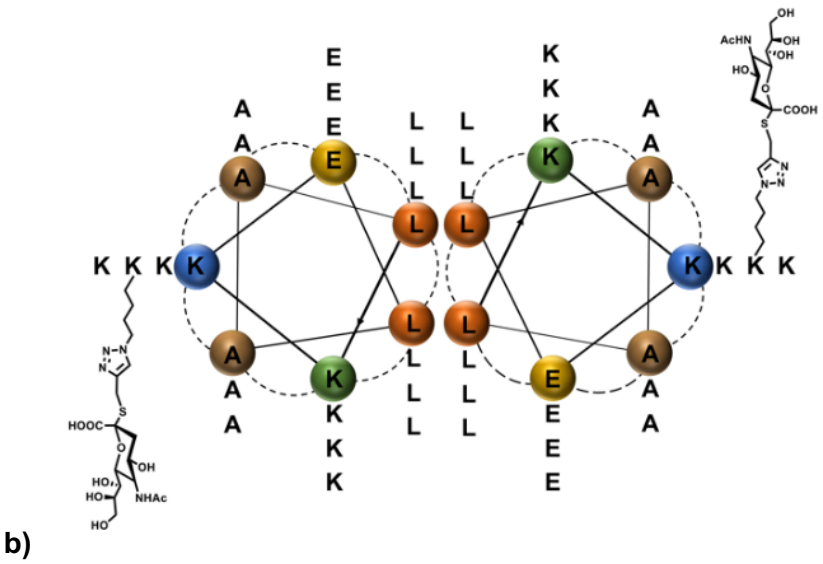

b)

Figure 5.26. Helical wheel projections of FF03 (a) and hFF03 (b) scaffolds, both bearing sialic acid moieties in position K17.

5.3.1 Synthesis of sialic acid bearing coiled-coil peptides

The carbohydrate-building block conjugated to the coiled-coil peptides was chosen with regards to suitability in SPPS. Sialic-acid carries several functional groups. The hydroxygroups as well as the carboxy-functionality at the anomeric C-atom of the hexose have to be protected by acetyl-groups (OH-functionalities) and a methylester (COOH-group). The protecting groups can easily be removed after full-length synthesis of the peptide and full-cleavage from the resin under basic conditions. The carbohydrate-building block carries an alkyne group for coupling *via* Huisgen copper-catalyzed azide-alkyne cycloaddition (CuAAC).[137] CuAAC is a popular method to conjugate different alkyne-functionalized *O*-, *S*-, and *C*-glycosides[138] or other alkynylated molecules[139] through a triazole ring to peptides or other azide-bearing partners. An advantage of CuAAC is the stability of azides towards a lot of organic solvents, as well as H_2O,[140–142] which makes it suitable for applications in SPPS and organic synthesis. Taking this into consideration, two different approaches are possible to conjugate the sugar to a coiled-coil peptide. Both methods need an alkyne-functionalized sialic-acid component for conjugation to the azide-bearing partner.

The first conjugation method is the synthesis of an amino acid building block carrying the sialic acid moiety in their side chain. In that case, the alkynylated-carbohydrate (2) will be coupled to the Fmoc-protected azido-L-lysine (1) in the presence of Cu(I) in a solvent mixture of THF and H_2O (see Figure *5.*). After complete conversion of the educts the product Fmoc-L-Lys-Sial-OH (3) will be purified by extraction and preparative HPLC. This approach has several advantages like the possibility to include the building-block (3) by standard SPPS protocols and the inclusion of the building block into several positions of the peptide sequence to bear the carbohydrate moiety simultaneously. The synthesis occurs in low yields between 10% to 22.5% as a result of several necessary purification steps such as extraction and preparative HPLC.

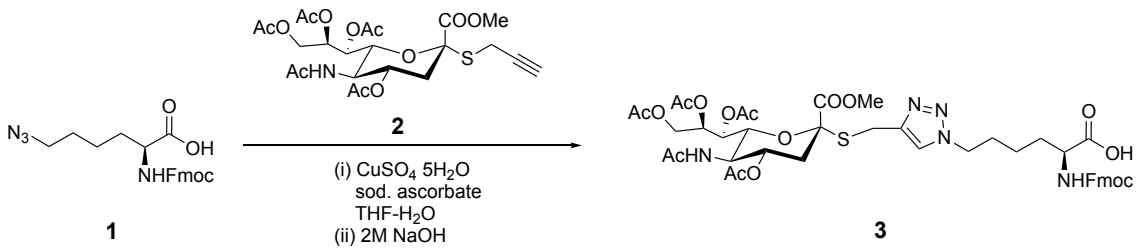

Figure 5.27. Conjugation of sialic-acid component (2) to Fmoc-protected azido-L-lysine (1) via CuAAC resulting in Fmoc-protected building block Fmoc-l-Lys-Sial-OH (3) suitable for SPPS.

A second approach includes full-length synthesis of the peptide and incorporation of the azide-bearing lysine-side chain by coupling of Fmoc-L-azido-lysine in position 17 of the peptide sequence according to a literary known procedure.[143] Similar to the synthetic route described above 5 eq. of the sialic acid component 2 (with respect to resin loading) was conjugated to the azide-group in lysine side chain in position 17 by CuAAC on solid-phase (see Figure 5.28). This method requires a low amount of alkynylated carbohydrate component which is a big advantage in comparison to the building block strategy. There is also no necessity of purification afterwards except of the peptide purification after full-cleavage from the resin.

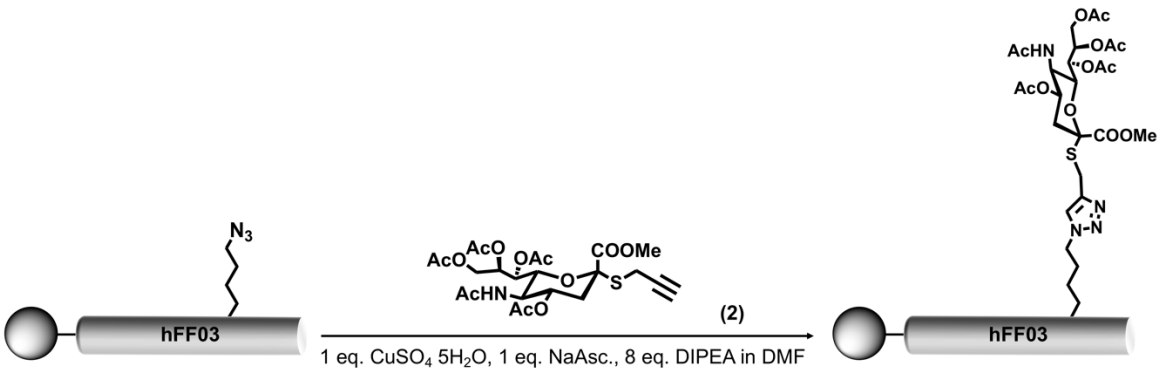

Figure 5.28. CuAAC of alkyne-sialic acid to azide functionality beared by the side-chain of lysine in position 17 of the coiled-coil scaffold (grey cylinder) on solid phase.

Comparing both approaches conjugation of the sialic acid component (2) on solid-phase has a higher efficiency than coupling of sialic acid conjugated amino acid building block.

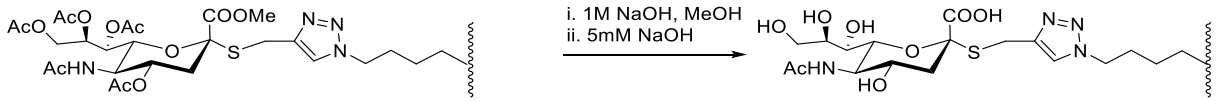

Figure 5.29. Deprotection of hydroxy-groups and hydrolysis of methylester of sialic-acid moiety conjugated to coiled-coil scaffold, schematically presented by the waved line.

Independent of the implemented synthesis route, after full-cleavage from the resin, the protecting groups of OH- and COOH-functionalities of the sialic-acid have to be removed (Figure 5.29). Firstly, the acetyl-groups were removed by treatment of the peptide in MeOH at a pH of 10 to 11 adjusted with aqueous NaOH, followed by hydrolysis of the methyl ester of the neuramic-acid moiety attached to anomeric C-atom with a low concentrated

aqueous NaOH at carefully controlled pH 11.5.[144,145] After successful cleavage of protecting groups, peptides were purified by preparative HPLC.

5.3.2 Structural characterization of sialic acid conjugated coiled-coil peptides and their compositions

For determination of peptides secondary structure, the sample concentrations were set to a total peptide concentration of 75 µM and all tested peptides and - mixtures were measured using CD spectroscopy at 20 °C and 37 °C. Conditions were chosen to study whether the ligand, the combination with an undecorated parent peptide or a temperature of 37 °C is interfering with the self-assembly of the peptides. CD spectra of pure peptides and their mixtures are shown in Figure 5.30.

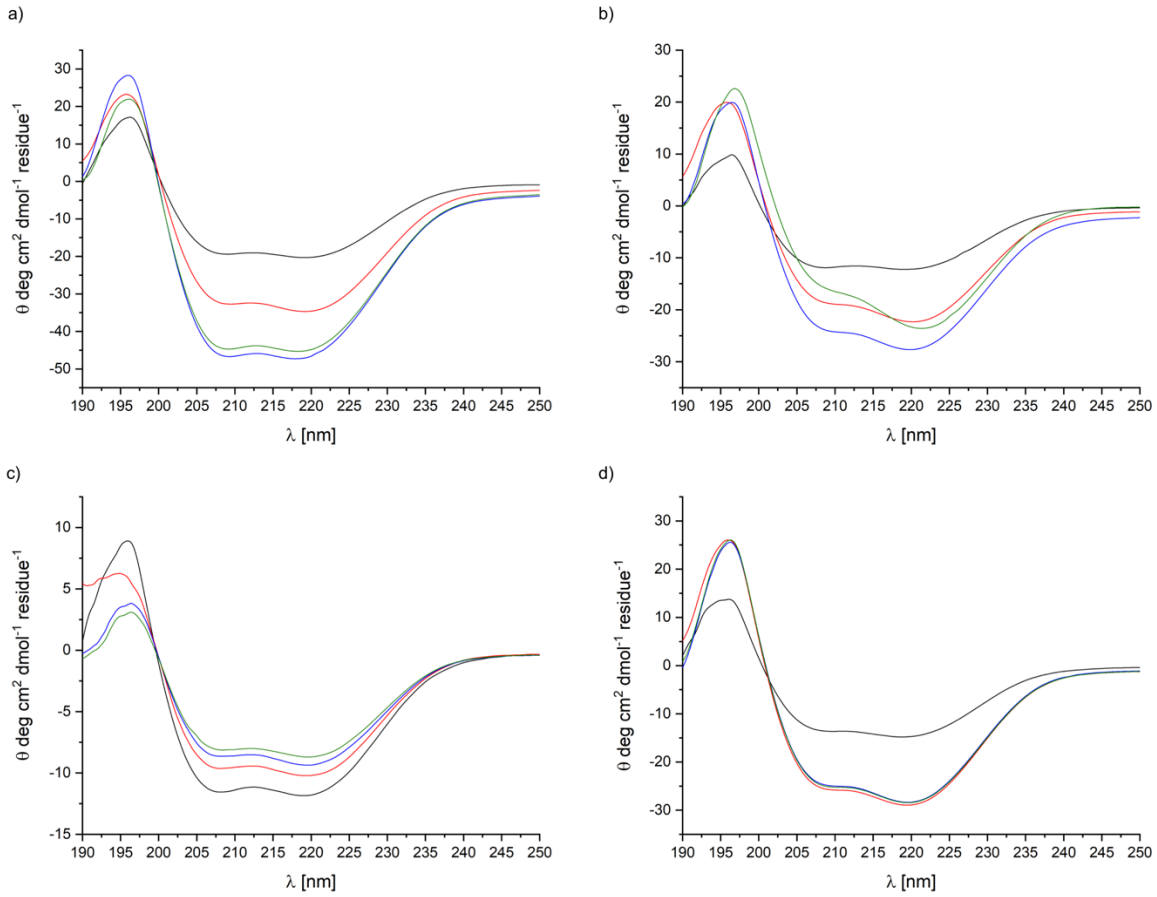

Figure 5.30. CD spectra of all pure undecorated and sialic acid-conjugated FF03 (a and b) and hFF03 (c and d) peptides at 20 °C over a period of 6 days. Peptide concentrations was 75 µM in D-PBS (pH 7.4). Black line 5 min, red line 24h, blue line 72h, green line 6 days.

All tested coiled-coil peptides have CD-profiles characteristic for α-helical secondary structure with minima around 208 nm and 222 nm and a maximum around 195 nm. CD spectra of the pure peptides (Figure 5.30) as well as their compositions show no significant difference, except in their intensities. CD spectra collected at 20 °C clearly display a stable secondary structure over at least six days. Interestingly, CD spectra of FF03 at 20 °C shows that the intensity of the minima at 208 nm and 222 nm is increasing in the same order, whereas the intensities of the minima in the spectrum of FF03-K17-Sial are increasing until 72 h and subsequently decreasing after 6 days with an obvious higher intense minimum at 222 nm. This effect could be explained by the self-assembly of the coiled-coil peptide resulting in peptide fibers, which leads to higher intense minima at 222 nm and due to peptide aggregation to an overall less intense spectrum compared to earlier time points. While the intensity of the CD minima of hFF03 are continuously decreasing over the tested period of six days, the intensities of its sialic acid conjugated variant are not significantly changing after 24 h. However, the minimum at 222 nm is of higher intensity compared to the other minimum at 208 nm, which may be an indicator for the formation of fibers, respectively.

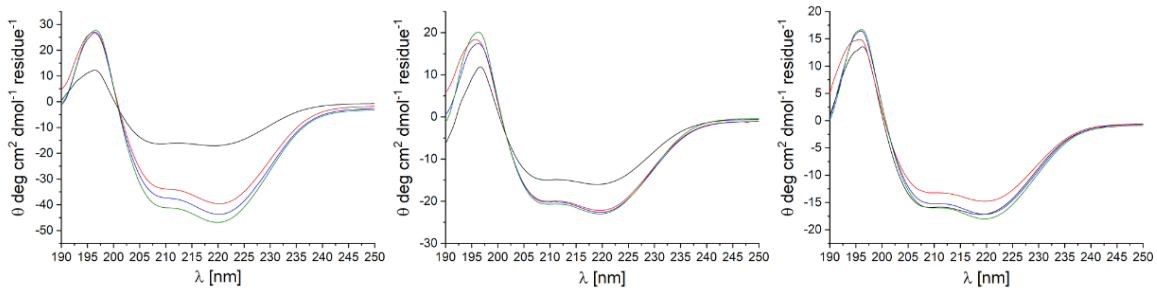

Figure 5.31. CD spectra of 1:1 peptide mixtures of (a) FF03 - FF03-K17-Sial, (b) FF03-K17-Sial : hFF03-K17-Sial and (c) hFF03 : hFF03-K17-Sial at 20 °C over a period of 6 days. Total peptide concentrations was 75 µM in D-PBS (pH 7.4). Black line 5 min, red line 24h, blue line 72h, green line 6 days.

Like the pure peptides, mixed peptides with a 1:1 ratio show similar CD results. There are a few differences in the intensity of the minima. Notably, by comparing the mixed CD spectra the characteristics of the decorated coiled-coil peptides are dominating resulting in the more intense minimum at 222 nm. All these results indicate that the conjugation of sialic acid to FF03 and hFF03 has no influence on their secondary structure, but possibly on their self-assembly into fibers as observable by the shape and the intensities of their CD profiles.

5.3.3 Inhibition studies

To verify the optimal scaffold for sialic acid presentation and ligand density for Influenza A Virus inhibition, peptide mixtures were prepared in different ratios to tune the density of sialic acid moieties presented to the virus surface (see Table 5.6). Unconjugated coiled-coil peptide was used as a control. The highest total concentration of each peptide solution was set to 150 µM for all inhibition tests, which corresponds to a mean concentration of 500 µg/mL.

Table 5.6. Ratios of different coiled-coil peptides bearing sialic-acid to study their inhibition potential of Influenza A Virus binding.

a)	***hFF03***	***hFF03-K17-Sial***	*b)*	***hFF03-K17-Sial***	***FF03-K17-Sial***	*c)*	***FF03-K17-Sial***	***FF03***
	---	1		---	--		1	---
	1	1		1	1		1	1
	1	2		1	2		1	2
	2	1		2	1		2	1
	1	5		1	5		1	5
	5	1		5	1		5	1

5.3.4 Hemagglutination Inhibition Assay (HAI)

To study the inhibition potential of multivalent coiled-coil scaffolds with varying densities of sialic acid moieties against Influenza A/X31/1 Virus hemagglutination inhibition (HAI) assays were performed. This assay is commonly used to verify the potential of a compound to inhibit the binding of the virus to cells.[81] It is based on the ability of the presented sialic acid to prevent attachment of the IAV to erythrocytes.[146] It is quantitatively expressed by the inhibition constant titer Ki, which is the lowest concentration of compound or the highest dilution of the serum. This leads to a complete prevention of IAV binding.[146] The virus binds either to the offered compound or to the blood cells, which is easily visible by eye in the respective wells of the well plates. If a compound prevents the binding of the virus to erythrocytes, the blood cells fall down to the bottom of the well and are visible as a red point. This process is named sedimentation and should also occur when compound and blood cells are mixed without virus particles to exclude interaction between component

and blood cells. However, if a compound or the virus interacts with the erythrocytes, the cells are coagulating which is visible as a red gel-like structure in the well. This process is called agglutination. A schematic representation in Figure 5.32 shows how the assay is performed, and how results are visualized upon mixing sialic acid presenting coiled-coil constructs with virus and erythrocytes. Mixing of erythrocytes either with virus or coiled-coil peptides represents the control experiments.

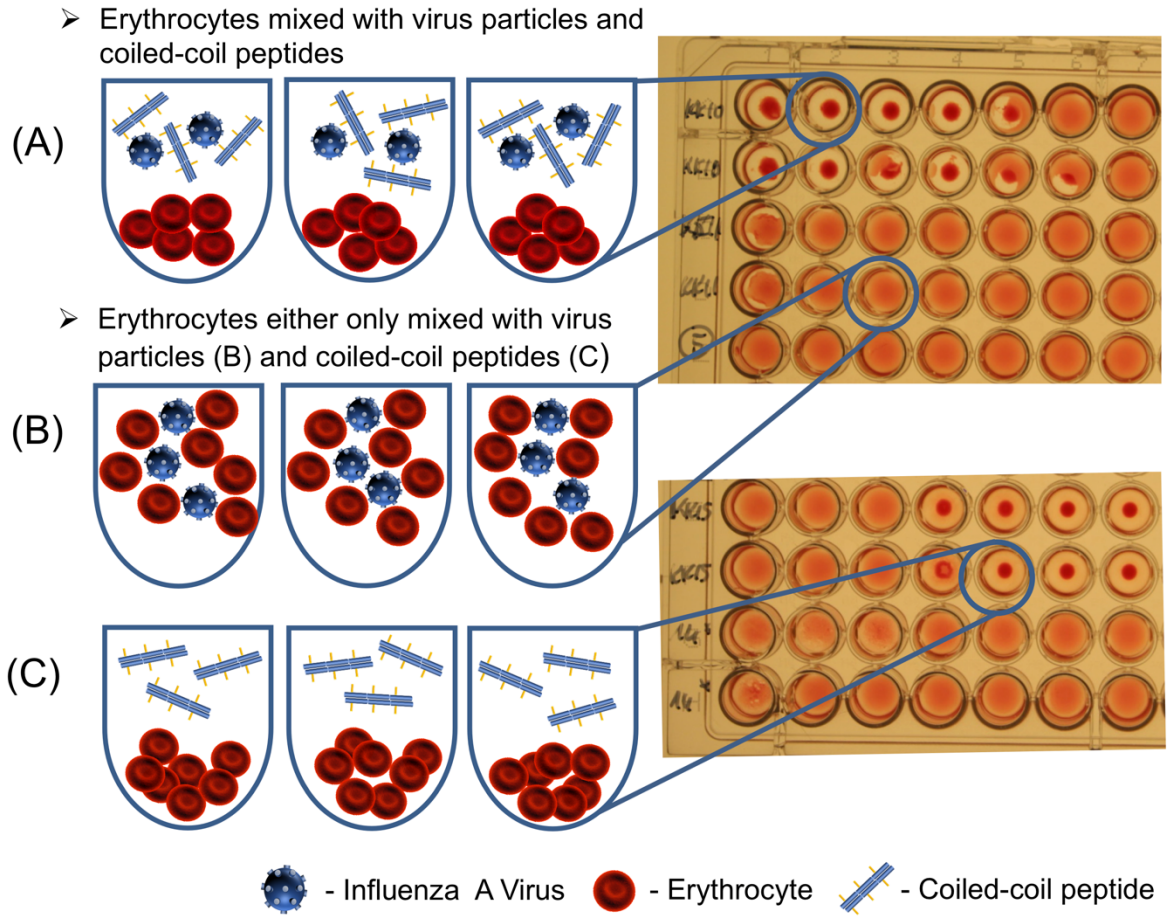

Figure 5.32. Scheme of HAI assay to test the inhibition potential of coiled-coil constructs of binding of Influenza A Virus to erythrocytes. Sedimentation takes places upon mixing of blood cells with virus particles and active coiled-coil constructs (A) or without virus and active coiled-coil constructs (C). Interaction of blood cells and virus particles leads to agglutination (B). The figure was kindly provided by M.Sc. Malte Hilsch, Group of Prof. Andreas Herrmann, Humboldt-Universität zu Berlin.

Table 5.7. Hemagglutination inhibition constants Ki HAI of tested sets a and b of sialic-acid conjugated coiled-coil peptides incubated with Influenza Virus X31.

	Construct			***Ki HAI [µg/mL]***	***Ki HAI [µM]***
	Peptide		ratio		
a)	hFF03	hFF03-K17-Sial	0:1	41.56	12.23
			1:0	>175.00	>51.50
			1:1	175.00	51.50
			1:2	>250.00	---
			2:1	>250.00	---
			1:5	>175.00	---
			5:1	>250.00	---
b)	FF03-K17-Sial	hFF03-K17-Sial	1:1	218.75	---
			1:2	>250.00	---
			2:1	250.00	---
			1:5	>250	---
			5:1	>250.00	---

All sialic acid constructs were tested against Influenza A Virus/X31, a H3N2 virus. Tested compositions set a and b and their inhibition potential against X31 are summarized in Table 5.7. Peptides and peptide composition of set c showed no inhibition effect and are therefore not mentioned in Table 5.7. Highest inhibition potential was detected for pure hFF03-K17-Sial peptide, which showed an inhibition until lowest concentration of 12.23 µM. All other peptide compositions of set a (see Table 5.7) present lower concentrations of sialic acid moieties due to hetero assemblies by mixing decorated and undecorated peptides. However, no inhibition potential was observed up to concentrations of 51.5 µM for all mixtures beside the 1:1 mixture of hFF03-K17-Sial and hFF03, which showed very low inhibition with a Ki HAI of 51.50 µM. All other peptide sets included constructs with the peptide FF03 and/or peptide FF03-K17-Sial. Whereas no inhibition potential could be detected for all mixtures of 1:2 or 2:1 ratio of hFF03-K17-Sial and hFF03 (Table 5.7), as well as all constructs of set c (see Table 5.6). A weak inhibition was

observed for hFF03-K17-Sial and FF03-K17-Sial in 1:1, 1:2 and 2:1 ratio, respectively. This effect could be due to high concentration of sialic acid molecules carried by the assembled peptide fibers, as their concentration corresponds directly with the concentration of peptides decorated with the carbohydrate. Surprisingly, FF03-K17-Sial and all peptide mixtures of the set c showed no prevention of binding of Influenza A/X31 to blood cells.

Table 5.8. HAI titer constants Ki of control experiments without virus incubation of selected constructs of the sets a and c of sialic-acid conjugated coiled-coil peptides.

	Construct			***Ki HAI [µg/mL]***	***Ki HAI [µM]***
	Peptide		ratio		
a)	hFF03	hFF03-K17-Sial	0:1	>175.00	---
			1:0	41.02	12.07
			1:1	65.63	19.32
			5:1	65.63	19.31
c)	FF03	FF03-K17-Sial	0:1	>250.00	
			2:1	5.47	
			5:1	2.45	

As constructs including hFF03-K17-Sial and FF03 show weak inhibition, whereas FF03-K17-Sial itself does not inhibit binding of X31 to blood cells, hFF03-K17-Sial seems to cause the detected effects. Two main reasons could affect the inhibitory potential of the tested peptides. The geometry of the assemblies plays a crucial role to detect an inhibitory potential. As the hetero assemblies of hFF03-K17-Sial : FF03-K17-Sial show a very low effect, whereas hFF03-K17-Sial shows the best inhibitory results of all tested components the flexibility of the assemblies could be a reason for the high Ki HAI values of FF03-constructs (low inhibition). Another reason could be due to interactions of the peptide scaffolds with red blood cells. Therefore, control experiments without virus addition were performed to study the interaction of the constructs with erythrocytes. Results of control experiments are summarized in Table 5.8. Data show that agglutination could be observed for pure hFF03 with a Ki HAI of 12.07 µM, whereas hFF03-K17-Sial showed no interaction with red blood cells. Ki HAI values of FF03-constructs reveal that increasing amounts of

FF03 mixed with its sialic acid decorated variant leads to increasing interaction with red blood cells. This interaction is stronger for FF03 than for hFF03.

Comparing the amino acid composition and the helical wheel projections (see Figure 5.26) of the peptides, it is obvious that FF03 carries more positive charges by lysine-side chains in its solvent exposed domain. These charges could be reasonable for interaction with red blood cells, as also for hFF03 a similar, but lower effect was observed resulting in visible agglutination within the control experiments. It can be concluded that electrostatic interactions between positively charged side chains of both undecorated peptides in the outside of their peptide bundle and negatively charges cell membranes of erythrocytes led to interaction. This effect was previously reported for adhesion of cell membranes on poly-L-Lysine surfaces.[147] From this point of view it can be explained that control experiments demonstrated an interaction of the undecorated peptides with the erythrocytes. Comparing these results with the results of the control experiment of the sialic acid conjugated peptides it was shown that only the hFF03 conjugated variant has no interaction with the erythrocytes, which presents a lower amount of lysines than FF03 in its outer sphere. Conjugated to hFF03 sialic acid seems to have a “shielding” effect to the lysines. Moreover, the lysines alternate occupying positions *b* and *c* in FF03 have a higher accessibility if *f*-positions are “shielded” and could facilitate the interaction with negatively charged membranes.

To verify this hypothesis the galactose-conjugated hFF03 (discussed in chapter 5.2) was tested under the same conditions than the discussed peptide sets with sialic acid conjugated coiled-coil peptides. Like expected the galactose conjugated peptide showed no inhibitory effect, namely no sedimentation but agglutination when the construct was incubated with virus. In order to exclude the risk of interaction of positively charged side chains in *f*-positions of the peptide scaffold, the sequence was newly designed in order to prevent agglutination caused by positive charges at the outside of the coiled-coil bundle. Therefore, *f* positions of the coiled coil sequence of hFF03 were exchanged to the unpolar amino acid serine.

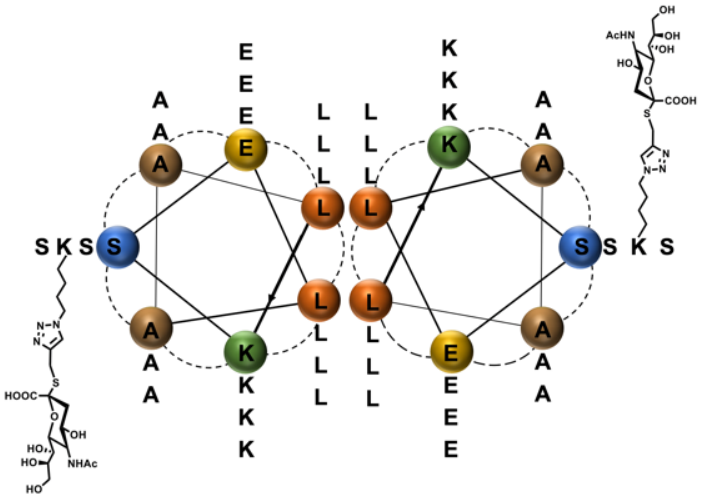

	1	2	3	4	5	6	7	8	9	10	11	12	13	14	15	16	17	18	19	20	21	22	23	24	25	26
	d	e	f	g	a	b	c	d	e	f	g	a	b	c	d	e	f	g	a	b	c	d	e	f	g	a
hFF03-*f*S Abz	L	K	S	E	L	A	A	L	K	S	E	L	A	A	L	K	**K**	E	L	A	A	L	K	S	E	L

Figure 5.33. Helical wheel projection and sequence of the re-designed peptide scaffold hFF03-fS-K17-Sial (table shows only the scaffold sequence without attached ligand in position 17).

Sialic acid conjugation occurs by CuAAC to azide-bearing lysine side-chain in position 17 as described above (Figure 5.28). CD-spectroscopy (spectra see appendix) showed that formation of α-helical conformation will not be interrupted by the attached sialic acid moiety. Testing this candidate for its ability to inhibit the Influenza A Virus binding showed no virus inhibition upon highest concentration of 150 µM and no agglutination in control experiments. The substitution of all *f*-positions in hFF03 with serine-residues led to exclusion of agglutination of erythrocytes. To further try to optimize the optimal conditions for IAV inhibition with sialic acid conjugated hFF03 a series of mixtures with hFF03-K17-Sial and hFF03-*f*S was tested according to the same conditions described above. For all testing of this set of peptide-mixtures the concentration of the peptide solution was set to 75 µM, which corresponds to a total peptide concentration of 250 µg. The concentration was halved because of results of all previously tested peptide sets show no inhibition for all non-conjugated coiled coil peptides. As hFF03-K17-Sial was the only coiled-coil peptide showing an inhibitory effect on IAV mediated cell binding, the ratios of the peptide set existing of hFF03-*f*S and hFF03-K17-Sial were chosen in low concentrations and are summarized in Table 5.9. However, the results of the HAI test with peptide mixtures of hFF03-*f*S and hFF03-K17-Sial showed no decrease of Ki HAI.

Table 5.9. Hemagglutination inhibition constants Ki HAI of tested peptide mixtures containing hFF03-fS and hFF03-K17-Sial incubated with Influenza Virus X31.

Construct			***Ki HAI [µM]***
Peptide		ratio	
hFF03-*f*S	hFF03-K17-Sial	1:0	>56.25
		1:1	56.25
		1:2	56.25
		2:1	>56.25
		1:5	>56.25
		5:1	>56.25

To finalize and sum up the second project of this thesis, we could show a promising approach to study several parameters like density of sialic acid groups and geometry and flexibility of the peptidic scaffold regarding Influenza A Virus inhibition simultaneously. Within this study different coiled-coil peptides were investigated and conjugated with a sialic acid moiety. Conjugation with sialic acid occurred by means of CuAAC, either with building block strategy by synthesis of a conjugated amino acid building block and by CuAAC on solid phase. Comparing both synthetic routes CuAAC on solid phase was found to be more efficient than building block strategy due to expensive purification of the synthesized amino acid and low yields. Finding the optimal strategy different coiled-coil peptides were conjugated to the carbohydrate to test the optimal peptide scaffold for Influenza A Virus inhibition. By mixing different peptides the optimal density of the sialic acid moieties was evaluated. Hemagglutination inhibition assays showed that of 23 tested peptides and peptide compositions only the candidate hFF03-K17-Sial showed an efficient Ki HAI value of 12.23 µM. Other candidates showed higher Ki HAI values and/or even no interaction with erythrocytes which may be due to electrostatic interactions with the partial positively charged peptide backbone. More investigations should be done to find the optimal geometry and density of presented sialic acid groups by the coiled-coil scaffold hFF03. To verify the “shielding” effect of the sialic acid group other *f*-positions to conjugate the carbohydrate to the peptides should be tested. Furthermore, the peptide should be equipped with two sialic acid moieties simultaneously to test whether an optimal geometry can be achieved to address hemagglutinin binding sites on the virus surface.

6 Summary and Outlook

Within this thesis, the potential of coiled-coil peptides as scaffolds for an extracellular matrix mimic or as an Influenza A Virus inhibitor were presented. The design and development of these peptide structures was the main goal. The final evaluation in biological assays as well as the determination of the structural parameters showed that hFF03-*b*A*c*A fulfills all needed parameters. With this in hand, an exactly tunable, reproducible and defined 3D scaffold can be built up to present ligands and – densities to the host and therefore enables the use as a biomaterial in the demonstrated applications.

To reach this aim, different coiled-coil systems were evaluated regarding their suitability to present relevant ligand and - densities without disturbing their self-assembly into stable fibers. The peptide hFF03-*b*A*c*A was exclusively the only synthesized peptide, which was able to form self-supporting hydrogels. Therefore, it was chosen to be decorated with biologically relevant peptide and carbohydrate ligands. These designed peptides were tested regarding their ability to build up hydrogels for three-dimensional scaffold formation. A small library was successfully ascertained and combined to build up complex networks, which present their covalently attached ligands within the three-dimensional structure of the hydrogel.

On the one side, the pure peptide hydrogels, as well as their mixtures were systematically studied regarding their morphology and structure and mechanical properties. Structural analysis by cryo-TEM and rheological experiments demonstrated that the peptide hydrogels are built of fiber-networks, which have a viscoelastic behavior. Further rheological characterizations revealed that stiffness of tested peptides hydrogels increases with temperature. The viability of these hydrogels was tested with NIH/3T3 cells and hMSCs. A high biocompatibility was demonstrated by viability assays of cultured NIH/3T3 populations on peptide hydrogels, which show excellent viability profiles. These results demonstrated that mixing different ligand bearing coiled-coil peptide hydrogels is a promising approach for the development of biomaterials. However, a low viability of hMSCs required the modification of the conditions and so higher tolerance of hMSCs to the coiled coil hydrogels has to be achieved.

On the other side, the conjugation of coiled-coil peptides with sialic acid ligands led to suitable scaffolds for inhibition of Influence A Virus binding to host cells. Different coiled-coil scaffolds and different ligand densities were studied to evaluate the most potent candidate for Influenza A Virus inhibition. Hemagglutination-inhibition assays revealed that sialic acid-conjugated hFF03-*b*A*c*A enables virus inhibition in the micromolar range.

Furthermore, control experiments showed interaction with erythrocytes of non-conjugated hFF03-*b*A*c*A and other conjugated and non-conjugated FF03 variants. To get more insights about this interaction, positive charged lysine was substituted to polar, uncharged serine into the solvent exposed positions f of the coiled-coil sequence of hFF03-*b*A*c*A. Control experiments of the peptide hFF03-*f*S without virus particles showed that the peptide not interacts with erythrocyte. These findings support the hypothesis that this interaction arises from positively charged lysine-residues in f-positions of the hFF03-*b*A*c*A. As an outlook, investigations should be done to evaluate the optimal ligand densities to address hemagglutinin-receptors on virus surface. Coiled-coil systems carrying several sialic acid ligands and/or the extension of the coiled-coil sequences are possible approaches to study optimal geometry and density of ligands. Also, investigations for heterodimeric coiled-coil systems, which initially assemble by mixing the second coiled-coil strain are promising to adapt their ligands and geometry based on the hemagglutinin-receptors presented by virus surface.

To finalize and perfect, hFF03-*b*A*c*A showed all needed parameters for both applications as a newly designed and synthesized coiled-coil peptide. The developed peptide hydrogels are providing a platform of tunable 3D materials for applications in tissue engineering and regenerative medicine, as commercially available 3D materials have big disadvantages like their reproducibility, their unknown composition and limited tunability. The herein presented system enables the adjustment of parameters like ligand type and density or the stiffness of the material. It complies the requirements of a 3D material to mimic the natural environment of cells. A big advantage of this system is its ease of synthesis and high reproducibility in forming chemically well-defined scaffolds. These unique properties of this system make it ideal to further develop formulations and materials for biological applications. As only a few examples of chemically well-defined and peptide-based 3D scaffolds exist, we decided to make an invention disclosure and to patent the herein described system. This enables us the development of materials for the use in (stem) cell culture and improvement of our current understanding of the extracellular matrix in the future.

As an outlook, further investigations should be done regarding the design of more complex hydrogels, which present the ligands of native ECMs. One strategy can be the exchange of the counter ion of the coiled-coil peptides. In the presented thesis the counter ion of the peptides was exchanged to chloride ions that led to a higher biocompatibility. Another possibility might be the exchange of TFA counter ion against acetate residues. As an alternative strategy, hFF03-K17-Man, the first carbohydrate conjugated coiled-coil hydrogel presented in this thesis, can be used for more detailed studies of the stem cell

fate. Further investigations are necessary to get more insights about their differentiation behavior and regarding more complex moieties. As an example, several polysaccharides were demonstrated to influence the differentiation behavior of stem cells, e.g. heparin-functionalized or chitosan-gelatin-chondroitin scaffolds. The modular units of these polymers could be promising to conjugate to the presented coiled-coil peptide, to increase the complexity of the presented ligands. Units of these carbohydrate derived from the described polysaccharides are presented in Figure 6.1.

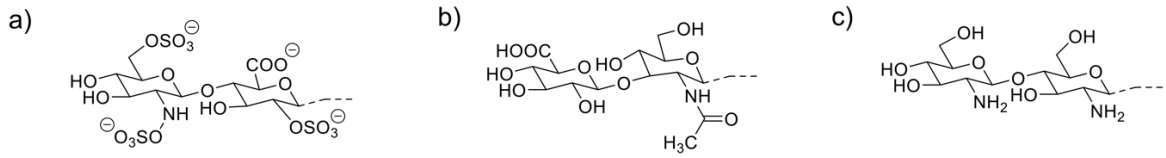

Figure 6.1. Suggested carbohydrate units of a) heparansulfate, b) hyaluronic acid and c) chitosan for conjugation to coiled-coil peptides to direct the fate of stem cells towards different specializations.

7 Materials and Methods

All reagents and solvents were used without further purification. Resins for solid-phase peptide synthesis were purchased from Novabiochem® (Merck KGaA, Darmstadt, Germany). Standard protected canonical orthogonal side-chain protected Fmoc-amino acids were purchased from ORPEGEN Peptide Chemicals GmbH (Heidelberg, Germany). Fmoc-L-Azido-Lysine was bought from Iris Biotech GmbH (Marktredwitz, Germany), Boc-Abz-OH was bought from Bachem (Bachem AG; Bubendorf, Switzerland) and Fmoc-Lys (Mtt)-OH was bought from Carbolution (Carbolution Chemicals GmbH, St. Ingbert, Germany). Coupling reagents for solid-phase peptide synthesis were obtained from Carbolution (Carbolution Chemicals GmbH, St. Ingbert, Germany), Novabiochem® (Merck KGaA, Darmstadt, Germany) or Sigma-Aldrich® (Merck KGaA, Darmstadt, Germany). Solvents used for peptide synthesis were synthesis grade and were purchased from Fisher Scientific (Schwerte, Germany), Acros Organics (Thermo Fisher Scientific, Geel, Belgium), VWR (VWR International GmbH, Darmstadt, Germany) or Merck (Merck Chemicals GmbH, Darmstadt, Germany). Solvents for preparative HPLC were HPLC or spectroscopy grade from Fisher Scientific (Schwerte, Germany) or Merck (Merck Chemicals GmbH, Darmstadt, Germany).

Deionized water for HPLC or buffer preparation was produced by a Milli-Q® Advantage A10 Ultrapure Water Purification System (Merck KGaA, Darmstadt, Germany).

TFA for peptide cleavage from resin was synthesis grade and taken from Sigma-Aldrich (Merck KGaA, Darmstadt, Germany), TFA for HPLC solvents was used as spectroscopy grade (Uvasol) and bought from Merck (Merck Chemicals GmbH, Darmstadt, Germany).

Further chemicals were purchased from Acros Organics (Thermo Fisher Scientific, Geel, Belgium), abcr GmbH (Karlsruhe, Germany), Alfa Aesar (Thermo Fisher (Kandel) GmbH, Karlsruhe, Germany), chemPUR (Karlsruhe, Germany), Fluorochem (Hadfield, United Kingdom), Merck (Darmstadt, Germany), Novabiochem® (Merck KGaA, Darmstadt, Germany), Sigma-Aldrich® (Merck KGaA, Darmstadt, Germany), Roth (Carl Roth GmbH + Co. KG, Karlsruhe, Germany) or VWR (Darmstadt, Germany) in highest quality.

Spectra/Por® Float-A-Lyzer® G2 (MWCO 500 $g*mol^{-1}$) were purchased from Roth (Carl Roth GmbH + Co. KG, Karlsruhe, Germany) and used according to suppliers' instructions.

Dulbecco's modified eagle medium with high glucose content (hG, 4.5 g/L) and Dulbecco's phosphate buffered saline (w/o calcium and magnesium) was purchased from Lonza (Lonza Group AG, Basel, Switzerland), cell counting Kit-8 (CCK-8) was bought from Sigma-Aldrich® (Merck KGaA, Darmstadt, Germany) and LIVE/DEAD™

Viability/Cytotoxicity Kit for mammalian cells was bought from Thermo Fisher Scientific (Thermo Fisher Scientific Inc., Waltham, Massachusetts, USA) and were used as received. NIH/3T3 cells were kindly provided by Dr. Marie Weinhart (Freie Universität Berlin) and hMSCs came from Sigma Aldrich (Catalogue Number SCR108, Merck KGaA, Darmstadt, Germany).

7.1 HPLC

7.1.1 Analytical HPLC

Semi-micro Chromaster HPLC system (fixer Fritz)

Analytical HPLC performed on semi-micro Chromaster HPLC system consisted of a VWR-Hitachi Chromaster HPLC 600 bar system (VWR International GmbH, Darmstadt, Germany) working with a low-pressure gradient. The system consists of a 5160 pump with a 6-channel solvent degasser, an organizer, a 5260 autosampler with a 20 µL sample loop, a 5310-column oven and a 5430-diode array detector with a high pressure semi-micro flow cell (5 mm). A Purospher® STAR RP-C18 endcapped UHPLC column (2 µm, 120 Å, 50x2.1 mm, Merck, Germany) was used. Eluents were deionized water (solvent A) and ACN (solvent B), both containing 0.1% (v/v) TFA. The column was heated to 24°C and a flow rate of 0.6 mL/min was used. UV-detection was performed at 220 nm for unlabeled peptides and at 320 nm for Abz-containing peptides. HPLC methods applied a linear gradient of ACN in water containing 0.1% TFA (v/v). Collected data were analyzed using EZChrom *Elite* software (Version 3.3.2 SP2, Agilent Technologies, Santa Clara, CA; USA).

Chromaster HPLC system (slow Fritz)

Analytical HPLC was performed on a VWR-Hitachi Chromaster HPLC 600 bar system (VWR International GmbH, Darmstadt, Germany). It works with a low-pressure gradient and consist of a 5160 pump with a 6-channel solvent degasser, a 5260 autosampler with a 100 µL sample loop, a 5310-column oven and a 430-diode array detector with a standard flow cell (10 mm optical path length). A Kinetex® C18 column (5 µm, 100 Å, 250 x 4.6 mm, Phenomenex®, Torrance, CA, USA) and a SecurityGuard™ Cartridge Kit (Ea, Phenomenex®, Torrance, CA, USA) equipped with a C18 catridge (4 x 3.0 mm) as pre-column was used. Eluents were deionized water (solvent A) and ACN (solvent B), both containing 0.1% (v/v) TFA. The column was heated to 24°C and a flow rate of 1 mL/min was used. UV-detection was performed at 220 nm for unlabeled peptides and at 320 nm for Abz-containing peptides. HPLC methods applied a linear gradient of ACN containing

0.1% TFA (v/v). Collected data were analyzed using EZChrom *Elite* software (Version 3.3.2, Agilent Technologies, Santa Clara, CA; USA).

LaChrom ELITE® HPLC system (Rosi)

The LaChrom ELITE®-HPLC-System was purchased from VWR-Hitachi (VWR International GmbH, Darmstadt, Germany) and consists of an organizer, two L-2130 HPLC-pumps with a solvent degasser, an L-2200 autosampler with a 100 µL sample loop, a L-2455 diode array flow detector and a high-pressure mixer. A Kinetex® C18 column (5 µm, 100 Å, 250 x 4.6 mm, Phenomenx®, Torrance, CA; USA) and a SecurityGuard™ Cartridge Kit (Ea, Phenomenex®, Torrance, CA, USA) equipped with a C18 catridge (4 x 3.0 mm) as pre-column was used. The flow rate was set to 1 mL/min. Eluents were deionized water (solvent A) and ACN (solvent B), both containing 0.1% (v/v) TFA. UV-detection was performed at 220 nm for unlabeled peptides and at 320 nm for Abz-containing peptides. HPLC methods applied a linear gradient of ACN containing 0.1% TFA (v/v). Collected data were analyzed using EZChrom *Elite* software (Version 3.3.2, Agilent Technologies, Santa Clara, CA; USA).

7.1.2 Preparative HPLC

Synthesized peptides were purified using a LaPrepΣ HPLC system (VWR International GmbH, Darmstadt, Germany), consisting of a LaPrepΣ LP 1200 preparative solvent pump with 100 mL titanium pump head, a ternary low-pressure gradient, a dynamic mixing chamber, a 6-port-3-channel injection valve with an automated preparative 10 mL sample loop, a LaPrepΣ LP 3101 1-channel UV-detector, a LaPrepΣ semi-preparative flow cell with 0.5 mm path length and a LaPrepΣ LP2016 17-port/1-channel fractionation valve. A Kinetex® C18 RP-HPLC-column with TMS endcapping (5 µm, 100 Å, 250x21.2 mm, Phenomenex®, Torrance, CA, USA) and a SecurityGuard™ Cartridge Kit (Ea, Phenomenex®, Torrance, CA, USA) equipped with a C18 catridge (4 x 3.0 mm) as pre-column was used. Eluents were deionized water (solvent A) and ACN (solvent B), both containing 0.1% (v/v) TFA. UV-detection was performed at 220 nm for unlabeled peptides and at 280 nm for purification of Fmoc-L-Lys-Sial-OH. Collected data were analyzed using EZChrom *Elite* software (Version 3.3.2 SP2, Agilent Technologies, Santa Clara, CA; USA).

Lyophilization

Synthesized compounds were lyophilized with a laboratory freeze dryer ALPHA 1-2 LD (Christ Gefriertrocknungsanlagen GmbH, Osterode im Harz, Germany) which was

connected to chemistry hybrid pump RC 6 (Vacuubrand GmbH + Co KG, Wertheim, Germany).

7.2 Analytical methods

Preparation of peptide stock solutions and concentration determination

Peptide stock solutions were prepared by dissolving lyophilized peptide powder in HFIP and treatment for 15 min in an ultrasound-bath. Then an aliquot of 10 µL was taken and evaporated in gentle stream of argon or N_2. The residue was dissolved in D-PBS containing 6M Guanidine-Hydrochloride (pH 7.4). If necessary, pH was adjusted to 7.4.

Determination of peptide concentration occurred by UV detection in half micro polymethylmethacrylate cuvettes. Spectra were automatically baseline corrected by the software with a reference spectrum of a sample containing solely buffer solution. Peptide concentrations were determined by measuring the absorbance of 4-amino-benzoic-acid containing peptides at 320 nm at pH 7.4. The concentration of the solution was calculated according to a recorded calibration curve of different concentrations of H_2N-Abz-Gly-OH x H_2O (Bachem AG, Bubendorf, Switzerland) in D-PBS (Lonza Group AG, Basel, Switzerland) containing 6M Guanidin-Hydrochloride at pH 7.4.

Sample preparation

For certain peptide concentrations the corresponding aliquots were completely evaporated and dissolved in the required solution. In case of hydrogel-mixtures the aliquots of desired peptide stock-solutions were mixed before evaporation. After evaporation peptides were dissolved in required volume of D-PBS (Lonza, w/o Mg^{2+}, Ca^{2+}), deuterated D-PBS or DMEM (Lonza, 4.5 g/L glucose). The pH of the solution was controlled and adjusted to pH 7.4 with 1M NaOH or in case of deuterated buffer with 1M NaOD. In case of pD adjustment, correlation between pH and pD was calculated according to Krężel et al.[148]

CD spectroscopy

CD spectroscopy was performed on a Jasco J-810 spectropolarimeter (JASCO Deutschland GmbH, Pfungstadt, Germany). For temperated samples, the instrument was connected to Jasco PTC-432S Peltier temperature control system and a HAAKE WKL water recirculatory (Thermo Electron GmbH, Karlsruhe, Germany). Data were analyzed using the software Spectra Manager J-700 (JASCO Deutschland GmbH, Pfungstadt,

Germany). Data processing was performed using the software OriginPro 2019b version 9.55 (OriginLab Corporation, Northampton, MA, USA).

CD spectra were recorded using Quartz Suprasil® cuvettes with a path length of 1.0 mm (Hellma Analytics, Müllheim, Germany) for samples with a concentration of >500 µM. CD spectra of peptide hydrogels were recorded using a Quartz Suprasil® cuvette with detachable windows and a path length of 0.1 mm (Hellma Analytics, Müllheim, Germany). Concentration of the peptides is given with the respective CD spectra. Measurements of the peptides were performed in D-PBS (pH 7.4) at 20°C and 37°C. If not stated otherwise the shown CD spectra are the mean of 3 independent measurements. CD spectra are background-corrected by subtraction of the corresponding buffer spectra at the corresponding temperature. During measurement an N_2-flow between 3.0 and 3.5 L/min was adjusted. Instrumental parameters of CD measurements are summarized in Table 7.1

Table 7.1. Instrumental parameters of CD spectroscopy.

Parameter	***adjustment***
sensitivity	Standard (100 mdeg)
start wavelength	250 nm
end wavelength	190 nm
data pitch	0.5 nm
scanning mode	continuous
scanning speed	100 nm/min
response	4 sec
band width	2 nm
accumulation	3

Electron Microscopy

For all electron microscopy measurements, the peptide samples were freshly prepared as needed in D-PBS and were performed ***in cooperation*** with the group of PD Dr. Christoph Böttcher (FU Berlin). The electron microscopy measurements were performed by PD Dr. Christoph Böttcher (FU Berlin) and Dr. Kai Ludwig.

Cryo-Transmission Electron Microscopy (cryo-TEM)

5 µl aliquots of the respective peptide solution were applied to pre-cleaned 200 mesh perforated carbon film-covered microscopical grids (R1/4 batch of Quantifoil, MicroTools GmbH, Jena, Germany). The grids were cleaned with chloroform and hydrophilized by 60 s glow discharging at 8 W in a BALTEC MED 020 device (Leica Microsystems, Wetzlar, Germany). Vitrifying of the samples occured by automatic blotting and plunge freezing with a FEI Vitrobot Mark IV (Thermo Fisher Scientific Inc., Waltham, Massachusetts, USA) using liquid ethane as cryogen. The vitrified samples were transferred to the autoloader of a FEI TALOS ARCTICA electron microscope (Thermo Fisher Scientific Inc., Waltham, Massachusetts, USA). The microscope is equipped with a high-brightness field-emission gun (XFEG), which operates at an acceleration voltage of 200 kV. Acquisition of the micrographs was carried out on a FEI Falcon 3 direct electron detector (Thermo Fisher Scientific Inc., Waltham, Massachusetts, USA) using a 70 µm objective aperture at a nominal magnification of 28,000 or 36,000 x, corresponding to a calibrated pixel size of 3.69 or 2.97 Å/pixel, respectively.

"Negative-stain" Transmission Electron Microscopy

5 µL aliquots of the respective peptide solution were absorbed onto hydrophilized 400 mesh carbon-coated collodium film that covered the copper grids. The supernatant fluid was removed by blotting with a filter paper, and the sample was allowed to dry in air. Contrast-enhancing heavy-metal stain solution (1% phosphotungstic acid at pH 7.4) was subsequently applied for 45 s and blotted again. A standard holder was used to transfer the dried samples into a FEI Talos L120C transmission electron microscope (Thermo Fisher Scientific Inc., Waltham, Massachusetts, USA) equipped with a LaB6 cathode. Images were taken at an accelerating voltage of 120 kV.

Mass Spectrometry

High resolution mass spectrometry was performed on an Agilent 6220 ESI-ToF LC-MS spectrometer (Agilent Technologies Inc., Santa Clara, CA, USA) and an Agilent Technologies 6230 TOF LC/MS spectrometer with ESI-injector (Agilent Technologies Inc., Santa Clara, CA, USA). Samples were dissolved either in pure ACN or a 1:1 (v/v) of ACN and water, both containing 0.1% TFA. Sample volumes between 50 and 100 µL were directly injected into the spray chamber using a syringe pump with a flow rate of 20 µL/min. Instrumental settings are summarized in table Table 7.2.

Table 7.2. Instrumental settings of high-resolution mass spectrometry.

Mass spectrometer	*Instrument settings*
Agilent 6220	gas temperature: 300°C flow drying gas: 5.0 L/min nebulizer: 20 psi voltage fragmentor: 200 V
Agilent 6230	gas temperature: 300°C flow drying gas: 5.0 L/min nebulizer: 20 psi voltage fragmentor: 250 V

The data was analyzed using the MassHunter Workstation software version B.02.00 or B.08.00 (Agilent Technologies Inc., Santa Clara, CA, USA). For calculation of monoisotopic mass series of peptides, respectively mass-to-charge values, Peptide Mass Calculator v3.2 was used. The ChemDraw Professional software Version 16.0.1.4 (Perkin Elmer Informatics, Inc., Waltham, MA, USA) was used to calculate molar masses of ligands and small molecules.

NMR-Spectroscopy

^{1}H- and ^{13}C-NMR spectra were recorded at a Bruker 600 MHz AVIII HD BRUKER (BRUKER, Billerica, MA, USA). ^{19}F-NMR spectra were recorded at a JEOL ECX400 (^{19}F: 376 MHz, JEOL, Tokyo, Japan). The MestReNova software version 10.0 (Mestrelab Research S. L., Santiago de Compostela, Spain) was used for depiction and analysis of NMR spectra.

Chemical shifts δ are given in parts per million (ppm) and are referenced to the deuterated solvent chloroform ($CDCl_3$, δ(1H)= 7.26 ppm, δ(13C)= 77.16 ppm)[149,150] for ^{1}H- and ^{13}C-NMR spectra. Values of chemical shifts of deuterated solvents are referenced to trimethylsilane as internal standard.[149,151] ^{19}F-NMR spectra were recorded in deuterium oxide (D_2O) and served as control of complete TFA/chloride exchange and were therefore not referenced to $CFCl_3$.

NMR data were reported in the following order: chemical shift, multiplicity (s = singlet, d = doublet, t = triplet, m = multiplet), integration as number of H-atoms, coupling constant *J* in Hertz (Hz).

Optical Microscopy

A Zeiss Observer Z1 microscope (Carl Zeiss Jena GmbH, Jena, Germany) combined with a well-plate holder was used for optical microscopy and fluorescence imaging. Images were acquired using a 10x objective in brightfield mode. Fluorescence imaging was performed in fluorescence mode. Microscopy images were depicted and analyzed with the software Zen 2 blue edition from Carl Zeiss Jena GmbH (Carl Zeiss Jena GmbH, Jena, Germany).

Oscillatory Rheology

Determination of mechanical properties of the peptide hydrogels was done by oscillatory rheology.

For all characterization of peptide hydrogels by oscillatory rheology the peptide samples were freshly prepared as needed for the measurement and were performed ***in cooperation*** with the group of Prof. Dr. Michael Gradzielski (TU Berlin). The experiments were performed by *M.Sc. Benjamin von Lospichl* at the Technische Universität Berlin.

Peptide hydrogels were measured within the plate-plate geometry (plate diameter 40 mm) at the physiological temperature of 37°C using a Bohlin 200 HR nano rheometer. The gap size is set to 200 µm.

Determination of the LVE regime of the sample and amplitude sweeps in the deformation-controlled mode (γ = 0.05 – 50%) was performed at a constant frequency of 1 Hz. The LVE regime is found for γ< 25%. For not overstressing the sample the deformation is fixed at γ = 2.0% for the subsequent oscillatory experiments. As a next step a frequency sweep is performed covering a frequency range from 0.05 to 50 Hz to determine the storage (G') and loss (G'') modulus.

UV-Spectroscopy

UV spectra were recorded using a Varian Cary 50 spectrophotometer (Varian Medical Systems, Palo Alto, CA, USA). Half micro polymethylmethacrylate cuvettes with a path length of 10 mm and a volume of 1.5 mL were used.

Small Angle Neutron Scattering (SANS)

For all SANS-experiments the peptide samples were freshly prepared as needed for the measurement and were performed ***in cooperation*** with the group of Prof. Dr. Michael

Gradzielski (TU Berlin). The SANS experiments were performed by *M.Sc. Benjamin von Lospichl* at Helmoltz Zentrum Berlin (HZB, Berlin, Germany) with the spectrometer V4 and at Laboratoire Leon Brillouin (LLB, Saclay, France) with the spectrometer PAXY.

7.3 Solid phase peptide synthesis (SPPS)

All peptides were synthesized from C- to N-terminus on solid support by standard Fmoc/*t*Bu protecting group strategy. Synthesis was performedat 0.05 mmol or 0.1 mmol scale on Fmoc-Leu-OH NovaSyn® TGA resin (0.2 g/mmol loading). In case of hFF03-fS the synthesis was conducted at 0.1 mmol scale on a resin (0.43 g/mmol loading).

The following protected standard canonical amino acids were used:

Fmoc-L-Ala-OH x H_2O, Fmoc-L-Arg(Pbf)-OH, Fmoc-L-Asn(Trt)-OH, Fmoc-L-Asp(O^tBu)-OH, Fmoc-L-Gln(Trt)-OH, Fmoc-L-Glu(O^tBu)-OH x H_2O, Fmoc-Gly-OH, Fmoc-L-His(Trt)-OH, Fmoc-L-Ile-OH, Fmoc-L-Leu-OH, Fmoc-L-Lys(Boc)-OH, Fmoc-L-Met-OH, Fmoc-L-Pro-OH, Fmoc-L-Phe-OH, Fmoc-L-Ser(^{t}Bu)-OH, Fmoc-L-Thr(^{t}Bu)-OH, Fmoc-L-Val-OH.

The following reagents and protected amino acids were used for synthesis: glutaric anhydride, 1-amino-1-deoxy-galactose, 1-amino-1-deoxy-mannose, prop-2-ynyl α-thiosialoside, Fmoc-L-Lys(Mtt)-OH, Fmoc-L-Lys(N_3)-OH, Boc-2-Abz-OH.

7.3.1 Automated peptide synthesis

Peptide synthesis of the described peptides was performed almost completely *via* automated peptide synthesis. Synthesis of described peptides was carried out using a fully automatic parallel peptide synthesizer Syro XP (Multi-Syn Tech GmbH, Witten, Germany), with an Activo-P11 Automated Peptide Synthesizer (Activotec, Cambridge, United Kingdom) or with a Liberty Blue™ (CEM Corporation, Matthews, NC, USA) microwave assisted peptide synthesizer.

Automated peptide synthesis on MultiSynTech Syro XP

Synthesis performed on a MultiSynTech Syro XP fully automated, parallel peptide synthesizer (Multi-Syn Tech GmbH, Witten, Germany) followed the protocol described in Table 7.3 and was conducted at 0.05 mmol scale.

Table 7.3. Synthesis protocol for automated peptide synthesis at 0.05 mmol scale using a MultiSynTech XP peptide synthesizer.

procedure		*reagents*	*time*
Start	Swelling	2.5 mL DMF	2 x 15 min
	Fmoc-deprotection	2 mL 2% piperidine, 2% DBU in DMF	4 x 5 min
	Washing	2.5 mL DMF	6 x 1 min
	Amino acid coupling	5 eq. Fmoc-X-OH + 0.5M NaClO4 in DMF 5 eq. TBTU in DMF 10 eq. DIPEA in NMP	60 min
	washing	2.5 mL DMF	1 x 1 min
Double coupling	Amino acid coupling	5 eq. Fmoc-X-OH + 0.5M NaClO4 in DMF 5 eq. TBTU in DMF 10 eq. DIPEA in NMP	60 min
	Washing	2.5 mL DMF	4 x 1 min
	Fmoc-deprotection	2 mL 2% piperidine, 2% DBU in DMF	4 x 5 min
	washing	2.5 mL DMF	6 x 1 min

Synthesis starts with two swelling steps of the resin for 15 min each in 2.5 mL DMF. Amino Acids were coupled by TBTU/HOBt/DIPEA activation. To prevent on resin aggregation during the coupling step, the corresponding amino acids were dissolved in a mixture of 0.5M $NaClO_4$ in DMF. Then, five equivalents of the corresponding amino acid, TBTU and HOBt and ten equivalents of DIPEA in NMP (1:2) were added to the resin. After one hour, the resin was washed with 2.5 mL DMF. Double coupling was repeated according to the same procedure, followed by four washing steps with 2.5 mL DMF. Fmoc-deprotection was performed by treatment of the resin with 2 mL of a solution of 2%(v/v) piperidine and

2% (v/v) DBU in DMF for five minutes. The deprotection step was performed four times, followed by six washing steps with 2.5 mL DMF.

Peptide synthesis on Activo-P11 Automated Peptide Synthesizer

Peptide synthesis performed on an Activo-P11 Automated Peptide Synthesizer (Activotec, Cambridge, United Kingdom) was performed according to the protocols in Table 7.4 and Table 7.5. Coupling of the amino acids was done either by activation by HOAt/DIC (see Table 7.4) or HATU/DIPEA or HBTU/DIPEA (see Table 7.5) activation. Coupling of amino acids by activation with HATU/DIPEA or HBTU/DIPEA followed the same procedure in both cases and is exemplarily explained by activation *via* HATU/DIPEA.

Table 7.4. Synthesis protocol for automated peptide synthesis at 0.05 mmol scale using an Activo-P11 peptide synthesizer with activation by HOAt/DIC.

	procedure	***reagents***	***time***
Start	Swelling	2.0 mL DMF	2 x 15 min
	Fmoc-deprotection	2.0 mL 2% piperidine, 2% DBU in DMF	4 x 5 min
	Washing	2.0 mL DMF	6 x 1 min
Double coupling	Double-coupling of amino acid	8 eq. Fmoc-X-OH, 8 eq. HOAt and 8 eq. DIC in 1.6 mL in 1.6 mL 0.5M NaO4Cl DMF	2x60 min
	Washing	2.0 mL DMF	5 x 1 min
	Fmoc-deprotection	2.0 mL 2% piperidine, 2% DBU in DMF	4 x 5 min
	washing	2.0 mL DMF	6 x 1 min

Prior to synthesis the resin was swelled two times with 2.0 mL of DMF for 15 min each. In case of 0.1 mmol scale synthesis the resin was swelled with 4.0 mL DMF for 15 min each. Synthesis with activation by HOAt/DIC was performed at 0.05 mmol scale. Therefore 8 equivalents of HOAt, 8 equivalents of DIC and 8 equivalents of the corresponding amino acid were dissolved in 1.6 mL of a 0.5M $NaClO_4$ in DMF, added to the resin and shaken for 1 hour. $NaClO_4$ was supplemented to the coupling solution to prevent aggregation during synthesis. Double coupling was performed under the same conditions. The resin

was washed five times with 2.0 mL DMF. Fmoc-deprotection was done by treatment of the resin with 2.0 mL of a solution of 2%(v/v) piperidine and 2% (v/v) DBU in DMF for 4 x 5 min followed by six washing steps with 2.0 mL of DMF.

In case of activation *via* HATU/DIPEA (see Table 7.5) synthesis was performed at 0.1 mmol scale. Therefore 5 eq. of amino acid, 4.9 eq. HATU and 10 eq. DIPEA in 3.2 mL of a 0.5M $NaClO_4$ DMF were added to the resin. $NaClO_4$ was supplemented to the coupling solution to prevent aggregation during synthesis. Amino acid coupling was performed for 30 min. Double coupling was performed under the same conditions. The resin was washed five times with 4.0 mL DMF. Fmoc-deprotection was performed by treatment of the resin with 4.0 mL of a solution of 2%(v/v) piperidine and 2% (v/v) DBU in DMF for 4 x 5 min followed by six washing steps with 4.0 mL of DMF.

Table 7.5. Synthesis protocol for automated peptide synthesis at 0.1 mmol scale using an Activo-P11 peptide synthesizer with activation by HATU/DIPEA.

	procedure	***reagents***	***time***
Start	Swelling	4.0 mL DMF	2 x 15 min
	Fmoc-deprotection	4.0 mL 2% piperidine, 2% DBU in DMF	4 x 5 min
	Washing	4.0 mL DMF	6 x 1 min
Double coupling	Double-coupling of amino acid	5 eq. Fmoc-X-OH, 4.9 eq. HATU and 10 eq. DIPEA in 3.2 mL 0.5M NaO4Cl DMF	2 x 30 min
	Washing	4.0 mL DMF	5 x 1 min
	Fmoc-deprotection	4.0 mL 2% piperidine, 2% DBU in DMF	4 x 5 min
	washing	4.0 mL DMF	6 x 1 min

Peptide synthesis on a CEM Liberty Blue™ Automated Microwave Peptide Synthesizer

Synthesis of hFF03, hFF03-K17(Mtt) and FF03-K17(N_3) were performed *via* automated microwave-assisted solid phase peptide synthesis on a CEM Liberty Blue™ Automated Microwave Peptide Synthesizer (CEM Corporation, Matthews, NC, USA) at 0.05 mmol or

0.1 mmol scale with Oxyma/DIC as activating agents. Prior to synthesis the resin was swelled in 5.0 mL of DMF for 30 min. Coupling of amino acids occurred in 5 eq. of the corresponding amino acid and 5 eq. of Oxyma/DIC. The first 19 amino acids of the corresponding sequences were coupled in single couplings, the rest of the sequences was coupled in double couplings.

Table 7.6. Synthesis protocol for automated peptide synthesis at 0.05 mmol scale using a CEM Liberty Blue TM automated microwave peptide synthesizer with activation by Oxyma/DIC.

	procedure	***reagents***	***conditions***
Start	Swelling	5 mL DMF	30 min
	Washing	4*4 mL DMF	5 s
	Fmoc-deprotection	3 mL 20 % piperidine in DMF	75 °C, 155 W, 10 s + 90 °C, 30 W, 50 s
	washing	3 mL DMF	3 x 5 s
coupling of amino acids	Single-coupling of first 19 amino acids	1.25 mL Fmoc-X-OH (0.2 M) in DMF (5 eq.) 1.0 mL activator (0.25 M DIC) in DMF (10 eq.) 0.5 mL activator base (0.5 M Oxyma) in DMF (5 eq.)	75 °C, 170 W, 15 s + 90 °C, 30 W, 110 s
	Double-coupling of last amino acids	2* [1.25 mL Fmoc-X-OH (0.2 M) in DMF (5 eq.) 1.0 mL activator (0.25 M DIC) in DMF (10 eq.) 0.5 mL activator base (0.5 M Oxyma) in DMF (5 eq.)]	2* [75 °C, 170 W, 15 s + 90 °C, 30 W, 110 s]

In case of synthesis at 0.05 mmol scale (see Table 7.6) 1.25 mL of a 0.2 M solution of the corresponding Fmoc-protected amino acid, 1.0 mL 0.25 M DIC in DMF (activator) and 0.5 mL 0.5M Oxyma in DMF (activator base) were added to the resin. The resin was treated for 15 s at 75 °C and a microwave energy of 170 W followed by heating up to 90 °C for 110 s and a microwave energy of 30 W. Fmoc-deprotection was done with 3.0 mL 20 % piperidine (v/v) in DMF for 10 s at 75 °C and a microwave energy of 155 W followed by heating up to 90 °C for 50 s at 30 W.

Table 7.7. Synthesis protocol for automated peptide synthesis at 0.1 mmol scale using a CEM Liberty Blue TM automated microwave peptide synthesizer with activation by Oxyma/DIC.

	procedure	*reagents*	*conditions*
start	Swelling	5 mL DMF	30 min
	Washing	4*4 mL DMF	5 s
	Fmoc-deprotection	3 mL 20 % piperidine in DMF	75 °C, 155 W, 10 s + 90 °C, 30 W, 50 s
	washing	3 mL DMF	3 x 5 s
coupling of amino acids	Single-coupling of first 19 amino acids	1.25 mL Fmoc-X-OH (0.2 M) in DMF (5 eq.) 1.0 mL activator (0.5 M DIC) in DMF (10 eq.) 0.5 mL activator base (1.0 M Oxyma) in DMF (5 eq.)	75 °C, 170 W, 15 s + 90 °C, 30 W, 110 s
	Double-coupling of last amino acids	2* [1.25 mL Fmoc-X-OH (0.2 M) in DMF (5 eq.) 1.0 mL activator (0.5 M DIC) in DMF (10 eq.) 0.5 mL activator base (1.0 M Oxyma) in DMF (5 eq.)]	2* [75 °C, 170 W, 15 s + 90 °C, 30 W, 110 s]

The 0.1 mmol scale (see Table 7.7) peptide synthesis was performed with 1.25 mL of a 0.2 M solution of the corresponding Fmoc-amino acid. Then 1.0 mL 0.5 M DIC in DMF (activator) and 0.5 mL 1.0 M Oxyma in DMF (activator base) were added to the resin and treated at 75 °C with a microwave energy of 170 W for 15 s, followed by heating up the reaction mixture to 90 °C and decreasing the microwave energy to 30 W for 110 s. Fmoc-deprotection occurred with 3.0 mL 20 % piperidine (v/v) in DMF at 75 °C and a microwave energy of 155 W for 10 s followed by heating up to 90 °C for 50 s at 30 W.

7.3.2 Manual Peptide Synthesis

Conditions for manual peptide synthesis are described in the following parts of this section individually. Polypropylene syringe reactors (10 mL) with plunger and polyethylene frit (MultiSynTech GmbH, Witten, Germany) were used. After washing the resin with DCM and DMF, each two times, the resin was allowed to swell in 5 mL of DMF for 30 min. The cycle of peptide synthesis started with treatment of the resin with 3 mL of a solution of 2%

piperidin (v/v), 2% DBU (v/v) in DMF three times for 5 min. After three washing steps, either with DMF or DCM, the following coupling step was carried out as described in the next sections for each ligand individually.

Manual coupling of Boc-2-amino-benzoic acid

In case of synthesis of peptide *via* automated peptide synthesis with the Syro XP synthesizer, coupling of boc-2-amino-benzoic acid occurred manually. Eight equivalents of boc-2-amino-benzoic acid with respect to resin loading were mixed with eight equivalents of HATU and twice the amount of DIPEA in 4 mL DMF. The mixture was shaken for 30 min. In case of coupling with HBTU the same procedure as described for HATU was performed.

Manual coupling of Fmoc-L-Lysine (Mtt)

Manual coupling of Fmoc-L-Lysine (Mtt) was performed in four equivalents relative to resin loading. The amino acid was mixed with four equivalents of HATU and twice the amount of DIPEA in 4 mL DMF. The mixture was shaken for 30 min. In case of coupling with HBTU the same procedure as described for HATU was performed.

Manual coupling of Fmoc-L-Lys-Sial-OH

Manual coupling of Fmoc-L-Lys-Sial-OH was conducted in 1.2 equivalents relative to resin loading. Therefore, the amino acid was dissolved in 0.8 mL DMF and mixed with a solution containing 1.1 equivalent of HATU in 0.2 mL. Afterwards, 2.2 equivalents of DIPEA were added to this mixture, the complete solution was added to the resin and was shaken for 1.5 h. Double coupling was done by the same conditions.

Deprotection of Mtt-protected NH_2-Group in Lysine-Side-Chain

Cleavage of the methyltrityl-group in lysine-side chain was performed by treatment of the resin with 5 mL of a cleavage cocktail containing 1 % MeOH (v/v), 1 % TFA (v/v) in DCM for 1 min. Afterwards the solvent was removed (how?) and the resin was treated again with 5 mL of the cleavage cocktail overnight. After removing the solvent, the resin was washed with 5 mL DMF, 5 mL 10 % DIPEA (v/v) in DMF, three times with 5 mL DMF and three times with 5 mL DCM.

Manual coupling of glutaric anhydride

To couple the amino-sugar building blocks the amino-group in the side-chain of lysine 17 of FF03 and hFF03 had to be switched to carboxy functionality. Three equivalents of glutaric anhydride were coupled to the lysine-side chain by the aid of catalytic amounts of DIPEA for 3h at room temperature. After finishing the reaction, the resin was washed 3 times with 5.0 mL of DMF to couple the amino-functionalized sugar.

Manual coupling of 1-amino-1-deoxy-hexoses

Coupling of 1-amino-1-deoxy-galactose and 1-amino-1-deoxy-mannose was performed according to the same procedure. The procedure will be explained exemplarily by coupling of 1-amino-1-deoxy-mannose. After switching the amino-functionality of lysine side-chain to COOH, the peptide resin was treated with a mixture of three equivalents of COMU and six equivalents of DIPEA in DMF at 40°C in an ultrasound bath for 1 min to activate the carboxy functionality on resin. Afterwards three equivalents of 1-amino-1-deoxy-mannose in DMF were coupled for 30 min at 40°C with ultrasound treatment. After finishing the reaction, the resin was washed with 5.0 mL DMF and DCM, each three times.

On-resin CuAAC of prop-2-ynyl α-thiosialoside

Copper assisted azide-alkyne cycloaddition was performed according to the literature.[143] The synthesis is described for coupling of prop-2-ynyl α-thiosialoside to 0.05 mmol peptide resin. For this purpose, 5 eq. of prop-2-ynyl α-thiosialoside (136.29 mg, 0.25 mmol), 1 eq. $CuSO_4 \cdot 5\ H_2O$ (12.48 mg, 0.05 mmol), 1 eq. sodium ascorbate (9.91 mg, 0.05 mmol) and 8 eq. DIPEA (69.67 µL, 0.40 mmol) were dissolved in 5 mL of argon flushed DMF. The solution was added to the resin presenting the corresponding azide-functionality in lysine side-chain (K17) and shaken overnight. Afterwards the solvent was removed (how?) and resin was washed one after another with MeOH (3x5 mL), 0.5% (w/v) EDTA in DMF (3x5 mL), DMF (3x5 mL) and DCM (3x5 mL).

Cleavage of acetyl-groups and methylester-hydrolysis of protected sialic acid moieties

After cleavage from the resin it is necessary to also cleave the acetyl- and methylester groups of the corresponding sialic acid moiety before purification. The procedure was performed according to protocols from the literature.[144,145] The peptide was dissolved in 50 mL MeOH and an aqueous solution of 5 mM NaOH was added to get a final pH value

between 10 and 11. The solution was stirred 3.5 h at room temperature. Then the solution was neutralized with 90 mM AcOH to pH 6. After removing the solvent under reduced pressure, the residue was dissolved in 30 mL of an aqueous solution of 5 mM NaOH and pH was adjusted to 11.5 for methylester hydrolysis. The solution was allowed to stir for another 4 h. Afterwards the pH of the solution was adjusted to pH 6 using 90 mM AcOH and lyophilized.

7.4 Organic Synthesis

Synthesis of (*S*)-2-((((9*H*-fluoren-9-yl)methoxy)carbonyl)amino)-6-(4-((((2*S*,4*S*,5*R*,6*R*)-5-acetamido-4-acetoxy-2-(methoxycarbonyl)-6-((1*S*,2*R*)-1,2,3-triacetoxypropyl)tetrahydro-2*H*-pyran-2-yl)thio)methyl)-1*H*-1,2,3-triazol-1-yl)hexanoic acid (3)

Synthesis of (*S*)-2-((((9*H*-fluoren-9-yl)methoxy)carbonyl)amino)-6-(4-((((2*S*,4*S*,5*R*,6*R*)-5-acetamido-4-acetoxy-2-(methoxycarbonyl)-6-((1*S*,2*R*)-1,2,3-triacetoxypropyl)tetrahydro-2*H*-pyran-2-yl)thio)methyl)-1*H*-1,2,3-triazol-1-yl)hexanoic acid (3) (Synthesis scheme see Figure 5.27) was performed according to the protocol for CuAAC of prop-2-ynyl α-thiosialoside to N_3-functioanlities described in literature.[81]

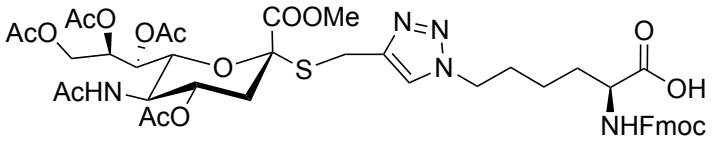

Figure 7.1. Chemical structure of the synthesized Fmoc-l-Lys-Sial-OH (3).

Fmoc-azidolysin (27.79 mg, 0.070 mmol, 1.0 eq.) was dissolved in 2.0 mL of THF:H_2O (1:1, v/v) followed by addition of prop-2-ynyl α-thiosialoside (50 mg, 0.090 mmol, 1.3 eq) dissolved in 0.5 mL THF and stirred in a 10 mL three-necked flask. A few drops of DMF were added to the solution to dissolve the educts completely. Then $CuSO_4 \cdot 5\ H_2O$ (3.52 mg, 0.014 mmol, 0.2 eq.) was dissolved in 0.1 mL H_2O and added to a solution of sodiumascorbat (27.93 mg, 0.140 mmol, 2.0 eq.) in 0.2 mL H_2O. This solution was slowly added to the stirring reaction mixture. After flushing the reaction mixture with argon for five minutes the reaction mixture was allowed to stir for three days at room temperature under argon atmosphere until HPLC revealed complete conversion of the starting material. The solvent was evaporated under reduced pressure. The residue was dissolved in 50 mL of $CHCl_3$ and extracted with a solution of 2% EDTA in H_2O (5x50 mL, w/v). The aqueous

phase was again extracted with $CHCl_3$ and the combined organic phases were dried over Na_2SO_4. The solvents were evaporated under reduced pressure and the residue was dried in vacuo to get rid of remaining DMF traces.

The dried residue was dissolved in 4 mL of ACN and filtered through a 0.45 µm Acrodisc® syringe filter with a GHP membrane (Pall Corporation, Port Washington, NY, USA). Purification of the crude amino acid was performed by reversed phase HPLC. Organic solvent of combined fractions was evaporated under reduced pressure and lyophilized, obtaining 14.9 mg (0.016 mM, 22.5%) of a white solid.

Purity of the amino acid was confirmed *via* analytical HPLC on a LaChrom ELITE® HPLC system. Identification of the product occurred by high resolution ESI-ToF-MS and NMR-spectroscopy (^1H, ^{13}C).

ESI-MS (ES+) $[M+H]^+$ for $C_{44}H_{53}N_5O_{16}S$ (939.99) calcd.: 940.3208 obs.: 940.3359

^{1}H-NMR (600 MHz, $CDCl_3$): δ = 7.74 (d, 2H *J* = 7.5 Hz), 7.62 – 7.54 (m, 2H), 7.38 (t, 2H, *J* = 7.5, 1.3 Hz), 7.29 (t, 2H, *J* = 7.4, 1.1 Hz), 5.64 (d, 1H, *J* = 7.8 Hz), 5.57 (d, 1H, *J* = 10.0 Hz), 5.46 – 5.42 (m, 1H), 5.31 (dd, 1H, *J* = 8.3, 2.2 Hz), 4.87 (td, 1H, *J* = 11.1, 4.6 Hz), 4.40 – 4.27 (m, 7H), 4.20 (t, 1H, *J* = 6.9 Hz), 4.09 – 3.93 (m, 5H), 3.92 – 3.86 (m, 1H), 3.73 – 3.64 (m, 3H), 2.71 (dd, 1H, *J* = 12.7, 4.7 Hz), 2.16, 2.14, 2.01 (d, 13H, *J* = 5.9 Hz), 1.87, 1.82 – 1.75 (m, 4H), 1.44, 1.27 (d, 3H, *J* = 30.9 Hz).

^{13}C-NMR (151 MHz, $CDCl_3$): δ = 171.31, 171.08, 170.86, 170.36, 143.85, 141.40, 127.85, 127.20, 120.12, 74.21, 69.57, 62.72, 53.22, 47.27, 23.20, 21.37, 20.95, 20.88.

7.5 Cleavage from the resin and purification

Test cleavage to monitor synthetic progress

To monitor completeness of coupling and the progress of peptide synthesis test cleavages were performed with a small amount of peptide resin (approximately. 250 mg) in a small reaction vessel. The resin beads were treated with 100 µL of cleavage cocktail containing 95% TFA (v/v), 3% H_2O (v/v) and 2% TIS (v/v) for 2.5 – 3 h in a shaker. The peptide was then precipitated with 1.5 mL ice-cold diethyl ether, centrifugated and ether decanted. The precipitate was dissolved in a mixture of H_2O/ACN containing 0.1% TFA (1:1, v/v). The resin beads were separated *via* centrifugation and the solution containing the peptide was injected into analytical HPLC to monitor the synthetic progress.

Full cleavage

After full length synthesis of the peptide was finished, the resin was dried in vacuo. The dried resin was shaken with a cleavage cocktail (2.5 mL per 150 mg resin) containing 95% TFA (v/v), 3% H_2O and 2% TIS (v/v) for 3 - 3.5 h at room temperature. In case of the peptide hFF03-K17-SP the dried resin was shaken with a cleavage cocktail (2.5 mL per 150 mg resin) containing 82.5% TFA (v/v), 5% H_2O (v/v), 5% Phenol (w/v), 5% Thioanisol (v/v) and 2.5% 1,2-Ethandithiol (EDT) (v/v). The cleavage cocktail containing the peptide was filtered and the supernatant was collected in a 100 mL flask, then the resin was washed with 2.0 mL TFA and 5 mL DCM and combined with the cleavage cocktail. Excess of solvent was removed by under reduced pressure and peptide was precipitated by addition of 75 mL ice-cold diethyl ether. Diethyl ether was centrifuged (4°C, 4.4 rpm, 5 min) to separate the precipitate from solvent. The peptide residue was again washed with ice-cold diethyl ether (50 mL), centrifuged and the solid was dried in vacuo.

Purification

The crude peptides were dissolved in H_2O/ACN (95%/5%, v/v) containing 0.1% TFA giving a final concentration of ~30 mg/mL. The content of ACN was increased when solubility problems of the peptides occurred. To increase the pH of the solution a few µL of 1M NaOH were added to get a final pH of ~ 4-5. Purification of the peptides was performed by reversed phase HPLC with a Kinetex ® C18 column (5 µm, 100 Å, 250x21.2 mm, Phenomenex®, Torrance, CA, USA) using a linear gradient of ACN in H_2O containing 0.1% TFA. The peptide solutions were filtered through a 0.45 µm Acrodisc® syringe filter with GHP membrane (Pall Corporation, Port Washington, NY, USA) prior to injection. After filtration the syringe filter was washed with ~1.0 mL of H_2O/ACN (1:1, v/v) containing 0.1% TFA (v/v) and combined with the peptide solution. Per run a maximum of 70 mg crude peptide dissolved in 3.0 mL of solvent was injected. Analysis of the collected fractions occurred *via* analytical HPLC on the semi-micro Chromaster system. Fractions of the same peptide were combined. After evaporation of ACN under reduced pressure, the remaining aqueous solution was lyophilized yielding the peptides as white powder. Purity of the peptides was confirmed *via* analytical HPLC on a LaChrom ELITE® HPLC system. Identification of the peptides occurred by high resolution ESI-ToF-MS.

Exchange of TFA against chloride

To increase biocompatibility of the synthesized peptides TFA counterion of NH-groups resulting from full cleavage was exchanged against chloride according to literature

established protocols.[152] In the context of this thesis TFA was exchanged against chloride in the following peptides: hFF03, hFF03-K17-Man and hFF03-K17-RGD.

Pure peptides were dissolved in water at a concentration of 0.52 mM. Afterwards 6 M HCl was added to the peptide solutions to give a final concentration of 7.5 mM HCl. The solutions were allowed to stir at room temperature for 1 minute and lyophilized. This procedure was repeated 5 times. Completeness of TFA exchange was verified by ^{19}F-NMR in deuterium oxide.

Dialysis of peptides after ion-exchange

Peptides were dialyzed to get rid of abundant salts to decrease the risk of interference of excess of different salts.

Dialysis of peptides was achieved by Spectra/Por® Float-A-Lyzer® (Carl Roth) with molecular weight cut-off of 500 Da and performed according to the instructions of the company. Peptides were dialyzed against water over three days. Water was changed thrice a day. After completion, the peptide solutions were freeze dried.

7.6 Cell culture

NIH/3T3 cells

NIH/3T3 cells were cultured in DMEM culture medium containing high glucose (4.5 g/L, hG), 10% FCS and 1% P/S in a humidified incubator at 37 °C under 5.0% CO_2 atmosphere. They were grown in 175 cm^2 cell culture flasks and medium was changed every second to third day. Upon confluency of 70 – 80% the cell population was subcultured according to the detected cell number.

hMSCs

hMSCs were cultured in DMEM culture medium containing high glucose (4.5 g/L, hG), 10% FCS, 1% P/S and 1 ng/mL bFGF in a humidified incubator at 37 °C under 5.0% CO_2 atmosphere. They were grown in 25 cm^2 cell culture flasks and medium was changed every second day.

7.7 Cytotoxicity assay by use of Cell Counting Kit-8 (CCK-8)

Cytotoxicity studies of NIH/3T3 cells cultured on coiled-coil peptide hydrogels

A suspension of NIH/3T3 fibroblasts in DMEM (hG, 10% FCS, 1% P/S) was seeded in a transparent, tissue-culture treated 96-well plate with a *Chimney-Wall*. The well-plate was preloaded with the peptide hydrogels. In case of hydrogel candidates summarized in Table 5.3 (section 5.2.2) cells were seeded in a density of $1.00 \cdot 10^4$ per well suspended in an overall volume of 100 µL. In case of hydrogel candidates summarized in of section 5.2.3 cells were seeded in a density of $2.00 \cdot 10^3$ per well suspended in an overall volume of 100 µL. After 24h and 72h, respectively, 10 µL of CCK-8 solution were added to each well. After 90 min of incubation at 37 °C under 5.0% CO_2-atmosphere, absorbance at 450 nm was measured using a Tecan Infinite® 200PRO microplate reader. Hydrogel candidates were tested in triplicates per experimental run. For hydrogel candidates summarized in Table 5.3 (section 0) three experimental runs were performed. For hydrogel candidates discussed in section 5.2.3one experimental run was performed.

hMSCs

A suspension of hMSCs in DMEM (hG, 10% FCS, 1% P/S, 1 ng/mL bFGF) was seeded in a transparent, tissue-culture treated 96-well plate with a *Chimney-Wall*. The well-plate was preloaded with the peptide hydrogels. Cells were seeded in a density of $1.80 \cdot 10^3$ per well suspended in an overall volume of 100 µL. After 24h and 72h, respectively, 10 µL of CCK-8 solution were added to each well. After 90 min of incubation at 37 °C under 5.0% CO_2-atomosphere, absorbance at 450 nm was measured using a Tecan Infinite® 200PRO microplate reader. One experimental run was performed in triplicates per hydrogel candidate.

Cytocompatibility of tested hydrogel candidates of NIH/3T3 cells and hMSCs *via* live-dead-staining

To study cytocompatibility of NIH/3T3 cells and hMSCs cultured on coiled-coil based peptide hydrogels, live-dead-staining was performed using LIVE/DEAD® Viability/Cytotoxicity Kit for mammalian cells to discriminate live cells from dead cells. The Kit includes stock solutions of Calcein AM (fluoresces green inside living cells) and ethidium homodimer-1 (fluoresces red inside dead cells). Then 20 µL of the supplied ethidium homodimer-1 solution and 5 µL of the supplied Calcein AM solution were diluted

together to 1.00 mL to D-PBS (w/o Mg^{2+}, Ca^{2+}). Afterwards10 µL of this solution were added to each hydrogel candidate 20 minutes prior to fluorescence imaging. During this time the plate was covered with aluminum foil to prevent photo bleaching of the dyes.

7.8 Hemagglutination Inhibition tests

Hemagglutination inhibition tests were performed to test the inhibitory potential of coiled-coil peptides against binding of Influenza A Virus/X31 to erythrocytes.

For all HAI tests the peptides were mixed out of HFIP stock solutions and evaporated by a gentle N_2-stream. The peptide samples were freshly prepared directly before starting the experiment by dissolving the peptides in certain amount of PBS to achieve a final total peptide concentration of 150 µM. The measurement was performed ***in cooperation*** with the group of Prof. Dr. Andreas Herrmann (HU Berlin). The experiments were performed by *M.Sc. Malte Hilsch* at the Institute of Biology of the Humboldt-Universität zu Berlin (IfB, HUB, Berlin, Germany).

A twofold serial dilution of each peptide candidate was pipetted into a 96-well plate. Then, a fixed amount of 4HA Units X31 virus (~$4 \cdot 10^7$ virus particles) was added to each well and allowed to incubate for 30 min at rt under gently agitation. Afterwards 50 µL of a1% human erythrocyte solution was added and further incubated for 60 min at rt without shaking. The results were recorded by visible sedimentation or agglutination at the respective concentration of peptide solution. The Ki HAI reflects the lowest amount of an inhibitor which induced inhibition of virus binding to erythrocytes.

7.9 Coiled-coil peptide datasheets

hFF03

Abz-LKKELAALKKELAALKKELAALKKEL-OH

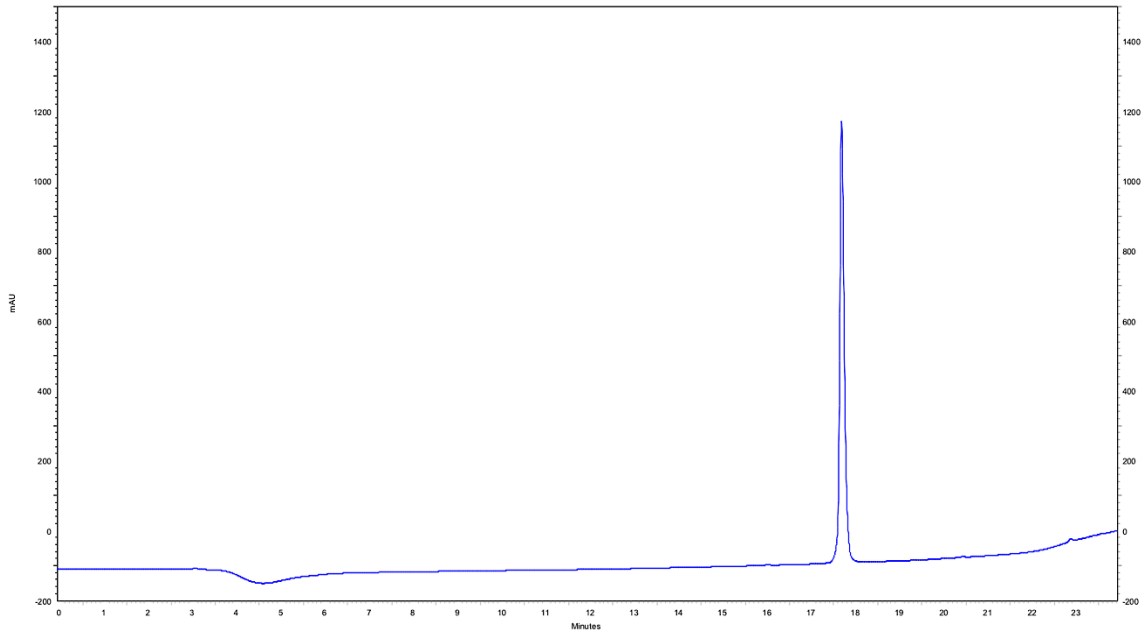

Analytical HPLC

Gradient: 5% ACN (0.1 %TFA) to 70 % ACN in Water (18 min), Rosi

Retention time: 17.8 min

ESI-ToF-MS

ESI-HRMS (m/z)	*Calculated mass (monoisotopic)*	*Observed mass*
$[M+2H]^{2+}$	1505.9956	1505.9489
$[M+3H]^{3+}$	1004.3330	1004.3037
$[M+4H]^{4+}$	753.5017	753.4801

hFF03-fA

Abz-LKAELKELKAELEKLKAELKELKAEL-OH

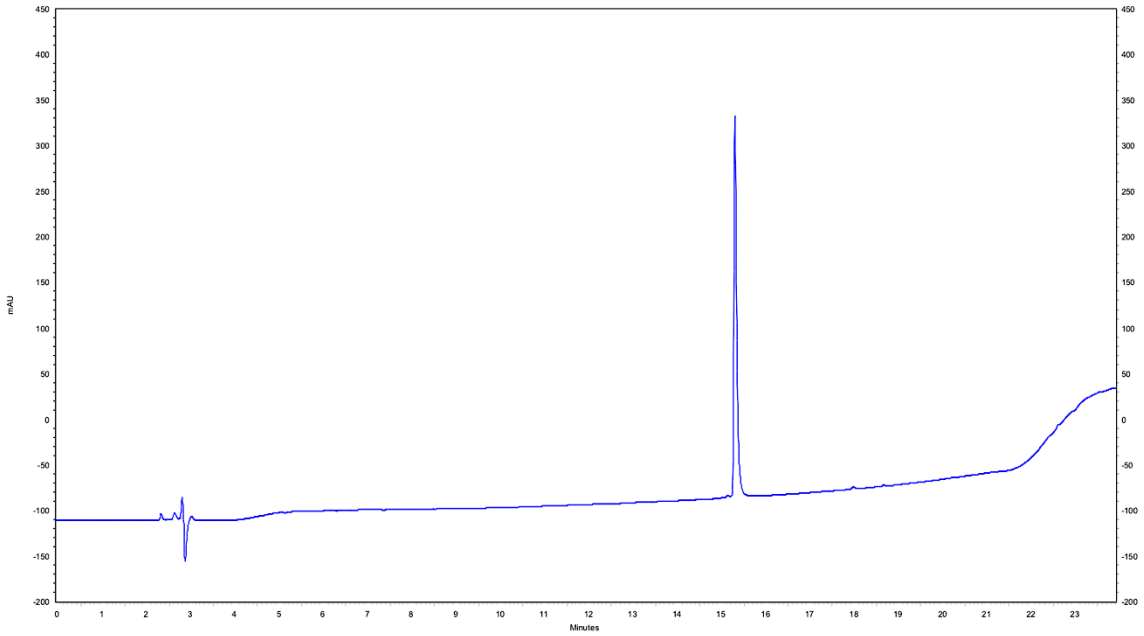

Analytical HPLC

Gradient: 5% ACN (0.1 %TFA) to 70 % ACN in Water (18 min), slow Fritz

Retention time: 15.4 min

ESI-ToF-MS

ESI-HRMS (m/z)	*Calculated mass (monoisotopic)*	*Observed mass*
$[M+3H]^{3+}$	1043.3192	1043.2907
$[M+4H]^{4+}$	782.7414	782.7199
$[M+5H]^{5+}$	626.3946	626.3780

***hFF03-b*AcA*f*A**

Abz-LKAELAALKAELAALKAELAALKAEL-OH

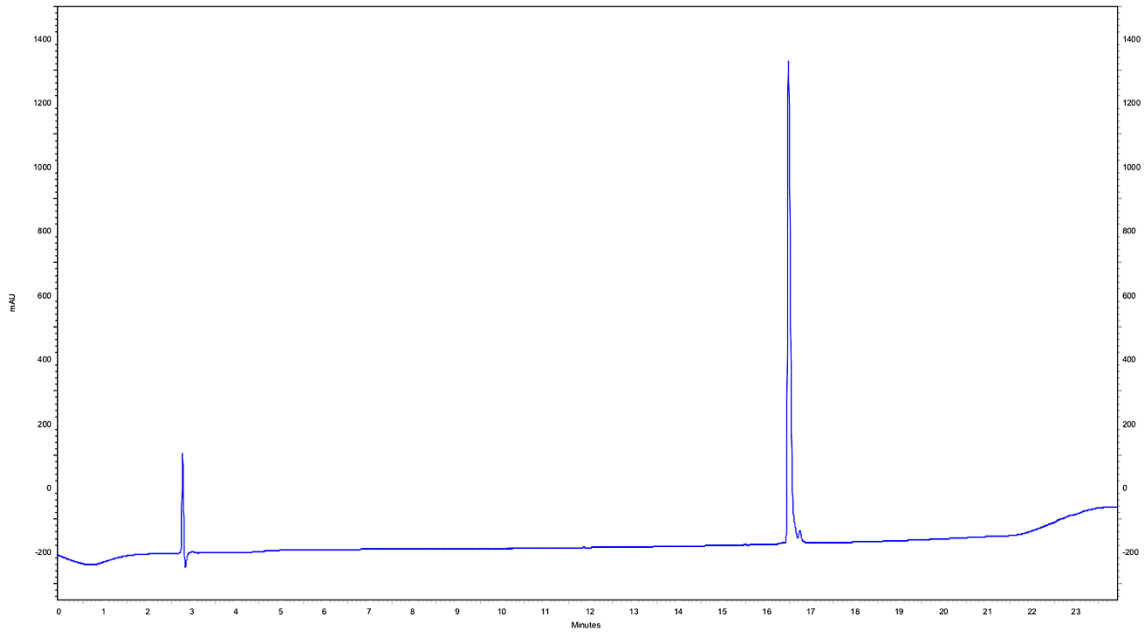

Analytical HPLC

Gradient: 5% ACN (0.1 %TFA) to 70 % ACN in Water (18 min), slow Fritz

Retention time: 16.6 min

ESI-ToF-MS

ESI-HRMS (m/z)	*Calculated mass (monoisotopic)*	*Observed mass*
$[M+2H]^{2+}$	1391.8799	1391.8293
$[M+3H]^{3+}$	928.2559	928.2252
$[M+4H]^{4+}$	696.4439	696.4205

***E-hFF03-b*AcA**

Abz-LEKELAALEKELAALEKELAALEKEL-OH

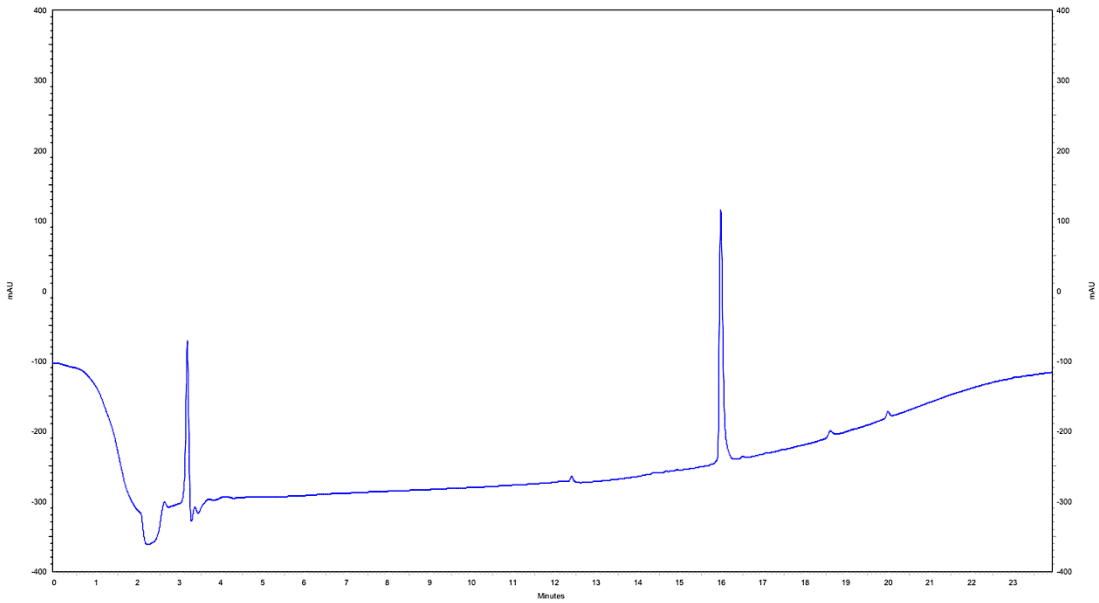

Analytical HPLC

Gradient: 5% ACN (0.1 %TFA) to 100 % ACN in Water (18 min), Rosi

Retention time: 16.1 min

ESI-ToF-MS

ESI-HRMS (m/z)	*Calculated mass (monoisotopic)*	*Observed mass*
$[M+2H]^{2+}$	1507.8909	1507.8433
$[M+3H]^{3+}$	1005.5965	1005.5664
$[M+4H]^{4+}$	754.4493	754.4284

K-hFF03-bAcA

Abz-LKKKLAALKKKLAALKKKLAALKKKL-OH

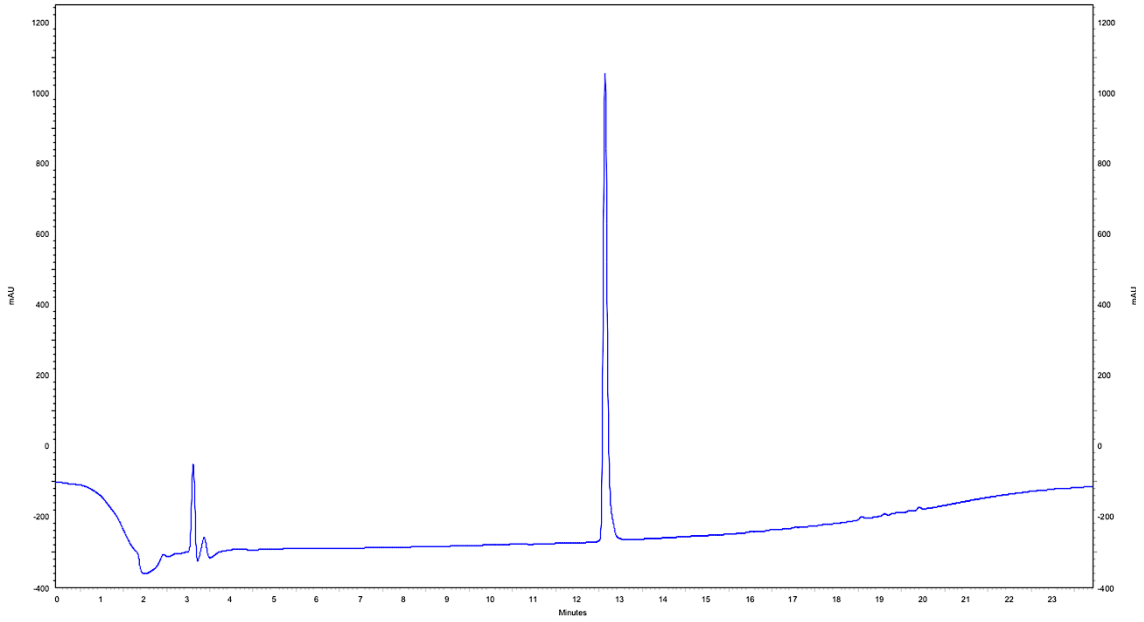

Analytical HPLC

Gradient: 5% ACN (0.1 %TFA) to 100 % ACN in Water (18 min), Rosi

Retention time: 12.7 min

ESI-ToF-MS

ESI-HRMS (m/z)	*Calculated mass (monoisotopic)*	*Observed mass*
$[M+2H]^{2+}$	1504.1004	1504.0536
$[M+3H]^{3+}$	1003.0695	1003.0401
$[M+4H]^{4+}$	752.5541	752.5325

hFF03-K17-RGD

Abz-LKKELAALKKELAALKK(-RGD) ELAALKKEL-OH

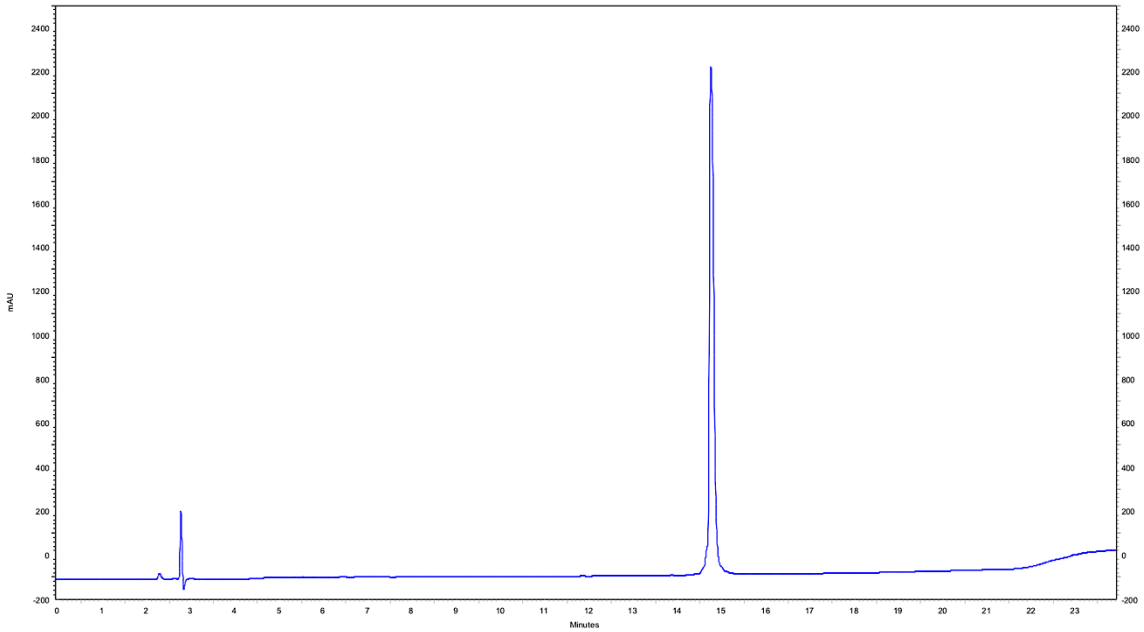

Analytical HPLC

Gradient: 5% ACN (0.1 %TFA) to 70 % ACN in Water (18 min), slow Fritz

Retention time: 14.8 min

ESI-ToF-MS

ESI-HRMS (m/z)	*Calculated mass (monoisotopic)*	*Observed mass*
$[M+2H]^{2+}$	1670.0757	1670.0205
$[M+3H]^{3+}$	1113.7197	1113.6831
$[M+4H]^{4+}$	835.5417	835.5148

hFF03-K17-Man

Abz-LKKELAALKKELAALKK(-GA-Man) ELAALKKEL-OH

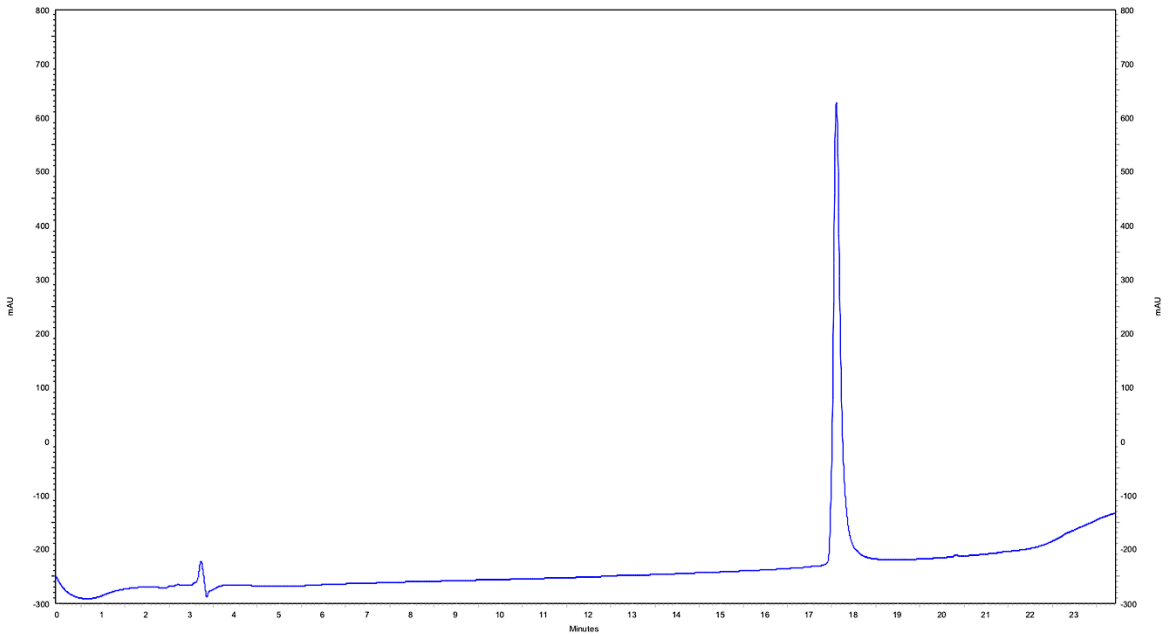

Analytical HPLC

Gradient: 5% ACN (0.1 %TFA) to 70 % ACN in Water (18 min), Rosi

Retention time: 17.7 min

ESI-ToF-MS

ESI-HRMS (m/z)	*Calculated mass (monoisotopic)*	*Observed mass*
$[M+2H]^{2+}$	1643.6782	1643.5009
$[M+3H]^{3+}$	1096.1214	1096.0038
$[M+4H]^{4+}$	822.3430	822.2552

hFF03-K17-Gal

Abz-LKKELAALKKELAALKK(-GA-Gal) ELAALKKEL-OH

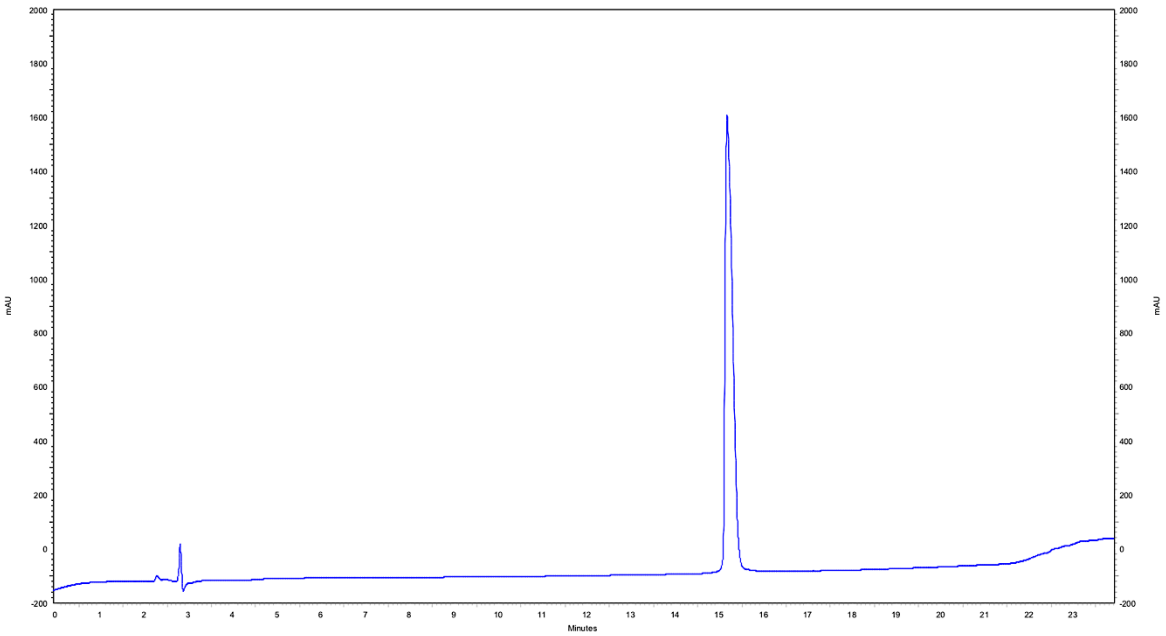

Analytical HPLC

Gradient: 5% ACN (0.1 %TFA) to 70 % ACN in Water (18 min), slow Fritz

Retention time: 15.3 min

ESI-ToF-MS

ESI-HRMS (m/z)	*Calculated mass (monoisotopic)*	*Observed mass*
$[M+2H]^{2+}$	1643.6782	1643.5087
$[M+3H]^{3+}$	1096.1214	1096.0046
$[M+4H]^{4+}$	822.3430	822.2545

hFF03-RGD

Abz-LKKELAALRGDLAALKKELAALKKEL-OH

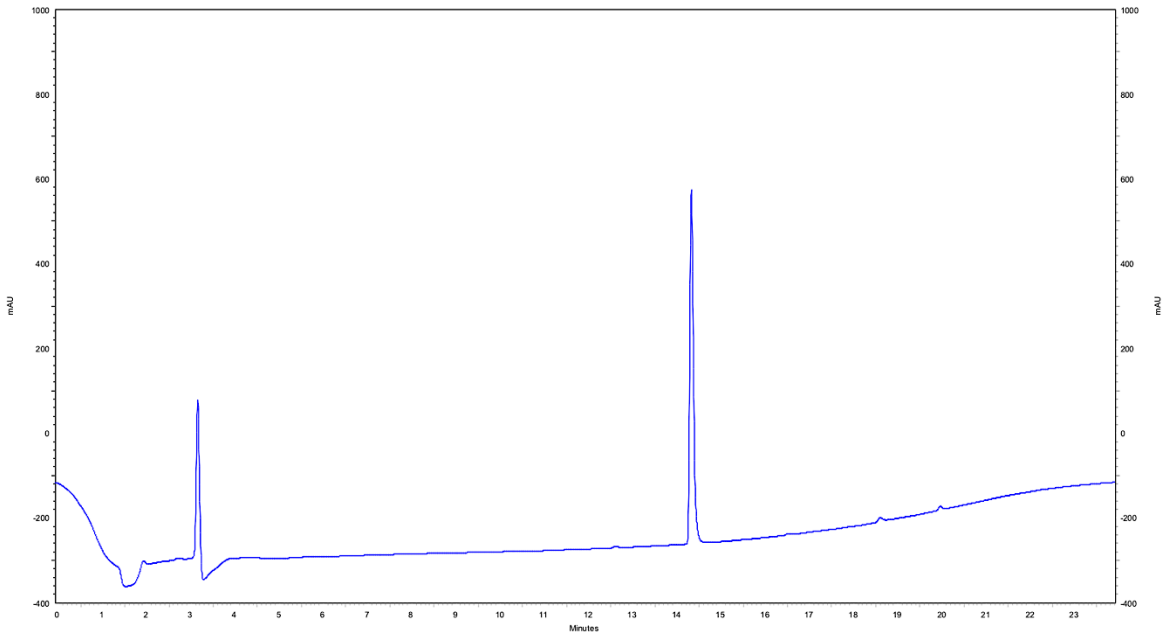

Analytical HPLC

Gradient: 5% ACN (0.1 %TFA) to 100 % ACN in Water (18 min), Rosi

Retention time: 14.4 min

ESI-ToF-MS

ESI-HRMS (m/z)	*Calculated mass (monoisotopic)*	*Observed mass*
$[M+2H]^{2+}$	1477.4541	1477.4202
$[M+3H]^{3+}$	985.3054	985.3846
$[M+4H]^{4+}$	739.2310	739.2164

hFF03-K17-NAIP

Abz-LKKELAALKKELAALKK(-SKPPGTSS) ELAALKKEL-OH

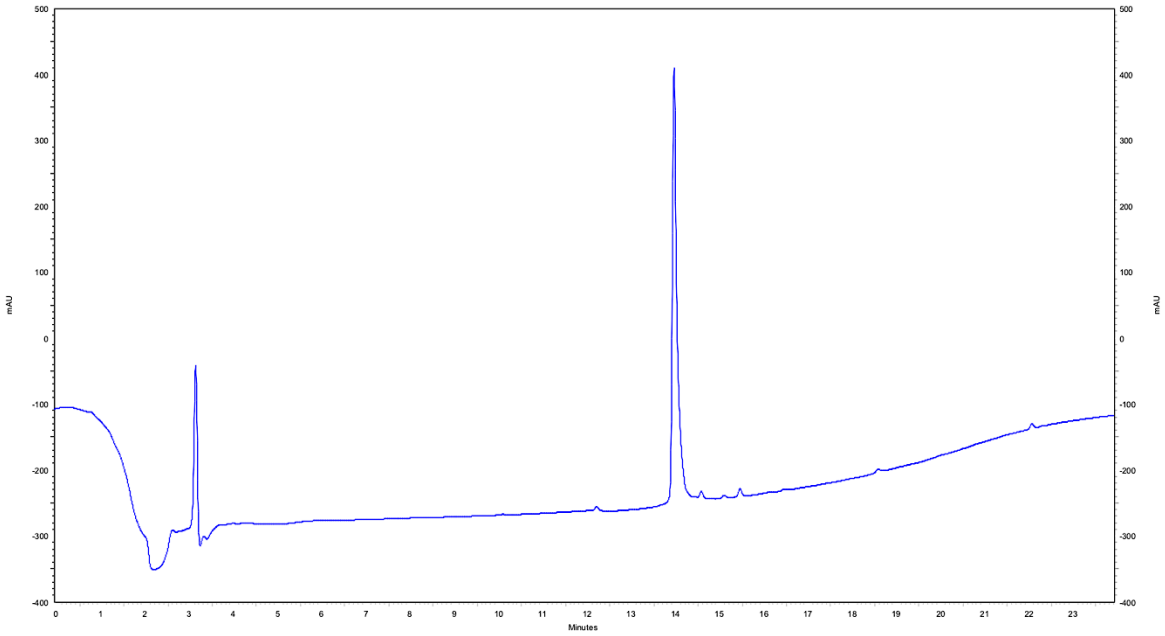

Analytical HPLC

Gradient: 5% ACN (0.1 %TFA) to 100 % ACN in Water (18 min), slow Fritz

Retention time: 14.0 min

ESI-ToF-MS

ESI-HRMS (m/z)	*Calculated mass (monoisotopic)*	*Observed mass*
$[M+2H]^{2+}$	1876.4482	1876.1189
$[M+3H]^{3+}$	1251.3014	1251.4193
$[M+4H]^{4+}$	938.7280	938.8162

hFF03-K17-SP

Abz-LKKELAALKKELAALKK(-RPLPNNFFGLM) ELAALKKEL-OH

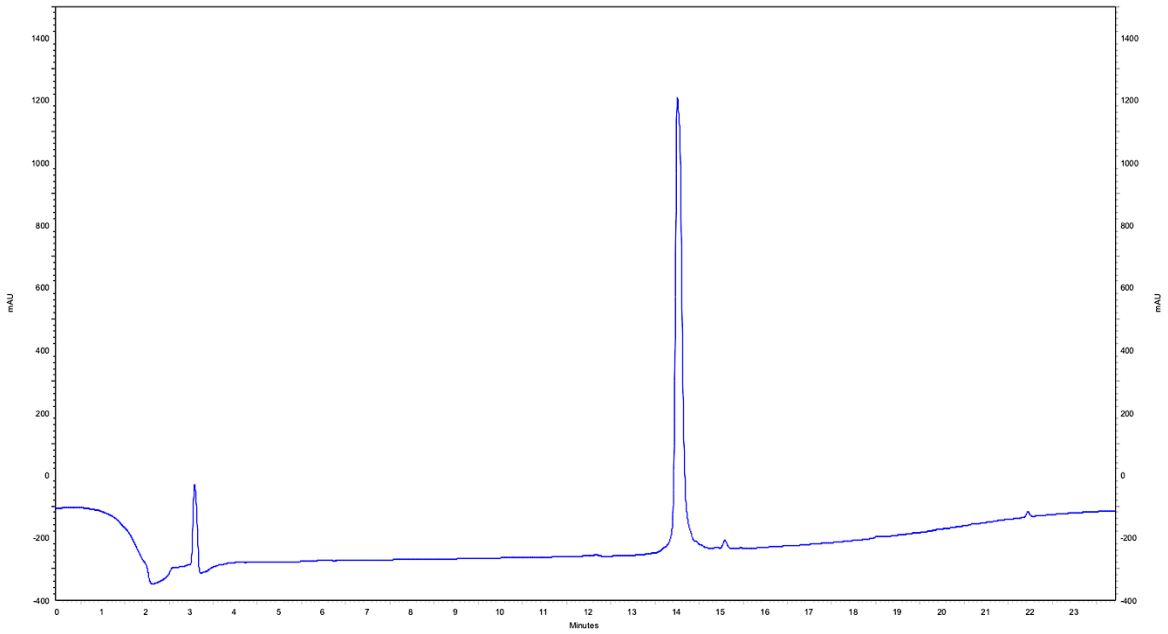

Analytical HPLC

Gradient: 5% ACN (0.1 %TFA) to 100% ACN in Water (18 min), Rosi

Retention time: 14.1 min

ESI-ToF-MS

ESI-HRMS (m/z)	*Calculated mass (monoisotopic)*	*Observed mass*
$[M+3H]^{3+}$	1447.5704	1447.5448
$[M+4H]^{4+}$	1085.9297	1085.9121
$[M+5H]^{5+}$	868.9453	868.9321

hFF03-K17-VT

Abz-LKKELAALKKELAALKK(-GKKQRFRHRNRKG) ELAALKKEL-OH

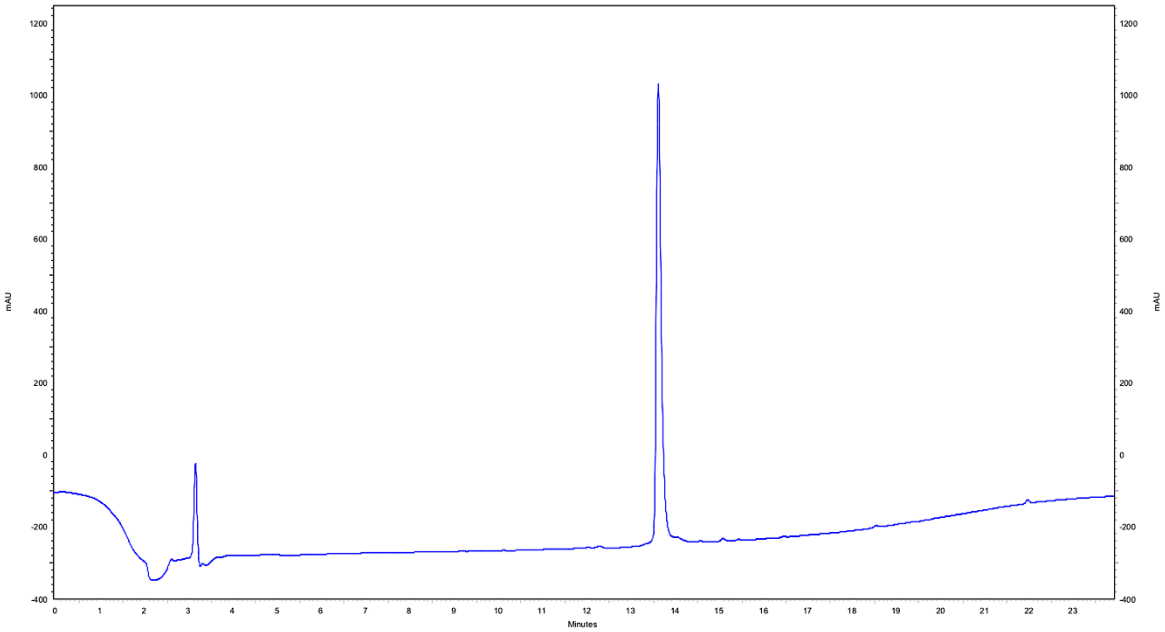

Analytical HPLC

Gradient: 5% ACN (0.1 %TFA) to 100% ACN in Water (18 min), Rosi

Retention time: 13.7 min

ESI-ToF-MS

ESI-HRMS (m/z)	*Calculated mass (monoisotopic)*	*Observed mass*
$[M+3H]^{3+}$	1553.9902	1553.9631
$[M+4H]^{4+}$	1165.7446	1165.7275
$[M+5H]^{5+}$	932.7972	932.7832

FF03

Abz-LKKELKELKKELEKLKKELKELKKEL-OH

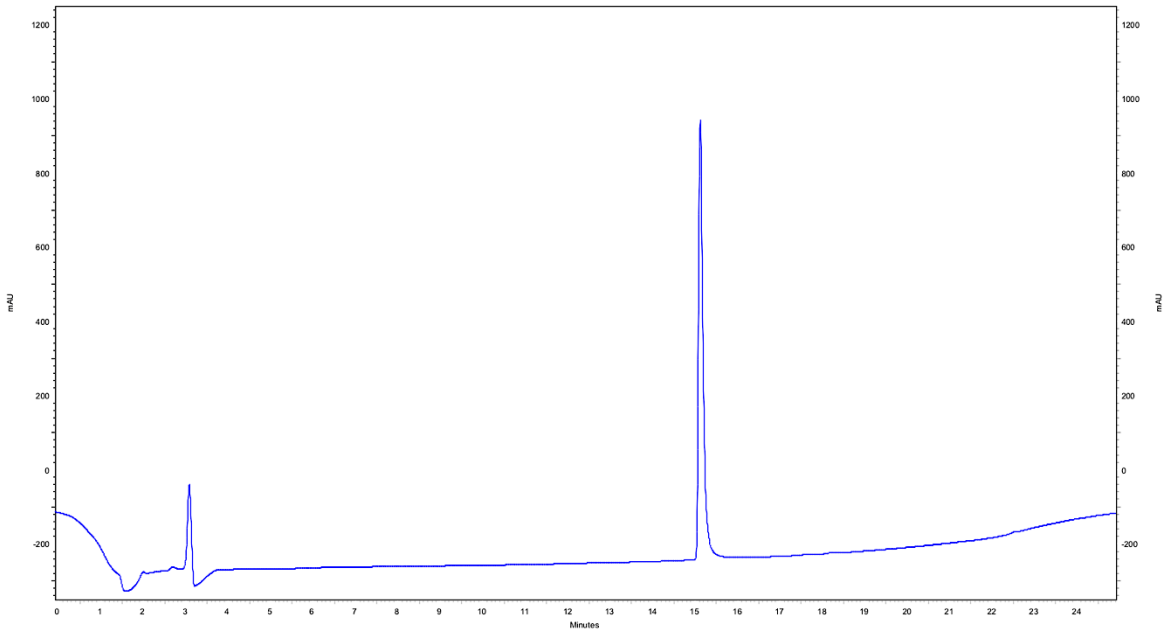

Analytical HPLC

Gradient: 10% ACN (0.1 %TFA) to 80% ACN in Water (18 min), Rosi

Retention time: 15.2 min

ESI-ToF-MS

ESI-HRMS (m/z)	*Calculated mass (monoisotopic)*	*Observed mass*
$[M+2H]^{2+}$	1678.5906	1678.5290
$[M+3H]^{3+}$	1119.3963	1119.3558
$[M+4H]^{4+}$	839.7992	839.7698

***hFF03-f*S**

Abz-LKSELAALKSELAALKKELAALKSEL-OH

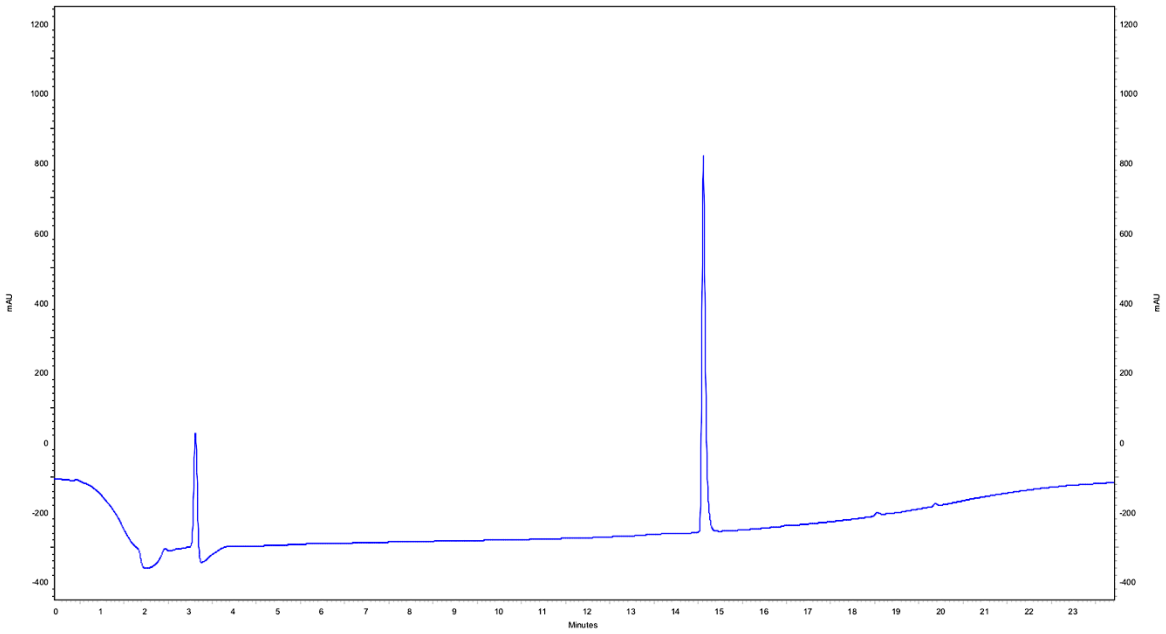

Analytical HPLC

Gradient: 5% ACN (0.1 %TFA) to 100% ACN in Water (18 min), Rosi,

Retention time: 14.7 min

ESI-ToF-MS

ESI-HRMS (m/z)	*Calculated mass (monoisotopic)*	*Observed mass*
$[M+2H]^{2+}$	1423.8698	1423.8166
$[M+3H]^{3+}$	949.5824	949.5475
$[M+4H]^{4+}$	712.4388	712.4126

FF03-K17-Sial

Abz-LKKELKELKKELEKLKK(-Sial)ELKELKKEL-OH

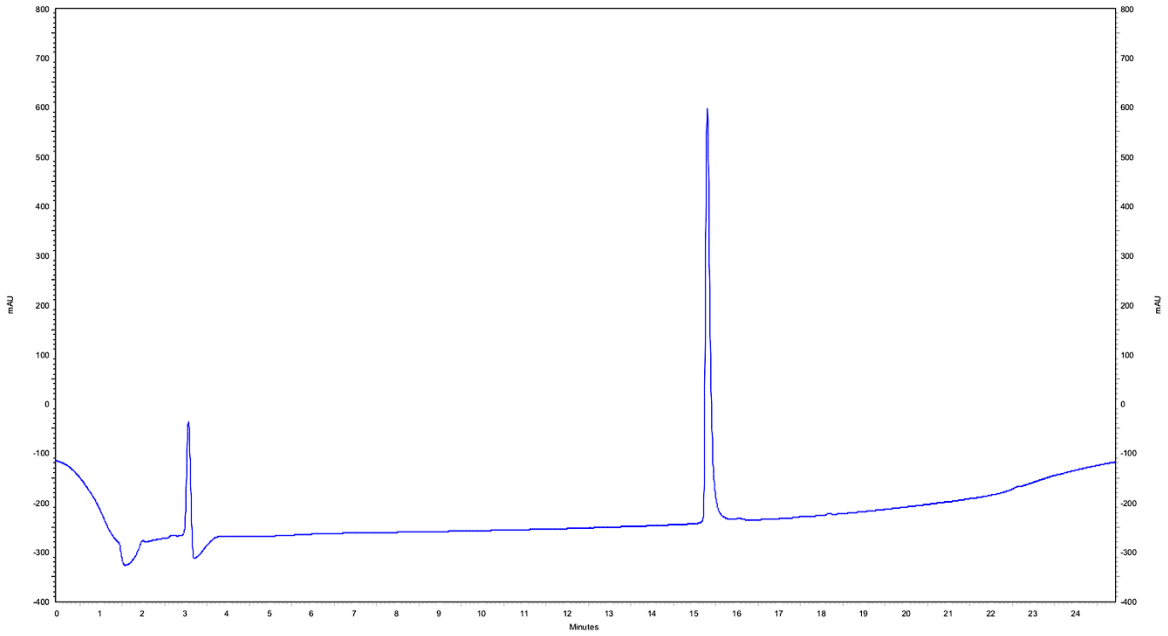

Analytical HPLC

Gradient: 10% ACN (0.1 %TFA) to 80 % ACN in Water (18 min), Rosi

Retention time: 15.4 min

ESI-ToF-MS

ESI-HRMS (m/z)	*Calculated mass (monoisotopic)*	*Observed mass*
$[M+3H]^{3+}$	1249.0947	1249.0742
$[M+4H]^{4+}$	937.0730	937.0582
$[M+5H]^{5+}$	749.8599	749.8491

hFF03-K17-Sial

Abz-LKKELAALKKELAALKK(-Sial)ELAALKKEL-OH

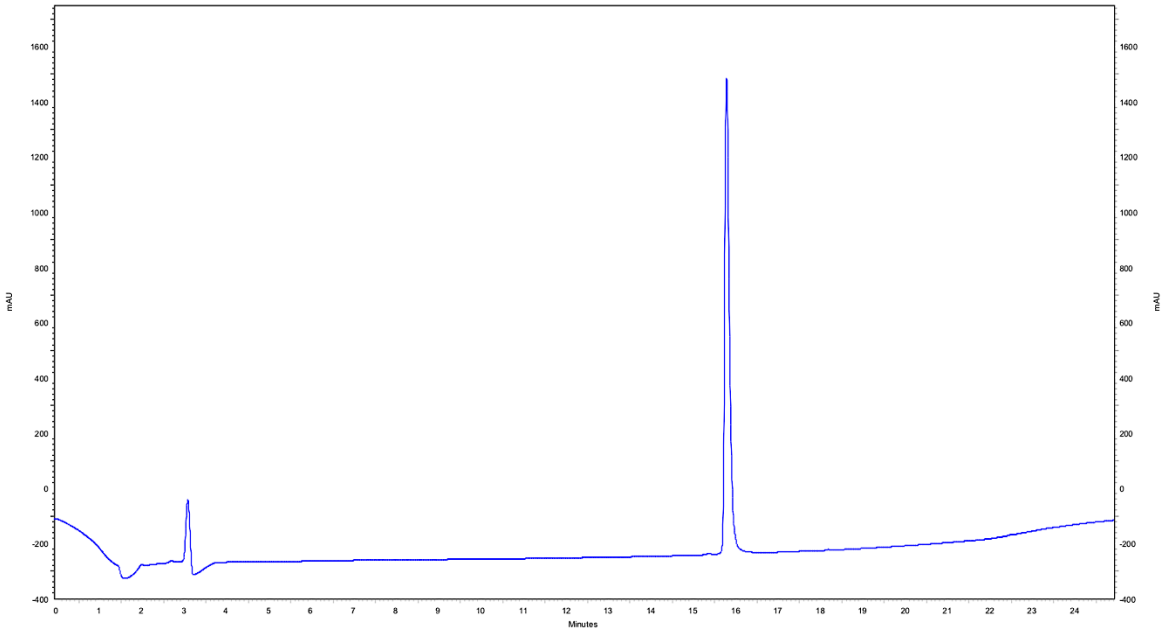

Analytical HPLC

Gradient: 10% ACN (0.1 %TFA) to 80 % ACN in Water (18 min), Rosi,

Retention time: 15.9 min

ESI-ToF-MS

ESI-HRMS (m/z)	*Calculated mass (monoisotopic)*	*Observed mass*
$[M+2H]^{2+}$	1700.5432	1700.5056
$[M+3H]^{3+}$	1134.0314	1134.0098
$[M+4H]^{4+}$	850.7755	850.7604

hFF03-fS-K17-Sial

Abz-LKSELAALKSELAALKK(-Sial)ELAALKSEL-OH

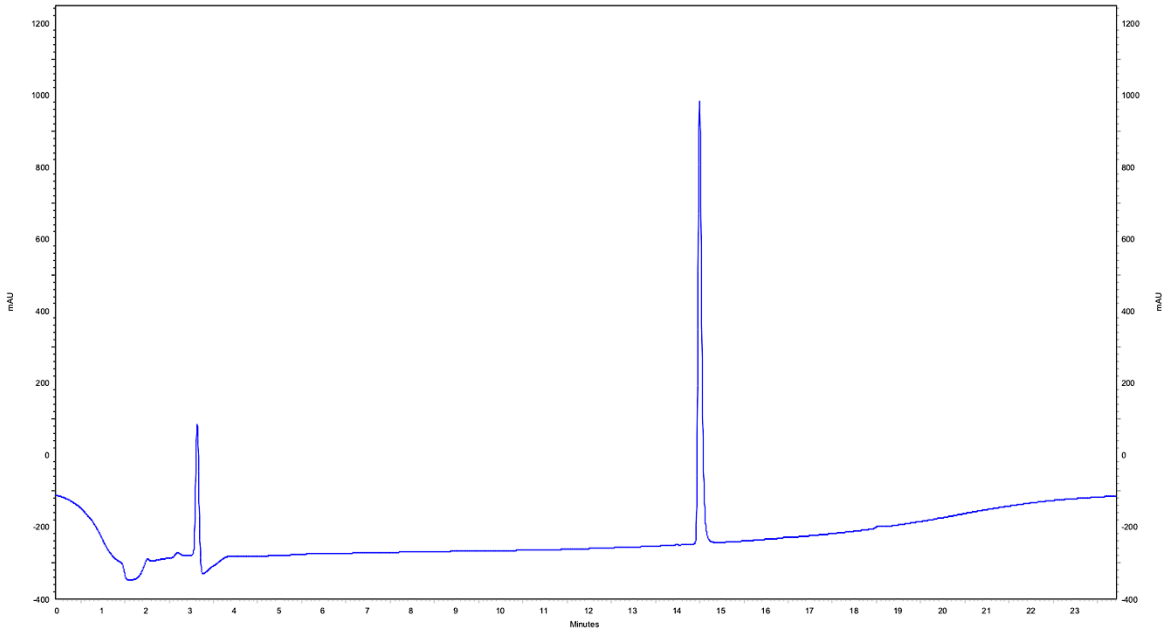

Analytical HPLC

Gradient: 5% ACN (0.1 %TFA) to 100 % ACN in Water (18 min), Rosi,

Retention time: 14.6 min

ESI-ToF-MS

ESI-HRMS (m/z)	*Calculated mass (monoisotopic)*	*Observed mass*
$[M+2H]^{2+}$	1638.9488	1638.9047
$[M+3H]^{3+}$	1092.9684	1092.9411
$[M+4H]^{4+}$	819.9783	819.9594

8 References

[1] *Eur. J. Biochem.* **1984**, *138*, 9–37.

[2] F. H. C. Crick, *Nature* **1952**, *170*, 882–883.

[3] L. Pauling, R. B. Corey, *Proc. Natl. Acad. Sci.* **1951**, *37*, 729–740.

[4] S. Lou, X. Wang, Z. Yu, L. Shi, *Adv. Sci.* **2019**, *1802043*, DOI 10.1002/advs.201802043.

[5] E. C. Wu, S. Zhang, C. A. E. Hauser, *Adv. Funct. Mater.* **2012**, *22*, 456–468.

[6] P. Burkhard, J. Stetefeld, S. V. Strelkov, *Trends Cell Biol.* **2001**, *11*, 82–88.

[7] Y. Wu, J. H. Collier, *Wiley Interdiscip. Rev. Nanomedicine Nanobiotechnology* **2017**, *9*, 1–17.

[8] M. Wolny, M. Batchelor, G. J. Bartlett, E. G. Baker, M. Kurzawa, P. J. Knight, L. Dougan, D. N. Woolfson, E. Paci, M. Peckham, *Sci. Rep.* **2017**, *7*, 1–14.

[9] D. N. Woolfson, *Adv. Protein Chem.* **2005**, *70*, 79–112.

[10] C. Chothia, M. Levitt, D. Richardson, *J. Mol. Biol.* **1981**, 215–250.

[11] J. A. Falenski, U. I. M. Gerling, B. Koksch, *Bioorg. Med. Chem.* **2010**, *18*, 3703–3706.

[12] F. Lapenta, J. Aupič, Ž. Strmšek, R. Jerala, *Chem. Soc. Rev.* **2018**, *47*, 3530–3542.

[13] A. N. Lupas, M. Gruber, in *Adv. Protein. Chem.*, **2005**, pp. 37–38.

[14] P. B. Harbury, T. Zhang, P. S. Kim, T. Alber, *Science* **1993**, *262*, 1401–1407.

[15] E. Zacco, C. Anish, C. E. Martin, H. v. Berlepsch, E. Brandenburg, P. H. Seeberger, B. Koksch, *Biomacromolecules* **2015**, *16*, 2188–2197.

[16] E. Zacco, J. Hütter, J. L. Heier, J. Mortier, P. H. Seeberger, B. Lepenies, B. Koksch, *ACS Chem. Biol.* **2015**, *10*, 2065–2072.

[17] J. M. Fletcher, A. L. Boyle, M. Bruning, Sg. J. Bartlett, T. L. Vincent, N. R. Zaccai, C. T. Armstrong, E. H. C. Bromley, P. J. Booth, R. L. Brady, et al., *ACS Synth. Biol.* **2012**, *1*, 240–250.

[18] E. Wolf, P. S. Kim, B. Berger, *Protein Sci.* **1997**, *6*, 1179–1189.

[19] P. B. Harbury, P. S. Kim, T. Alber, *Nature* **1994**, *371*, 80–83.

[20] M. G. Ryadnov, D. N. Woolfson, *Angew. Chemie - Int. Ed.* **2003**, *42*, 3021–3023.

[21] M. G. Ryadnov, D. N. Woolfson, *J. Am. Chem. Soc.* **2005**, *127*, 12407–12415.

[22] M. G. Ryadnov, D. N. Woolfson, *Nat. Mater.* **2003**, *2*, 329–332.

[23] M. J. Pandya, G. M. Spooner, M. Sunde, J. R. Thorpe, A. Rodger, D. N. Woolfson, *Biochemistry* **2000**, *39*, 8728–8734.

[24] M. J. Haider, H. V. Zhang, N. Sinha, J. A. Fagan, K. L. Kiick, J. G. Saven, D. J. Pochan, *Soft Matter* **2018**, *14*, 5488–5496.

[25] H. V. Zhang, F. Polzer, M. J. Haider, Y. Tian, J. A. Villegas, K. L. Kiick, D. J. Pochan, J. G. Saven, *Sci. Adv.* **2016**, *2*, DOI 10.1126/sciadv.1600307.

[26] S. . Potekhin, T. . Melnik, V. Popov, N. . Lanina, A. . Vazina, P. Rigler, A. . Verdini, G. Corradin, A. . Kajava, *Chem. Biol.* **2001**, *8*, 1025–1032.

[27] R. Schofield, *Blood Cells* **1978**, *4*, 7–25.

[28] F. Guilak, D. M. Cohen, B. T. Estes, J. M. Gimble, W. Liedtke, C. S. Chen, *Cell Stem Cell* **2009**, *5*, 17–26.

[29] D. L. Jones, A. J. Wagers, *Nat. Rev. Mol. Cell Biol.* **2008**, *9*, 11–21.

[30] S. Kühl, M. Kühl, *Stammzellbiologie*, **2012**, Stuttgart: Verlag Eugen Ulmer.

[31] E. Fuchs, T. Tumbar, G. Gausch, Howard Hughes Medical Institute, *Cell* **2004**, *116*, 769–778.

[32] L. Li, T. Xie, *Annu. Rev. Cell Dev. Biol.* **2005**, *21*, 605–631.

[33] S. Ding, P. G. Schultz, *Nat. Biotechnol.* **2004**, *22*, 833–840.

[34] M. F. Griffin, P. E. Butler, A. M. Seifalian, D. M. Kalaskar, *World J. Stem Cells* **2015**, *7*, 37.

[35] J. A. Knoblich, *Cell* **2008**, *132*, 583–597.

[36] F. M. Watt, B. L. Hogan, *Science* **2000**, *287*, 1427–1430.

[37] J. S. Odorico, D. S. Kaufman, J. a Thomson, *Stem Cells* **2001**, *19*, 193–204.

[38] J. M. Gimble, F. Guilak, M. E. Nuttall, S. Sathishkumar, M. Vidal, B. A. Bunnell, *Transfus. Med. Hemotherapy* **2008**, *35*, 228–238.

[39] R. Hynes, *Science* **2009**, *326*, 1216–1219.

[40] F. M. Watt, W. T. S. Huck, *Nat. Rev. Mol. Cell Biol.* **2013**, *14*, 467–73.

[41] K. J. Lampe, S. C. Heilshorn, *Neurosci. Lett.* **2012**, *519*, 138–146.

[42] M. P. Lutolf, P. M. Gilbert, H. M. Blau, *Nature* **2009**, *462*, 433–41.

[43] K. S. Hellmund, B. Koksch, *Front. Chem.* **2019**, *7*, 172.

[44] E. R. Aurand, K. J. Lampe, K. B. Bjugstad, *Neurosci. Res.* **2012**, *72*, 199–213.

[45] H. Lv, L. Li, M. Sun, Y. Zhang, L. Chen, Y. Rong, Y. Li, *Stem Cell Res. Ther.* **2015**, *6*, 103.

[46] A. Lakshmanan, S. Zhang, C. A. E. Hauser, *Trends Biotechnol.* **2012**, *30*, 155–165.

[47] J. R. Klim, L. Li, P. J. Wrighton, M. S. Piekarczyk, L. L. Kiessling, **2010**, *7*, DOI 10.1038/nmeth.1532.

[48] C. Cha, W. B. Liechty, A. Khademhosseini, N. A. Peppas, *ACS Nano* **2012**, *6*, 9353–9358.

[49] C. Tuzmen, P. G. Campbell, *Connect. Tissue Res.* **2018**, *58*, 81–90.

[50] H. S. Hong, J. Lee, E. Lee, Y. S. Kwon, E. Lee, W. Ahn, M. H. Jiang, J. C. Kim, Y. Son, *Nat. Med.* **2009**, *15*, 425–435.

[51] H. Hong, D. Y. Kim, K. J. Yoon, Y. Son, **2011**, *34*, 2003–2006.

[52] S. Zhang, F. Gelain, X. Zhao, *Semin. Cancer Biol.* **2005**, *15*, 413–420.

[53] Y. Yanlian, K. Ulung, W. Xiumei, A. Horii, H. Yokoi, Z. Shuguang, *Nano Today* **2009**, *4*, 193–210.

[54] X. Liu, X. Wang, X. Wang, H. Ren, J. He, L. Qiao, F. Z. Cui, *Acta Biomater.* **2013**, *9*, 6798–6805.

[55] I. L. Ivanovska, J. W. Shin, J. Swift, D. E. Discher, *Trends Cell Biol.* **2015**, *25*, 523–532.

[56] R. K. Das, O. F. Zouani, C. Labrugère, R. Oda, M.-C. C. Durrieu, *ACS Nano* **2013**, *7*, 3351–3361.

[57] A. Horii, X. Wang, F. Gelain, S. Zhang, *PLoS One* **2007**, *2*, e190.

[58] H. Hosseinkhani, M. Hosseinkhani, H. Kobayashi, *Biomed. Mater.* **2006**, *1*, 8–15.

[59] H. Hosseinkhani, M. Hosseinkhani, F. Tian, H. Kobayashi, Y. Tabata, *Biomaterials* **2006**, *27*, 4079–4086.

[60] C. E. Semino, J. R. Merok, G. G. Crane, G. Panagiotakos, S. Zhang, *Differentiation* **2003**, *71*, 262–270.

[61] M. A. Bokhari, G. Akay, S. Zhang, M. A. Birch, *Biomaterials* **2005**, *26*, 5198–5208.

[62] Z. Zhang, J. Hu, P. X. Ma, *Adv. Drug Deliv. Rev.* **2012**, *64*, 1129–1141.

[63] B. Brodsky, J. A. M. Ramshaw, *Matrix Biol.* **1997**, *15*, 545–554.

[64] B. Brodsky, A. V Persikov, *Adv. Protein Chem.* **2005**, *70*, 302–333.

[65] T. Wess, *Adv. Protein Chem.* **2005**, *70*, 341–374.

[66] L. Cen, W. Liu, L. Cui, W. Zhang, Y. Cao, *Pediatr. Res.* **2008**, *63*, 492–496.

[67] K. M. Hennessy, B. E. Pollot, W. C. Clem, M. C. Phipps, A. A. Sawyer, B. K. Culpepper, S. L. Bellis, *Biomaterials* **2009**, *30*, 1898–1909.

[68] H. J. Lee, J.-S. Lee, T. Chansakul, C. Yu, J. H. Elisseeff, S. M. Yu, *Biomaterials* **2006**, *27*, 5268–5276.

[69] H. J. Lee, C. Yu, T. Chansakul, N. S. Hwang, S. Varghese, S. M. Yu, J. H. Elisseeff, *Tissue Eng. Part A* **2008**, *14*, 1843–1851.

[70] T. L. Deans, J. Elisseeff, *World Stem Cell 2009* **2010**, 97–100.

[71] O. Yasa, O. Uysal, M. S. Ekiz, M. O. Guler, A. B. Tekinay, *J. Mater. Chem. B* **2017**, *5*, 4890–4900.

[72] F. Gelain, D. Bottai, A. Vescovi, S. Zhang, *PLoS One* **2006**, *1*, DOI 10.1371/journal.pone.0000119.

[73] T. Y. Cheng, M. H. Chen, W. H. Chang, M. Y. Huang, T. W. Wang, *Biomaterials* **2013**, *34*, 2005–2016.

[74] M. Yamada, Y. Kadoya, S. Kasai, K. Kato, M. Mochizuki, N. Nishi, N. Watanabe, H. K. Kleinman, Y. Yamada, M. Nomizu, *Dev. Biol.* **2002**, *530*, 48–52.

[75] T. C. Holmes, S. de Lacalle, X. Su, G. Liu, a Rich, S. Zhang, *Proc. Natl. Acad. Sci. U. S. A.* **2000**, *97*, 6728–6733.

[76] E. F. Banwell, E. S. Abelardo, D. J. Adams, M. A. Birchall, A. Corrigan, A. M. Donald, M. Kirkland, L. C. Serpell, M. F. Butler, D. N. Woolfson, *Nat. Mater.* **2009**, *8*, 596–600.

[77] N. Mehrban, E. Abelardo, A. Wasmuth, K. L. Hudson, L. M. Mullen, A. R. Thomson, M. A. Birchall, D. N. Woolfson, *Adv. Healthc. Mater.* **2014**, *3*, 1387–1391.

[78] N. Mehrban, B. Zhu, F. Tamagnini, F. I. Young, A. Wasmuth, K. L. Hudson, A. R. Thomson, M. A. Birchall, A. D. Randall, B. Song, et al., *ACS Biomater. Sci. Eng.* **2015**, *1*, 431–439.

[79] M. Hussain, H. D. Galvin, T. Y. Haw, A. N. Nutsford, M. Husain, *Infect. Drug Resist.* **2017**, *10*, 121–134.

[80] C. A. Russel, T. C. Jones, I. G. Barr, N. J. Cox, R. J. Garten, V. Gregory, I. D. Gust, A. W. Hampson, A. J. Hay, A. C. Hurt, et al., **2008**, *320*, 340–346.

[81] S. Bhatia, D. Lauster, M. Bardua, K. Ludwig, S. Angioletti-Uberti, N. Popp, U. Hoffmann, F. Paulus, M. Budt, M. Stadtmüller, et al., *Biomaterials* **2017**, *138*, 22–34.

[82] M. C. Zambon, *J. Antimicrob. Chemother.* **1999**, *44*, 3–9.

[83] J. K. Taubenberger, D. M. Morens, *Emerg. Infect. Dis.* **2006**, *12*, 15–22.

[84] P. R. Saunders-Hastings, D. Krewski, *Pathogens* **2016**, *5*, DOI 10.3390/pathogens5040066.

[85] D. Lauster, Entwicklung Multivalenter Inhibitoren des Eintritts von Influenzaviren in Wirtszellen, Humboldt-Universität zu Berlin, **2017**.

[86] N. M. Bouvier, P. Palese, *Vaccine* **2008**, *26*, 49–53.

[87] A. Harris, G. Cardone, D. C. Winkler, J. B. Heymann, M. Brecher, J. M. White, A. C. Steven, *Proc. Natl. Acad. Sci. U. S. A.* **2006**, *103*, 19123–19127.

[88] E. Vanderlinden, L. Naesens, **2013**, 301–339.

[89] W. Zhu, C. Wang, B. Z. Wang, *Int. J. Mol. Sci.* **2017**, *18*, 1–14.

[90] M. Gerber, C. Isel, V. Moules, R. Marquet, *Trends Microbiol.* **2014**, *22*, 446–455.

[91] R. U. Kadam, J. Juraszek, B. Brandenburg, C. Buyck, W. B. G. Schepens, B. Kesteleyn, B. Stoops, R. J. Vreeken, J. Vermond, W. Goutier, et al., **2017**, *2004*, 496–502.

[92] A. Moscona, *Annu. Rev. Med.* **2008**, *59*, 397–413.

[93] A. Moscona, *N. Engl. J. Med.* **2005**, *13*, 1363–1373.

[94] S. Li, C. Sieben, K. Ludwig, C. T. Höfer, S. Chiantia, A. Herrmann, F. Eghiaian, I. A. T. Schaap, *Biophys. J.* **2014**, *106*, 1447–1456.

[95] A. Osterhaus, R. Fouchier, G. Rimmelzwaan, *Philos. Trans. R. Soc. B Biol. Sci.* **2011**, *366*, 2766–2773.

[96] D. J. Smith, A. S. Lapedes, J. C. de Jong, T. M. Bestebroer, G. F. Rimmelzwaan, A. D. M. E. Osterhaus, R. A. M. Fouchier, *Science* **2004**, *305*, 371–376.

[97] D. Lauster, M. Glanz, M. Bardua, K. Ludwig, M. Hellmund, U. Hoffmann, A. Hamann, C. Böttcher, R. Haag, C. P. R. Hackenberger, et al., *Angew. Chemie* **2017**, *129*, 6025–6030.

[98] J. T. Skehel, D. C. Wiley, *Annu. Rev. Biochem.* **2000**, 531–69.

[99] S. Bhatia, L. C. Camacho, R. Haag, **2016**, DOI 10.1021/jacs.5b12950.

[100] C. Fasting, C. A. Schalley, M. Weber, O. Seitz, S. Hecht, B. Koksch, J. Dernedde, C. Graf, E. Knapp, R. Haag, **2012**, 10472–10498.

[101] M. Mammen, S.-K. Choi, G. M. Whitesides, *Angew. Chemie Int. Ed.* **1998**, *37*, 2754–2794.

[102] M. Mammen, G. Dahmann, G. M. Whitesides, *J. Med. Chem.* **1995**, *38*, 4179–4190.

[103] W. J. Lees, A. Spaltenstein, J. E. Kingery-Wood, G. M. Whitesides, *J. Med. Chem.* **1994**, *37*, 3419–3433.

[104] J. D. Reuter, A. Myc, M. M. Hayes, Z. Gan, R. Roy, D. Qin, R. Yin, L. T. Piehler, R. Esfand, D. A. Tomalia, et al., *Bioconjug. Chem.* **1999**, *10*, 271–278.

[105] G. B. Sigal, M. Mammen, G. Dahmann, G. M. Whitesides, *J. Am. Chem. Soc.* **1996**, *118*, 3789–3800.

[106] J. J. Landers, Z. Cao, I. Lee, L. T. Piehler, P. P. Myc, A. Myc, T. Hamouda, A. T. Galecki, J. R. Baker, Jr., *J. Infect. Dis.* **2002**, *186*, 1222–1230.

[107] S. J. Kwon, D. H. Na, J. H. Kwak, M. Douaisi, F. Zhang, E. J. Park, J. H. Park, H. Youn, C. S. Song, R. S. Kane, et al., *Nat. Nanotechnol.* **2017**, *12*, 48–54.

[108] V. Bandlow, S. Liese, D. Lauster, K. Ludwig, R. R. Netz, A. Herrmann, O. Seitz, *J. Am. Chem. Soc.* **2017**, *139*, 16389–16397.

[109] W. Lu, R. J. Pieters, *Expert Opin. Drug Discov.* **2019**, *14*, 387–395.

[110] K. Pagel, B. Koksch, *Curr. Opin. Chem. Biol.* **2008**, *12*, 730–739.

[111] E. H. C. Bromley, K. J. Channon, P. J. S. King, Z. N. Mahmoud, E. F. Banwell, M. F. Butler, M. P. Crump, T. R. Dafforn, M. R. Hicks, J. D. Hirst, et al., *Biophys. J.* **2010**, *98*, 1668–1676.

[112] M. J. Pandya, G. M. Spooner, M. Sunde, J. R. Thorpe, A. Rodger, D. N. Woolfson, *Biochemistry* **2000**, *39*, 8728–8734.

[113] M. MILLIPORE, *Novabiochem (R) Guide to Selection of Building Blocks*.

[114] R. S. Hodges, *Biochem. Cell Biol.* **1996**, *74*, 133–154.

[115] M. J. Hollamby, *Phys. Chem. Chem. Phys.* **2013**, *15*, 10566–10579.

[116] M. V. Petoukhov, D. I. Svergun, *Curr. Opin. Struct. Biol.* **2007**, *17*, 562–571.

[117] C. A. Dragolici, in *IntechOpen*, **2016**, pp. 37–64.

[118] R. Pynn, *Los Alamos Sci.* **1990**, *19*, 1–31.

[119] L. A. Feigin, D. I. Svergun, *Structure Analysis by Small-Angle X-Ray and Neutron Scattering*, **1987**.

[120] R. Richardson, in *Colloid Sci. Princ. Methods Appl.*, John Wiley & Sons Ltd, **2010**, pp. 273–297.

[121] B. Hammouda, **2012**.

[122] "https://www.sasview.org/publications/," (accessed 16th September 2019).

[123] J. S. Pedersen, P. Schurtenberger, *Macromolecules* **1996**, *29*, 7602–7612.

[124] A. A. Zamyatnin, *Prog. Biophys. Mol. Biol.* **1972**, *24*, 107–123.

[125] S. J. Perkins, *Eur. J. Biochem.* **1986**, *157*, 169–180.

[126] C. Yan, D. J. Pochan, *Chem. Soc. Rev.* **2010**, *39*, 3528–3540.

[127] K. Almdal, J. Dyre, S. Hvidt, O. Kramer, *Polym. Gels Networks* **1993**, *1*, 5–17.

[128] S. B. Ross-Murphy, *Polym. Gels Networks* **1994**, *2*, 229–237.

[129] C. W. Macosko, *Rheology: Principles, Measurements and Applications*, John Wiley & Sons Ltd, New York, NY, **1994**.

[130] T. G. Mezger, *The Rheology Handbook, 4th Edition*, Vincentz Network, Hanover, Germany, **2014**.

[131] R. Lewandowski, B. Chorazyczewski, *Comput. Struct.* **2010**, *88*, 1–17.

[132] L. B. Eldred, W. P. Baker, A. N. Palazotto, *AIAA J.* **1995**, *33*, 547–550.

[133] P. Decherchi, P. Cochard, P. Gauthier, *J. Neurosci. Methods* **1997**, *71*, 205–213.

[134] Q. L. Deveraux, J. C. Reed, **1999**, 239–252.

[135] S. Koutsopoulos, S. Zhang, *Acta Biomater.* **2013**, *9*, 5162–5169.

[136] M. J. Dubon, K.-S. Park, *Exp. Ther. Med.* **2015**, *9*, 1185–1191.

[137] M. Meldal, C. W. Tomøe, *Chem. Rev.* **2008**, *108*, 2952–3015.

[138] L. Moni, A. Marra, J. S. Skotnicki, F. E. Koehn, M. Abou-Gharbia, A. Dondoni, *Tetrahedron Lett.* **2013**, *54*, 6999–7003.

[139] C. W. Tornøe, C. Christensen, M. Meldal, *J. Org. Chem.* **2002**, *67*, 3057–3064.

[140] V. V. Rostovtsev, L. G. Green, V. V. Fokin, K. B. Sharpless, *Angew. Chemie - Int. Ed.* **2002**, *41*, 2596–2599.

[141] E. Saxon, C. R. Bertozzi, *Science* **2000**, *287*, 2007–2010.

[142] K. L. Kiick, E. Saxon, D. A. Tirrell, C. R. Bertozzi, *PNAS* **2002**, *99*, 19–24.

[143] H. Fittler, O. Avrutina, B. Glotzbach, M. Empting, H. Kolmar, *Org. Biomol. Chem.* **2013**, *11*, 1848–1857.

[144] B. Liebe, H. Kunz, *Helv. Chim. Acta* **1997**, *80*, 1473–1482.

[145] C. Brocke, H. Kunz, *Bioorganic Med. Chem.* **2002**, *10*, 3085–3112.

[146] S. V. Vemula, J. Zhao, J. Liu, X. W. Xue, S. Biswas, I. Hewlett, *Viruses* **2016**, *8*, 1–15.

[147] A. Hategan, K. Sengupta, S. Kahn, E. Sackmann, D. E. Discher, *Biophys. J.* **2004**, *87*, 3547–3560.

[148] A. Kręzel, W. Bal, *J. Inorg. Biochem.* **2004**, *98*, 161–166.

[149] H. E. Gottlieb, V. Kotlyar, A. Nudelman, *J. Org. Chem.* **1997**, *62*, 7512–7515.

[150] G. R. Fulmer, A. J. M. Miller, N. H. Sherden, H. E. Gottlieb, A. Nudelman, B. M. Stoltz, J. E. Bercaw, K. I. Goldberg, *Organometallics* **2010**, *29*, 2176–2179.

[151] R. K. Harris, E. D. Becker, S. M. C. de Menezes, R. Goodfellow, Pierre Granger, **2001**, *73*, 1795–1818.

[152] V. V. Andrushchenko, H. J. Vogel, E. J. Prenner, *J. Pept. Sci.* **2007**, *13*, 37–43.

9 Overview Figures

10 Overview Tables

11 Overview Equations

12 Appendix

Coiled-coil based ligand presenting 3D scaffolds as highly specialized biological microenvironments by K. S. Hellmund, Berlin, December 19.

Supporting Information

1) CD – spectra
2) NMR-Spectra
3) Microscopy Images
4) Rheology Data
5) Hydrogel-concentration

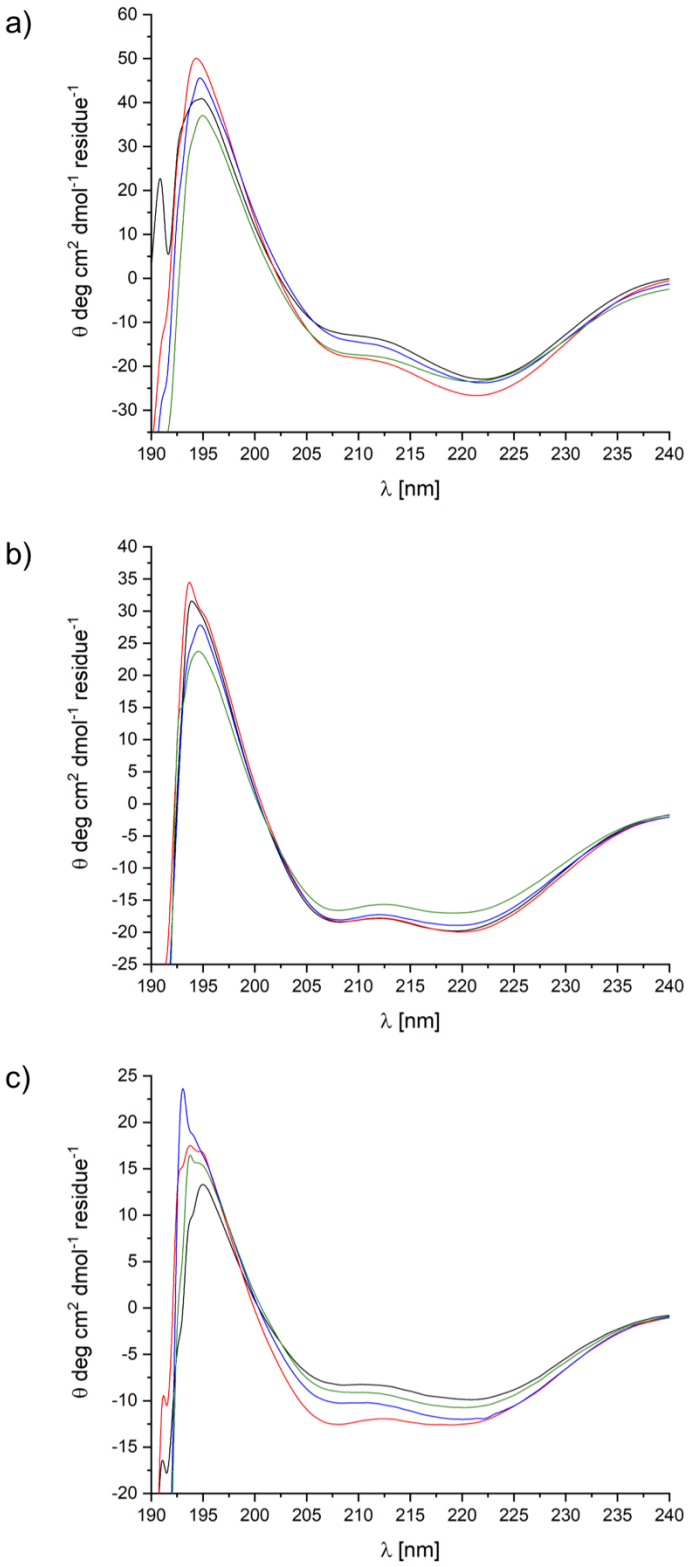

Figure 12.1. CD-spectra at 20°C of hFF03-*f*A (a), hFF03-*b*A*c*A (b) and hFF03-*b*A*c*A*f*A (50 µM each) in D-PBS over a period of six days directly after sample preparation (black line), 24h (red line), 72h (blue line) and 6 days (green line) after sample preparation to follow folding behavior.

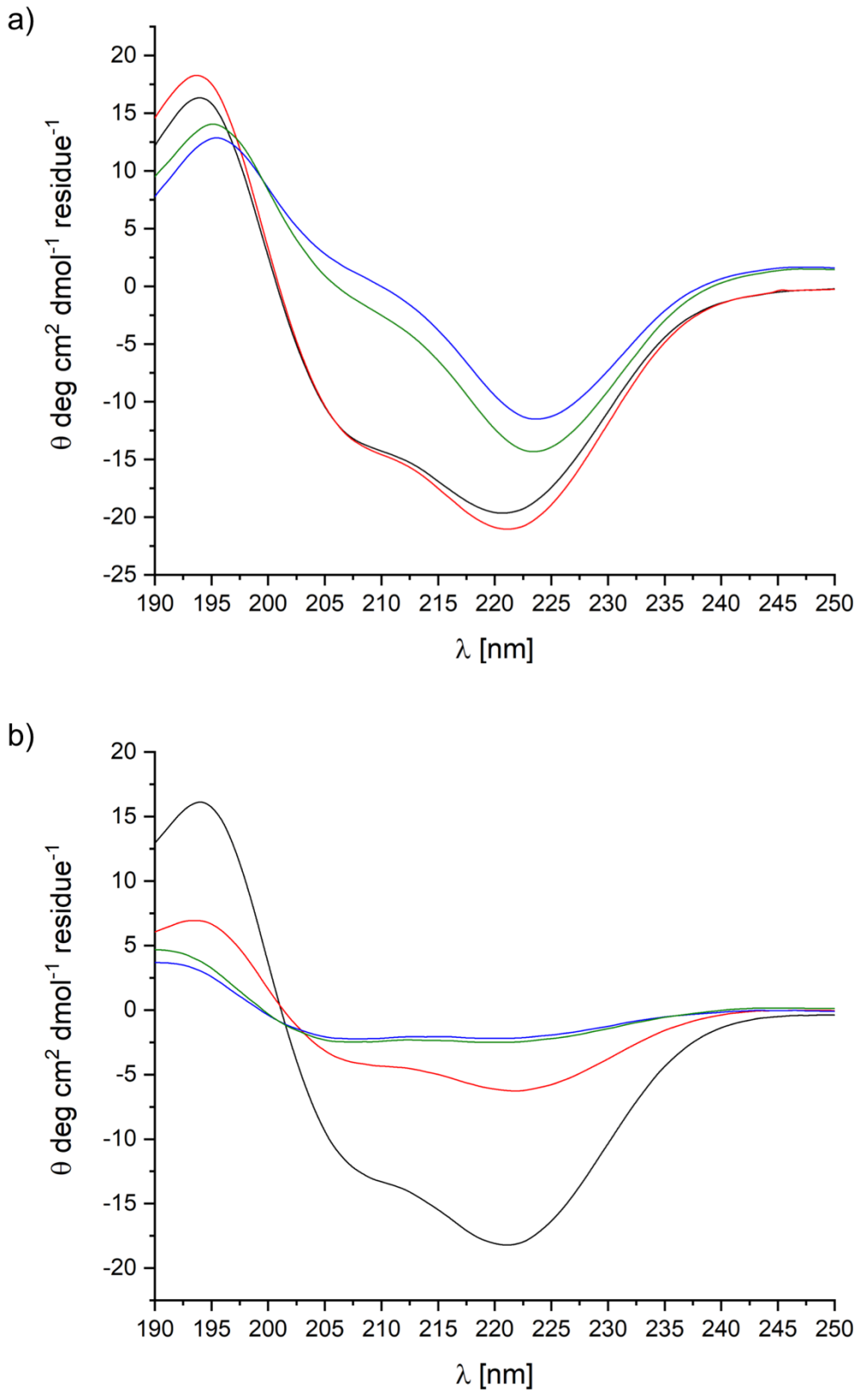

Figure 12.2. CD-spectra at 20°C (a) and 37°C (b) of 0.15 wt% hFF03 in D-PBS over a period of six days directly after sample preparation (black line), 24h (red line), 72h (blue line) and 6 days (green line) after sample preparation.

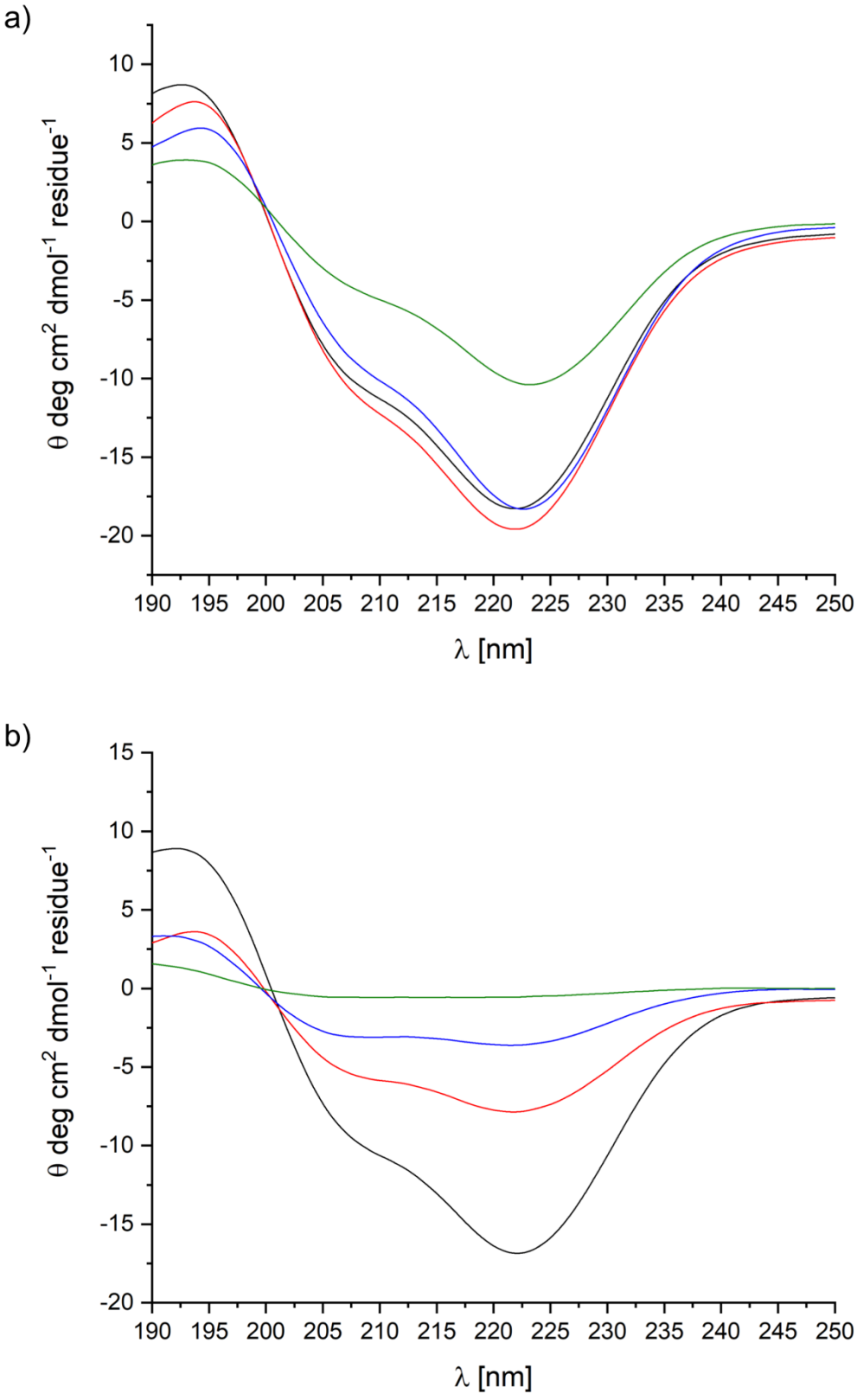

Figure 12.3. CD-spectra at 20°C (a) and 37°C (b) of 0.30 wt% hFF03 in D-PBS over a period of six days directly after sample preparation (black line), 24h (red line), 72h (blue line) and 6 days (green line) after sample preparation.

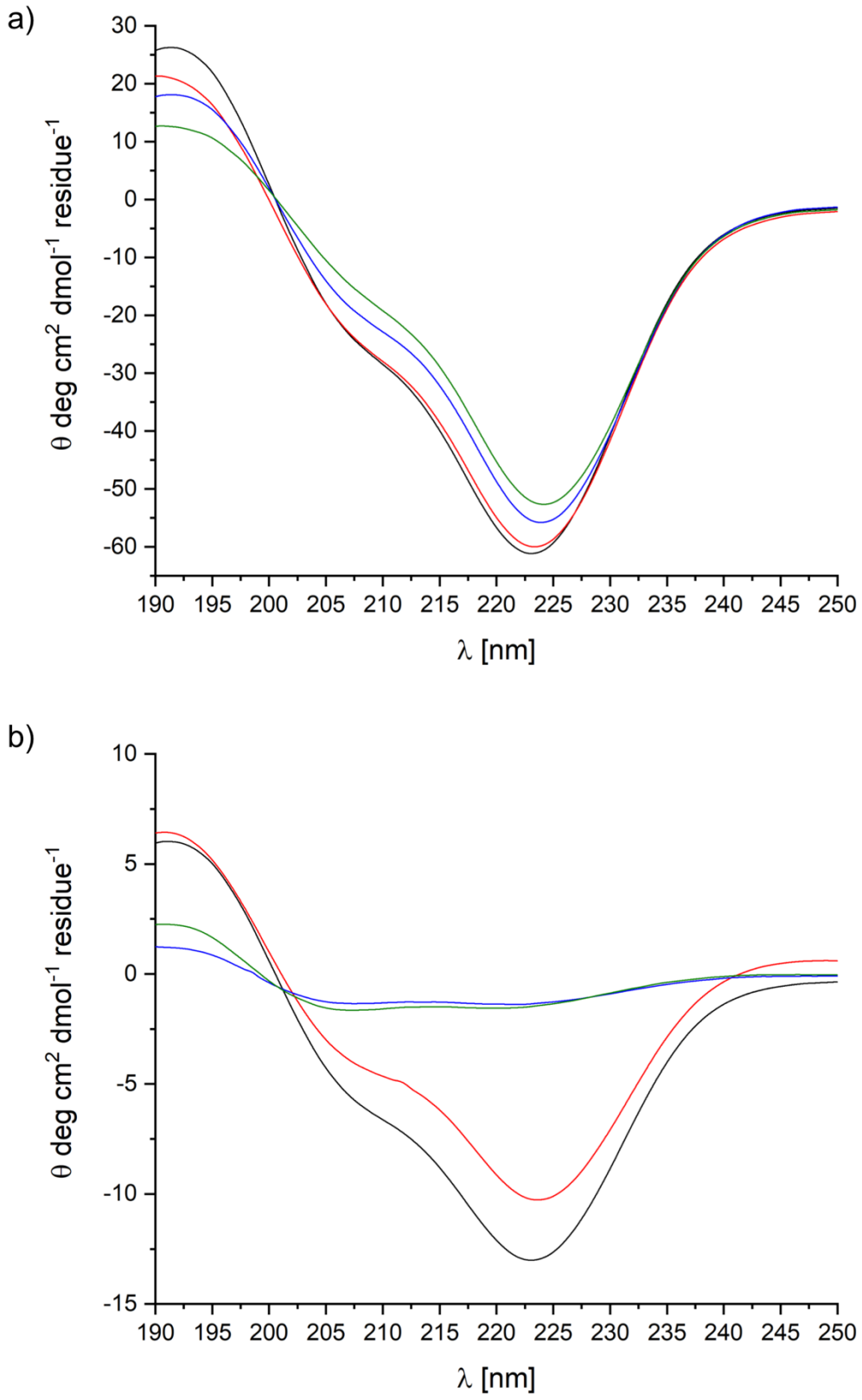

Figure 12.4. CD-spectra at 20°C (a) and 37°C (b) of 0.50 wt% hFF03 in D-PBS over a period of six days directly after sample preparation (black line), 24h (red line), 72h (blue line) and 6 days (green line) after sample preparation.

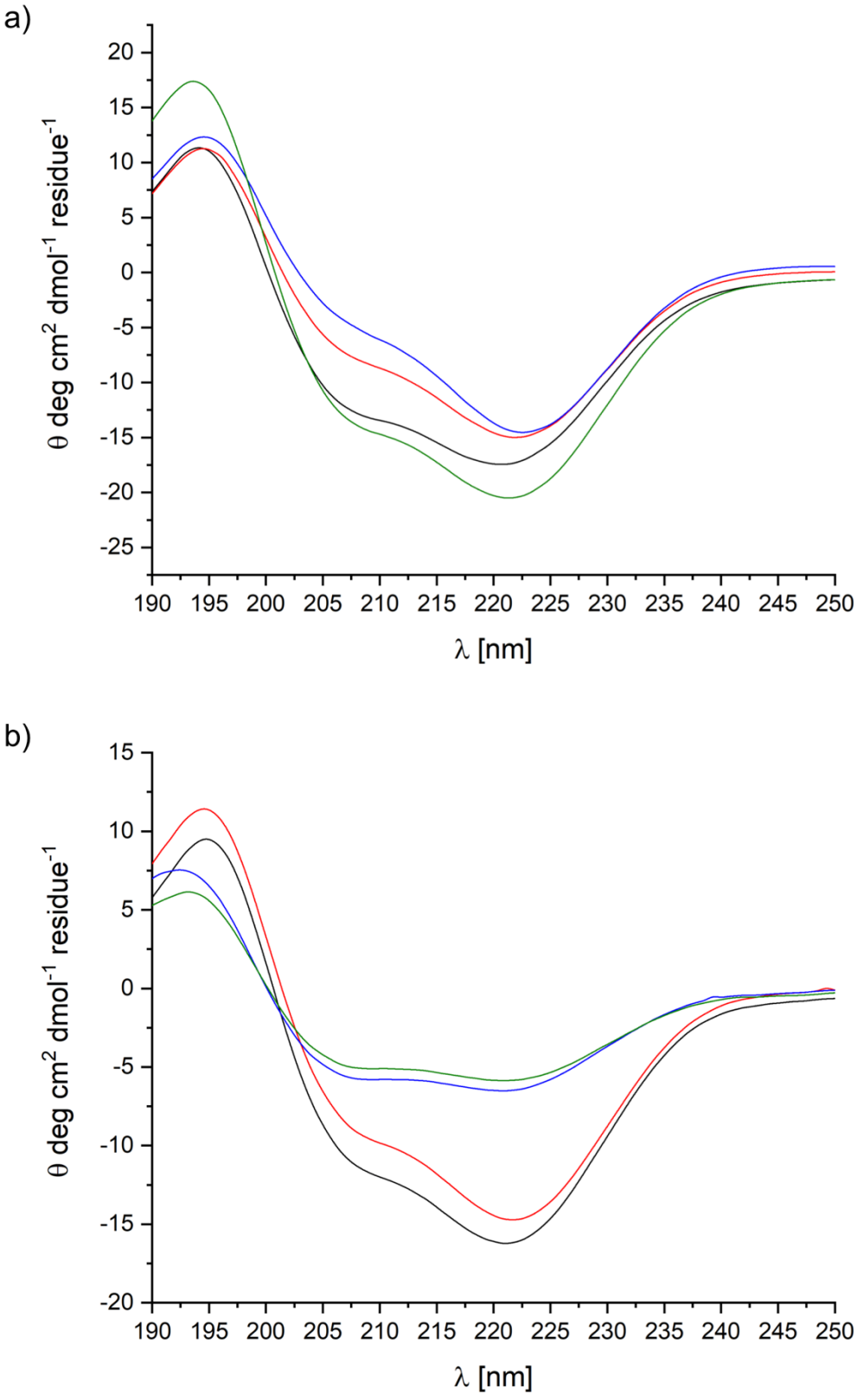

Figure 12.5. CD-spectra at 20°C (a) and 37°C (b) of 0.15 wt% hFF03-K17-Man in D-PBS over a period of six days directly after sample preparation (black line), 24h (red line), 72h (blue line) and 6 days (green line) after sample preparation.

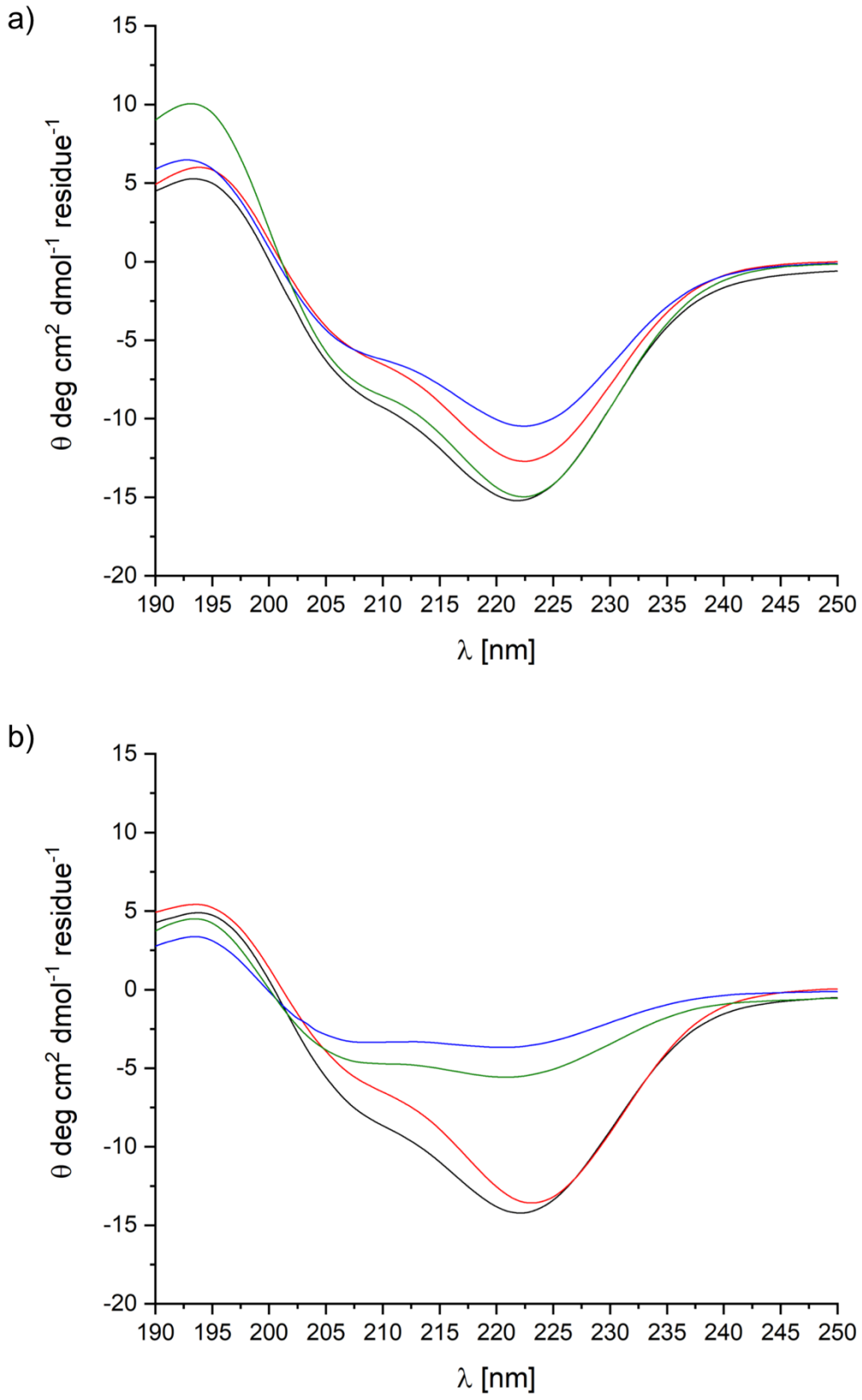

Figure 12.6. CD-spectra at 20°C (a) and 37°C (b) of 0.30 wt% hFF03-K17-Man in D-PBS over a period of six days directly after sample preparation (black line), 24h (red line), 72h (blue line) and 6 days (green line) after sample preparation.

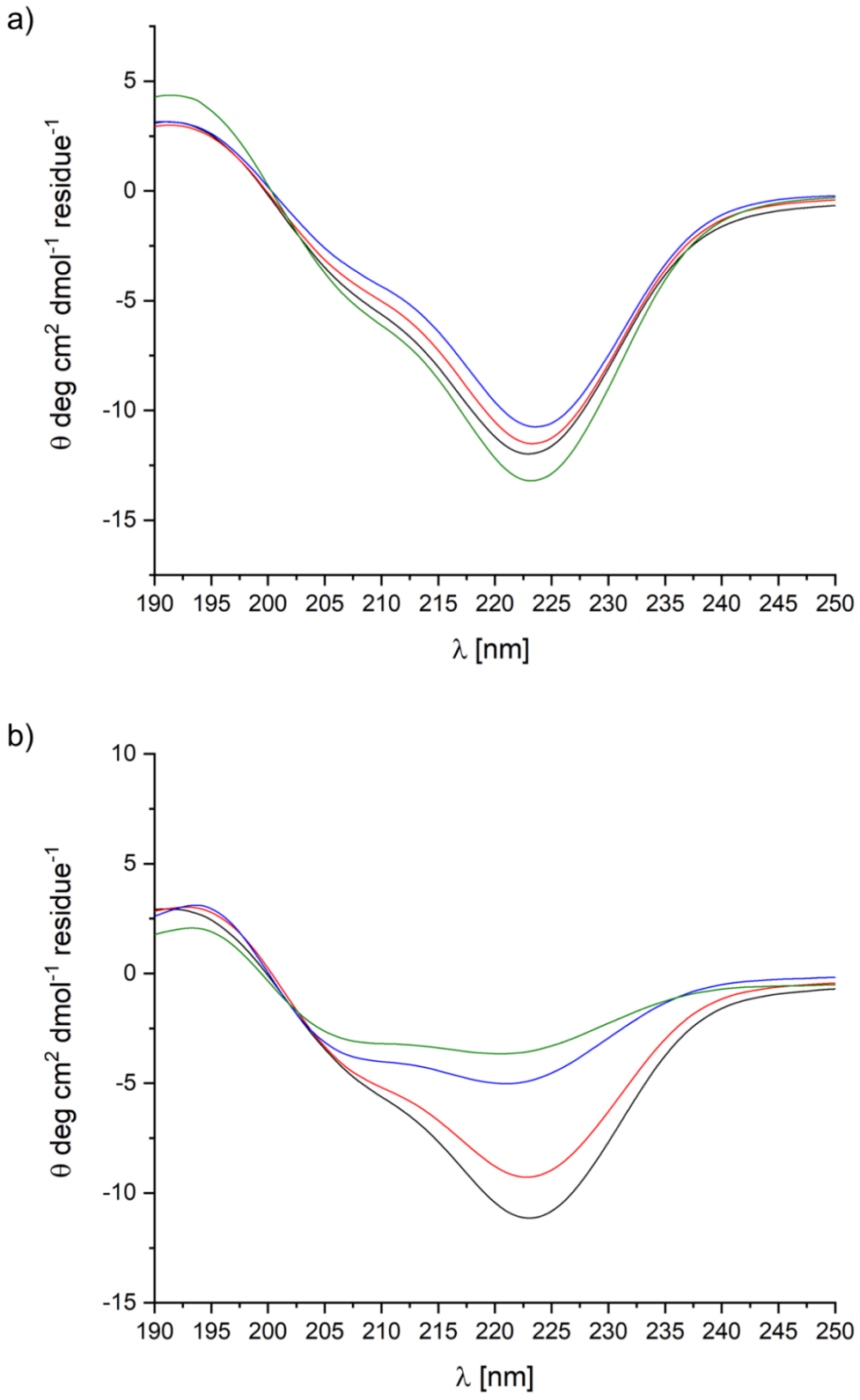

Figure 12.7. CD-spectra at 20°C (a) and 37°C (b) of 0.50 wt% hFF03-K17-Man in D-PBS over a period of six days directly after sample preparation (black line), 24h (red line), 72h (blue line) and 6 days (green line) after sample preparation.

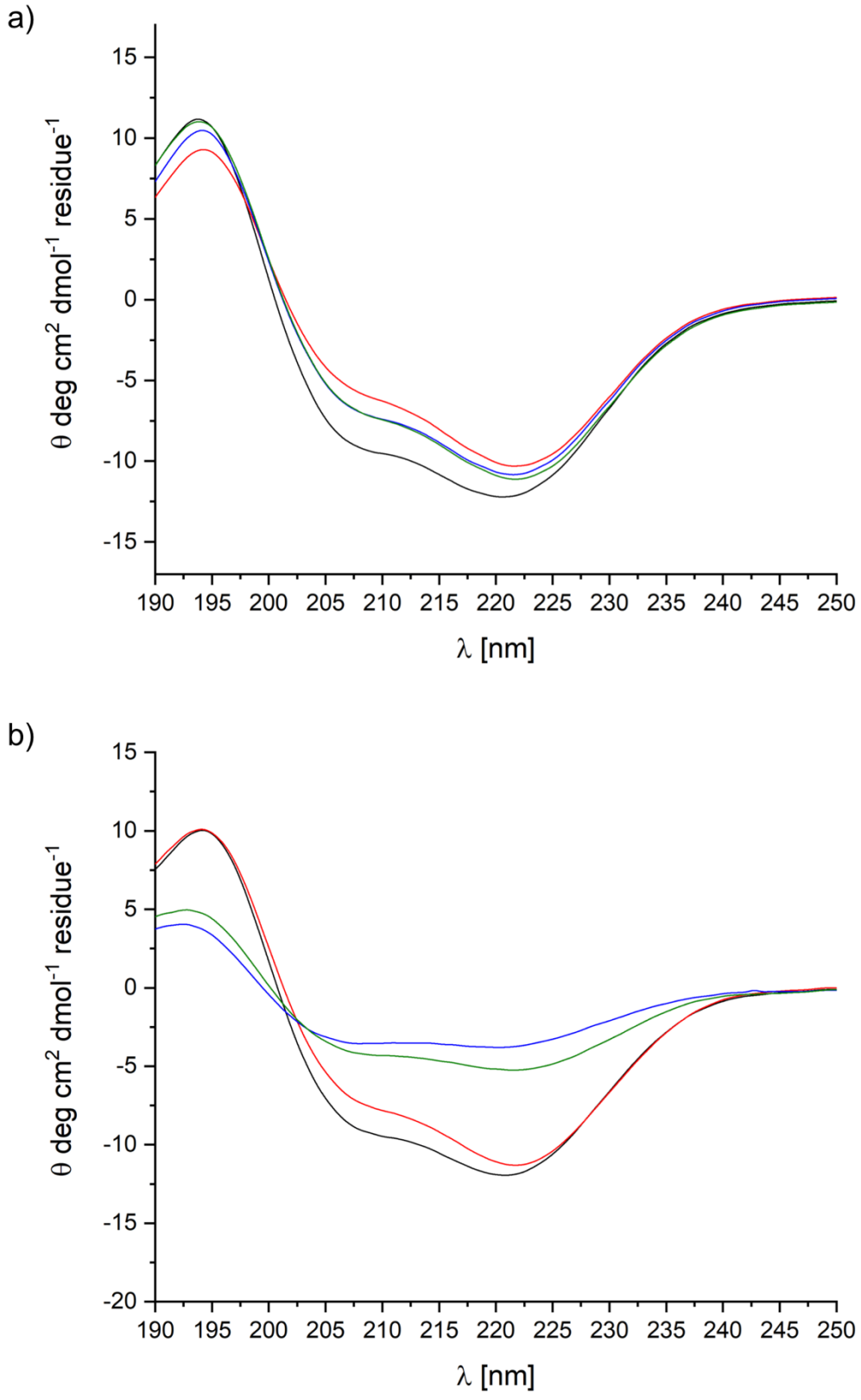

Figure 12.8. CD-spectra at 20°C (a) and 37°C (b) of 0.15 wt% hFF03-K17-RGD in D-PBS over a period of six days directly after sample preparation (black line), 24h (red line), 72h (blue line) and 6 days (green line) after sample preparation.

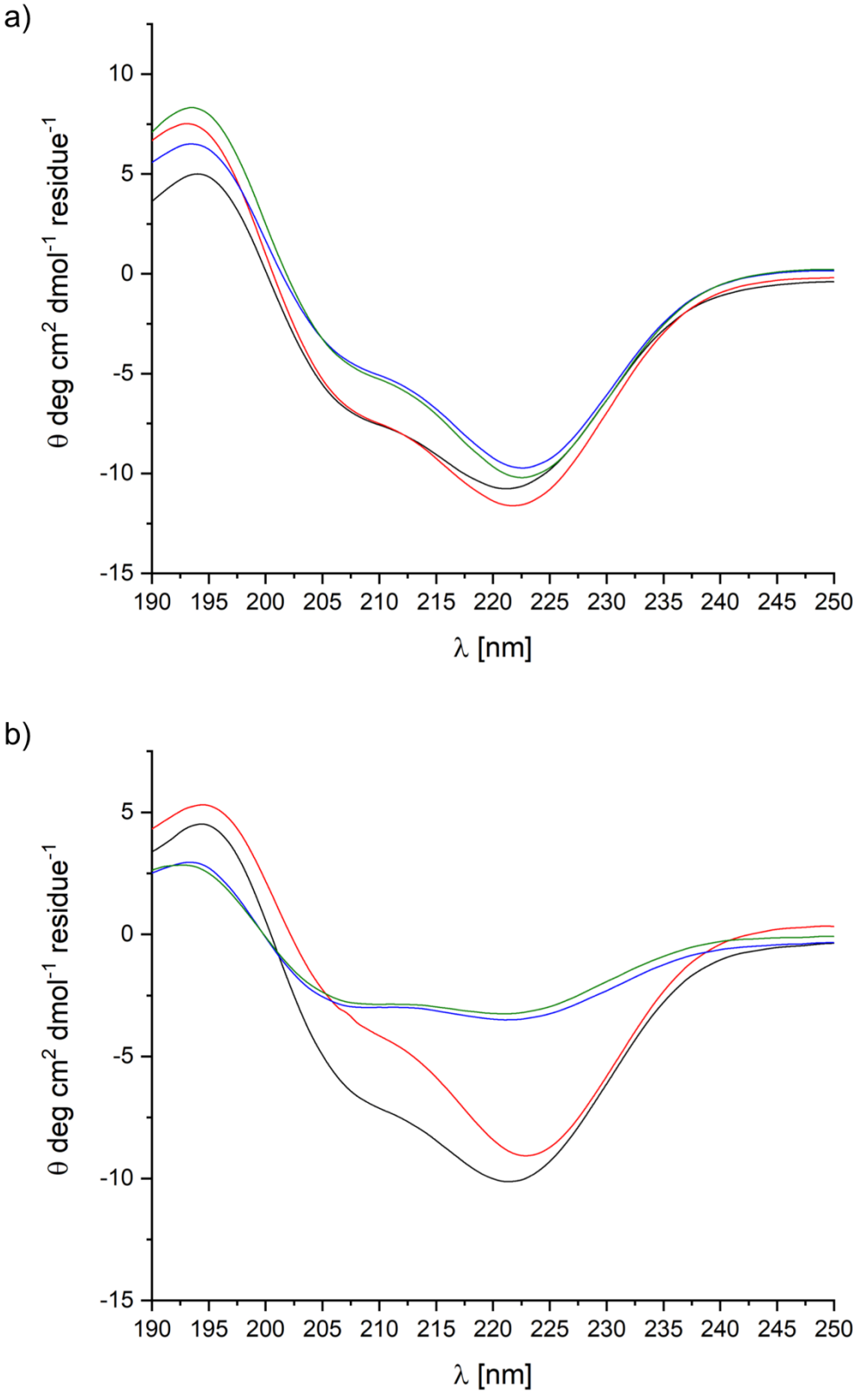

Figure 12.9. CD-spectra at 20°C (a) and 37°C (b) of 0.30 wt% hFF03-K17-RGD in D-PBS over a period of six days directly after sample preparation (black line), 24h (red line), 72h (blue line) and 6 days (green line) after sample preparation.

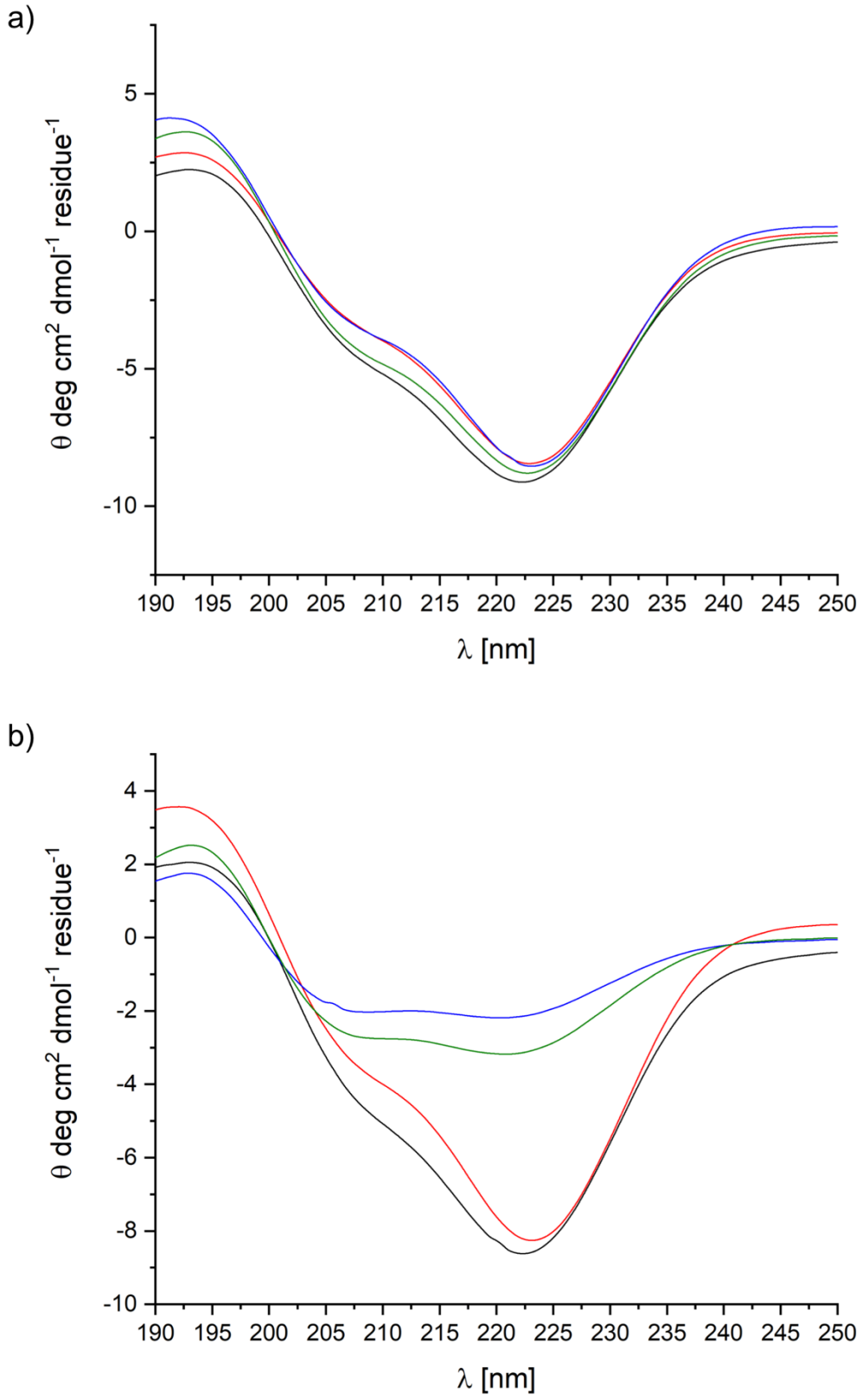

Figure 12.10. CD-spectra at 20°C (a) and 37°C (b) of 0.50 wt% hFF03-K17-RGD in D-PBS over a period of six days directly after sample preparation (black line), 24h (red line), 72h (blue line) and 6 days (green line) after sample preparation.

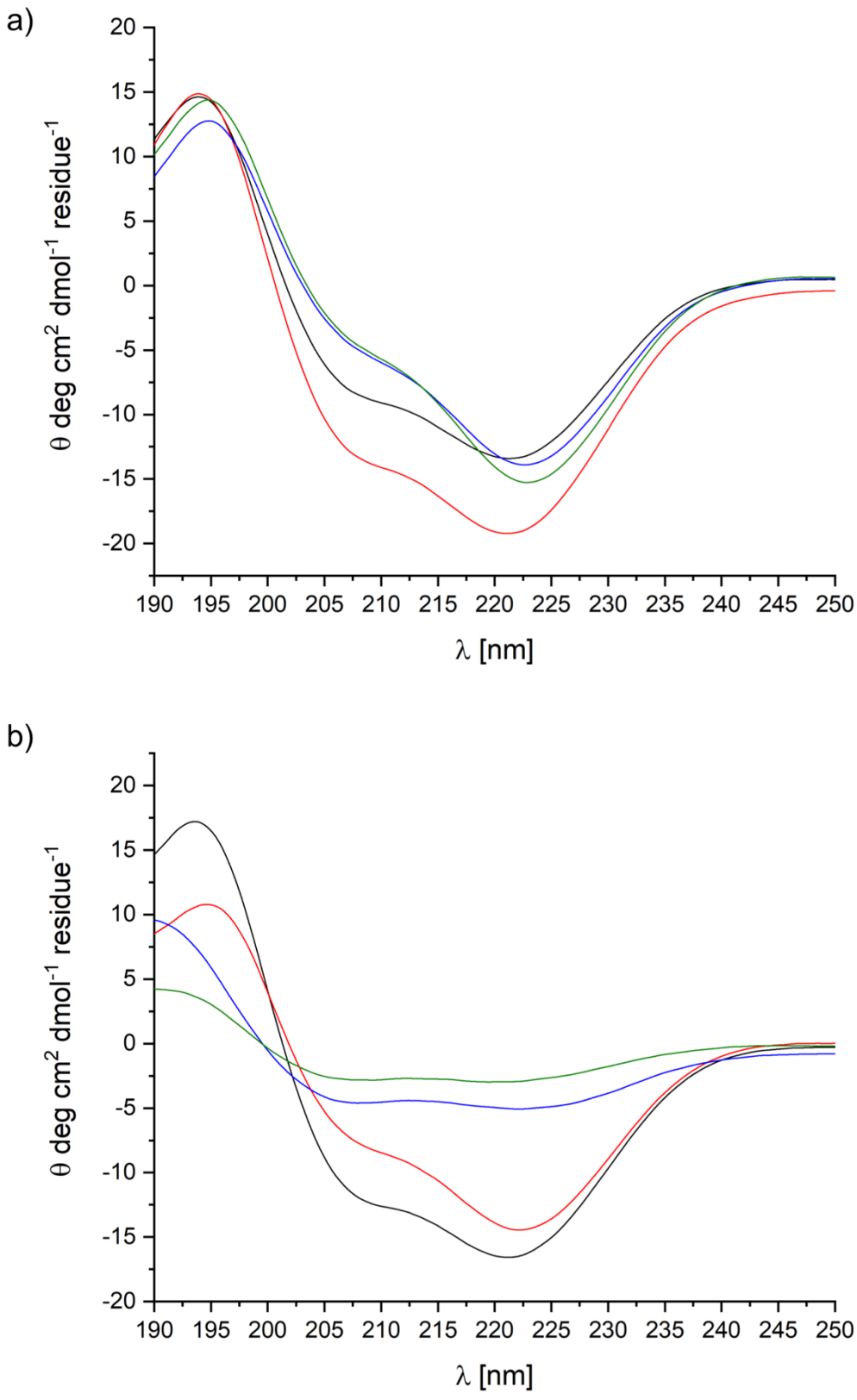

Figure 12.11. CD-spectra at 20°C (a) and 37°C (b) of 0.15 wt% hFF03 + 1% hFF03-K17-Man in D-PBS over a period of six days directly after sample preparation (black line), 24h (red line), 72h (blue line) and 6 days (green line) after sample preparation.

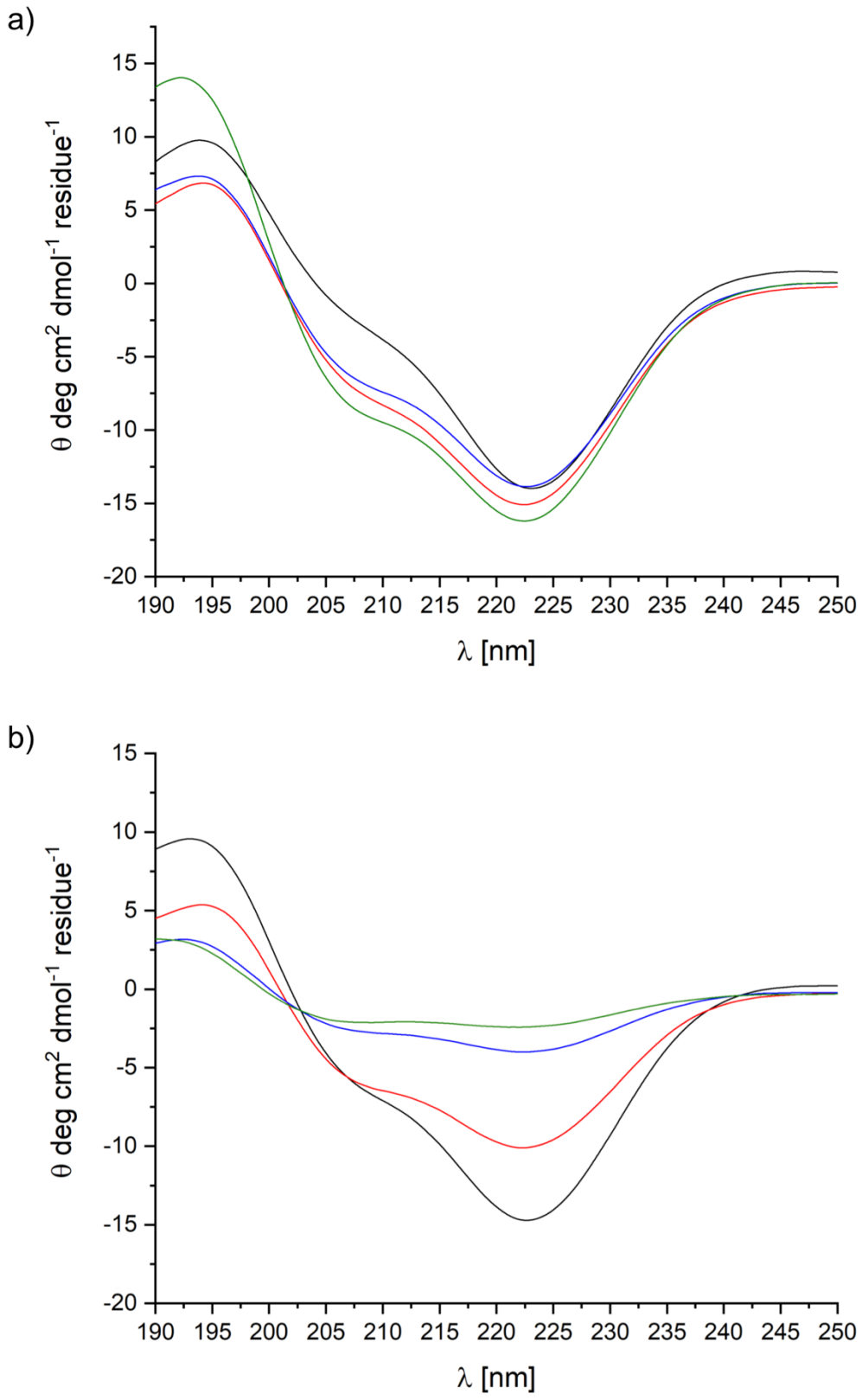

Figure 12.12. CD-spectra at 20°C (a) and 37°C (b) of 0.30 wt% hFF03 + 1% hFF03-K17-Man in D-PBS over a period of six days directly after sample preparation (black line), 24h (red line), 72h (blue line) and 6 days (green line) after sample preparation.

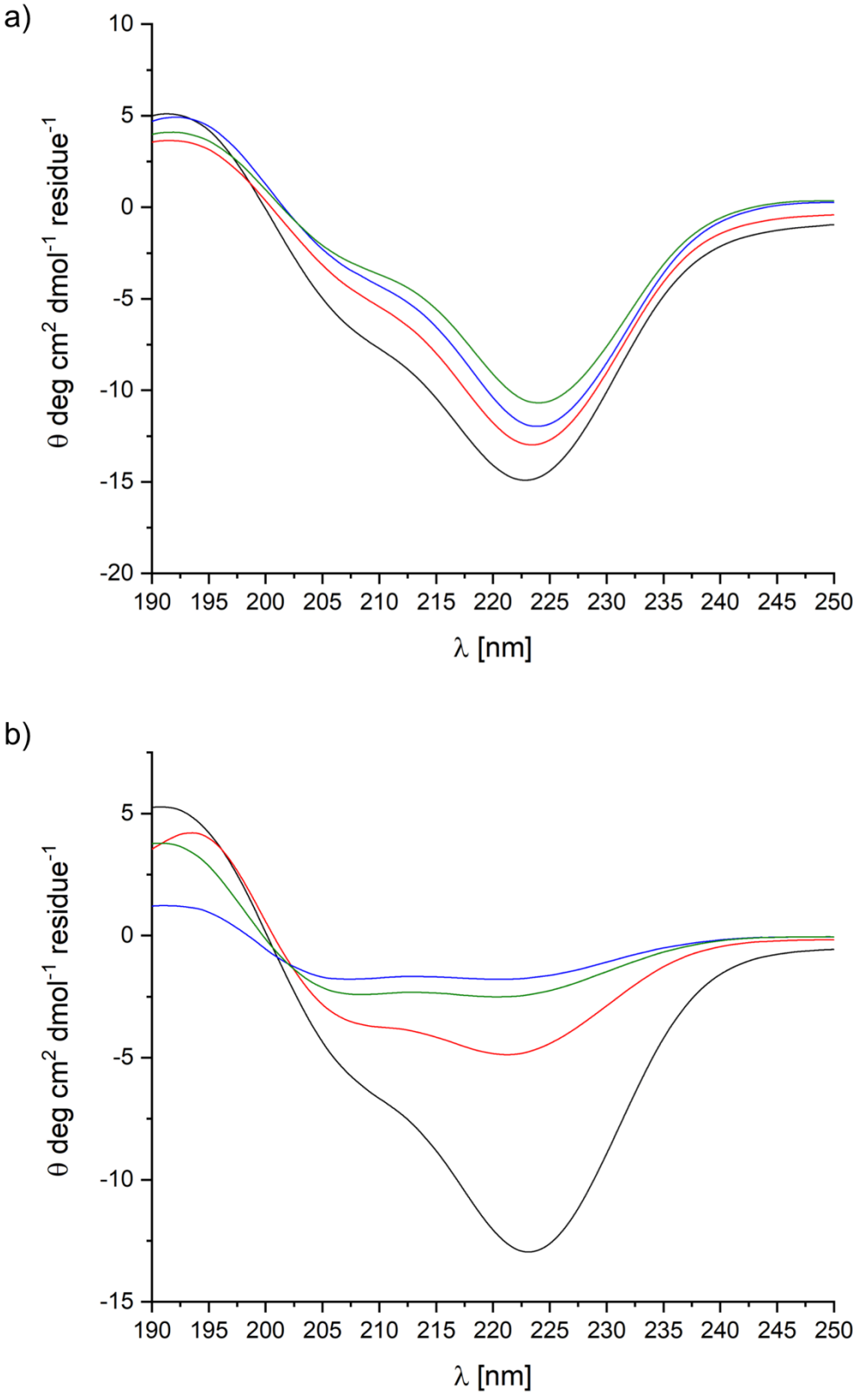

Figure 12.13. CD-spectra at 20°C (a) and 37°C (b) of 0.50 wt% hFF03 + 1% hFF03-K17-Man in D-PBS over a period of six days directly after sample preparation (black line), 24h (red line), 72h (blue line) and 6 days (green line) after sample preparation.

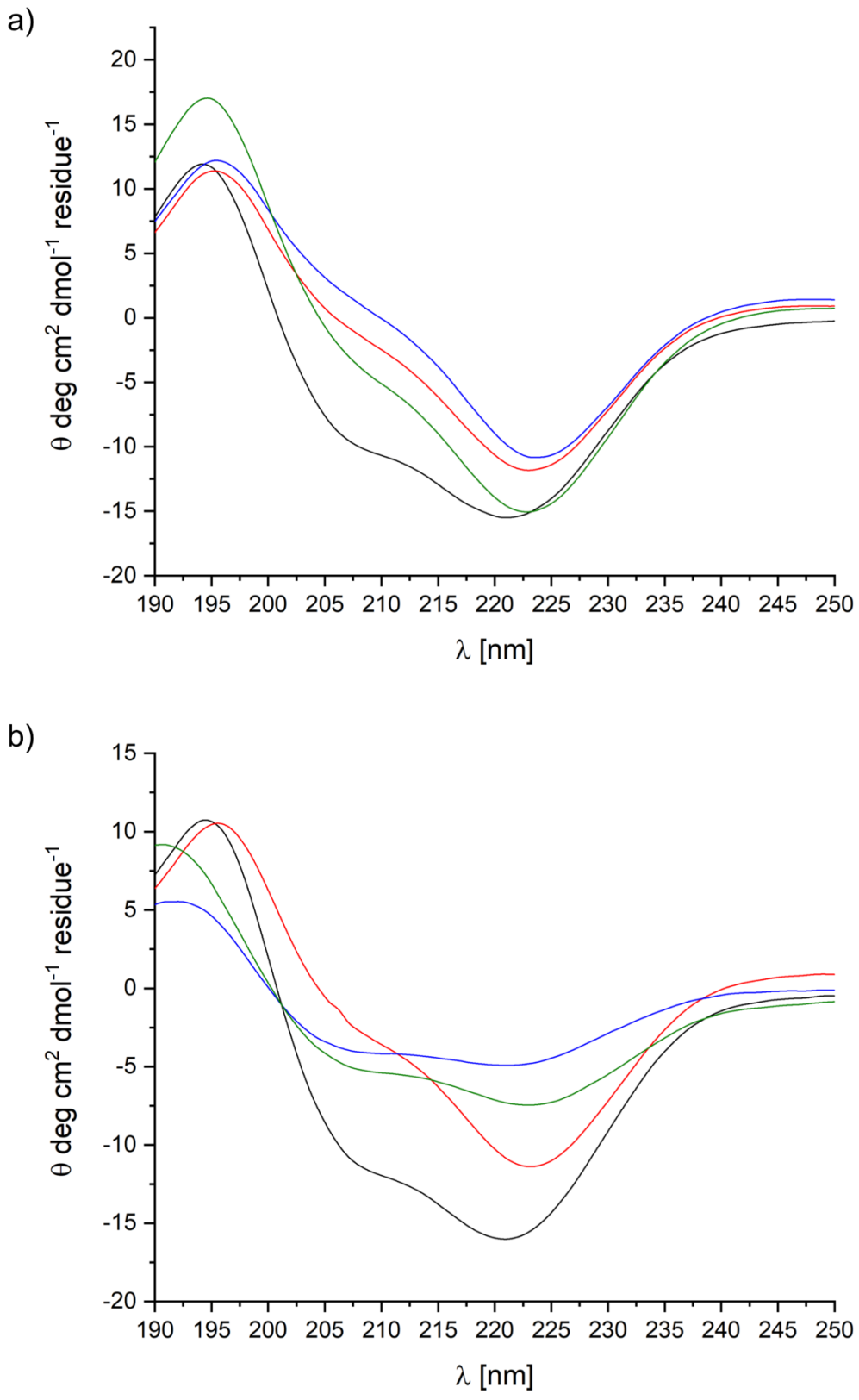

Figure 12.14. CD-spectra at 20°C (a) and 37°C (b) of 0.15 wt% hFF03 + 5% hFF03-K17-RGD in D-PBS over a period of six days directly after sample preparation (black line), 24h (red line), 72h (blue line) and 6 days (green line) after sample preparation.

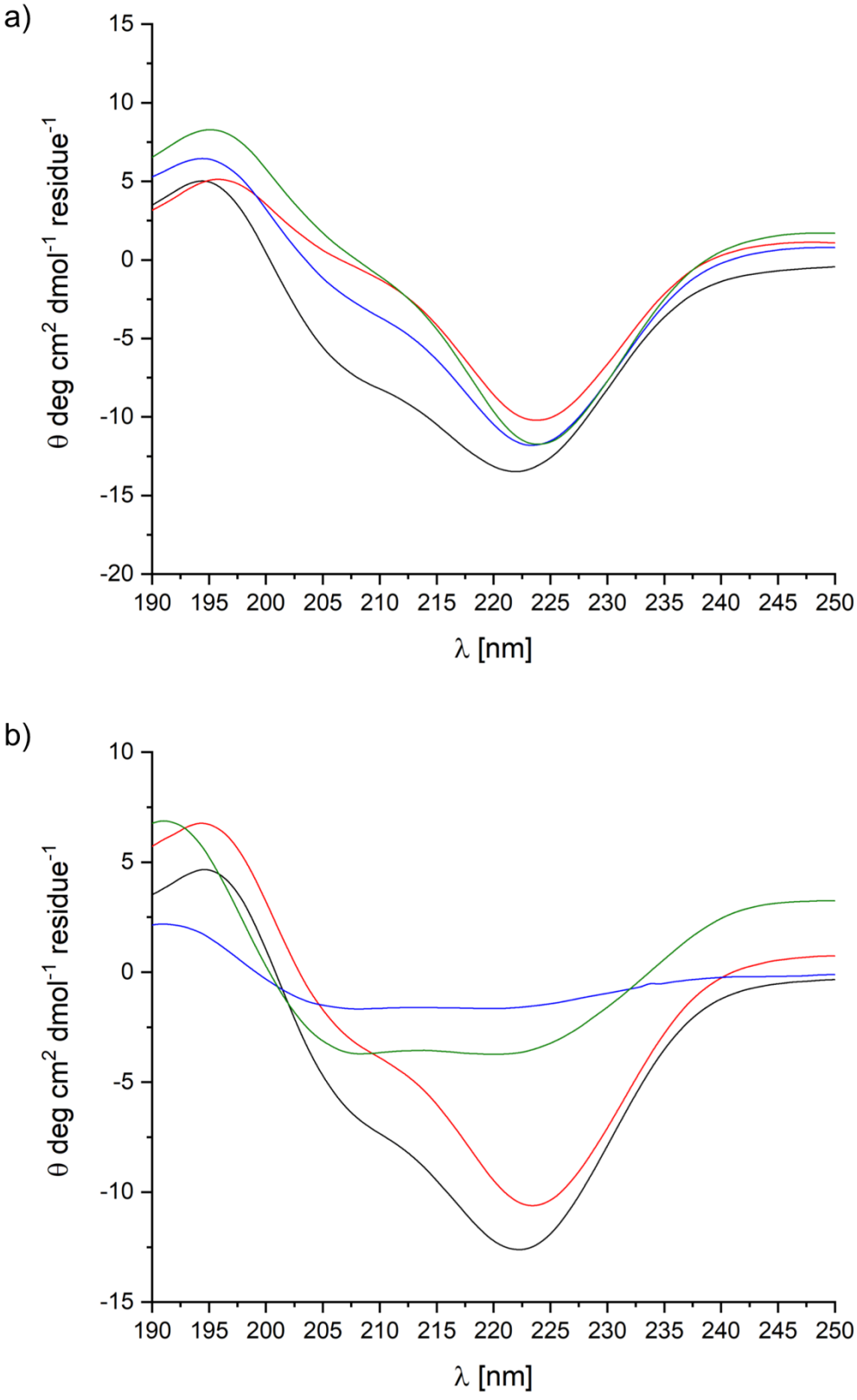

Figure 12.15. CD-spectra at 20°C (a) and 37°C (b) of 0.30 wt% hFF03 + 5% hFF03-K17-RGD in D-PBS over a period of six days directly after sample preparation (black line), 24h (red line), 72h (blue line) and 6 days (green line) after sample preparation.

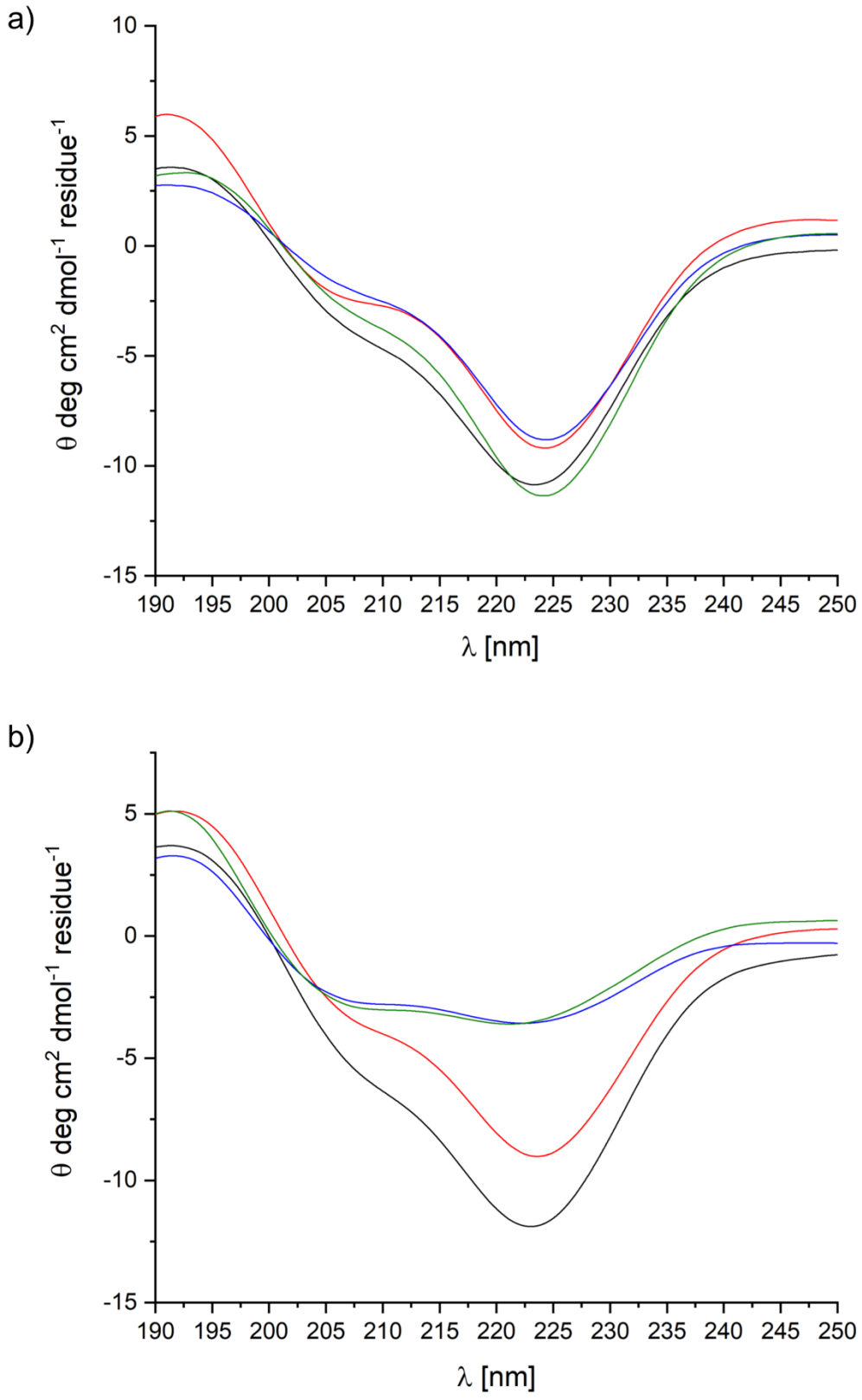

Figure 12.16. CD-spectra at 20°C (a) and 37°C (b) of 0.50 wt% hFF03 + 5% hFF03-K17-RGD in D-PBS over a period of six days directly after sample preparation (black line), 24h (red line), 72h (blue line) and 6 days (green line) after sample preparation.

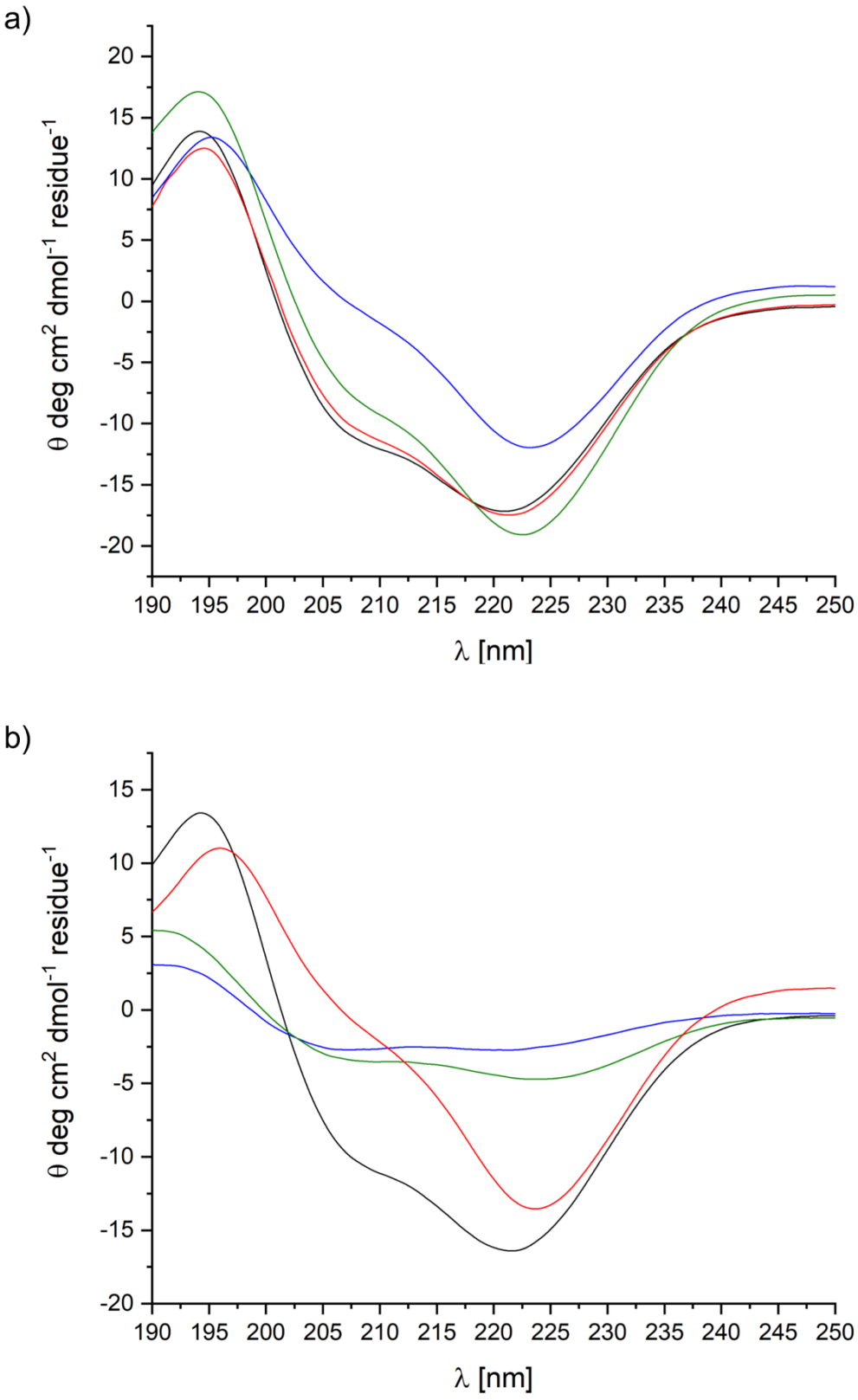

Figure 12.17. CD-spectra at 20°C (a) and 37°C (b) of 0.15 wt% hFF03 +1% hFF03-K17-Man + 5% hFF03-K17-RGD in D-PBS over a period of six days directly after sample preparation (black line), 24h (red line), 72h (blue line) and 6 days (green line) after sample preparation.

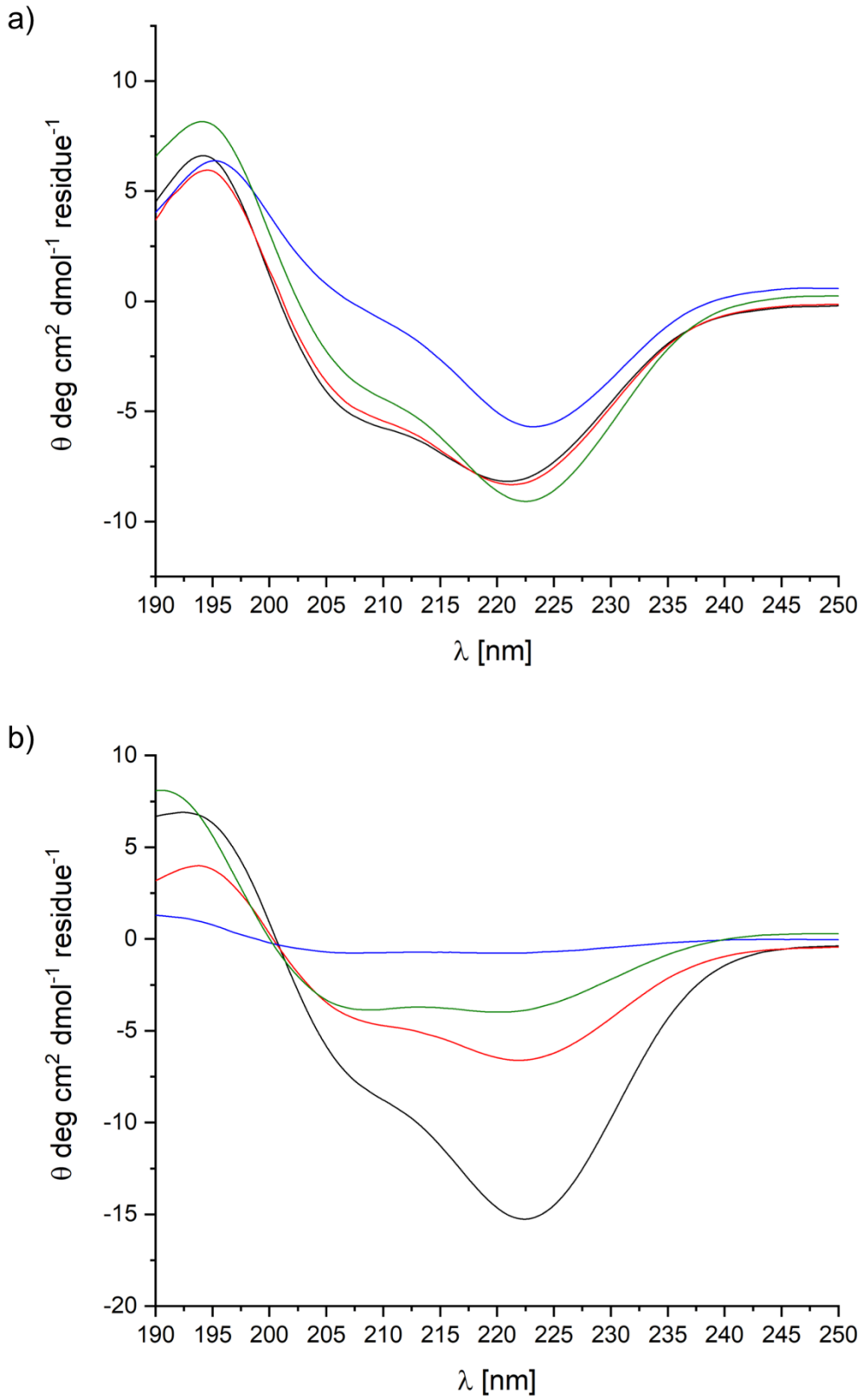

Figure 12.18. CD-spectra at 20°C (a) and 37°C (b) of 0.30 wt% hFF03 +1% hFF03-K17-Man + 5% hFF03-K17-RGD in D-PBS over a period of six days directly after sample preparation (black line), 24h (red line), 72h (blue line) and 6 days (green line) after sample preparation.

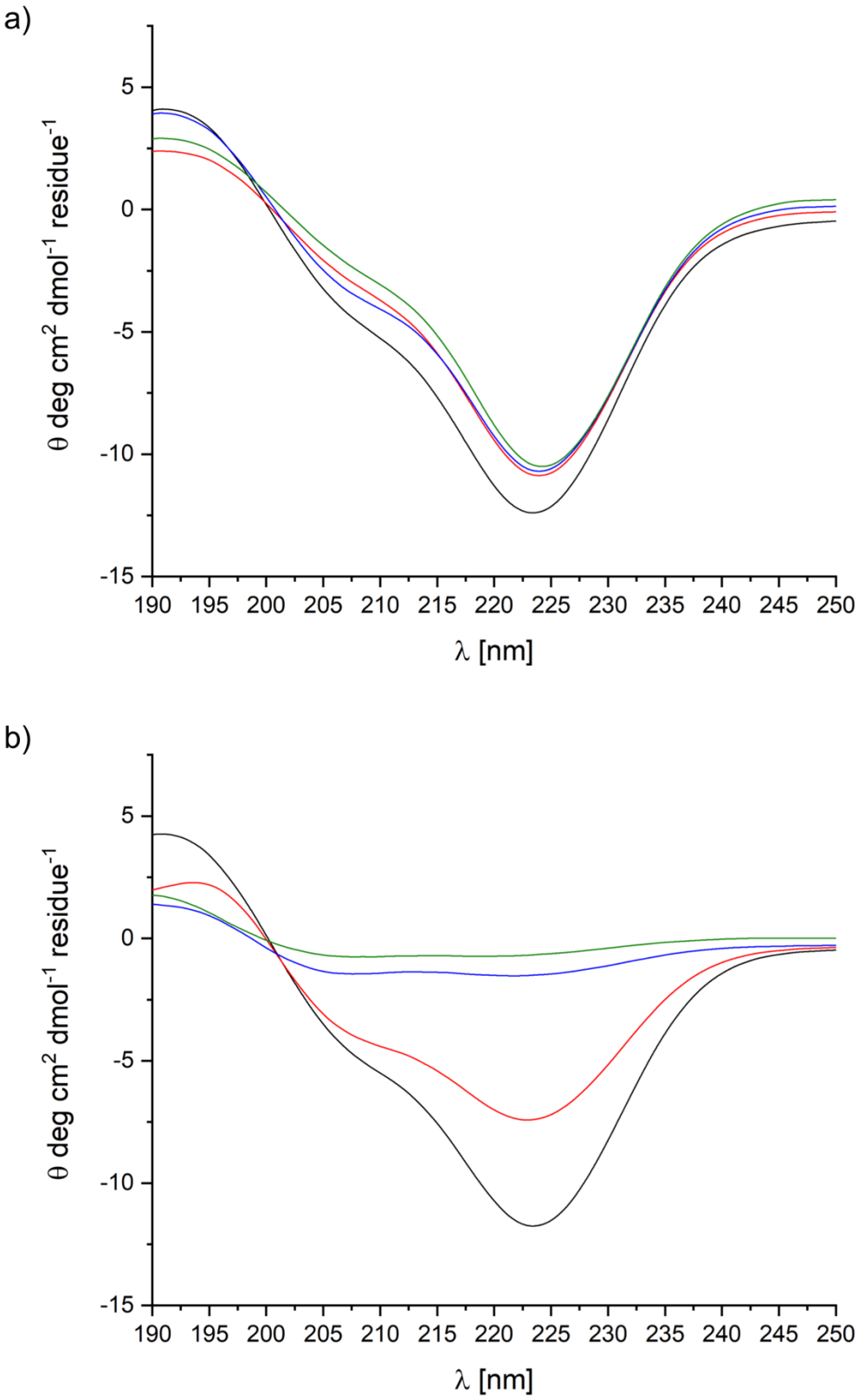

Figure 12.19. CD-spectra at 20°C (a) and 37°C (b) of 0.50 wt% hFF03 +1% hFF03-K17-Man + 5% hFF03-K17-RGD in D-PBS over a period of six days directly after sample preparation (black line), 24h (red line), 72h (blue line) and 6 days (green line) after sample preparation.

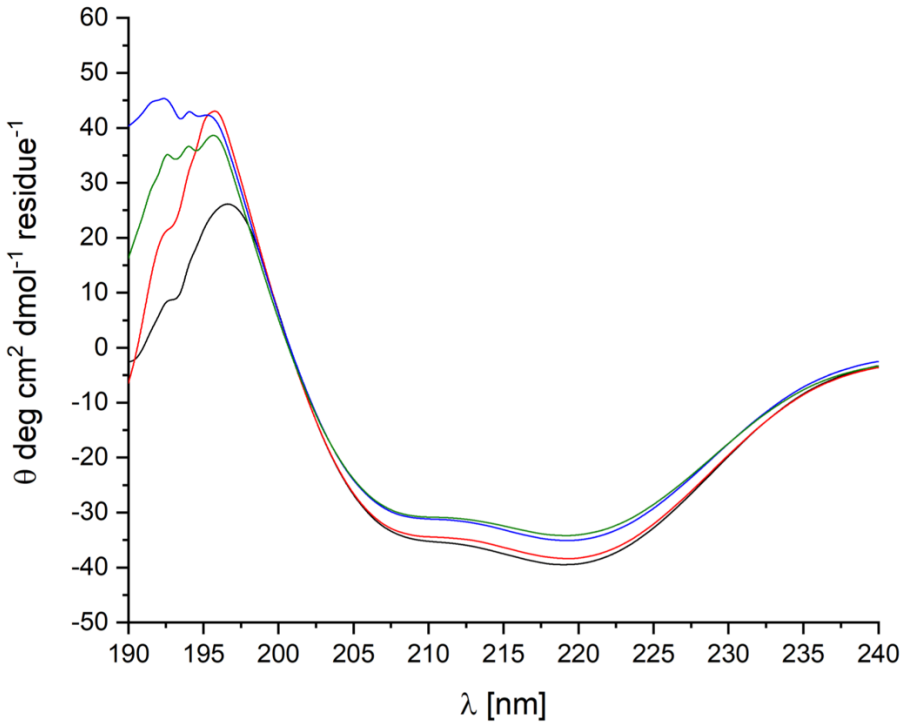

Figure 12.20. CD-spectra at 20°C of 50 µM hFF03-RGD in D-PBS over a period of six days directly after sample preparation (black line), 24h (red line), 72h (blue line) and 6 days (green line) after sample preparation.

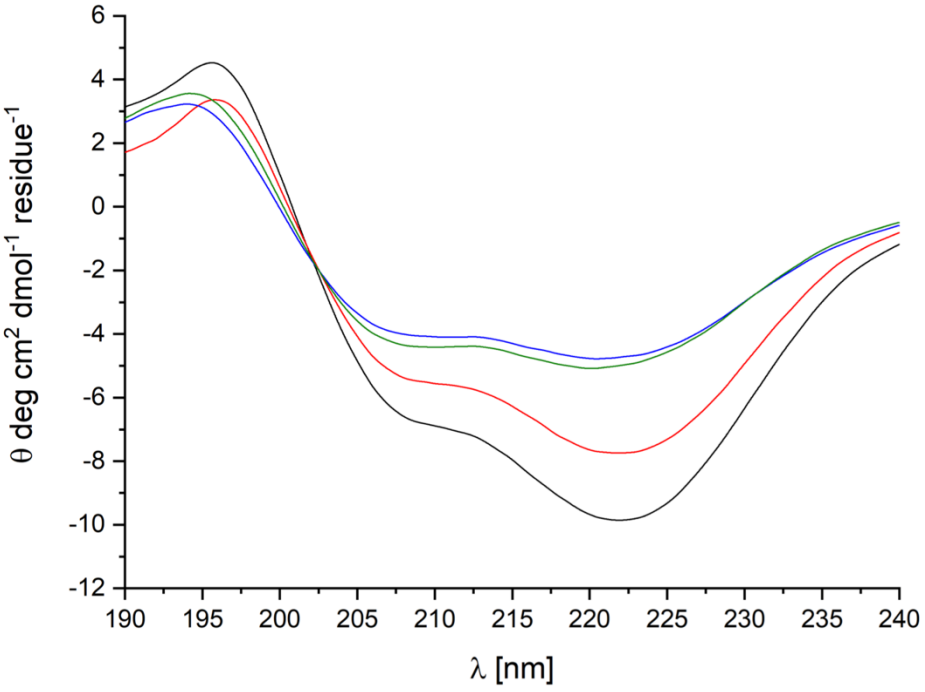

Figure 12.21. CD-spectra at 37°C of 1100 µM hFF03-K17-Gal in D-PBS over a period of six days directly after sample preparation (black line), 24h (red line), 72h (blue line) and 6 days (green line) after sample preparation.

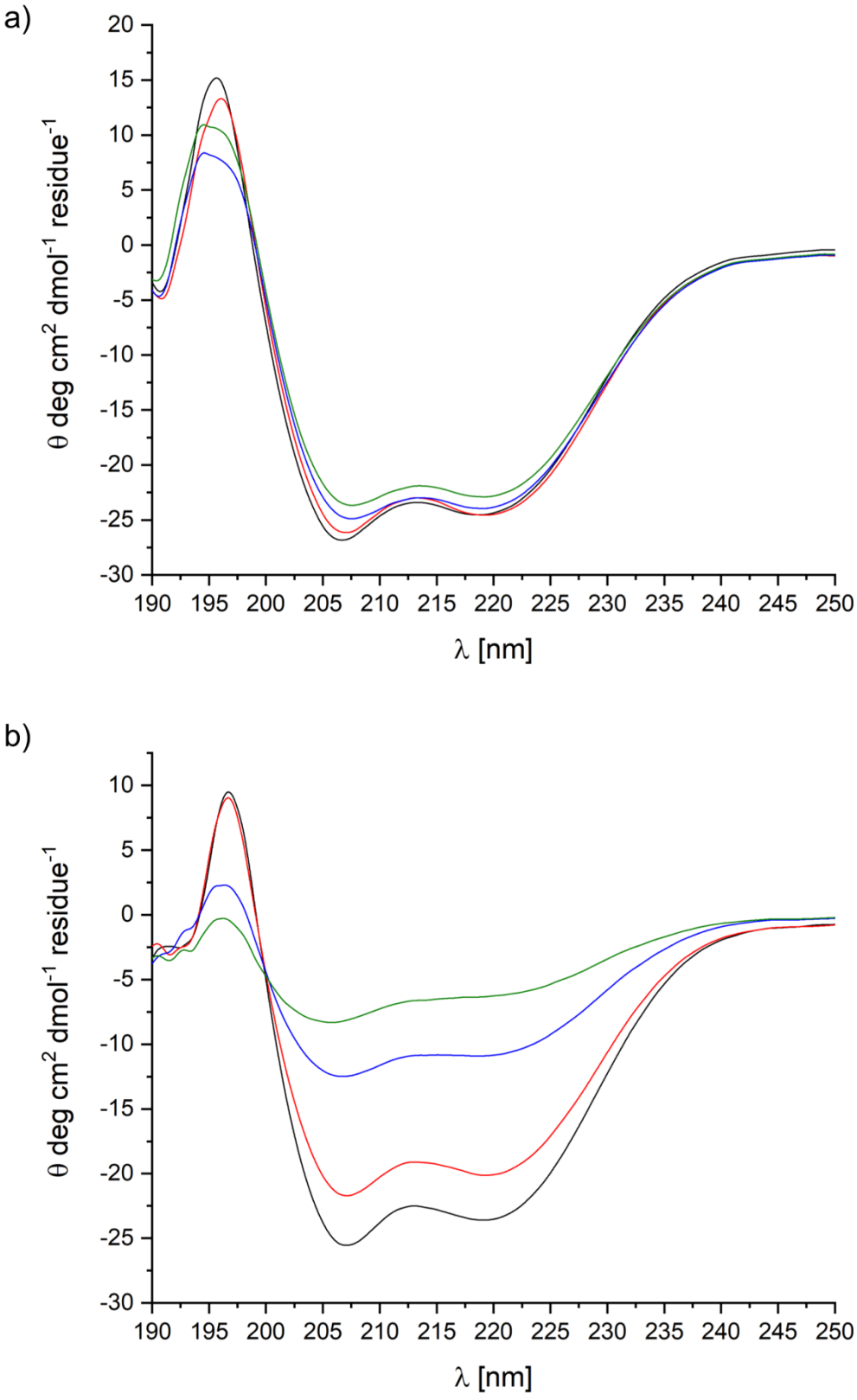

Figure 12.22. CD-spectra at 20°C (a) and 37°C (b) of 50 µM hFF03-K17-NAIP in D-PBS over a period of six days directly after sample preparation (black line), 24h (red line), 72h (blue line) and 6 days (green line) after sample preparation.

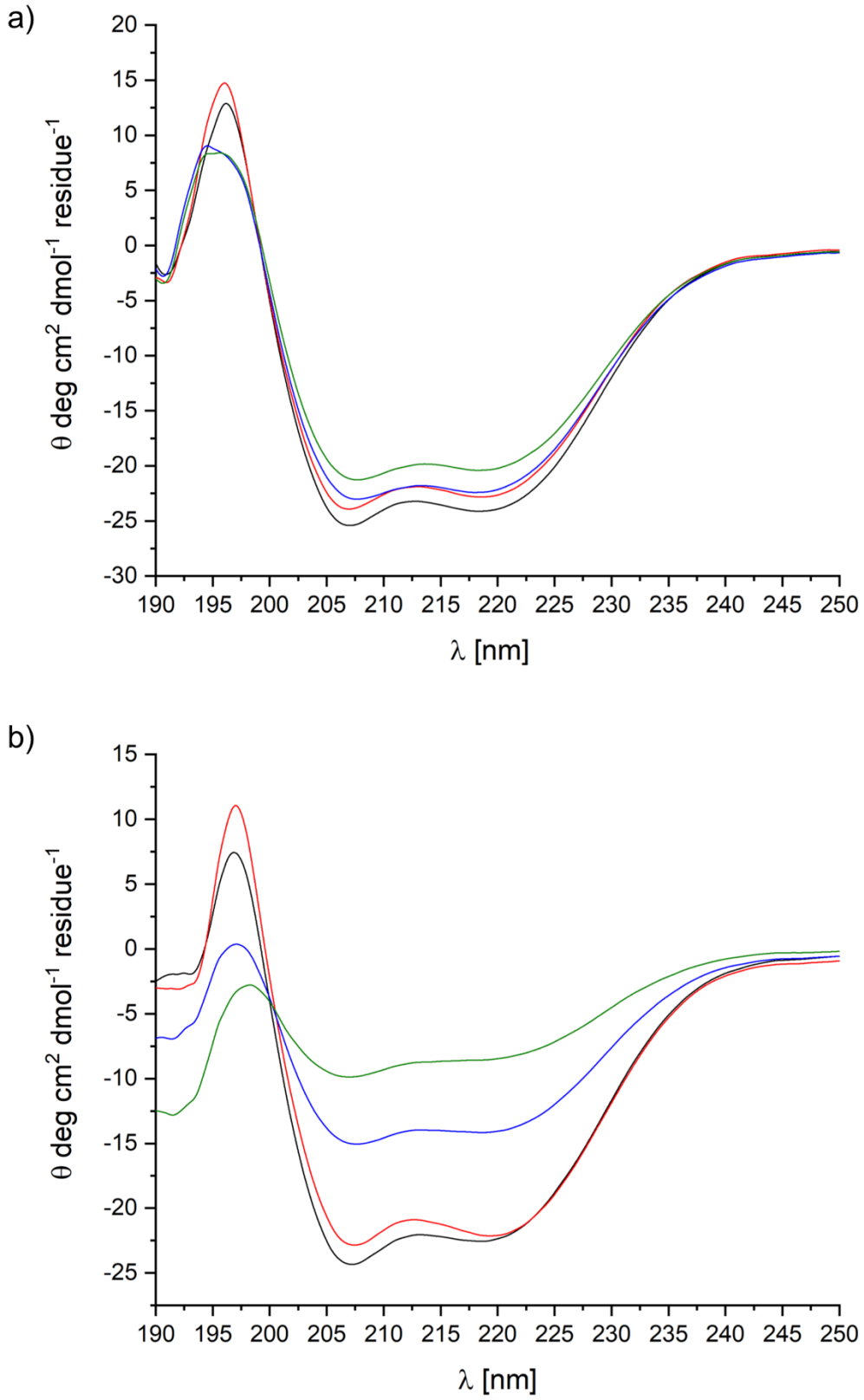

Figure 12.23. CD-spectra at 20°C (a) and 37°C (b) of 50 µM hFF03-K17-SP in D-PBS over a period of six days directly after sample preparation (black line), 24h (red line), 72h (blue line) and 6 days (green line) after sample preparation.

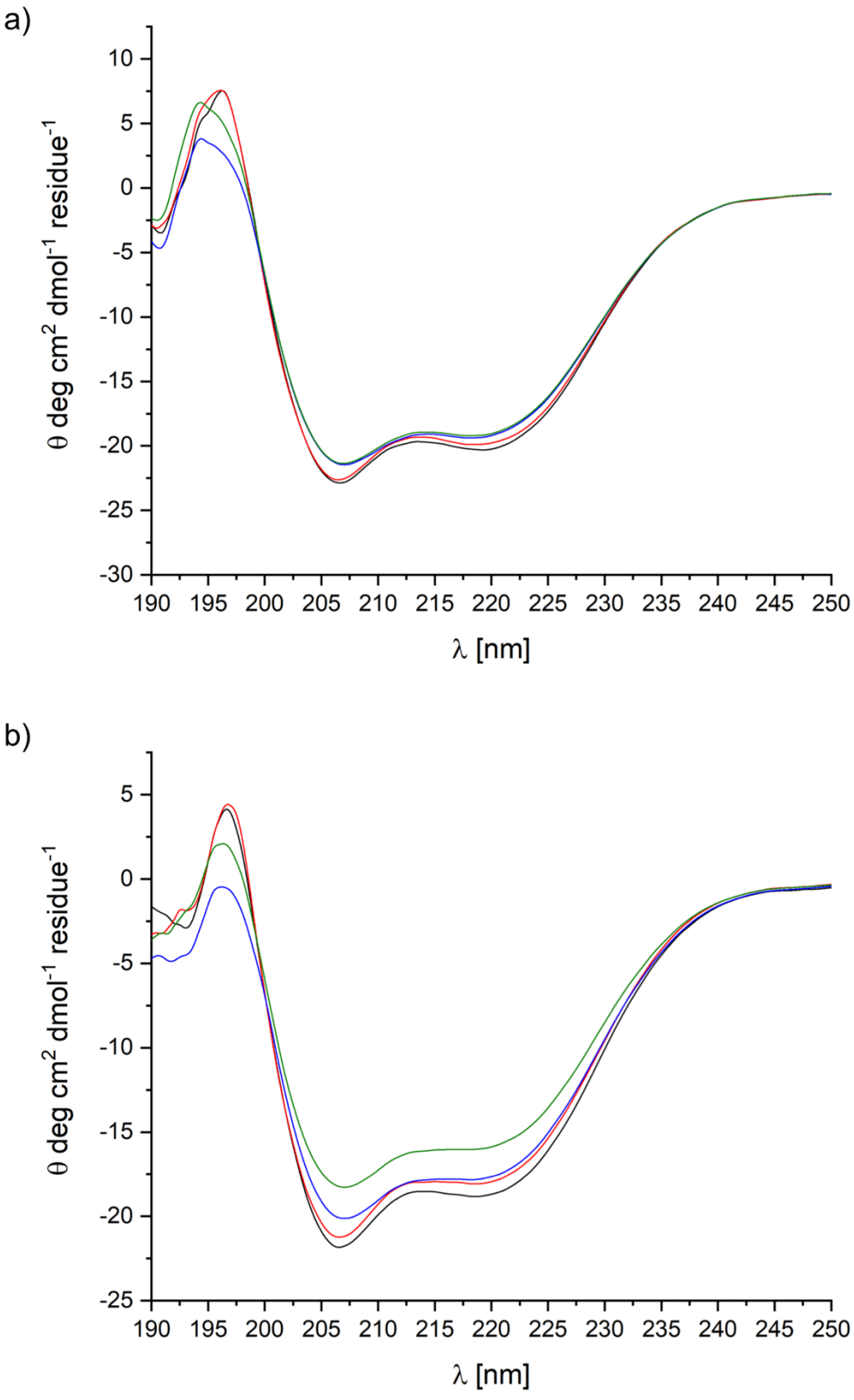

Figure 12.24. CD-spectra at 20°C (a) and 37°C (b) of 50 µM hFF03-K17-VT in D-PBS over a period of six days directly after sample preparation (black line), 24h (red line), 72h (blue line) and 6 days (green line) after sample preparation.

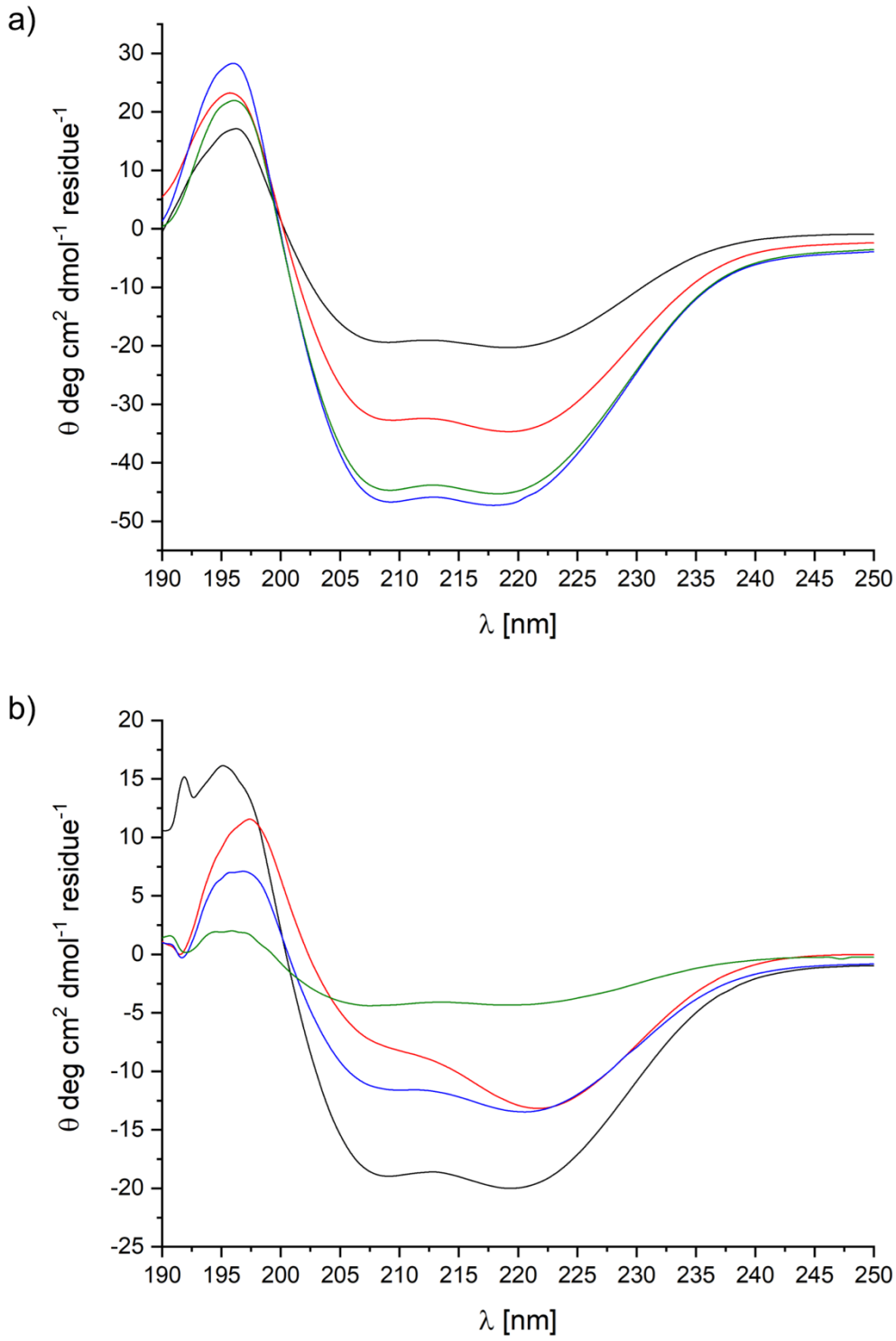

Figure 12.25. CD-spectra at 20°C (a) and 37°C (b) of 75 µM FF03 in D-PBS over a period of six days directly after sample preparation (black line), 24h (red line), 72h (blue line) and 6 days (green line) after sample preparation.

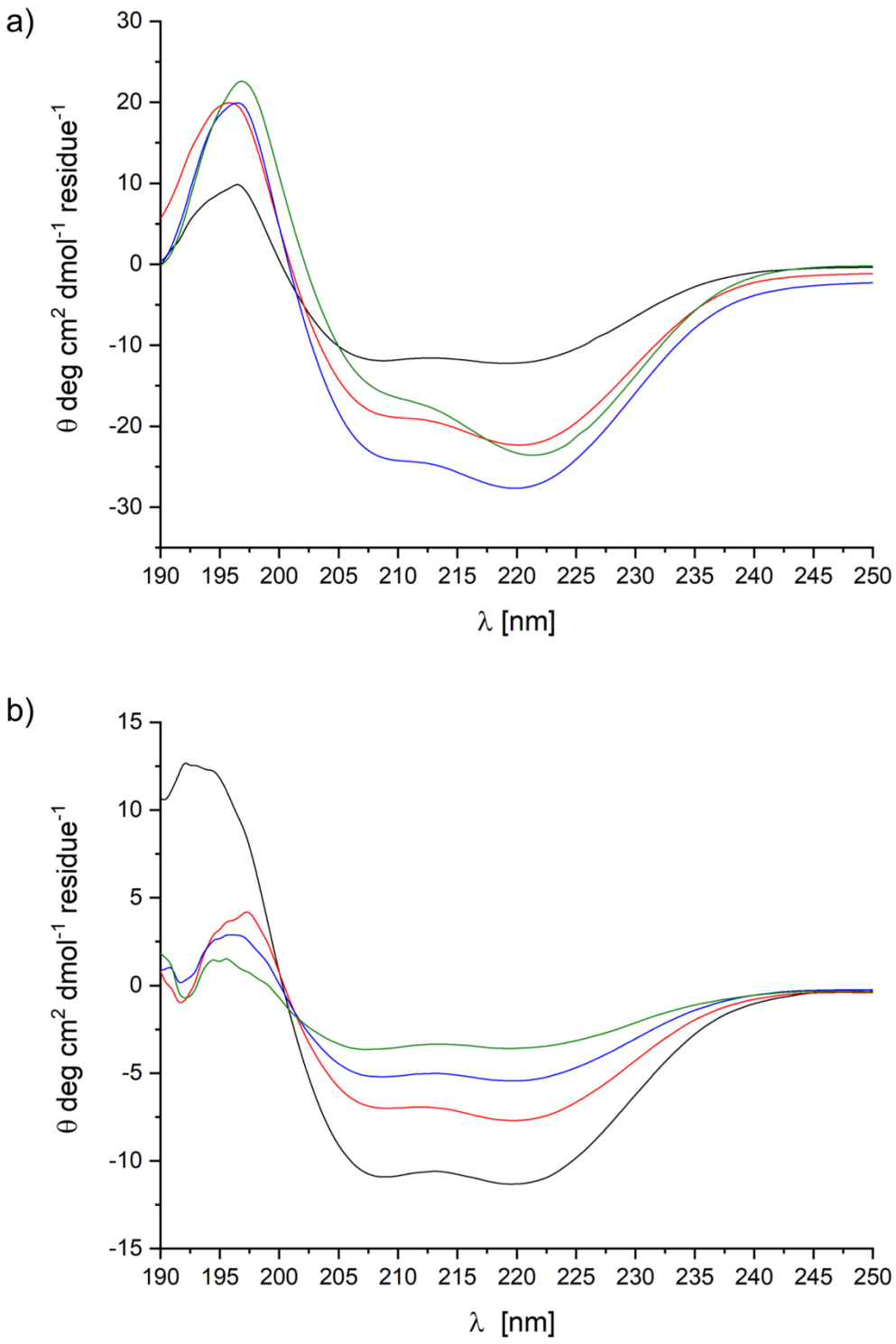

Figure 12.26. CD-spectra at 20°C (a) and 37°C (b) of 75 µM FF03-K17-Sial in D-PBS over a period of six days directly after sample preparation (black line), 24h (red line), 72h (blue line) and 6 days (green line) after sample preparation.

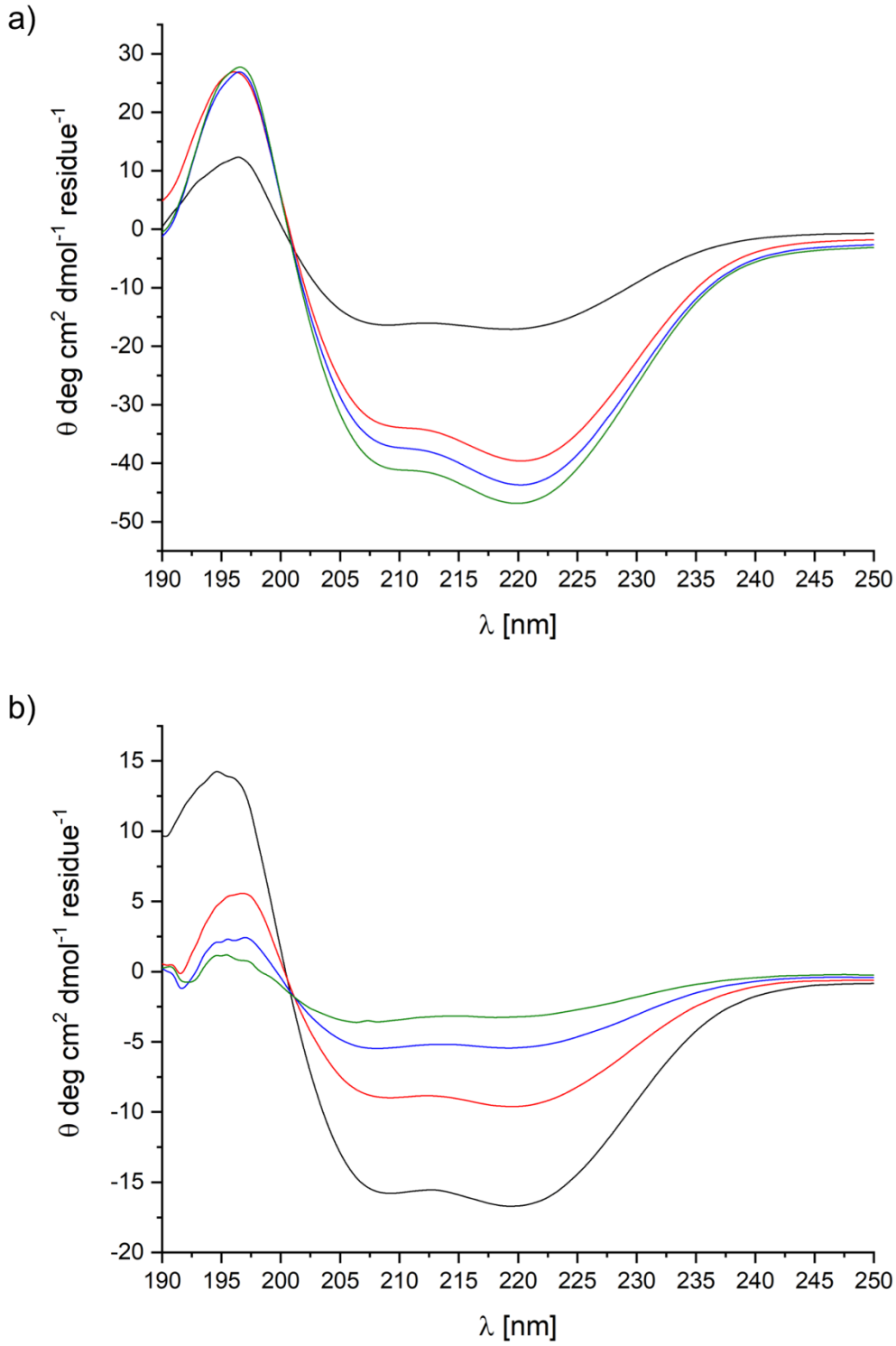

Figure 12.27. CD-spectra at 20°C (a) and 37°C (b) of FF03 + FF03-K17-Sial in D-PBS over a period of six days directly after sample preparation (black line), 24h (red line), 72h (blue line) and 6 days (green line) after sample preparation (75 µM total peptide concentration).

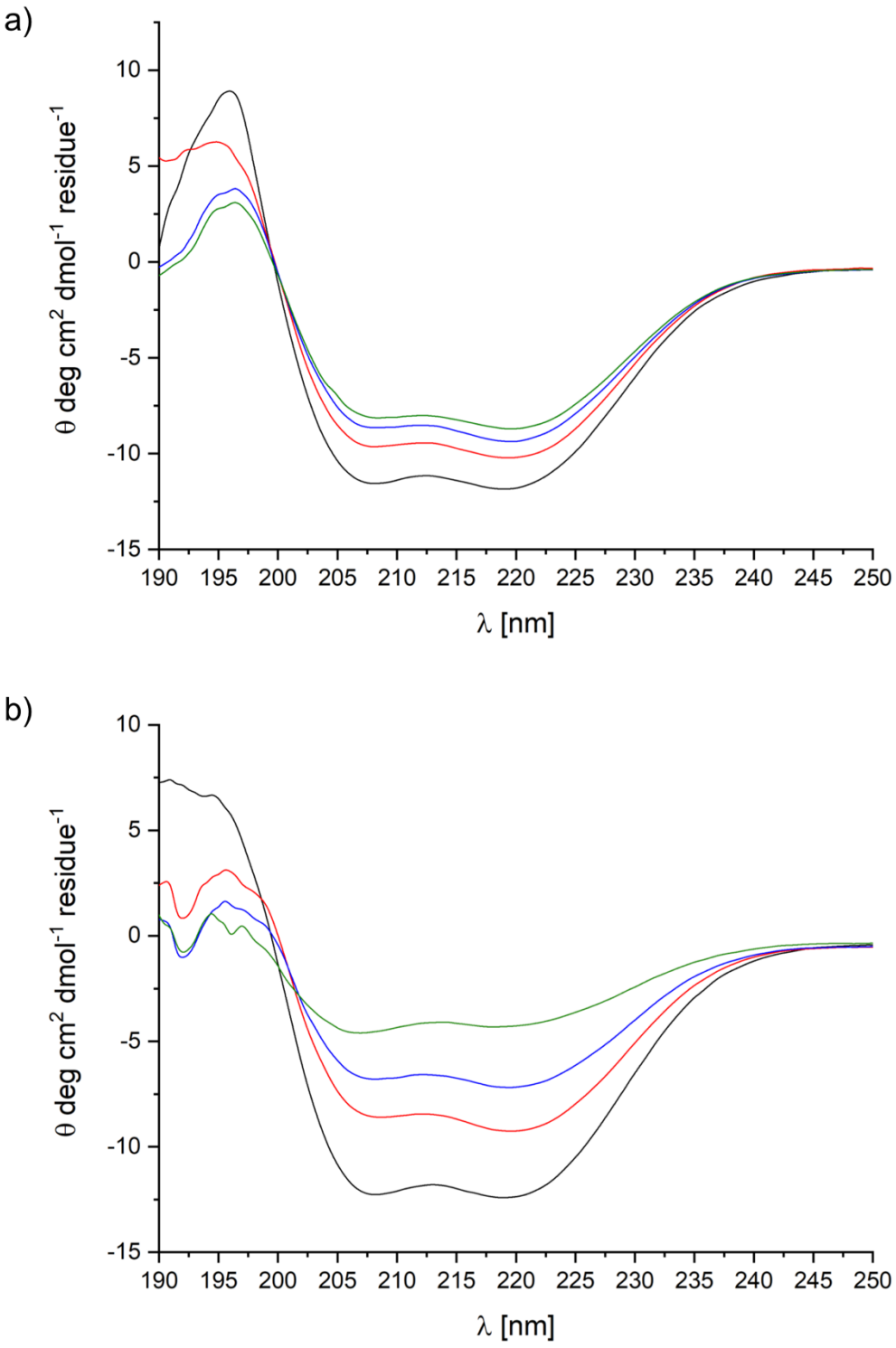

Figure 12.28. CD-spectra at 20°C (a) and 37°C (b) of 75 µM hFF03 in D-PBS over a period of six days directly after sample preparation (black line), 24h (red line), 72h (blue line) and 6 days (green line) after sample preparation.

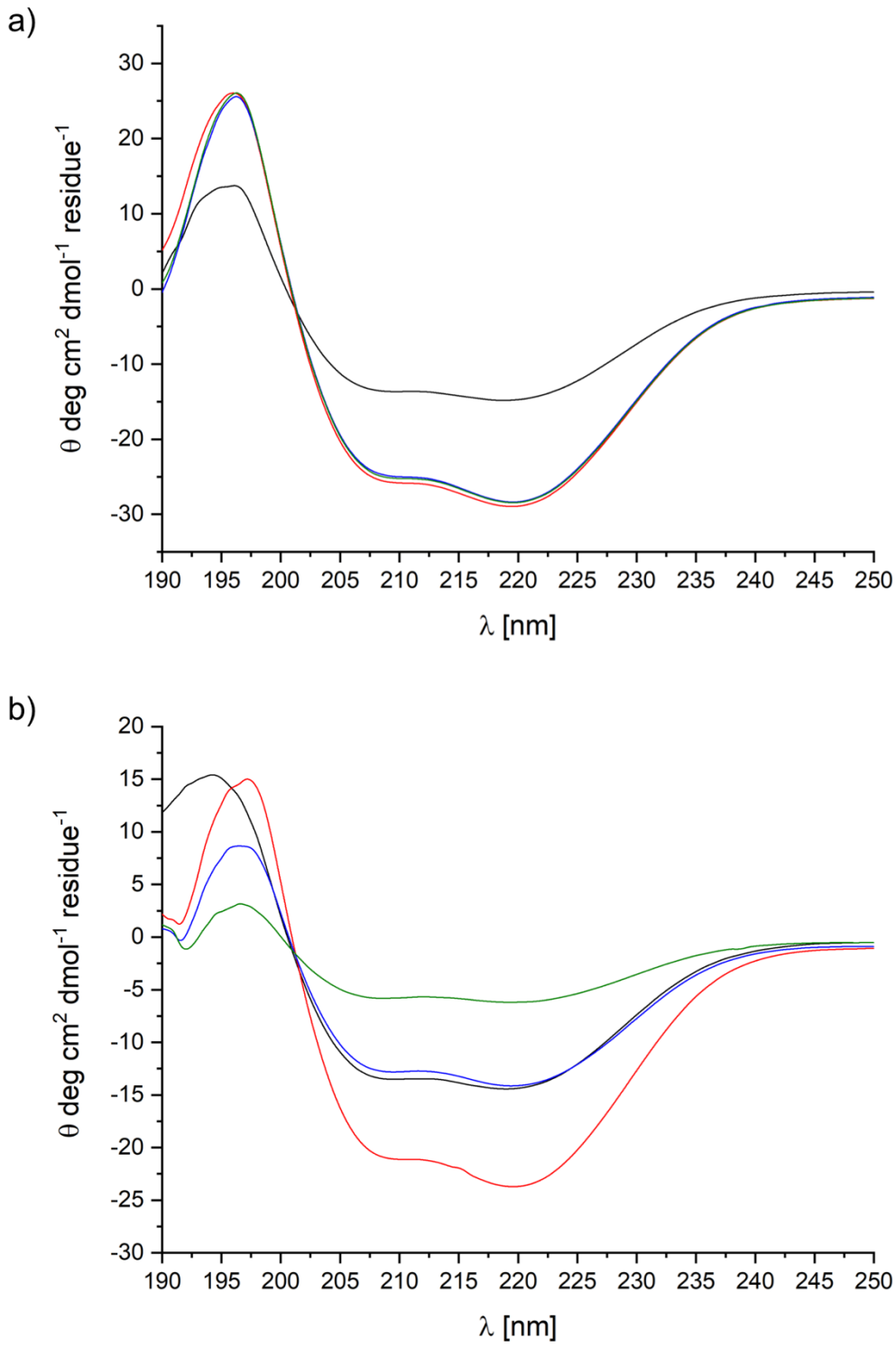

Figure 12.29. CD-spectra at 20°C (a) and 37°C (b) of 75 µM hFF03-K17-Sial in D-PBS over a period of six days directly after sample preparation (black line), 24h (red line), 72h (blue line) and 6 days (green line) after sample preparation.

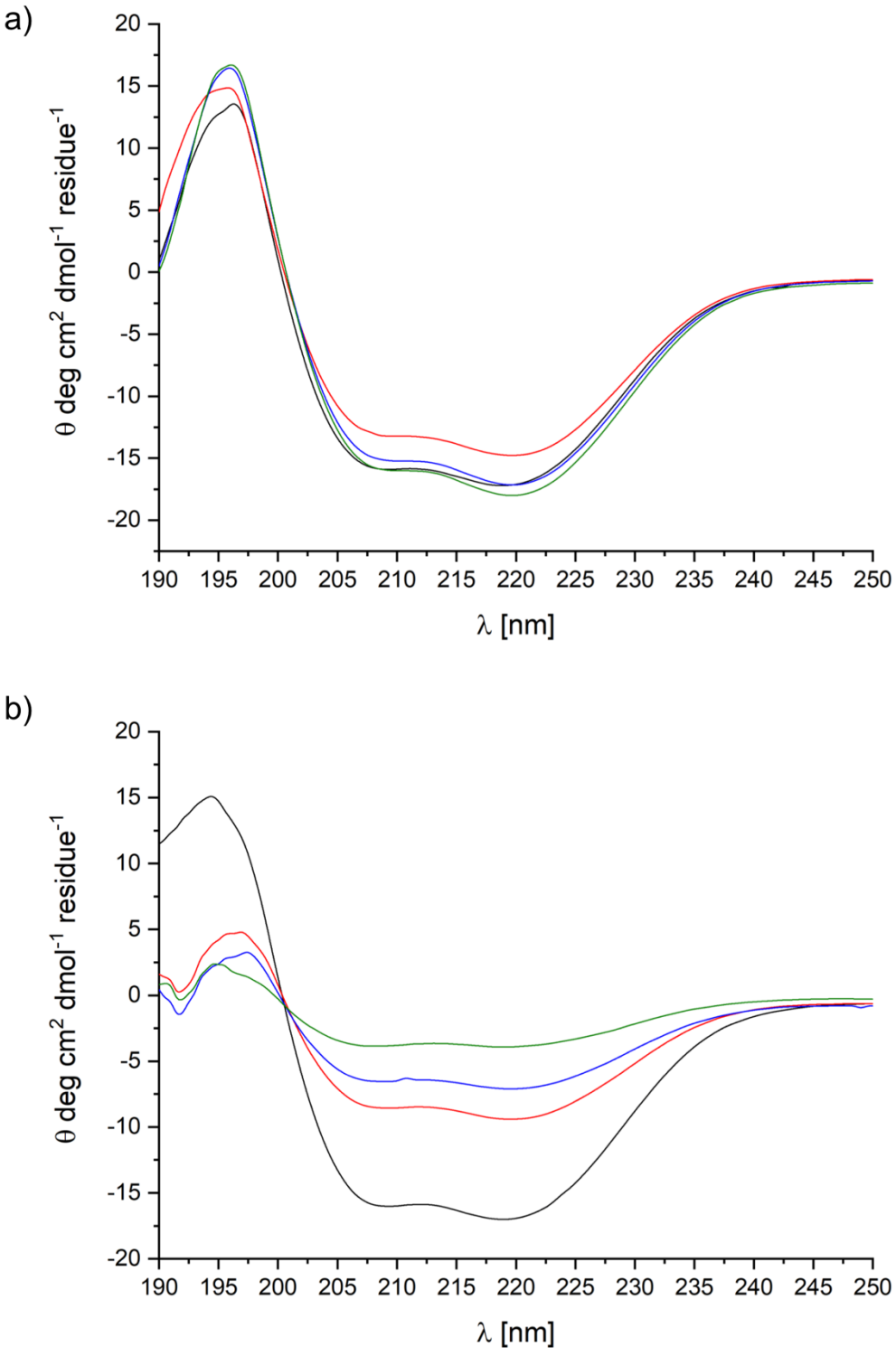

Figure 12.30. CD-spectra at 20°C (a) and 37°C (b) of hFF03 + hFF03-K17-Sial in D-PBS over a period of six days directly after sample preparation (black line), 24h (red line), 72h (blue line) and 6 days (green line) after sample preparation (75 µM total peptide concentration).

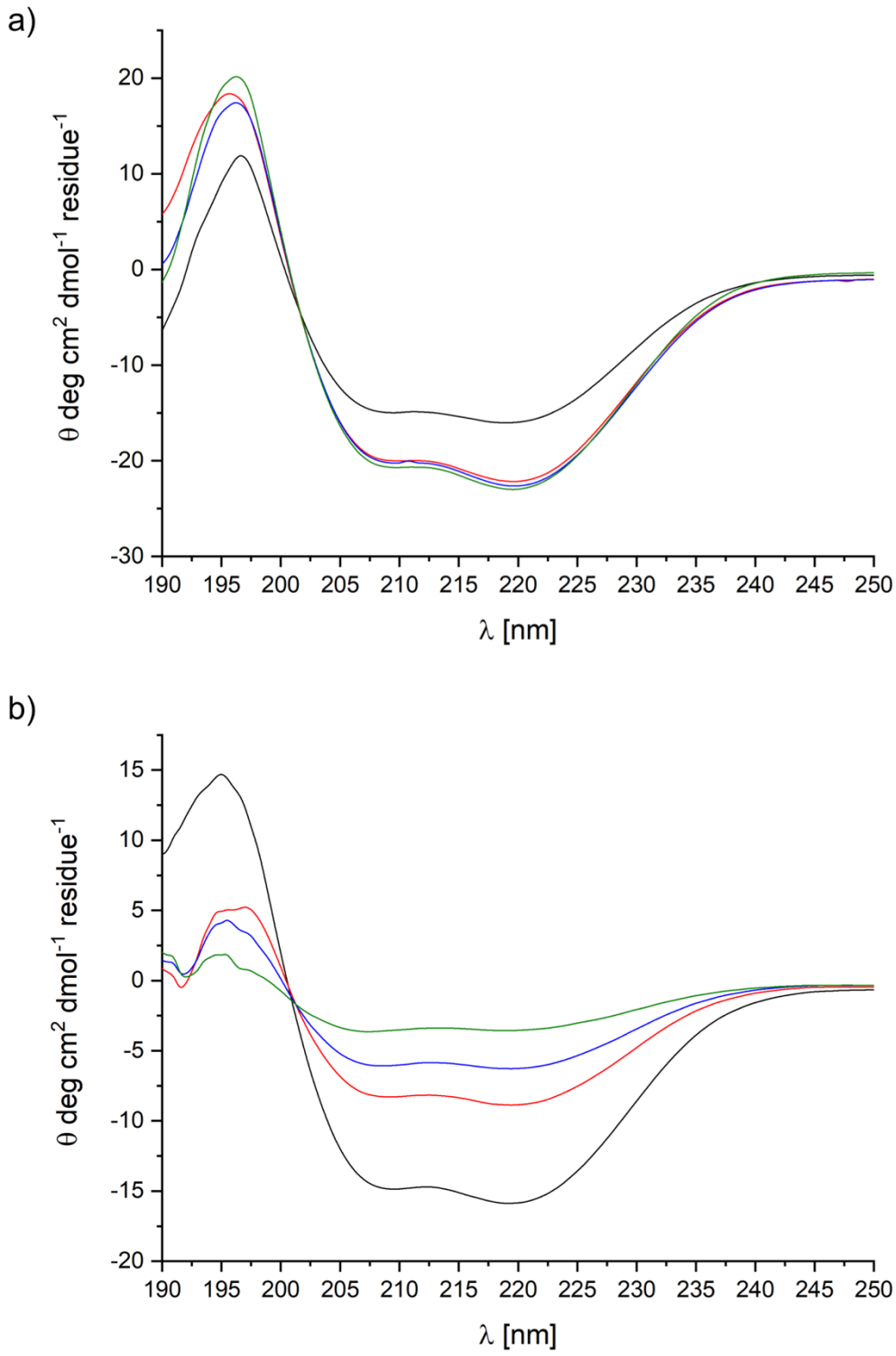

Figure 12.31. CD-spectra at 20°C (a) and 37°C (b) of FF03-K17-Sial + hFF03-K17-Sial in D-PBS over a period of six days directly after sample preparation (black line), 24h (red line), 72h (blue line) and 6 days (green line) after sample preparation (75 µM total peptide concentration).

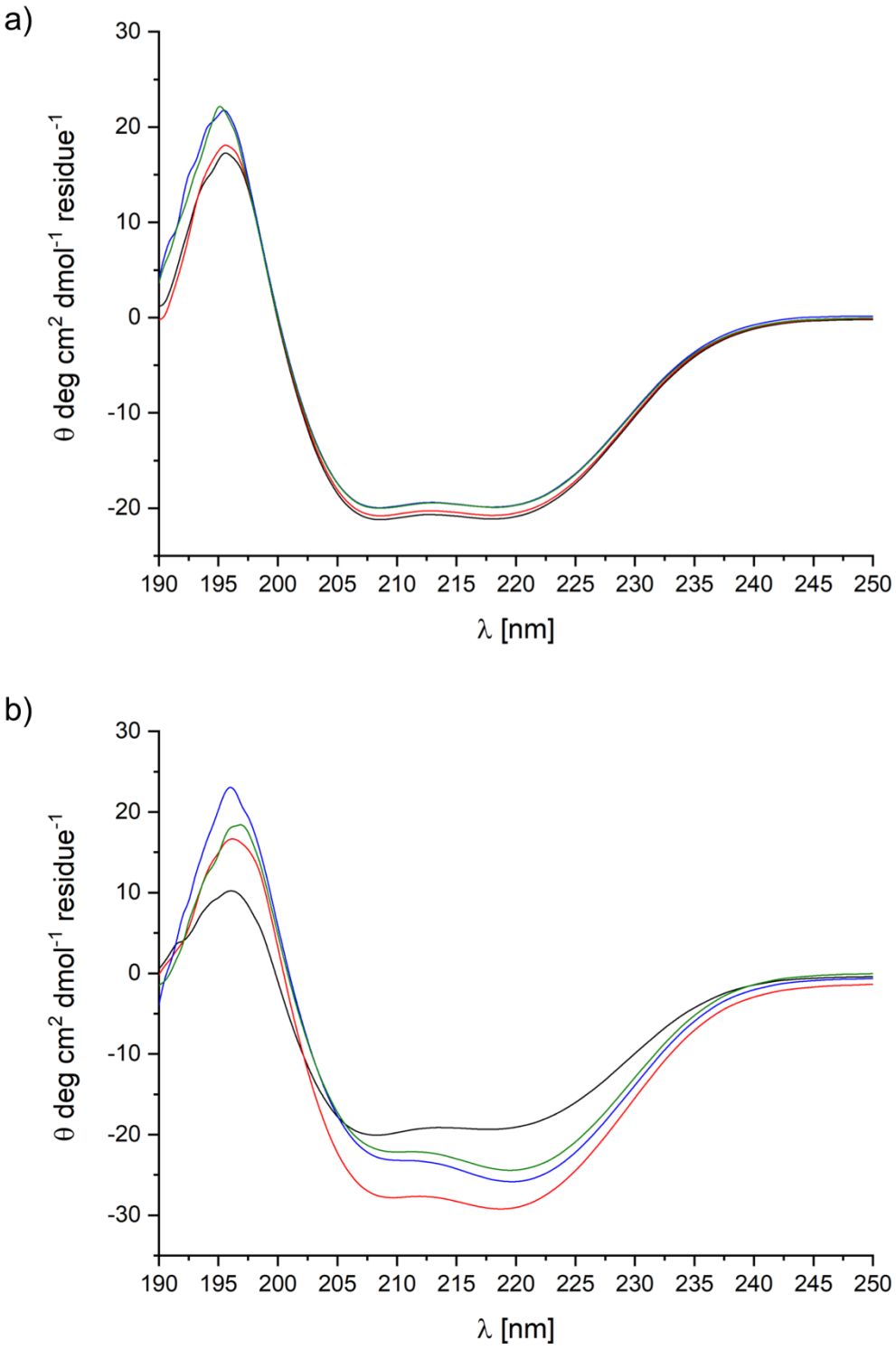

Figure 12.32. CD-spectra at 20°C (a) and 37°C (b) of 75 µM hFF03-fS-K17-Sial in D-PBS over a period of six days directly after sample preparation (black line), 24h (red line), 72h (blue line) and 6 days (green line) after sample preparation.

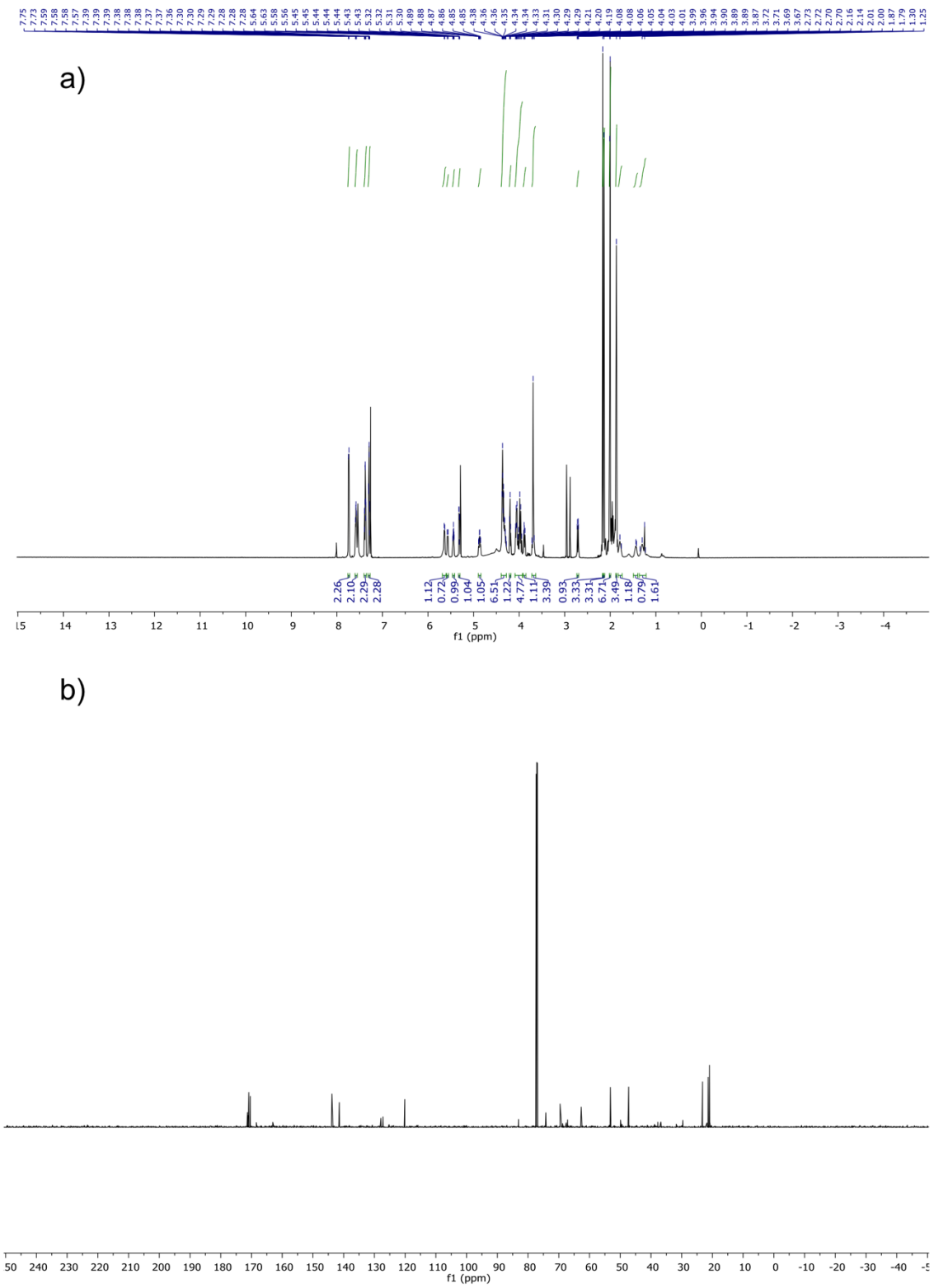

Figure 12.33. ^{1}H-NMR (panel a) and ^{13}C-NMR of Fmoc-L-Lys-Sial-OH (3) in $CDCl_3$.

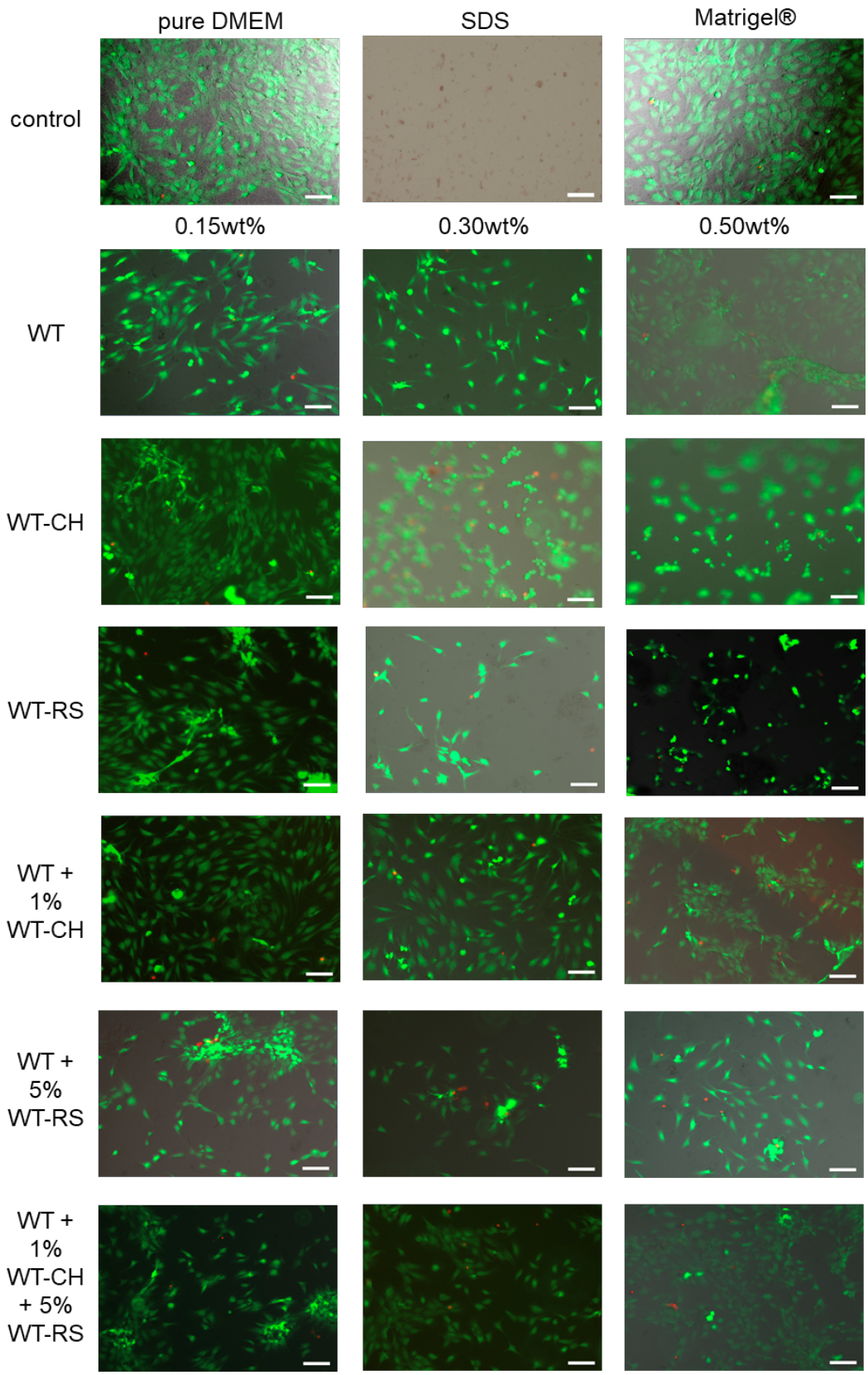

Figure 12.34. NIH/3T3 cells 24h after culturing on coiled-coil peptide hydrogels. Cells were stained by a LIVE/DEAD staining were living cells are stained green (calcein AM) and dead cells were stained red (ethidium homodimer-1). The scale bar denotes 100 µm.

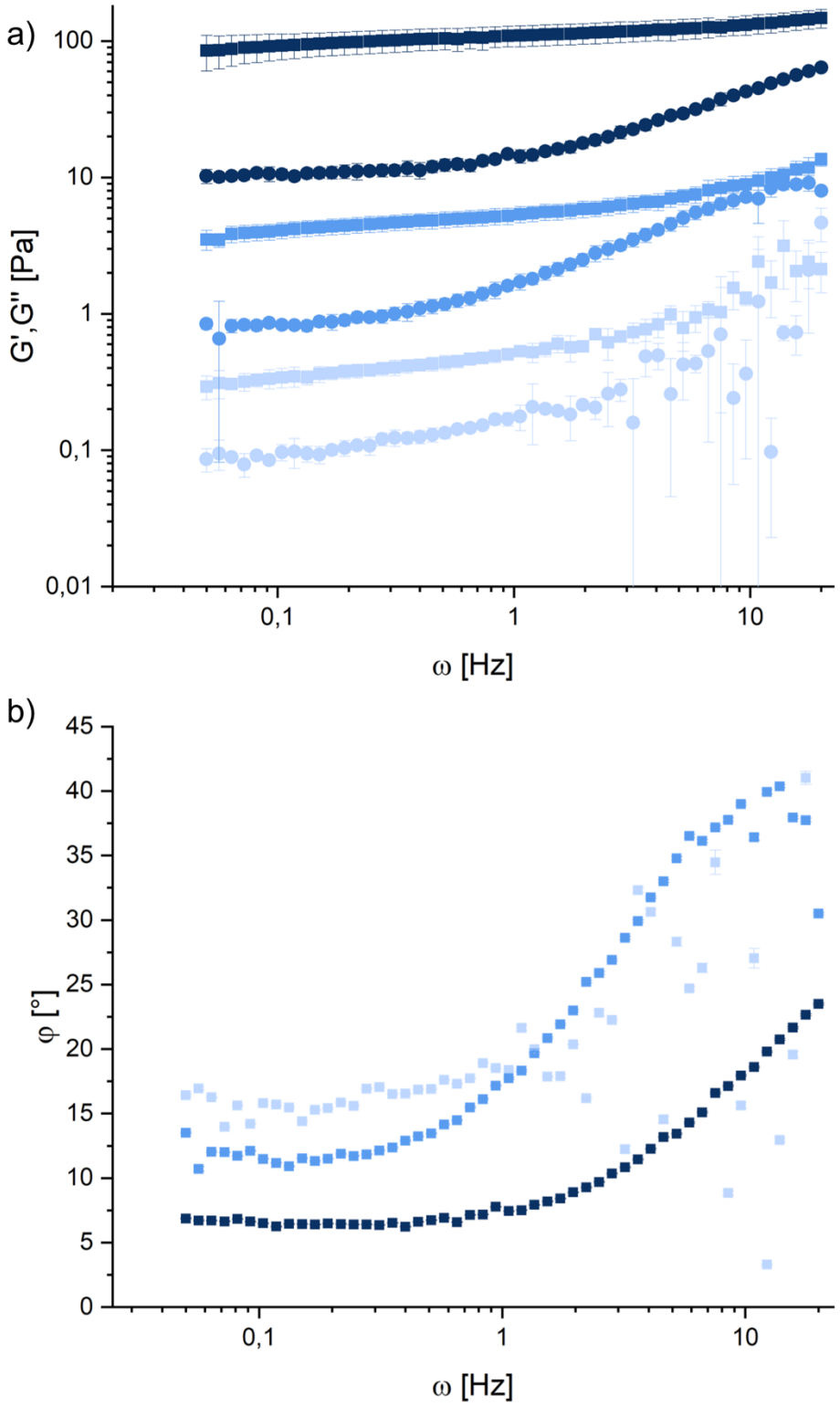

Figure 12.35. Storage modulus G' (squares) and loss modulus G'' (circles) as function of the applied frequencies (pattern a) and phase angle (pattern b) for WT hydrogel at 25°C of 0.15 wt% (light blue), 0.30 wt% (middle blue) and 0.50 wt% (dark blue).

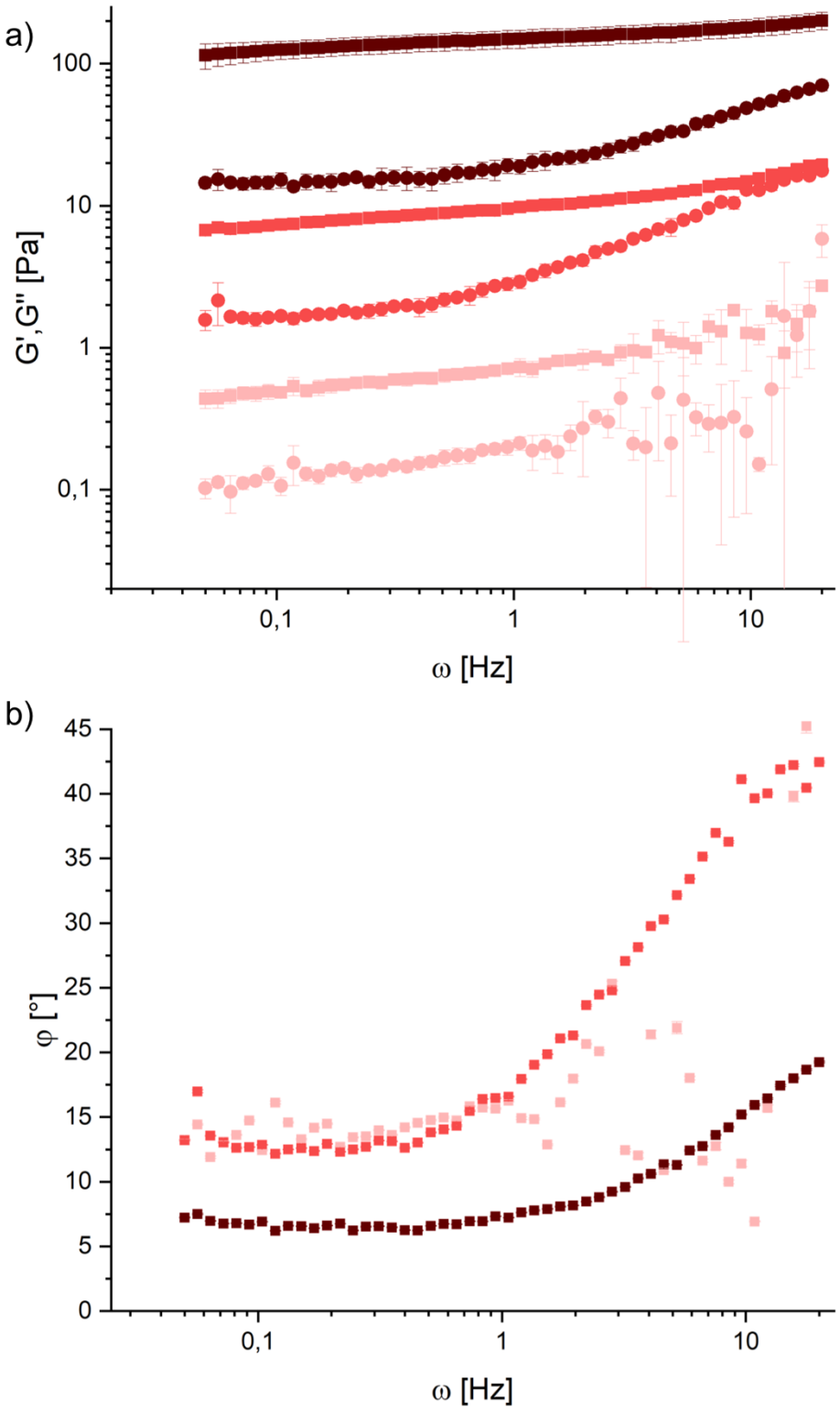

Figure 12.36. Storage modulus G' (squares) and loss modulus G'' (circles) as function of the applied frequencies (pattern a) and phase angle (pattern b) for WT hydrogel at 37°C of 0.15 wt% (light red), 0.30 wt% (red) and 0.50 wt%(dark red).

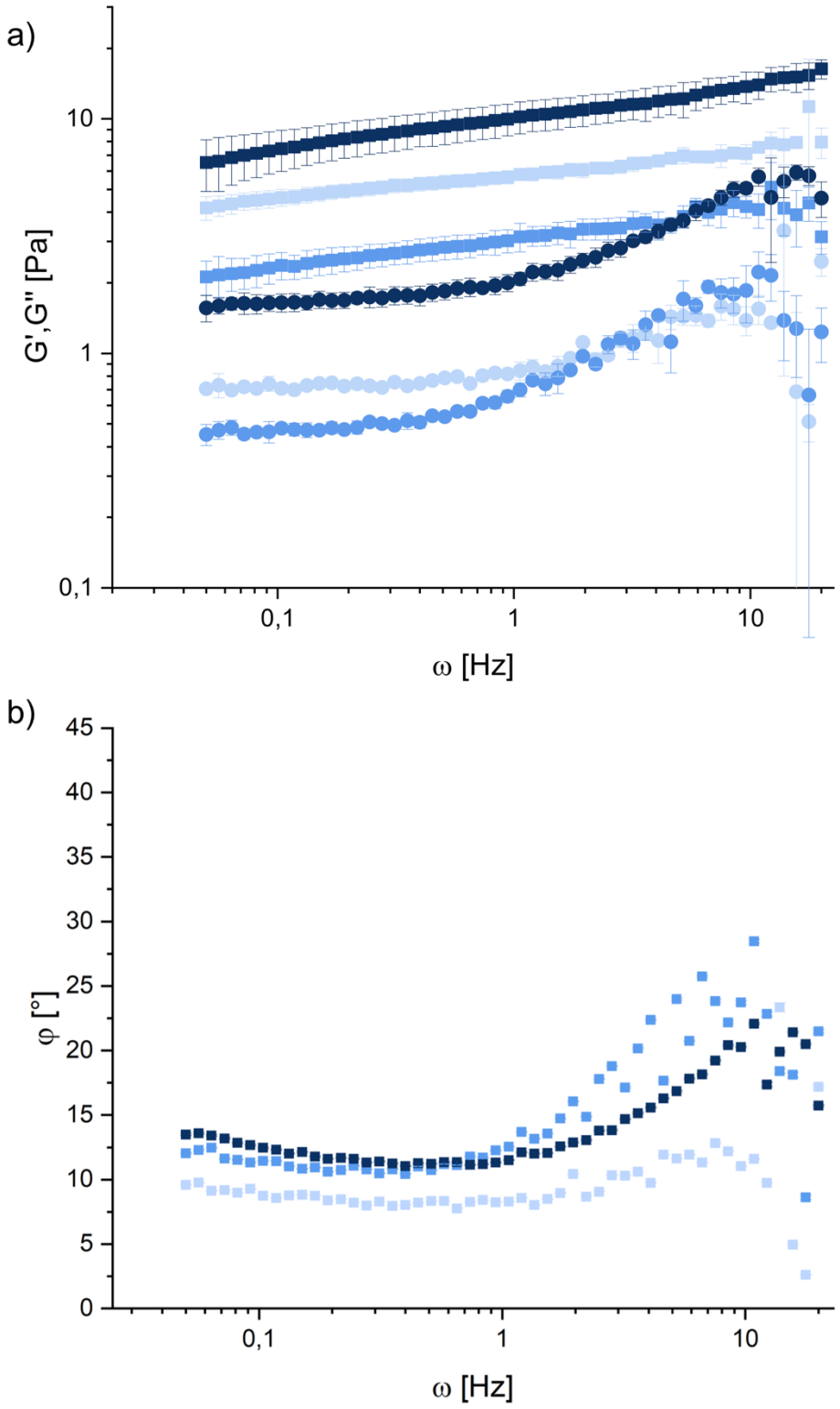

Figure 12.37. Storage modulus G' (squares) and loss modulus G'' (circles) as function of the applied frequencies (pattern a) and phase angle (pattern b) for WT-CH hydrogel at 25°C of 0.15 wt% (light blue), 0.30 wt% (middle blue) and 0.50 wt% (dark blue).

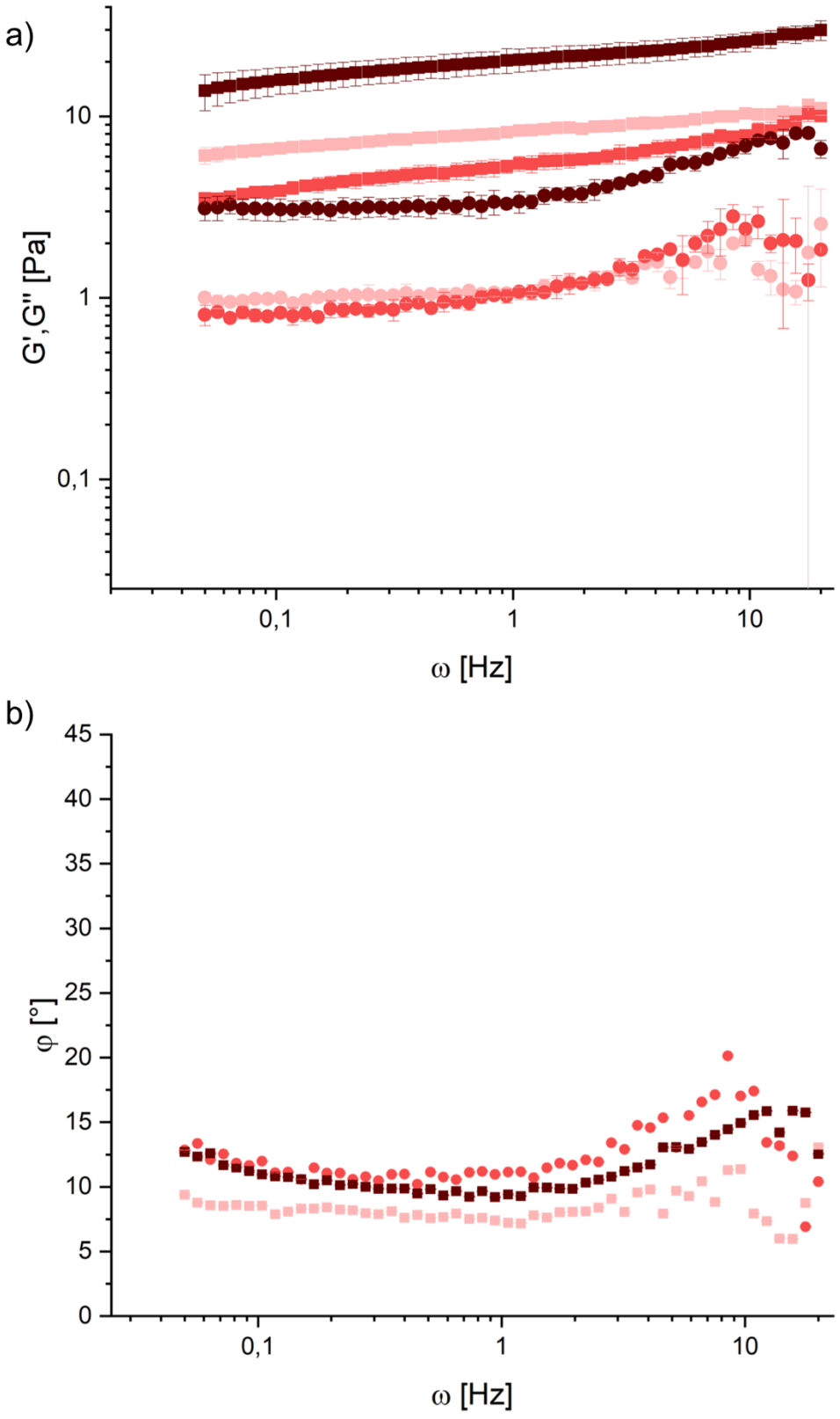

Figure 12.38. Storage modulus G' (squares) and loss modulus G'' (circles) as function of the applied frequencies (pattern a) and phase angle (pattern b) for WT-CH hydrogel at 37°C of 0.15 wt% (light red), 0.30 wt% (red) and 0.50 wt%(dark red).

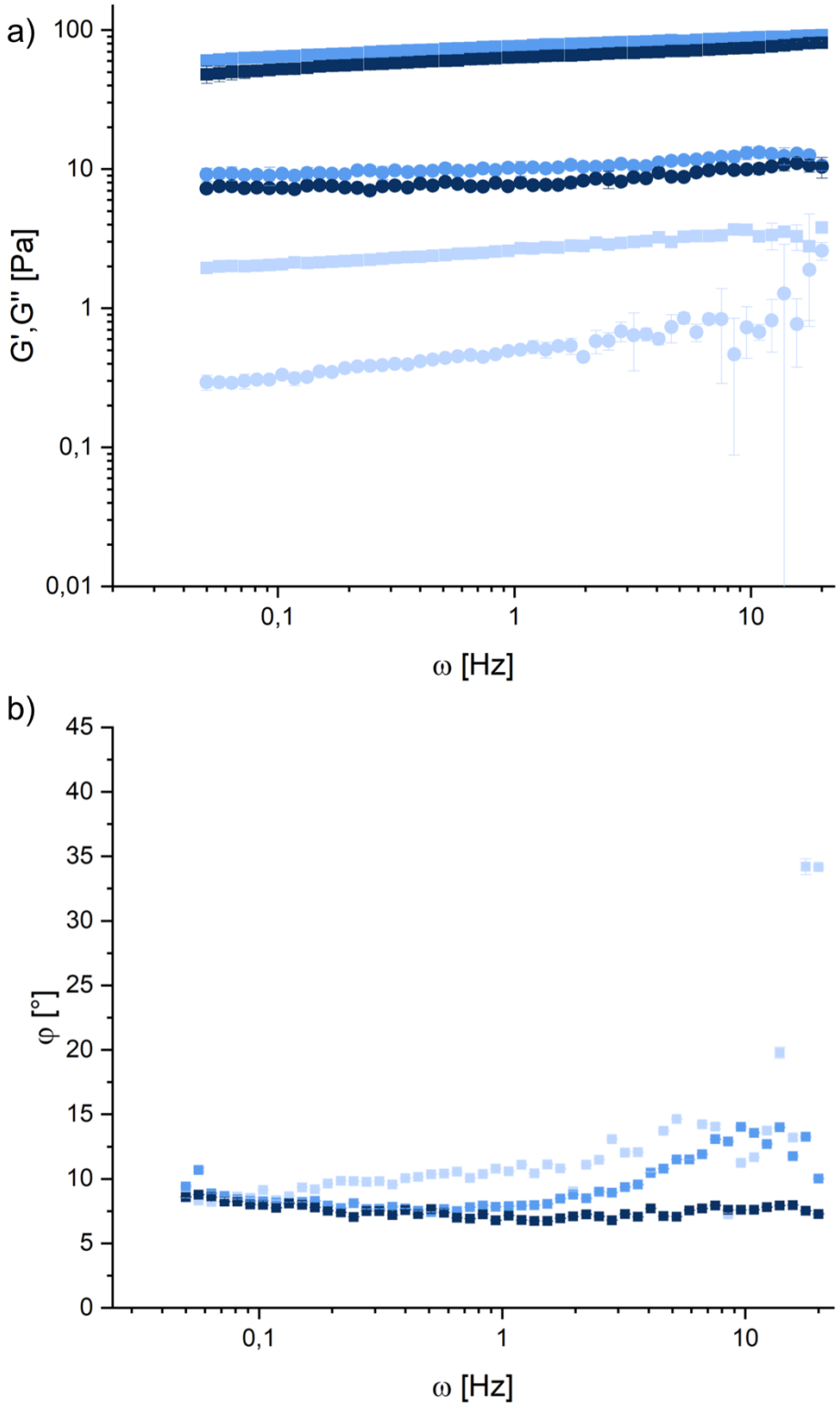

Figure 12.39. Storage modulus G' (squares) and loss modulus G'' (circles) as function of the applied frequencies (pattern a) and phase angle (pattern b) for WT-RS hydrogel at 25°C of 0.15 wt% (light blue), 0.30 wt% (middle blue) and 0.50 wt% (dark blue).

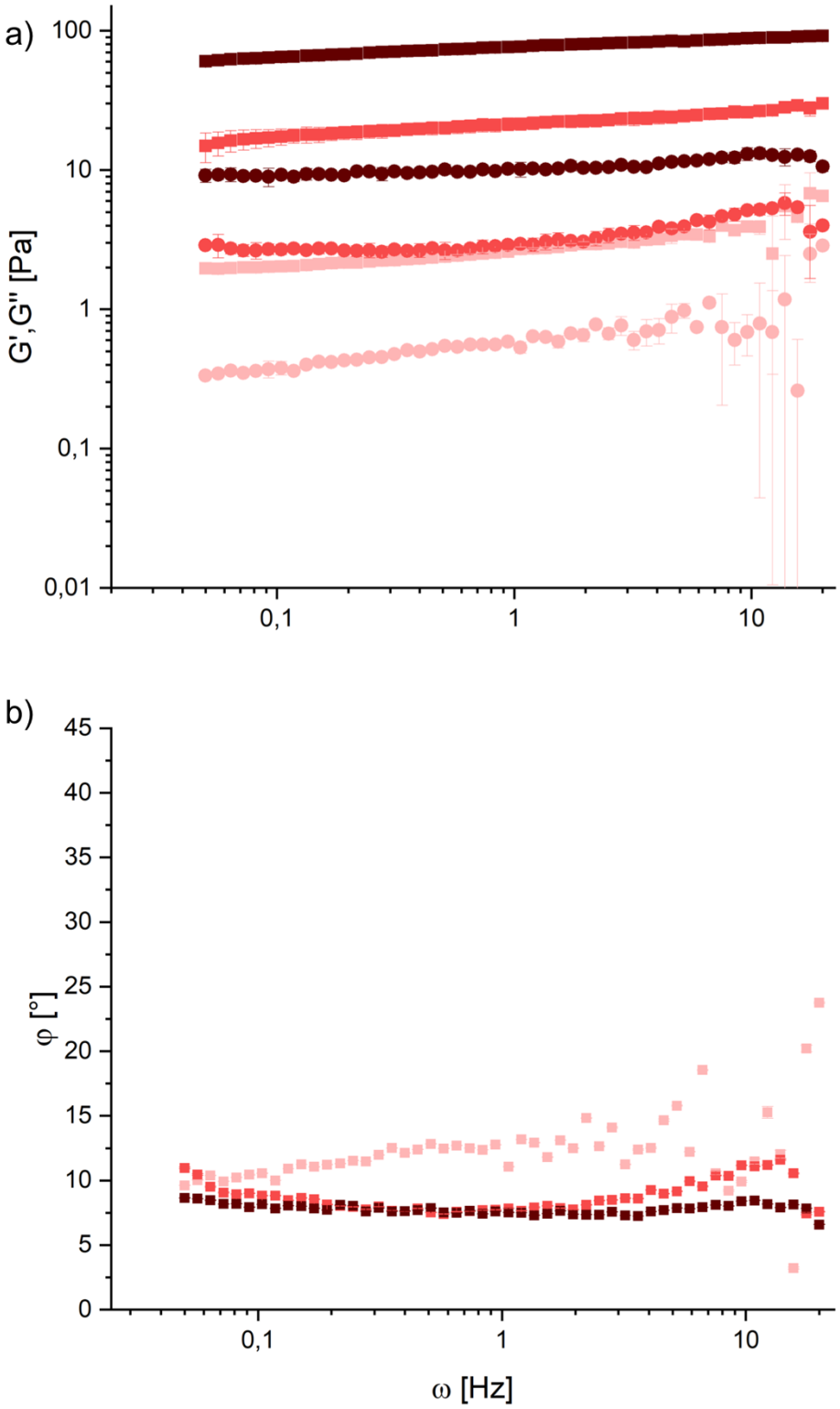

Figure 12.40. Storage modulus G' (squares) and loss modulus G'' (circles) as function of the applied frequencies (pattern a) and phase angle (pattern b) for WT-RS hydrogel at 37°C of 0.15 wt% (light red), 0.30 wt% (red) and 0.50 wt%(dark red).

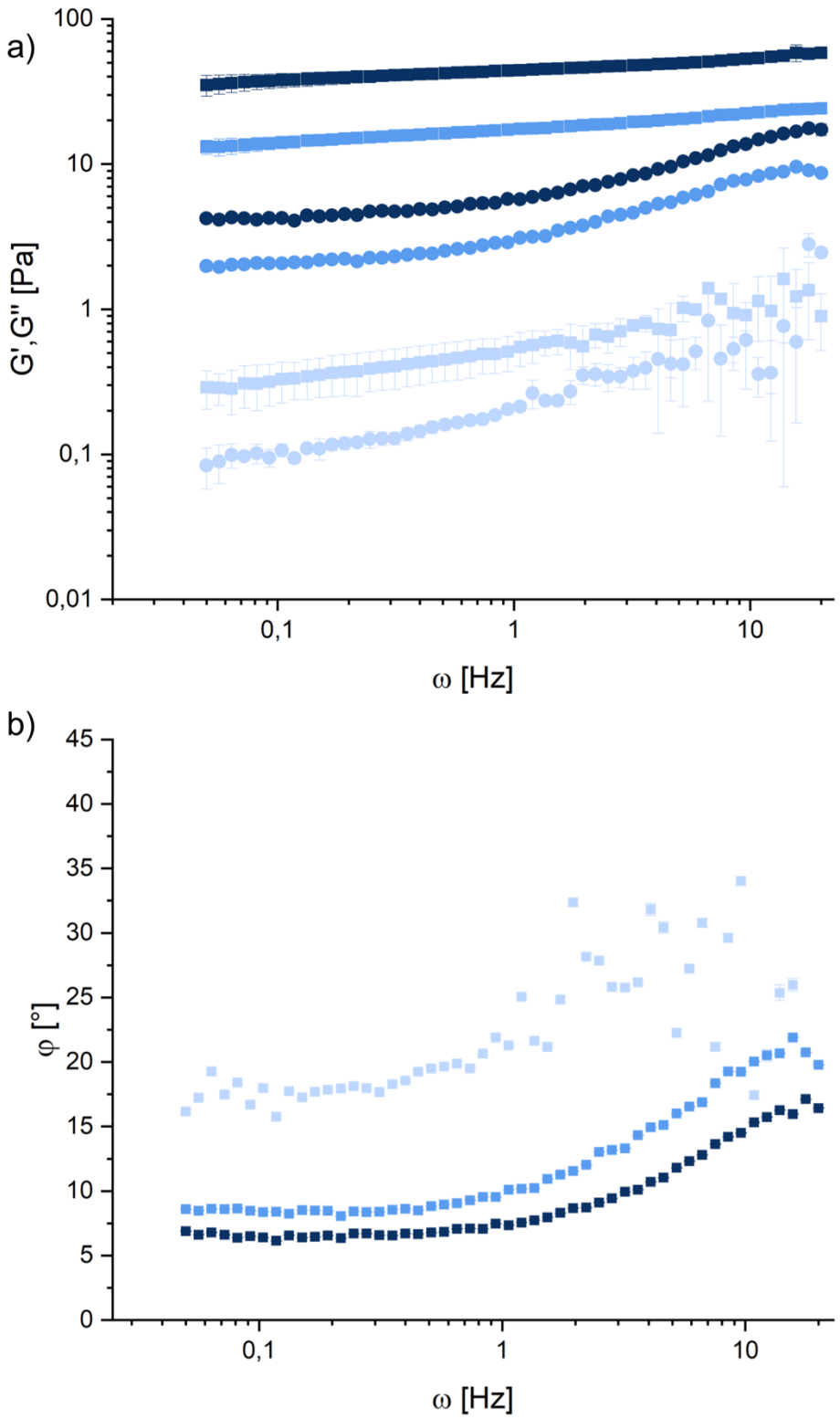

Figure 12.41. Storage modulus G' (squares) and loss modulus G'' (circles) as function of the applied frequencies (pattern a) and phase angle (pattern b) for WT +1% WT-CH hydrogel at 25°C of 0.15 wt% (light blue), 0.30 wt% (middle blue) and 0.50 wt% (dark blue).

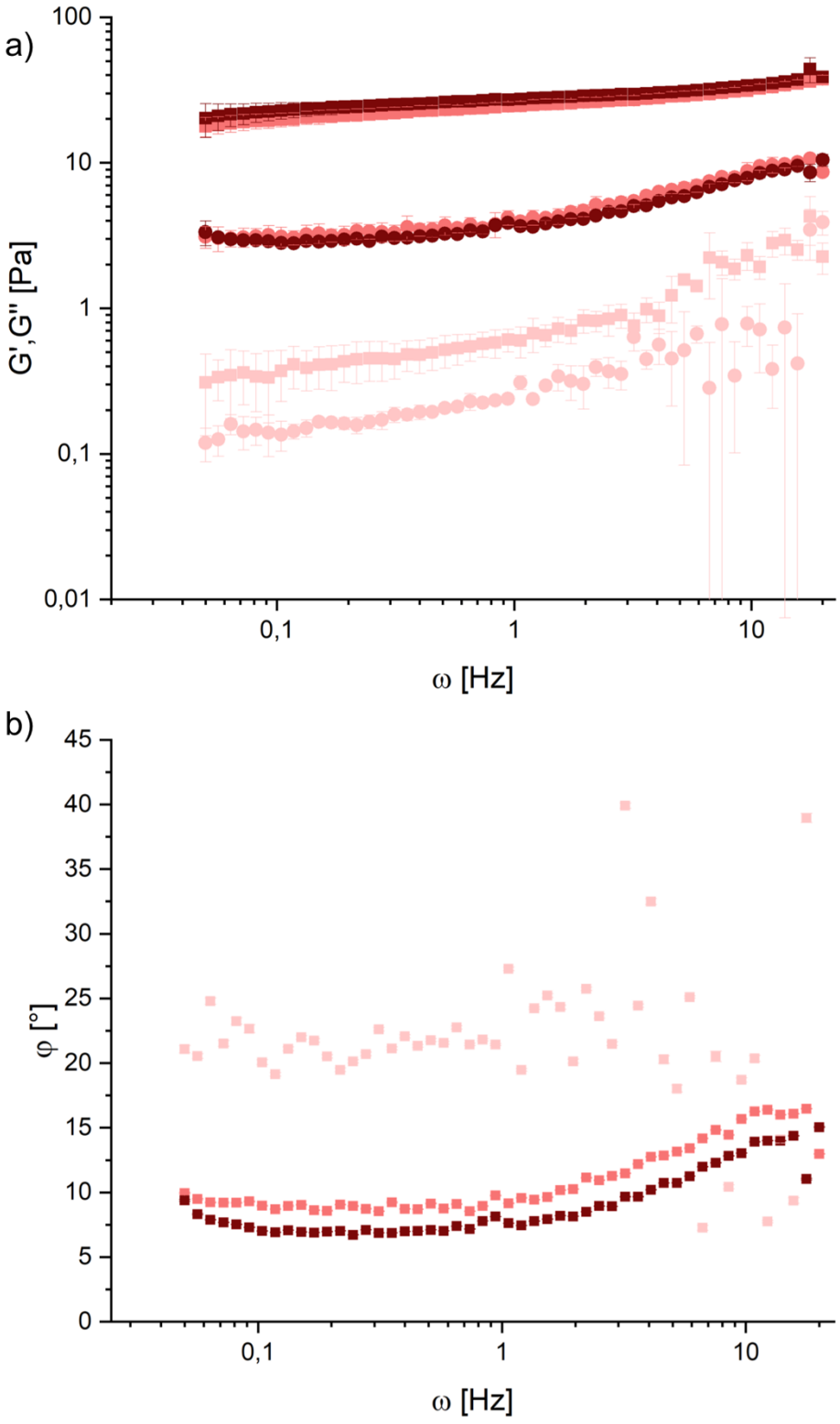

Figure 12.42. Storage modulus G' (squares) and loss modulus G'' (circles) as function of the applied frequencies (pattern a) and phase angle (pattern b) for WT +1% WT-CH hydrogel at 37°C of 0.15 wt% (light red), 0.30 wt% (red) and 0.50 wt%(dark red).

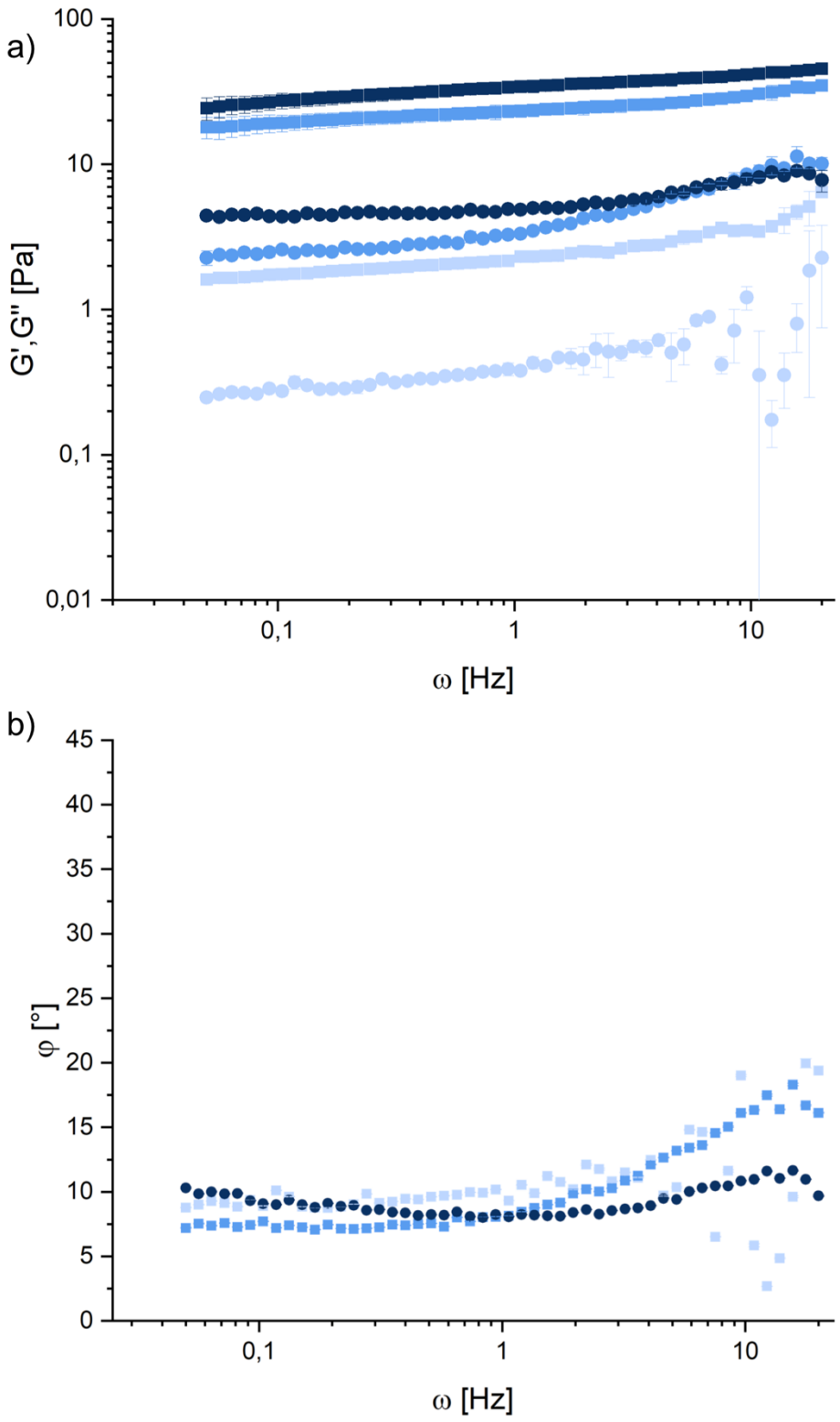

Figure 12.43. Storage modulus G' (squares) and loss modulus G'' (circles) as function of the applied frequencies (pattern a) and phase angle (pattern b) for WT +5% WT-RS hydrogel at 25°C of 0.15 wt% (light blue), 0.30 wt% (middle blue) and 0.50 wt% (dark blue).

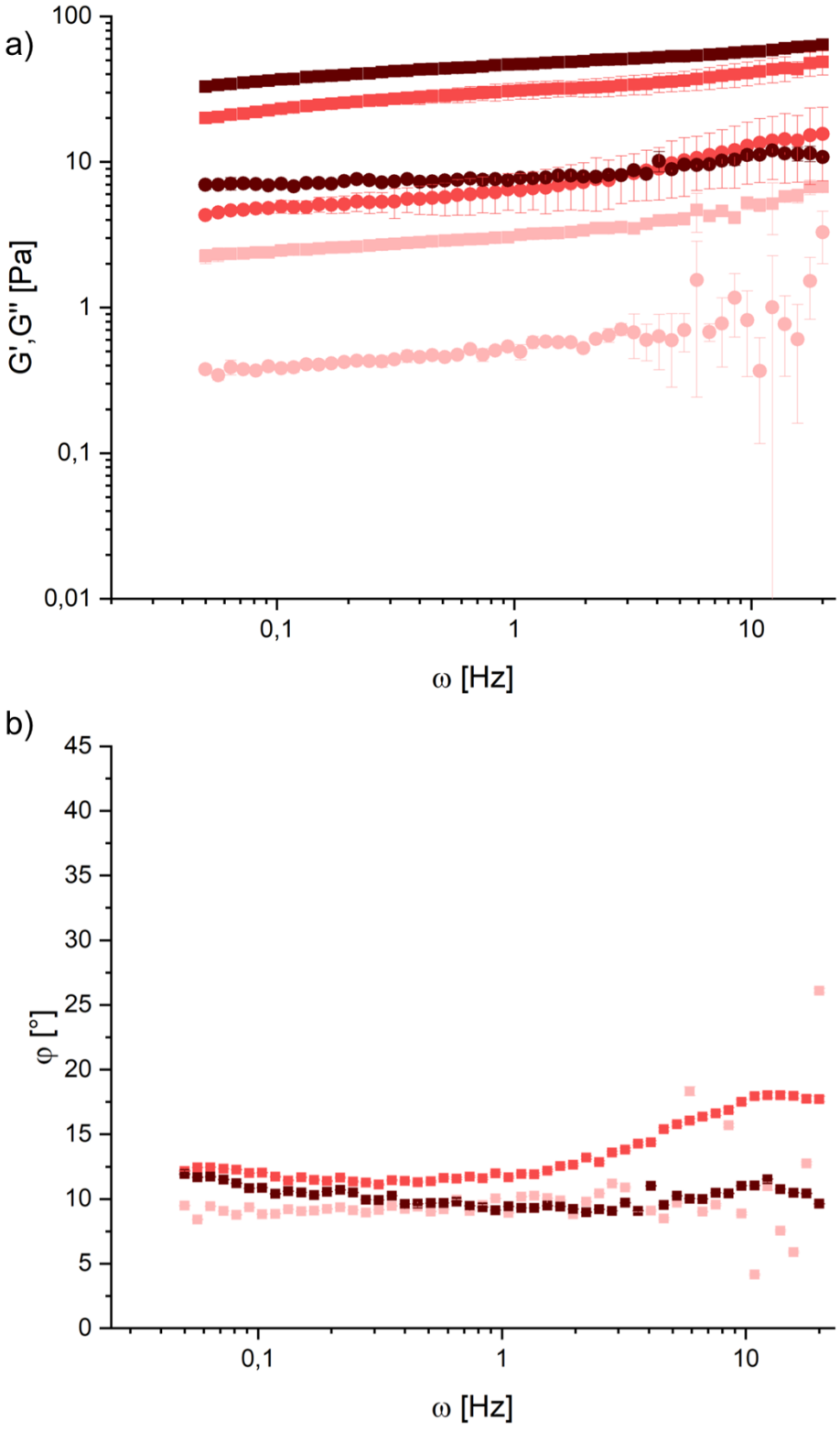

Figure 12.44. Storage modulus G' (squares) and loss modulus G'' (circles) as function of the applied frequencies (pattern a) and phase angle (pattern b) for WT + 5% WT-RS hydrogel at 37°C of 0.15 wt% (light red), 0.30 wt% (red) and 0.50 wt%(dark red).

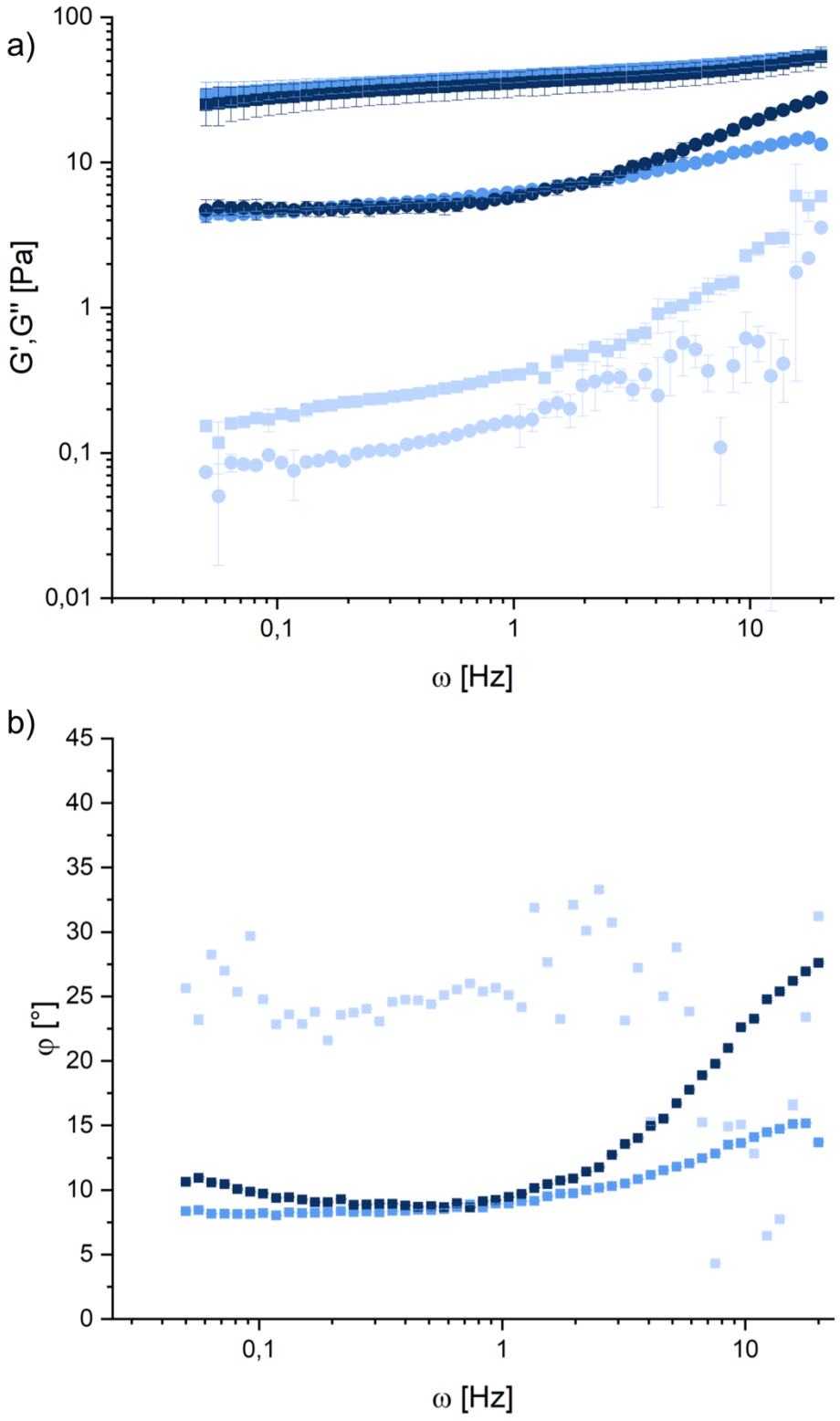

Figure 12.45. Storage modulus G' (squares) and loss modulus G'' (circles) as function of the applied frequencies (pattern a) and phase angle (pattern b) for WT +1% WT-CH + 5% WT-RS hydrogel at 25°C of 0.15 wt% (light blue), 0.30 wt% (middle blue) and 0.50 wt% (dark blue).

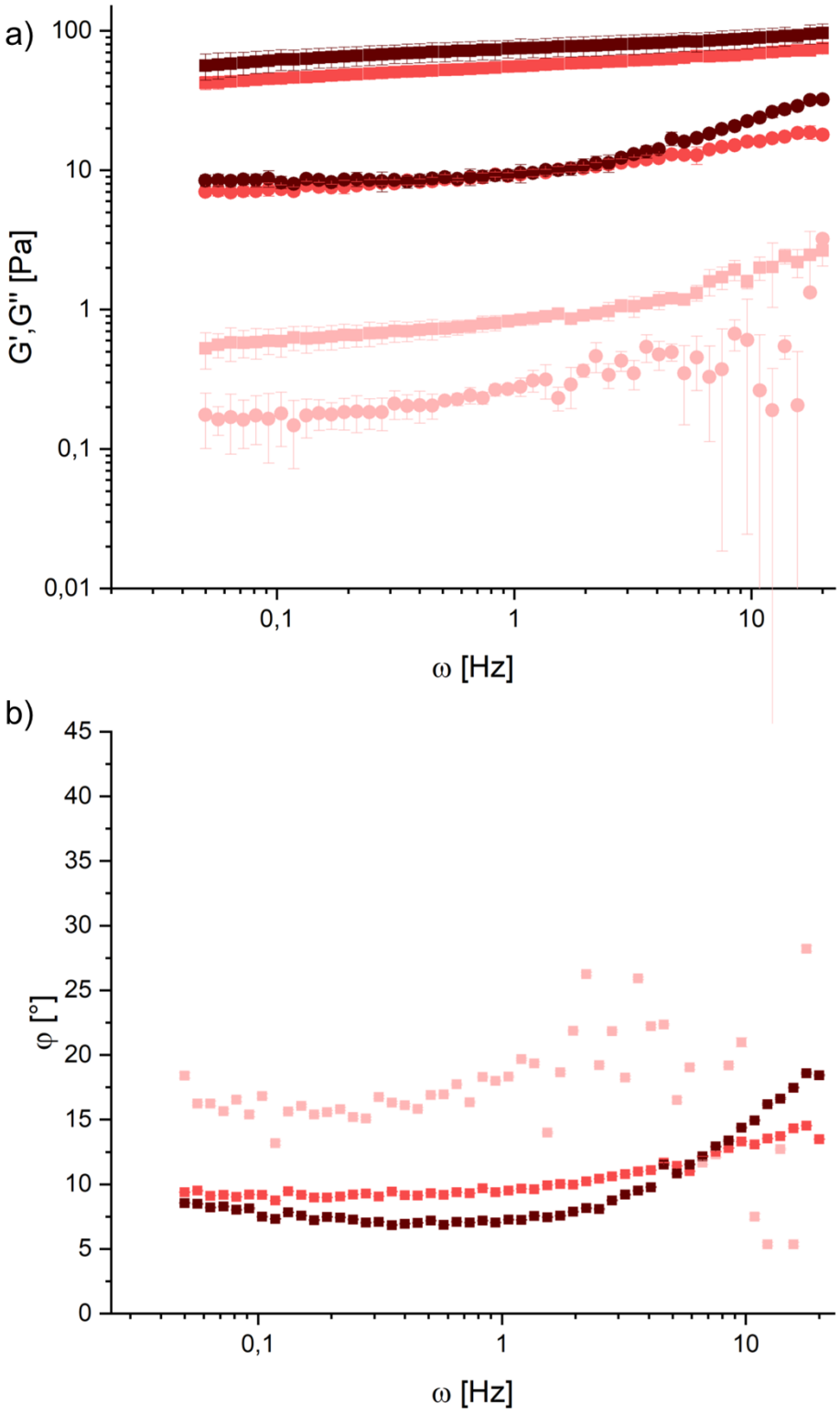

Figure 12.46. Storage modulus G' (squares) and loss modulus G'' (circles) as function of the applied frequencies (pattern a) and phase angle (pattern b) for WT + 1% WT-CH + 5% WT-RS hydrogel at 37°C of 0.15 wt% (light red), 0.30 wt% (red) and 0.50 wt%(dark red).

Table 12.1. Concentration of hydrogel-mixtures of section 5.2.2.

		Composition		
Sample	**wt%**	**hFF03 [µM]**	**hFF03-K17-Man [µM]**	**hFF03-K17-RGD [µM]**
WT	0.15	498.37	-	-
	0.30	996.73	-	-
	0.50	1661.22	-	-
WT-CH	0.15	-	456.50	-
	0.30	-	913.00	-
	0.50	-	1522.00	-
WT-RS	0.15	-	-	449.41
	0.30	-	-	898.81
	0.50	-	-	1498.02
WT + 1% WT-CH	0.15	498.37	4.98	-
	0.30	996.73	9.96	-
	0.50	1661.22	16.61	-
WT + 5% WT-RS	0.15	498.37	-	24.92
	0.30	996.73	-	49.84
	0.50	1661.22	-	83.05
WT + 1% WT-CH + 5% WT-RS	0.15	498.37	4.98	24.92
	0.30	996.73	9.96	49.84
	0.50	1661.22	16.61	83.05